Modulation of TMEM16 proteins: a novel therapeutic approach to Cystic Fibrosis therapy

DISSERTATION ZUR ERLANGUNG DES DOKTORGRADES
DER NATURWISSENSCHAFTEN (DR.RER.NAT.)
DER FAKULTÄT FÜR BIOLOGIE UND VORKLINISCHE MEDIZIN
DER UNIVERSITÄT REGENSBURG

Vorgelegt von
Roberta Benedetto
Aus Messina, Italien

im Jahr 2019

DAS PROMOTIONSGESUCH WURDE EINGEREICHT AM: 11.01.2019

DIE ARBEIT WURDE ANGELEITET VON:
PROF. DR. KARL KUNZELMANN

UNTERSCHRIFT:

DIE ARBEIT WURDE ANGELEITET VON: PROF. DR. KARL KUNZELMANN

PRÜFUNGSAUSSCHUSS:

VORSITZENDER: PROF. DR. MED. ARMIN KURTZ

1.GUTACHTER: PROF. DR. MED. KARL KUNZELMANN

2.GUTACHTER: MICHAEL GRAY Ph.D

3. PRÜFER: PROF. DR.RER.NAT. WOLF HAYO CASTROP

ERSATZPERSON: PROF. DR. RER. NAT. CHARLOTTE WAGNER

To see what is right and not to do it is want of courage.

Confucius

Summary

Cystic Fibrosis (CF) is caused by mutations in the gene encoding the CF transmembrane conductance regulator (CFTR) protein. CFTR is the apical cAMP activated Cl^- channel of epithelial cells. Mutations of this protein cause disruption of the electrolyte balance, leading to the formation of thick and sticky mucus in the lungs, and a variety of other problems. Cystic Fibrosis is a multifaceted disease and, despite being monogenic, its treatment is very challenging. Current therapies aim to modulate defective CFTR but are beneficial only to patients harboring a restricted number of mutations including F508del and G551D, thus excluding about 15% of the patients carrying so-called “unrescuable” mutations. Therefore, bypass therapies are of great importance to many patients who could benefit from them regardless of their genotype. This implies that with the increase in the number of mutations that are sensitive to a given therapy, the costs would diminish and the accessibility to the treatment should increase accordingly.

TMEM16A (Anoctamin 1; ANO1) is the major contributor to Ca^{2+} activated Cl^- secretion in the airways and is regarded as the ideal druggable channel to bypass defective CFTR dependent Cl^- secretion. In the present work we demonstrate that TMEM16A facilitates compartmentalized Ca^{2+} store release in membrane microdomains. Modulation of intracellular Ca^{2+} by TMEM16A is necessary for proper function as well as membrane insertion of CFTR. We showed that cAMP-dependent and Ca^{2+} activated Cl^- currents in airway epithelial cells strongly overlap due to crosstalk of intracellular signaling molecules. Intracellular Ca^{2+} rise mediated by TMEM16A triggers so-called Store Operated cAMP signaling (SOcAMPs) and activates Ca^{2+} regulated adenylyl cyclase 1 (ADCY1) and the exchange protein directly activated by cAMP (EPAC1). This crosstalk is compartmentalized and supports activation of both, TMEM16A and CFTR.

Our tissue specific knockout model for TMEM16A showed a peculiar phenotype due to intracellular mucus accumulation. We found that TMEM16A is essential for ATP-dependent constitutive exocytosis of mucus in airways and intestine. Moreover, we demonstrate that TMEM16A is upregulated in inflammatory airway disease. This upregulation occurs in epithelial cells as well as airway smooth muscle. We concluded that the effect of TMEM16A

on intracellular Ca^{2+} signaling contributes to mucus hypersecretion and airways bronchoconstriction. As further shown, inhibition of TMEM16 proteins has beneficial effects in inflammatory airway disease by inhibiting mucus release and promoting bronchorelaxation and in addition, shows anti-inflammatory effects. TMEM16 inhibitors are therefore suggested as novel potential drugs for the treatment of CF lung disease and other inflammatory airway diseases.

Zusammenfassung

Mukoviszidose (Zystische Fibrose, Cystic Fibrosis, CF) wird durch Mutationen im CFTR (Cystic Fibrosis Transmembrane Conductance Regulator) Gen verursacht. CFTR ist der apikale cAMP-aktivierte Cl^- Kanal in Epithelzellen. Mutationen im CFTR Protein führen zu einer Störung des Elektrolyttransports, was zur Bildung von hochviskösem und adhäsivem Schleim in Lunge und Darm sowie zu einer Vielzahl von Störungen in anderen Organen führt. Die Mukoviszidose ist eine vielschichtige Krankheit. Obwohl sie monogen vererbt wird, weist sie eine Vielzahl von zellulären Defekten und klinischen Symptomen auf. Die Behandlung der Erkrankung erweist sich als schwierig. Die derzeitigen Therapien zielen darauf ab, die Restfunktion des mutierten CFTRs zu aktivieren. Dies ist aber nur bei etwa 85 % der Patienten möglich. Etwa 15% der Patienten mit nicht korrigierbaren Mutationen sind von diesen Therapien ausgeschlossen. Daher sind neue therapeutische Ansätze erforderlich. Ein möglicher Ansatz besteht in der pharmakologischen Beeinflussung weiterer zellulärer Ionenkanäle, um den CFTR-Defekt zu kompensieren. Viele Patienten könnten von diesen sogenannten Bypass-Therapien unabhängig von ihrem Genotyp profitieren. Darüber hinaus könnte eine solche Behandlung für alle CF-Patienten zugänglich sein und die derzeit enormen Behandlungskosten senken.

TMEM16A (Anoctamin 1; ANO1) ist der Hauptfaktor für die Ca^{2+} aktivierte Cl^- Sekretion in den Atemwegen und gilt als idealer pharmakologischer Angriffspunkt zur Umgehung defekter CFTR-abhängiger Cl^- Sekretion. Die vorliegende Arbeit zeigt, dass TMEM16A die Freisetzung von Ca^{2+} in Membran-Mikrodomänen erleichtert. Die Modulation von intrazellulärem Ca^{2+} durch TMEM16A ist für die korrekte Funktion sowie für die Membraninsertion von CFTR notwendig. Weiterhin wurde deutlich, dass sich die cAMP-abhängigen und Ca^{2+}-aktivierten Cl^- Ströme in Atemwegsepithelzellen aufgrund des Nebeneinanders von intrazellulären Signalmolekülen stark überlappen. Der intrazelluläre Ca^{2+}-Anstieg, der durch TMEM16A vermittelt wird, löst das so genannte Store Operated cAMP-Signaling (SOcAMPs) aus und aktiviert die Ca^{2+} regulierte Adenylylcyclase 1 (ADCY1) und das Austauschprotein aktiviert durch cAMP (EPAC1). Diese kompartimentalisierten Wechselwirkungen von Signalmolekülen führen zusammen zur Aktivierung von TMEM16A und CFTR.

Gewebespezifische Knockout-Modelle für TMEM16A zeigen in den Atemwegen und im Darm aufgrund der intrazellulären Akkumulation von Schleim einen auffälligen Phänotyp. TMEM16A ist für die ATP-abhängige konstitutive Exozytose von Schleim in Atemwegen und Darm unerlässlich. Darüber zeigt die Arbeit, dass TMEM16A bei entzündlichen Atemwegserkrankungen hochreguliert ist. Die erhöhte Expression von TMEM16A tritt sowohl in Epithelzellen als auch in der glatten Muskulatur der Atemwege auf. Die erhobenen Daten lassen darauf schließen, dass die Wirkung von TMEM16A auf die intrazellulären Ca^{2+}-Signalwege zur Schleimhypersekretion und Atemwegsbronchokonstriktion beiträgt. Wie weiter gezeigt, hat die Hemmung der TMEM16-Proteine positive Auswirkungen auf die entzündliche Atemwegserkrankung durch Hemmung der Schleimfreisetzung und Bronchorelaxation. Darüber hinaus zeigt es entzündungshemmende Effekte. TMEM16-Hemmer werden daher als neuartige potenzielle Medikamente zur Behandlung von CF-Lungenerkrankungen und anderen entzündlichen Atemwegserkrankungen vorgeschlagen.

Preface

This work is the result of the combination of published papers under the form of book chapters. Therefore, the reader may encounter variations (e.g. mouse nomenclature), accordingly to the guidelines of the different journals.

The chapters consist of the following manuscripts:

Chapter 2: Cabrita I, **Benedetto R**, Fonseca A, Wanitchakool P, Sirianant L, Skryabin BV, Schenk LK, Pavenstadt H, Schreiber R, Kunzelmann K. Differential effects of anotamins on intracellular calcium signals. FASEB J. 2017 May; 31(5): 2123-2134.

Chapter 3: **Benedetto R**, Ousingsawat J, Wanitchakool P, Zhang Y, Holtzman MJ, Amaral M, Rock JR, Schreiber R, Kunzelmann K. Epithelial Chloride Transport by CFTR requires TMEM16A. Sci Rep. 2017 Sept; 7(1): 12397.

Chapter 4: Lérias J, Pinto M, **Benedetto R**, Schreiber R, Amaral M, Aureli M, Kunzelmann K. Compartmentalized crosstalk of CFTR and TMEM16A (ANO1) through EPAC1 and ADCY1. Cell Signal. 2018 Apr; 44:10-19.

Chapter 5: **Benedetto R**., Cabrita I., Schreiber R., and Kunzelmann, K. TMEM16A is indispensable for basal ATP-induced mucus secretion in airways and intestine. Faseb J. 2018 Dec:fj201801333RRR.

Chapter 6: Inês Cabrita, **Roberta Benedetto**, Rainer Schreiber, Karl Kunzelmann. Niclosamide repurposed for the treatment of inflammatory airway disease. (Submitted for publication).

List of Figures

List of tables

Chapter 1

Introduction

Cystic Fibrosis

Cystic Fibrosis (CF) is an autosomal recessive disorder caused by mutations in the Cystic Fibrosis transmembrane conductance regulator (CFTR) gene. The frequency of CF varies around the globe. It is particularly common among Caucasians of Northern European descent, with an incidence of 1 in every 2500-3000 newborns [1]. CFTR is a complex cAMP-activated chloride (Cl^-) channel and regulatory protein found in the apical membranes of epithelial cells in all exocrine tissues. Deficient CFTR causes imbalanced transport of chloride and bicarbonate and leads to the formation of a thick, viscous secretion in lungs, pancreas, liver, intestine, and reproductive tract. CF patients also show an increased salt content in their sweat [2,3]. Clinically, lung disease is the most severe problem in the majority of CF patients. However, the phenotypic spectrum of CF is complex and several organs can be affected. In the gastrointestinal tract, plugs of meconium appear in the distal ileum after the 17^{th} week of gestation, leading to an obstruction that causes dilatation and perforation of the ileal wall, a condition called meconium ileus. Due to their altered composition, pancreatic secretion in CF is characterized by low pH, reduced volume and higher protein content. Precipitation in the duct lamina results in obstruction, inflammation and general fibrosis. Intrahepatic and extrahepatic stones, due to the accumulation of mucus in the liver, are found in around 15% of CF patients. Gallbladder calculi, affecting around 12% of all CF cases, often accompany liver pathology. Kidney stones [4], renal amyloidosis and immune complex glomerulonephritis occur in a large number of CF patients. Around 97% of all males with CF suffer from the Congenital Absence of the Vas Deferens (CAVD), while 20% of affected women have reduced fertility due to thickened cervical mucus. Of all the various symptoms of CF, mucus hyperproduction with consequent obstruction of the distal airways and submucosal glands is the main cause for morbidity and mortality in affected individuals [5, 6].

The CFTR Cl^- channel

In 1989 the CF gene was discovered by linkage analysis by Riordan *et al.*, who located the gene on the long arm of chromosome 7 (7q31.2) [7]. CFTR encodes a member of the ATP-binding cassette (ABC) transporter superfamily that, unlike canonical ABC transporters, forms a Cl^- channel [8]. CFTR consists of two membrane spanning domains (MSDs) with six transmembrane helices each, two cytoplasmic nucleotide-binding domains (NBDs) that hydrolyze ATP, and a phosphorylation dependent regulatory (R) domain that allows the channel to open upon phosphorylation by cAMP-dependent protein kinase A (PKA) (Fig 1) [8-10]. Peculiar of CFTR is a N-terminal interfacial structure named lasso motif (represented in dark blue in Fig.1). It is speculated that the lasso domain interaction with the R domain regulates the gating of the channel [11], however no direct contact was reported [9]. The contributions of the different domains to the functions of CFTR have been thoroughly investigated over the years, through study of CFTR variants containing site-directed mutations [11]. By using Cl^- channel inhibitors of different sizes, the narrowest part of the pore was found to be around 5.3 Å [12].

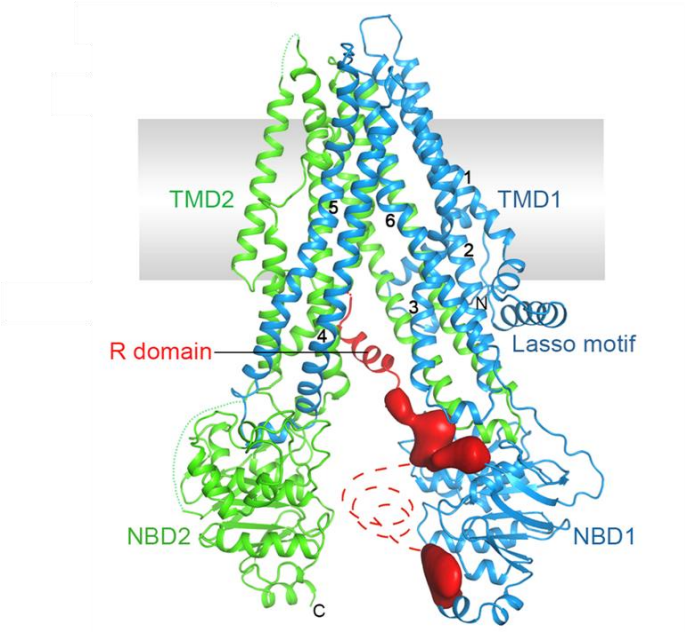

Fig 1.1 *Cryo-EM CFTR structure.*
Transmembrane domain 1 and 2 (TMD1, TMD2) are represented in green and blue (together with the respective nucleotide binding domains 1 and 2; NBD1, NBD2). The Lasso motive is in dark blue. The Regulatory domain (R domain) is in red. Reprinted from [9].

Whereas standard ABC transporters actively transport solutes by consuming ATP, CFTR

possesses the unique characteristic of using ATP hydrolysis to open the channel pore, through which ions flow only along their electrochemical gradient. Assembly of two MSDs forms the pore [12-14]. In patch clamp experiments the CFTR channel shows a small single-channel conductance (6-10 pS) with a linear current-voltage (I-V) relationship. In addition the channel displays a time and voltage-independent gating behavior, and an anion over cation selectivity. Its permeability sequence is $Br^- \geq Cl^- \geq I^-$, with a corresponding conductance sequence of $Cl \geq Br \geq I$ [15, 16].

There are currently 2027 known mutations of CFTR, 400 of which cause Cystic Fibrosis (www.genet.sickkids.on.ca). They are divided into seven classes, according to the mechanism by which they disrupt synthesis, trafficking, or function of CFTR (Table 1).

Class	Mutation type (s)	Examples
Class I: Lack of CFTR synthesis	Nonsense mutation, frameshift, deletions.	W1282X, R553X, G542X
Class II: Defective protein processing	Missense mutations and in frame deletions disrupt CFTR folding and trafficking	F508del, N1303K
Class III: Defective channel regulation or channel gating	Missense mutations resulting in aminoacid substitutions	G551D, G551S, G1349D
Class IV: Defective chloride conductance	Missense mutations resulting in changes to the CFTR pore region	R117H, R334W, R347P
Class V: Reduced amount of CFTR protein	Missense mutations resulting in alternative splicing that disrupt mRNA processing	2789+5G →A, A455E
Class VI: Increased turnover of CFTR channel at the cell surface	Various mutations resulting in unstable CFTR at the membrane	Rescued F508del, 120del23, N287Y
Class VII: "Unrescuable mutations"	Large deletions	CFTRdele2,3 (21 kb)

Table 1 *Classes of CFTR mutations, adapted from* [17].

The most common CF-associated mutation belongs to Class II. It is a phenylalanine deletion at residue 508, named F508del-CFTR, and is present in at least one allele in about 70% of all patients in Europe and North America [8]. CFTR bearing the F508del mutation is misfolded and does not progress through the normal biosynthetic pathway. Instead it is retained in the endoplasmatic reticulum (ER) by chaperone proteins (Hsp 70 [18], Hsp 90 [19], Hsp40 [20]) and undergoes premature degradation by the proteasome complex. The F508del-CFTR protein

shares similar biophysical properties with wild-type (wt)-CFTR: small single conductance (6-10pS), linear I-V relationship, selectivity for anions over cations, and equivalent permeability sequence [21]. However, the F508del mutation occurs at a critical interface, impairing the ATP-dependent CFTR gating [21,22]. Other common CF mutations, such as G542X (a Class I mutation, present in 5% of CF cases), affect production of the protein, while Class III mutations (e.g., G551D, found in 4%) lead to defective channel gating. The Class I mutations W1282X and R553X are each found in 2.5% of CF cases. R117H (Class IV) causes defective conductance and has a 1% incidence (http://www.genet.sickkids.on.ca/app).

Progress has been made with regard to symptomatic treatments and therapies that target the molecular defect of CF. Several therapies for CF are based on the use of pharmacological chaperones (correctors), designed to overcome defective trafficking of Class II mutants, combined with molecules that repair the gating defect that is associated with F508delCFTR and other mutants in classes III and IV (potentiators).

The identification and characterization of CFTR activators started in 2002 [23]. Verkman *et al*. screened 60,000 compounds to look for activators of wt-CFTR that would activate G551D-CFTR and F508del-CFTR. Out of 57 activators of wt-CFTR only three significantly activated G551D-CFTR, and a few more the F508del-CFTR. The same group screened 100,000 compounds [24] for potentiators to correct the defective F508del-CFTR gating. They were able to identify by high-throughput screening a collection of diverse small molecules (1000 compounds) with high affinity for F508del-CFTR. The search for compounds continued and eventually led to the discovery of VRT-532 and VRT-422/VRT-325. The former potentiates PKA-stimulated gating of defective F508del-CFTR, the latter corrects the trafficking defect of F508del-CFTR[25]. Vertex Pharmaceuticals screened over 228,000 compounds and identified VX-770 (Ivacaftor), a CFTR potentiator that enhances the activity of G551D-CFTR. Treatment of F508delCFTRcells with 1 µmol/l of VX-770 restored the channel activity to wt-CFTR levels [26]. In addition, CFBE with genotype F508del/G551D-CFTR incubated with VX-770 (10 µmol/l) increased airway surface liquid (ASL) volume and ciliary beat frequency (CBF) to levels about half of those of wt-CFTR [21]. VX-770 was the first potentiator that was tested in the clinic and it was approved by the US Food and Drug administration (FDA) in 2012. Ivacaftor is currently

used as a drug for patients (children ≥6 years) harboring the G551D mutation and was approved to treat 23 additional mutations[27]. Lumacaftor (VX-809), also developed by Vertex, is a CFTR corrector used in combination with Ivacaftor. It is marketed under the name Orkambi™ and used in patients homozygous for F508delCFTR[28, 29]. Despite great promises of these compounds, other studies showed controversial results. Veit *et al* demonstrated that chronic co-administration of Lumacaftor and Ivacaftor reduces biosynthesis of F508del-CFTR[30]. A study conducted by Cholon *et al* demonstrated that chronic treatment with Ivacaftor negatively affects the pharmacological correction of F508delCFTR by Lumacaftor and VX-661 [30]. Costs of these drugs are another major issue: Ivacaftor and Orkambi are rather expensive treatments, with costs ranging between 250.000 and 300.000 US$ per patient and year [31]. In 2018 the FDA approved Tezacaftor (VX-661), a corrector that aims to restore CFTR traffic to the membrane. It is sold in combination with Ivacaftor under the name Symdeko™ for patients having two copies of F508delCFTR [32]. A recent study identified three correctors (type I, II, and III) that individually exhibit only marginal effects, but in combination robustly restored expression and function of mutant CFTR [33]. These studies represent the proof of concept that compounds targeting distinct structural defects of CFTR can synergistically rescue mutant CFTR. In 2018 two new next generation correctors (VX-445 and VX-659) used in combination with Tezacaftor and Ivacaftor showed positive effects in CF patients who were heterozygous for the F508del-CFTR mutation and a minimal-function CFTR mutation (Phe508del–MF genotypes) or homozygous for the F508del-CFTR mutation (F508del–F508del genotype) [323,324].

Despite extensive research for suitable small molecules targeting mutant CFTR, there is still a need for treatments all CF patients would benefit from. For this reason the so-called ”mutation agnostic therapies”, whose aim it is to bypass the loss of the CFTR mediated Cl^- transport, are interesting. Along this line, alternative ion channels that may compensate for the lack of functional CFTR have long been proposed as a treatment in CF.

Alternative therapies for Cystic Fibrosis

Many ion channels and transporters are promising non-CFTR targets. Among which are

TMEM16A (also called Anoctamin 1) and possibly TMEM16F (Anoctamin 6), SLC9A3, SLC26A9 (Solute Carrier 9A3 and 26A9) and the Epithelial Sodium Channel ENaC. TMEM16A and TMEM16F are part of the Anoctamins protein family, and are both plasma membrane localized. TMEM16A is a Ca^{2+} activated Cl^- Channel (CaCC), present in many secretory epithelia, while the role of TMEM16F is somewhat controversial. In fact, TMEM16F is thought to be both an ion channel and phospholipid scramblase[34]. *SLC9A3* encodes for a sodium-proton exchanger. Its variant rs4957061 has been associated with lung decline and earlier onset age of *P.aeruginosa* infections[35] in children with CF. Interestingly SLC9A3 interacts with CFTR via a regulatory complex of NHERF2, Ezrin and PKA. Co-binding of CFTR and SLC9A3 to the PDZ domains of NHERF-2 lead to PKA mediated suppression of SLC9A3. Disruption of CFTR might lead to excessive SLC9A3 activity, and therefore acidification of the ASL [36]. Deletion of *SLC9A3* in a CF mouse model decreased the rate of intestinal obstruction and reverted the intestinal pathology [37]. SLC26A9 is a chloride-bicarbonate exchanger abundantly expressed in gastric epithelial cells. Variations of this protein are associated with diabetes mellitus [38] and meconium ileus [39]. In addition Slc26a9-null mice displayed impaired Cl^- gastric secretion [40]. ENaC is the essential channel for electrogenic Na^+ absorption in epithelial tissues[41]. Loss of CFTR has been linked to increased function of ENaC and therefore Na^+ hyperabsorption has been proposed as the main reason for CF lung disease[42]. In fact numerous findings supported the concept of Na^+ hyperabsorption[43-45] as a leading cause for CF lung and intestinal disease. Na^+ hyperabsorption causes airways dehydration, plugging with thickened mucus and impaired mucociliary clearance (MCC). Numerous groups, including ours, detected enhanced Na^+ conductance in nasal *ex vivo* tissue and nasal cells from CF patients[46]. However, this model was challenged by other studies, which did not provide evidence for Na^+ hyperabsorption in CF airways [47, 48].

In recent years the protons pump ATP12A that is expressed in airway epithelial cells, attracted attention. Several studies demonstrated that ATP12A mediates airway H^+ secretion. In normal conditions, H^+ secretion is counterbalanced by bicarbonate transport. This is unbalanced in CF. Proton accumulation causes acidification of the ASL, which compromises

local innate immune defense by ß-defensins, thereby favoring bacterial infections [49, 50]. Thus, inhibition of ATP12A might have a beneficial effect on CF airways.

Targeting alternative channels, transporters or pumps may be beneficial to all patients, regardless of their underlying CFTR-mutation. Activating alternative Cl^- channels may compensate for the lack of CFTR, and thus restore epithelial Cl^- secretion. Activation of CaCC was already tested in a clinical trial with Denofusol, a $P2Y_2$ agonist that stimulates Ca^{2+} activated chloride secretion. Despite the potential of this approach, the inhalation of Denofusol was unsuccessful in a phase III clinical trial. The likely reason for the negative outcome might be the limited half-life time of the compound in airways, which is only 17 minutes [51]. Direct activation of TMEM16A by small molecules has not yet been examined in patients. However, given the broad expression of TMEM16A in smooth muscle cells and its role in nociception, further studies are needed to clarify the consequences of activation of TMEM16A. In fact, stimulation of TMEM16A results in membrane depolarization causing muscular contraction and potentially bronchoconstriction[52]. During the experimental work on my PhD thesis, I focused on the role of TMEM16A and TMEM16F for Cl^- transport in the airways and other epithelial tissues. However, other members of the TMEM16 protein family have been shown to play a relevant role in cellular homeostasis. An overview, summarizing other TMEM16 proteins is given in Table 2 of Appendix I.

TMEM16A and TMEM16F

Epithelial and non-epithelial Ca^{2+} activated Cl^- channels (CaCC) are involved in many physiological processes such as electrolyte/fluid secretion, smooth muscle excitability, and olfactory perception. The molecular identity of these channels was unknown until 2008, when three independent groups identified TMEM16A as the Ca^{2+}-activated Cl^- channel[53-56]. TMEM16 proteins are a family of 10 transmembrane protein members (TMEM16A to TMEM16K) abundantly expressed in many cell types [57]. The first two members TMEM16A and TMEM16B function as Ca^{2+} activated chloride channels, while TMEM16C, D, G, J and in particular TMEM16F are phospholipid scramblases. Scramblases are proteins responsible for the translocation of phospholipids across the cell membrane. TMEM16A and TMEM16B are

voltage-dependent, small conductance (1-3 pS) chloride channels that are activated by an increase in intracellular Ca^{2+} above 150 nmol/l [58]. They produce time dependent currents with a strongly outwardly rectifying current-voltage (I-V) relationship. They are characterized by a permeability sequence of $I^- \geq Br^- \geq Cl^- \geq F$ with a similar conductivity for I^- and Cl^- [53]. Initial insights into the structure of these proteins were obtained from X-ray crystallography studies on the lipid scramblase of the fungus *Nectria haematococca* (nhTMEM16) in 2014 [59]. This study confirmed the homodimeric organization of TMEM16 proteins and identified ten membrane spanning helices rather than the to eight initially predicted. Most interestingly it recognized the presence of a dimer cavity (of unknown function) and of a subunit cavity (linked to Ca^{2+} activation) [59] (Fig 3).

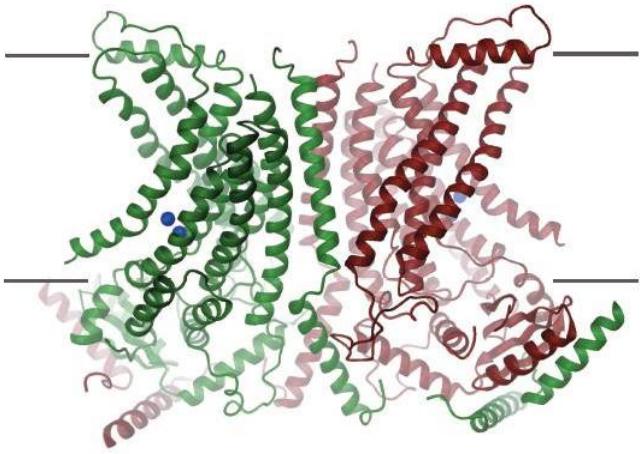

Fig 1. 2 *Ribbon representation of the nhTMEM16 dimer (green and red).*
The view is from within the membrane. Bound calcium ions are shown as blue spheres. Reprinted from [59].

Further studies in 2017 purified a murine Tmem16A in the absence and presence of Ca^{2+}, and determined the structure of the channel under both conditions by single-particle Cryo-Electron Microscopy (Cryo-EM) [60]. The study established the structure of the channel in both open and closed conformations, and proposed a mechanism of activation (Fig 4). The authors proved that the binding of Ca^{2+} alters the properties of the ion conduction path and triggers a rearrangement of the α-helix number six. The contact between the helix and the bound ligand causes the opening of the pore (Fig 1.3).

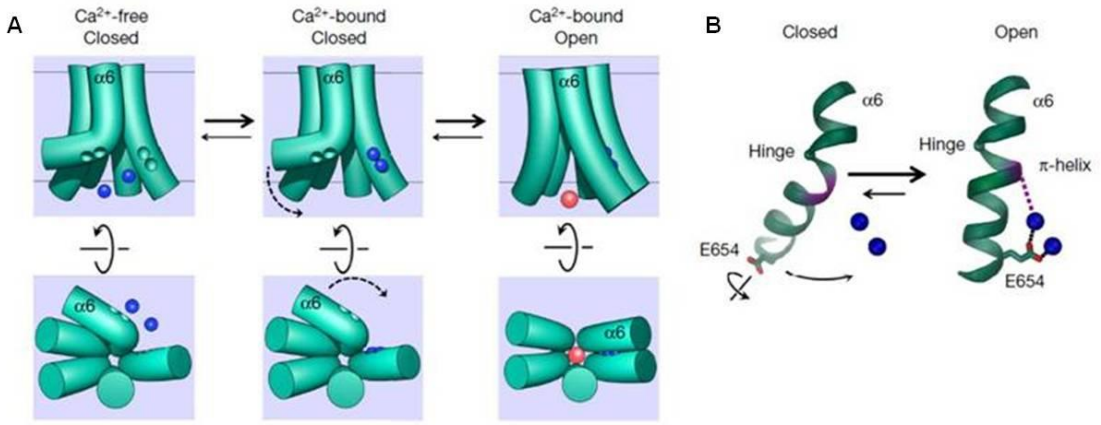

Fig 1. 3 *Cryo-EM model for mouse TMEM16A activation.*
A) Schematic representation of Tmem16a activation upon Ca^{2+} binding. Each transmembrane unit consists of ten membrane-spanning αhelices. In the closed state the α6 helix is in the relaxed state, leaving space for the binding of (presumably) two Ca^{2+} ions to four acidic residues on α7 and α8. B) Formation of a π-helix lead to the conformational change in α6 upon Ca^{2+} binding. Reprinted from[60].

TMEM16A is upregulated in various types of cancer such as head and neck squamous cell carcinoma (HNSCC) and colon cancer and is generally linked with cells hyperproliferation, migration, and apoptosis. TMEM16F is together with TMEM16A the most studied TMEM16 protein, although its physiological role remain controversial. It is highly expressed among various cells and tissues, and it has been endowed with both Ca^{2+} activated phospholipid scrambling activity [61] and with chloride [62] and cation [63] ion channel activity. TMEM16F is also activated during cell swelling [64]. Recent studies attributed a role of TMEM16F in mediating cell death through ROS-activation of the channel itself [65]. TMEM16F missense mutations have been reported in patients with the Scott syndrome, a rare congenital bleeding disorder caused by a defect in a platelet mechanism required for blood coagulation [61, 66].

TMEM16 proteins are an unusual family with dual functions. It is suggested that the phospholipid scrambling and the transmembrane ion flux could be mediated by the same pore. When TMEM16A and B were identifed as Ca^{2+} activated Cl^- channels [67, 68], it was expected that the remaining members of the family would have the same properties. However then TMEM16F was identified as a scramblase. The structural characterization of nhTMEM16, a TMEM16F homologue, from the fungus *Netria Hematococca,* revealed the presence of a hydrophilic enviroment required for phospholipid scrambling, but a separate

pore for ion transport could not be detected [60]. These results supported the hypothesis that phospholipid scrambling was the ancestral activity of TMEM16 proteins. Some members, namely TMEM16A and TMEM16B obviously have lost their ability to shuttle phospholipids between both membrane leaflets by narrowing the conductive pore, but maintaining the ability to conduct anions. In 2016 a study on the structure of a mouse Tmem16A (mTmem16A) unraveled how TMEM16 proteins use similar structures to accomplish different functions of Ca^{2+} activated Cl^- channel and phospholipid scrambles[69]. The authors claimed that the helices constituting the polar cavity in scramblases have changed their location in channels to form a protein-enclosed enviroment. To unravel this duality further functional studies are required. The localization of TMEM16 proteins within the plasma membrane is also of interest, as they seem to be localized in lipid rafts [70].

Membrane microdomains

The plasma membrane mediates exchange of metabolic material and biochemical signaling. Therefore, highly differentiated compartments are required. The plasma membrane is defined as a fluid mosaic [71], in which the lipid bilayer houses several components (transmembrane proteins, lipids) that can freely diffuse. The lipidic component can segregate in functionalized microdomains, also referred as lipid rafts [72]. Lipid rafts are believed to regulate signaling by providing concentrated microenvironments for lipid and protein components of signaling pathways [73]. These microdomains contain higher amounts of cholesterol (3 to 5 fold increase compared to the surrounding lipid bilayer), and are enriched in sphingomyelin. The hydrophobic residues contained in the lipids are more tightly packed and saturated than the rest of the membrane and interact with cholesterol in gluing and stabilizing the membrane [74]. Two kinds of lipid rafts have been described according to the presence of caveolin: caveolae and non caveolar or planar lipid rafts [75]. Caveolae can be invaginated or detached vesicles, and are mainly composed of cholesterol, sphingolipids and caveolin, while non-caveolar lipid rafts are composed of phospholipids [76].

Three different isoforms of Caveolin have been decribed: Caveolin 1, 2 and 3 (CAV1/2/3).

CAV1 and CAV2 are ubiquitously expressed while CAV3 is mostly expressed in skeletal and cardiac smooth muscles [77]. Membrane rafts have been reported to play a significant role in many biological processes, including signal transduction pathways, apoptosis, viral infections, cell adhesion and migration, synaptic transmission, organization of the cytoskeleton, and plasma membrane protein sorting during both exocytosis and endocytosis. For more than three decades lipid rafts have been proposed to influence the homeostasis of Ca^{2+} signaling. Recently the link between Ca^{2+} and lipid rafts has been further elucidated. A mechanism of Ca^{2+} entry via CAV1 has been proposed [78]. Evidence was provided that CAV1 containing lipid rafts may also contain TMEM16A and the proteins which are essential for the TMEM16A mediated Ca^{2+} activated chloride secretion [79]; namely $P2Y_2$ receptors, IP_3 receptors, GPCRs, and part of the ER [80].

Mucins and exocytosis

Mucus hypersecretion is a hallmark of chronic airway diseases such as asthma, chronic obstructive pulmonary disease (COPD), and Cystic Fibrosis. Goblet cell hyperplasia and persistent inflammation are characteristic pathologic features and the main causes of pulmonary complications and mortality in CF patients [81]. Under physiological conditions the mucus forms a barrier against bacteria, traps inhaled particles and prevents desiccation of the airways surfaces. Functioning as part of the innate immune system, mucus consists of a mixture of secreted polypeptides, water, ions and cellular debris [82], overlying the airway epithelial cells [83, 84]. In other epithelia such as the stomach and the colon, mucus is composed of two layers, an adherent layer secreted by goblet cells that is impermeable to bacteria, and a non-adherent layer formed by accumulation of mucins released from the adherent layer, which traps the bacteria [85, 86].

Mucins are the most abundant macromolecules present in mucus. They are heavily glycosylated proteins that can easily reach very high molecular weights and confer mucus its elastic and gel-forming properties. Mucins are mainly constituted of chains of oligosaccharids linked to a protein backbone and a high number of threonine/serine and proline rich tandem

repeats (TRs). The protein backbone of the mucins determines the class in which they belong [87] (Table 2).

Membrane tethered	MUC1, MUC3A, MUC3B, MUC4, MUC11, MUC12, MUC13, MUC16, MUC17, MUC20
Secreted cysteine rich	MUC2, MUC5AC, MUC5AB, MUC6, MUC19
Secreted non-cysteine rich	MUC7, MUC8, MUC9

Table 2 *Class of mucins, adapted from* [88].

In lung, the predominant mucins are MUC5AC (airway epithelium) and MUC5AB (in submucosal glands), while MUC2 is predominantly produced in the gastro intestinal tract [88]. Mucins are stored intracellularly in a highly condensed form and compacted in granules. In order to be properly unfolded the negative charges need to be shielded by positive ions, namely Ca^{2+} or H^{+} [89]. After being exocytosed the mucins virtually explode and expand within a couple of seconds to a volume that is up to three orders of magnitude larger than the condensed mucins. This process depends on HCO_3^-, which binds Ca^{2+} and H^+ and forms $CaHCO_3^-$, $CaCO_3$ and $H_2CO_3^-$, which ultimately will lead to the formation of water (H_2O) and carbon dioxide (CO_2). The negative core of mucins is then exposed and will force the compacted mucins into open-soluble and easily transportable strings [90, 91].

Exocytosis of mucin granules is a Ca^{2+} dependent event, following agonistic stimulation of $P2Y_2$ receptors (via ATP or UTP), A3 adenosine receptors or protease-activated receptors [92]. Unlike intestinal goblet cells [93], stimulation of CFTR by cAMP in the airways does not lead to mucin secretion [94]. Low stimulation of $P2Y_2$ and A3 adenosine receptors induce basal secretion of mucin by paracrine release of ATP and adenosine (constitutive exocytosis). On the contrary, high levels of these ligands as well as inflammatory mediators leads to massive secretion called compound exocytosis. Once the receptors are activated, a signaling cascade triggers the formation of diacylglycerol (DAG) and triphosphoinositol (IP_3) from phosphatidylinositol 4,5-bisphosphate (PIP2). IP_3 binds to the inositol trisphosphate receptor (IP_3R) and causes Ca^{2+} release from the ER. The Ca^{2+} represents the key signal to trigger exocytosis. It is involved in both the fusion of the secretory vesicles with the plasma

membrane [95] and in the maturation of the vesicles prior to fusion [96].

Myristoylated Alanine-Rich C Kinase Substrate (MARCKS) protein has been reported as one of the main players of exocytosis [97, 98]. It was shown that MARCKS binds to the mucin granules together with the Vesicle-associated membrane protein 8 (VAMP8) and the Cysteine String Protein (CSP), and that this interaction helps to position granules in place for secretion. The regulation of secretory granule (SG) exocytosis depends on the interaction of the GTPase Rab27 with the myosin V, which mediates the anchoring of the SG to the plasma membrane. After stimulation, the MARCKS protein mediates the recruitment of the SG to the actin cytoskeleton, and its successive transport to the periphery of the cell. Consecutively the SGs are tethered and docked to the plasma membrane in a process mediated by the soluble N-ethylmaleimide sensitive factor attachment receptor (SNARE) proteins that are present on secretory vesicles (v-SNAREs, such as VAMP) and their target membranes (t-SNAREs, such as Syntaxin and SNAP-25). The v- and t-SNAREs contain-helical domains that interact to form a tightly coiled four-helix bundle (the core complex) that brings together the opposing membrane [99-101]. However, this process requires the presence also of accessory components, such as the MUNC proteins. In particular MUNC18 and MUNC13 promote the interaction of the core complex and synthaxins [99]. Of note is the phenotype of Munc13-2 mice lacking a sensor of Ca^{2+} and DAG that displays accumulation of mucus in the goblet cells in the airways [102].

Inflammation and infection in Cystic Fibrosis

Colonization of the purulent material by opportunistic bacteria represents one of the hallmarks of Cystic Fibrosis. In fact, CF patients are particularly susceptible to infection with *Pseudomonas aeruginosa.* Hypotheses have been postulated to justify the frequent association of *P. aeruginosa* and CF lungs. One is that CFTR is also a specific receptor for internalization of the bacteria; therefore, loss of CFTR causes a reduction in the bacterial clearance from the airways [103]. Another is that CFTR, and in particular F508del-CFTR, influences the adherence of the bacteria to the epithelial cells [104]. The persistence of bacterial infection is associated with the evolution of the strain into a mucoid phenotype, which is

extremely hard to eradicate. The chronicity of the infection is the main trigger of the inflammatory state, characterized by neutrophil accumulation and IL-8 release. Neutrophil chemoattraction and degranulation is mediated by IL-8, IL-17 and macrophage derived cytokines. Neutrophil degranulation causes release of proteases such as MMP-9 (matrix metalloprotease 9) and elastase. The imbalance between protease production and antiprotease defenses leads to remodeling and structural weakening of the airways, and finally to bronchiectasis and bronchomalacia [105].

Infection is regarded as the main trigger of the inflammatory state. However, there is evidence pointing to an inflammatory response that is independent of infection. Adam *et al,* suggested that CFTR traffic defect causes ER stress and activation of the nuclear factor kappa-light-chain-enhancer of activated B cell (NF-$_K$B) [106]. Constant lung inflammation and progressive release of oxidants and enzymes cause epithelial surface damage and ultimately decline of the pulmonary function [3, 107]. The sequence of events at the onset of pulmonary infection and inflammation is still controversial and not yet fully characterized. Several studies have reported CF patients with normal lungs at birth [108]. In studies on newborn CF piglets no differences were observed between bronchoalveolar lavage (BAL) samples at 6h or 12h in terms of IL-8 release and leukocytes count [109]. However, cultured BAL of newborn CF piglet showed host-defense defects and impaired ability to eradicate bacteria. Several other studies reported neutrophil accumulation and elevated levels of IL-8 and elastase in bronchoalveolar lavage of CF compared to healthy controls [110]. To date the chicken-and-egg conundrum on whether inflammation or infection comes first in CF is still an open question.

Aim of the study

My research has focused on understanding the cellular functions and regulation of TMEM16A/F. Therefore, the role of TMEM16 proteins as modulators of intracellular Ca^{2+} signaling was investigated and is outlined in Chapter 2. The interaction between TMEM16A and CFTR, their regulation by Ca^{2+} and cAMP, and the mechanisms behind this crosstalk is described in Chapter 3 and is further expanded in Chapter 4. A novel concept that identifies TMEM16A as a major player in membrane exocytosis and the underlying molecular mechanisms are summarized in Chapter 5. Finally, in Chapter 6 a novel therapeutic strategy for the treatment of CF lung and intestinal disease is proposed, which is based on repurposing a FDA-approved drug for the inhibition of TMEM16A.

Chapter 2

Differential effects of anoctamins on intracellular calcium signals

Abstract

The Ca^{2+} activated Cl^- channel TMEM16A (Anoctamin 1 / ANO1) is homologous to yeast Ist2 and has been shown to tether the cortical endoplasmic reticulum (ER) to the plasma membrane. We therefore examined whether ANO1 and other members of the Anoctamin family affect intracellular Ca^{2+} signals. It is shown that expression of ANO1 augments Ca^{2+} store release upon stimulation of G-protein coupled receptors (GPCR), while knockdown of ANO1, or lack of Ano1 expression in $Ano1^{-/-}$ animals as shown in an earlier report, inhibits Ca^{2+} release. ANO 5, 6, 10 show similar effects, while expression of ANO4, 8, 9 attenuate filling of the ER store. The impact of ANO1 and ANO4 were examined in more detail. ANO1 colocalized and interacted with IP_3R, while ANO4 colocalized with SERCA Ca^{2+} pumps and interacted with ORAI1 channels, respectively. ANO1 chloride currents were rapidly activated exclusively through Ca^{2+} store release and remained untouched by influx of extracellular Ca^{2+}. In contrast expression of ANO4 caused a delayed activation of membrane localized ANO6 channels, solely through store operated Ca^{2+} entry (SOCE) via ORAI. Ca^{2+} signals were inhibited by knocking down expression of endogenous ANO1, 5, 6, 10, and were also reduced in epithelial cells from Ano10 null mice. The data suggest that anoctamins affect intracellular compartmentalized Ca^{2+} signals, which may explain some of the cellular defects related to Anoctamin mutations.

Keywords: TMEM16A, TMEM16D, TMEM16F, Anoctamin 1, Anoctamin 4, Anoctamin 6, Ca^{2+} signaling, Ca^{2+} store, store operated Ca^{2+} influx, SOCE, ORAI, SERCA

Published in: Inês Cabrita, **Roberta Benedetto**, Ana Fonseca, Podchanart Wanitchakool,

Lalida Sirianant, Boris V. Skryabin, Laura K Schenk, Hermann Pavenstädt, Rainer Schreiber, Karl Kunzelmann. Differential effects of anoctamins on intracellular calcium signals. *Faseb j*. 2017 May;31(5): 2123-2134.

Own experimental contribution: All patch clamping experiments.

Own written contribution: Methods, Results.

Other contributions: Designed experiments and analyzed data.

Introduction

Anoctamins form phospholipid scramblases and ion channels [61, 63, 111-114]. They are expressed and functional in all types of tissues and have a central role in many different diseases [112]. ANO1 is essential for chloride transport in epithelial tissues, controls smooth muscles contraction and arterial blood pressure and has various functions in neuronal and sensory cells [112, 115-118]. Many cellular functions of anoctamins, like effects on proliferation, tissue repair, bone mineralization and immunological processes are only poorly understood [119-124].

Recent studies suggest a role of anoctamins in controlling compartmentalized Ca^{2+} signals elicited by activation of G-protein coupled receptors (GPCRs): i) The yeast ANO1 homologue Ist2 tethers the endoplasmic reticulum (ER) to the plasma membrane, by means of anchoring in the ER membrane and binding of its polybasic C-terminus to the plasma membrane [125]. ii) In dorsal root ganglia, ANO1 has been shown to be activated exclusively by Ca^{2+} released from the ER. This is achieved by tethering of ANO1-containing plasma membrane to the ER membrane via ANO1/IP3R interaction [126]. iii) Mid-range Ca^{2+} signaling requires coupling between store-operated Ca^{2+} entry (SOCE) and IP3-dependent store release [127]. iv) Freshly isolated intestinal crypt cells from mice lacking Ano1 expression demonstrated abrogated GPCR-triggered Ca^{2+} signals [128]. v) Anoctamin-homologous transmembrane channel-like protein 8 (TMC8, EVER2) controls GPCR-induced intracellular Ca^{2+} signaling [129]. Here we identified a differential role of anoctamins in GPCR-induced Ca^{2+} signaling: They affect Ca^{2+} release via IP3R as well as the Ca^{2+} store content, possibly by operating as leakage channels or by controlling ORAI or the sarcoplasmic/endoplasmic reticulum Ca^{2+} ATPase (SERCA). These results may help to explain the ever-growing number of anoctamin-related cellular defects and diseases.

Materials and Methods

Animals, cells, cDNA, RT-PCR, siRNA. Generation of animals with a floxed Ano10 allele has been described in an earlier report[128]. Tissue specific renal tubular knockout was

achieved by crossbreeding ANO10$^{loxp/loxp}$ and Pax8Cre+ or Six2Cre+ mice. Offsprings were genotyped and tubular ANO10 knockout was verified by RT-PCR and Western blot analysis in isolated proximal tubular epithelial cells. All animal experiments were approved by the local ethics commission of the University of Regensburg and the University Münster and were conducted according to the guidelines of the American Physiological Society and the German law for welfare of animals. For isolation of renal proximal tubular epithelial cells, kidneys were removed and kept in ice cold PAN, PO4-41250 medium. Cortices were cut off, cells were isolated using collagenase type 2 (Worthington, S9H11286) and passed through a sieve. After washing, centrifugation and resuspension, cells were run though a percoll gradient (45% percoll, 55% 2X PBS-Glucose). Cells were resuspended in media and kept on ice until use. HEK293 were grown in DMEM-F12 (GIBCO, Karlsruhe, Germany) supplemented with 10% fetal bovine serum at 37°C in the absence of antibiotics in a humidified atmosphere with 5% CO2. HeLa cells were grown as described earlier. For expression of anoctamins, cells were plated on fibronectin- and collagen-coated 18 cm diameter coverslips and co-transfected with cDNA encoding either hTMEM16A, D, E, F, G, H, J, K, or empty pcDNA3.1 vector (mock) along with P2Y2 receptor and CD8. Transfected cells were detected by binding of anti-CD8 labeled beads. Construction of expression plasmids has been described earlier [130]. RT-PCR analyses were performed using standard conditions and appropriate primers as described earlier [130]. For semi-quantitative RT-PCR total RNA (1 µg) was isolated from HeLa, reverse-transcribed using a random primer and M-MLV reverse transcriptase (Promega, Mannheim, Germany). The RT-PCR reaction contained sense and antisense primers [130]. Knockdown of anoctamins by siRNA was reported in our previous study [131]. All experiments were performed 48h after the transfection.

Immunocytochemistry. Transfected HeLa cells were fixed for 10 minutes with 4% (w/v) PFA at RT. Bovine serum albumin (BSA) was added and left for 30 min at RT. Cells were incubated for 1 h with primary goat anti-GFP antibody (1:200; Rockland, Philadelphia, USA), rabbit anti-IP3R or mouse anti-SERCA (all 1:200; Abcam, UK) in PBS supplemented with 1% BSA at 4°C. Cells were washed three times with cold PBS and incubated with the secondary

antibody Alexa Fluor 488 conjugated Donkey Anti-Goat IgG (1:500; Molecular Probes, Invitrogen, Germany) and 0,1 µg/ml Hoechst 33342 (1:200; Aplichem, Darmstadt, Germany) for 1 h. Actin was labeled by Alexa Fluor 647-phalloidin (1:100; Molecular Probes, Invitrogen, Germany) and Fluor 555-conjugated donkey anti-rabbit IgG (1:500) or Alexa Fluor 546 conjugated donkey anti-mouse IgG (1:500; Molecular Probes). Cover slips were mounted with fluorescence mounting medium (DAKO Cytomation, Hamburg, Germany). For quantitative assays ANO1-GFP and ANO4-GFP transfected HeLa cells were fixed with 4% paraformaldehyde in PBS for 10 min, permeabilized with 0,1% Triton X-100 for 10 min at RT and incubated with primary antibodies goat anti-GFP, rabbit anti-human IP3 receptor (Abcam, UK), or mouse anti-SERCA (Abcam, UK) at 4°C overnight. Secondary antibodies were Alexa Fluor 488 goat anti rabbit IgG, Alexa Fluor 555 conjugated donkey anti- rabbit IgG or Alexa Fluor 546 conjugated donkey anti- mouse IgG (Molecular Probes, Invitrogen, Germany). Nuclei were counterstained with Hoechst 33342 (Sigma-Aldrich, Taufkirchen, Germany). Immunofluorescence was detected using an Axiovert 200 microscope equipped with an ApoTome and analyzed with the profile measurement tool of Carl Zeiss AxioVision software AxioVs40 V4.8.2.0 (Zeiss, Jena, Germany).

COIP and Western blotting. HeLa cells overexpressing ANO4-GFP or ANO1-GFP were collected using 1% CHAPs lysis buffer. 500 µg protein was incubated with antibody at 4°C for 1h by spinning on a rotator, followed by incubation with pre-cleaned protein G agarose (60 µl) at 4°C. Afterward, beads were centrifuged and washed three times with 1% CHAPs lysis buffer containing 1X proteinase inhibitor (Roche). Immune complexes were eluted by 2x sample buffer. IP samples were analyzed by Western blotting. Samples were separated by 8.5% and 12.5% SDS-PAGE and transferred onto PVDF membrane. Membrane was blocked with 5%NFM/TBS-T or 5%NFM/PBS-T for 1h at RT and incubated overnight at 4°C with rabbit anti-ORAI1 (1:1000 in 0.25% BSA/TBS-T), rabbit anti-IP3R (1:1000 in 1% BSA/TBS-T), rabbit anti-DOG1 (1:500 in 1% NFM/TBS-T) (Novus,USA), goat anti-GFP (1:1000 in 1% NFM/TBS-T), mouse anti-SERCa^2 (1:1000 in 0.25% BSA/TBS-T) and mouse anti-actin (1:750 in 5% NFM/PBS-T) (Santa Cruz, USA). The membrane was incubated with HRP-conjugated goat

anti-rabbit IgG (1:10,000 in 1% NFM/TBS-T) for 2 hrs, HRP-conjugated donkey anti-goat IgG (1:2,000 in 3% NFM/TBS-T) for 1 h and HRP-conjugated goat anti-mouse IgG (1:5,000 in 1% NFM/TBS-T or PBS-T) for 2 hrs at RT. Signals were detected using SuperSignal West Pico chemiluminescence substrate (Pierce, USA). Experiments were performed in triplicates.

Measurement of [Ca^{2+}]i: The plasma membrane bound calcium sensor GCAMP2 was modified by the addition of a N-terminal signal peptide (20 aa) from Neuromodulin (Pl-G-CaMP2 [132]). Addition of this peptide results in posttranslational palmitoylation of the protein, which facilitates anchoring of the protein to the plasma membrane [133]. HEK293 cells were transfected on coated glass cover slips with pcDNA31 Pl-G-CaMP2 and were mounted in a perfusion chamber 48h after transfection. ER Ca^{2+} signals were detected after expression of the Ca^{2+} sensor ER-LAR-GECO1. Cells were perfused with ringer solution at a rate of 8 ml/min at 37˚C. Cell fluorescence was measured continuously with an inverted microscope Axiovert S100 (Zeiss) using an x40 objective (Fluar 40x/1.3 Oil, Zeiss) and a high-speed polychromator system (VisiChrome, Visitron, Puchheim, Germany). Pl-G-CaMP2 was excited at 485 nm and 405 nm. Emission was recorded between 520 and 550 nm using a CCD-camera (CoolSnap HQ, Visitron). Control of experiments, imaging acquisition, and data analysis were done with the software package Meta-Fluor (Universal imaging, New York, USA). Alternatively, cells were loaded with Fura-2 and intracellular Ca^{2+} concentrations were determined as described earlier [134].

Patch Clamping. Cells were seeded and patch clamped on glass cover slips. If not indicated otherwise, patch pipettes were filled with a cytosolic-like solution containing (in mM): KCl 30, K-gluconate 95, NaH_2PO_4 1.2, Na_2HPO_4 4.8, EGTA 1, Ca-gluconate 0.758, MgCl2 1.03, D -glucose 5, ATP 3, pH 7.2. The Ca^{2+} activity was 0.1 µM. Cells were perfused with a bicarbonate free Ringer bath solution (in mM; NaCl 145, KH_2PO_4 0.4, K_2HPO_4 1.6, D-glucose 6, MgCl2 1, Ca-gluconate 1.3, pH 7.4). Coverslips were mounted in a perfused bath chamber on the stage of an inverted microscope (IM35, Zeiss) and kept at 37 °C. The bath was perfused continuously with Ringer solution at a rate of 8 ml/min. Patch clamp experiments were performed in the fast whole cell configuration. Patch pipettes had an input resistance of

2–4 MΩ when filled with the cytosolic like (physiological) solution. Currents were corrected for serial resistance. The access conductance was measured continuously and was 60–140 nS. Currents (voltage clamp) and voltages (current clamp) were recorded using a patch clamp amplifier (EPC 7, List Medical Electronics, Darmstadt, Germany), a LIH1600 interface and PULSE software (HEKA, Lambrecht, Germany) as well as Chart software (AD Instruments, Spechbach, Germany). Data were stored continuously on a computer hard disc and analyzed using PULSE software. In regular intervals, membrane voltage (Vc) was clamped in steps of 20 mV from -100 to +100 mV. Current density was calculated by dividing whole cell currents by cell capacitance.

Materials and statistical analysis. All compounds used were of highest available grade of purity and were from Sigma, Tocris Bioscience, or Merck. Mouse monoclonal anti- calreticulin and rabbit anti- actin were from Abcam and Sigma-Aldrich, respectively. Anti- ORAI1 was a generous gift from Prof. Dr. Veit Flockerzi (Institute for pharmacology, University of Saarlandes). Osmolarity of all solutions was measured using an osmometer. Data are reported as mean ± SEM. Student's t-test for unpaired samples or ANOVA were used for statistical analysis. A p-value < 0.05 was accepted as significant difference.

Results

Cl^- transport affects GPCR-controlled local Ca^{2+} increase.

The Ca^{2+} sensitive dye Fura-2 detects global Ca^{2+} signals throughout the cell. Activation of the purinergic receptors ($P2Y_2$) by ATP induced the typical intracellular Ca^{2+} peak and plateau increase, indicating a fast release of Ca^{2+} from the ER (peak), followed by Ca^{2+} influx through store operated Ca^{2+} influx channels (SOCE) (Fig 2.1A). Fura-2 detects both parts of receptor triggered Ca^{2+} signals, as it distributes more or less homogenously through the cytosol. In contrast, the Ca^{2+} sensor Pl-G-CaMP2 binds to the plasma membrane and detects preferentially Ca^{2+} signals in close proximity of the cell membrane. We found that Pl-G-CaMP2 detects Ca^{2+} release from IP3-sensitive ER stores (peak), but not Ca^{2+} influx (SOCE; plateau) (Fig 2.1A). Using GCAMP2 as Ca^{2+} monitor, we did not detect any Ca^{2+} rise in the ER store depletion protocol after adding CPA or after re-adding Ca^{2+} in the presence of CPA

(Fig 2.1B,C). Interestingly, a negative transient peak was detected by GCAMP2 upon re-addition of extracellular Ca^{2+} indicating a transient dip in the local Ca^{2+} concentration in close proximity to the store release site (IP3 receptor). This transient peak may somehow reflect refilling of the store, although the mechanisms remain currently obscure.

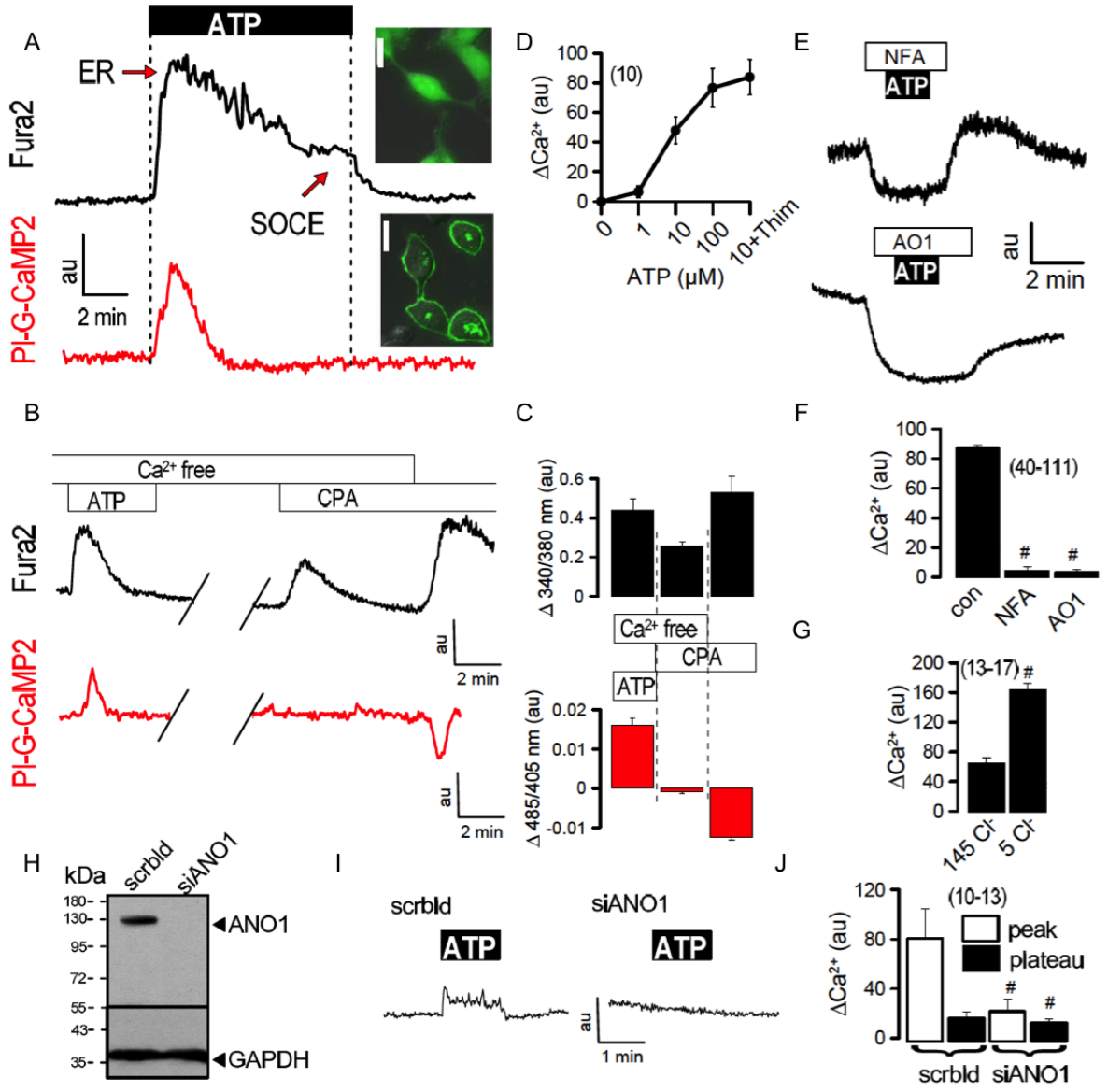

Fig 2.1 *Receptor-mediated increase in intracellular Ca^{2+} is Cl^- dependent.*
A) Increase in intracellular Ca^{2+} in HeLa cells by stimulation with ATP (100 µM) was detected by Fura-2 or by the membrane bound Ca^{2+} sensor PI-G-CaMP2, fused to a N-terminal signal peptide from neuromodulin. While Fura-2 detects Ca^{2+} release from ER (peak) and Ca^{2+} influx through store operated Ca^{2+} entry (SOCE; plateau), GCAMP2 detects only ER store release Ca^{2+}, indicating local separation of store release and Ca^{2+} influx. B, C) Ca^{2+} store release/depletion by stimulation with ATP (100 µM) and cyclopiazonic acid (CPA; 10 µM), as detected by Fura-2 (upper panels) or by PI-G-CAMP2 (lower panels). D) Concentration dependent increase in intracellular Ca^{2+} (arbitrary units; au) by ATP. Thimerosal (100 µM), a sensitizer of IP3 receptors was enclosed to detect maximal store

release. E,F) Anoctamin inhibitors Niflumic acid (NFA) and CaCCinhAO1 (AO1; both 20 µM) inhibited baseline Ca^{2+} and abolished ATP-induced Ca^{2+} release (ΔCa^{2+}). G) Summary of ATP-induce Ca^{2+} increase in the presence of physiological extracellular Cl^- concentration (145 mM) or low (5 mM) extracellular Cl^-. H) Western blot indicating knockdown of endogenous expression of ANO1 in CAL27 cells. I) ATP induced Ca^{2+} signal (measured by PI-G-CAMP2), which was abolished by knockdown of ANO1. J) Summary of Ca^{2+} peak and plateau induced by ATP in CAL27 cells. Mean ± SEM (number of cells). # significant inhibition by NFA and AO1, and augmented Ca^{2+} release in the presence of 5 Cl^- (ANOVA).

ANO1 is a membrane localized ion channel that probably accumulates in specific cholesterol-rich membrane compartments, called lipid rafts [79, 135]. As ANO1 is preferentially, if not exclusively, activated through ER store release [126], and because store release (but not SOCE) is picked up well by Pl-G-CaMP2, Pl-G-CaMP2 is probably colocalized together with ANO1 in a raft compartment that does not contain elements of the SOCE. Thus, there is a spatial separation between Ca^{2+} release and activation of ANO1, and SOCE influx pathways, as nicely demonstrated in an earlier report by Courjaret and Machaca [127]. In the present experiments maximal store release was achieved at 100 µM ATP (Fig 2.1D). Blockers of anoctamins such as NFA or AO1 strongly reduced baseline Ca^{2+} concentrations and completely abolished Ca^{2+} store release, suggesting a role of Cl^- transport through anoctamins for Ca^{2+} signaling (Fig 2.1E,F). Cl^- dependence was further supported by the finding that ATP-induced Ca^{2+} increase was augmented in the presence of a low (5 mM; $5Cl^-$) extracellular Cl^- concentration (Fig 2.1G). Possible artifacts of these inhibitors and of $5Cl^-$ on intracellular pH, fluorescence intensity or absorbance were excluded in control experiments. Moreover, both NFA and AO1 slightly hyperpolarized (11.2 ± 1.6 mV (n=13; NFA) and 12.2 ± 1.9 mV (n=9; AO1) the membrane voltage. Hyperpolarization of Vm is generally augmenting GPCR-mediated Ca^{2+} signaling, but in our experiments NFA and AO1 inhibited Ca^{2+} signaling, suggesting a role of Cl^- conductance for ATP induced Ca^{2+} transients. $5Cl^-$ depolarized Vm by 13.4 ± 1.8 mV (n=11). Depolarization of Vm is generally inhibitory on GPCR-mediated Ca^{2+} signaling [136]. However, in our experiments $5Cl^-$ augmented Ca^{2+} increase (Fig 2.1G), arguing against an artifact, but supporting the role of Cl^- / Cl^- conductance for ATP induced Ca^{2+} transients. We observed that siRNA-knockdown of endogenous expression of ANO1 in the

head and neck cancer cell line CAL27, inhibited GPCR-mediated Ca^{2+} increase (Fig 2.1G-J). We therefore examined in detail the impact of ANO1 and other anoctamins on intracellular Ca^{2+} signaling.

Anoctamins affect compartmentalized Ca^{2+} signals.

We analyzed if anoctamins affect compartmentalized Ca^{2+} signals triggered by GPCRs in HeLa cells. We found that expression of some anoctamins (ANO1, 5, 6, 10; green) augmented Ca^{2+} store release detected by Pl-G-CaMP2, while others (ANO4, 8, 9; red) largely reduced Ca^{2+} signals (Fig 2.2 A,B). ANO4, 6, 8, and 10 were found to be expressed endogenously in HeLa cells (not shown). When endogenous Ca^{2+}-enhancing ANO6 and ANO10 were knocked down by siRNA, ATP-induced Ca^{2+} signals were strongly attenuated (Fig 2.2 C). Effects of anoctamins on ATP-induced Ca^{2+} signals or ionomycin induced ER Ca^{2+} store depletion were only partially detected when Fura-2 was used as a global cytosolic Ca^{2+} sensor (data not shown). It appears unlikely that ANO1 affects hydrolysis of PIP2 and generation of IP3, when examining fluorescence changes during ATP stimulation of cells expressing GFP-tagged PLCδ1PH [137] (Supplementary Fig 2.2 A,B).

Immunofluorescence labeling of IP3 receptors (IP3R) and overexpressed ANO1 suggested colocalization of ANO1/IP3R in close proximity to the plasma membrane (Fig 2.2 D). In contrast SERCA colocalized with ANO4 in a cytosolic compartment, but did not co-localize with ANO1 (Fig 2.2 E,F). Colocalization of proteins is supported by scanning red (IP3R, SERCA) and green fluorescence (ANO1, ANO4) (Fig 2.2 D-F, lowest panels). Moreover, fluorescence labeling of the ER protein calreticulin suggested the presence of cortical ER close to ANO1, which is located in the plasma membrane, while most ANO4 localized to intracellular calreticulin (Supplementary Fig 2.1 C,D). Compounds known to deplete biological membranes of cholesterol and to disrupt lipid rafts like methyl-ß-cyclodextrin (MβCD) [138] or filipin [139], abolished the inhibitory effects of ANO4 on Ca^{2+} signaling (Supplementary Fig 2.1E). As ORAI1 was detected as the main isoform, ANO4 may be co-localized with ORAI1 in a raft population separate from the one containing ANO1.

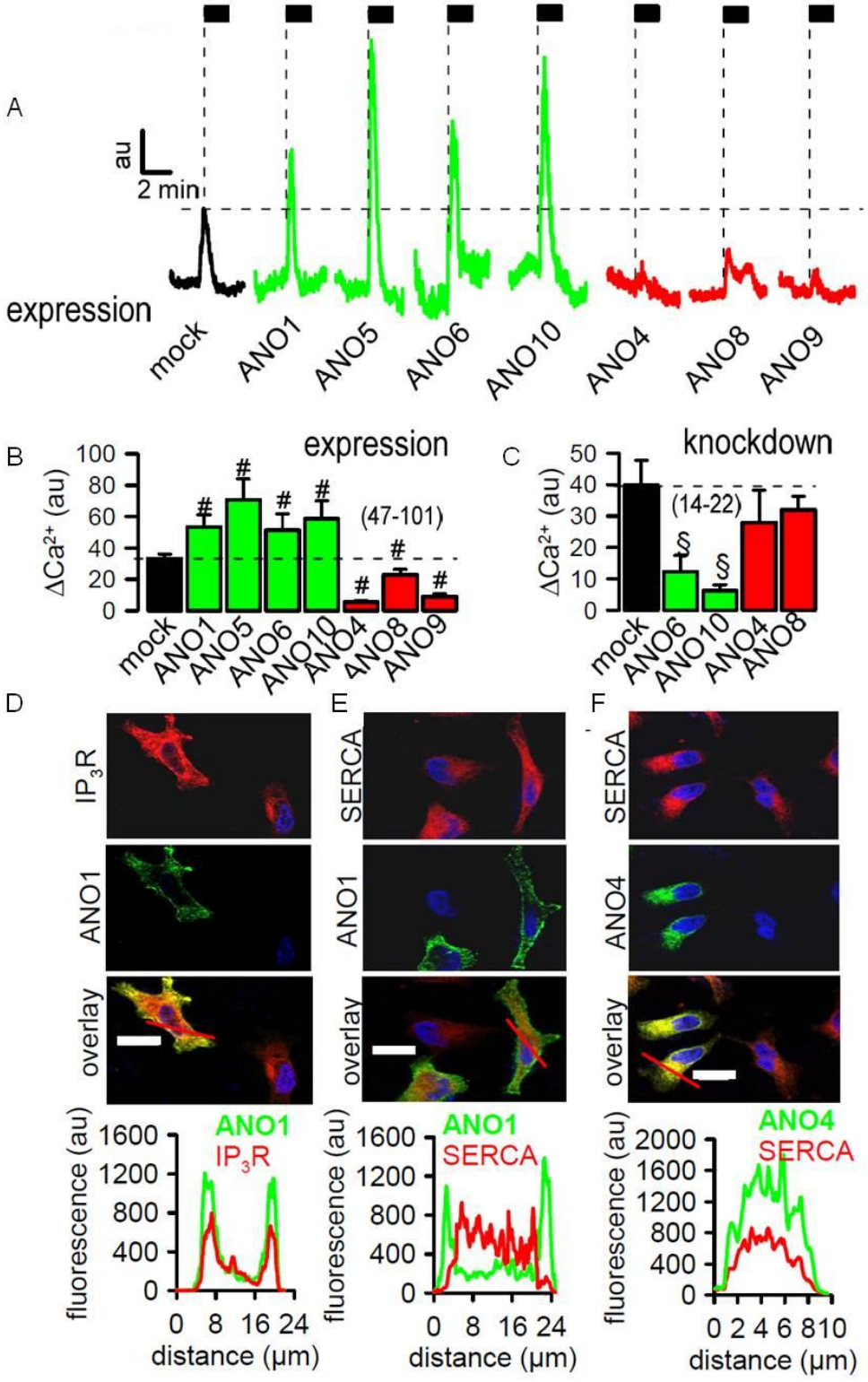

Fig 2. 2: *Anoctamins affect intracellular* Ca^{2+} *signals*.

A) Ca^{2+} store release detected by PI-G-CaMP2 fluorescence in HeLa cells overexpressing different anoctamins. B) Summary of ATP (100 µM) induced Ca^{2+} signals (arbitrary units; au) in the presence of different anoctamins, which augmented (ANO1, 5, 6,19; green) or reduced (ANO4, 8, 9; red) Ca^{2+} store

release. C) Summary of Ca^{2+} signals in cells treated with scrambled RNA or after knockdown of different endogenous anoctamins, which abolished (arbitrary units; au) enhancing (ANO6, ANO10) and inhibitory (ANO4, ANO8) effects of anoctamins on Ca^{2+} signals. Successful knockdown of anoctamins by siRNA is shown in Supplementary Fig 2.1F. D-F) Immunofluorescence of IP3 receptor, SERCA, ANO1 and ANO4 in HeLa cells (upper panels). Scanning of fluorescence intensities (arbitrary units, lowest panels) indicated colocalization of cortical IP3R (red) and ANO1 (green) close to the plasma membrane (D), but lack of colocalization of SERCA and ANO1 (F). ANO4 was found to be colocalized with SERCA (F). Mean ± SEM (number of cells). # significant increase (ANO1,5,6,10; green) and inhibition (ANO4,8,9; red) of Ca^{2+} signals by overexpression of anoctamins (ANOVA). § significant inhibition of Ca^{2+} signals and mRNA expression by siRNA-knockdown of anoctamins (ANOVA).

Differential interaction of ANO1 and ANO4 with IP_3R and ORAI.

ANO1 augmented but ANO4 strongly inhibited ATP-induced currents. While ANO1 is strictly plasma membrane localized, ANO4 is expressed intracellularly in an ER compartment. We therefore decided to examine the cellular functions of these anoctamins in more detail. Immunocytochemistry may suggest a differential molecular interaction of ANO1 with IP3R and ANO4 with ORAI or SERCA [126]. This assumption was supported by coimmunoprecipitation of ANO1 and IP3R in overexpressing HeLa cells (Fig 2.3 A). In contrast, SERCA (or ORAI; data not shown) could not be coimmunoprecipitated with ANO1 (Fig 2.3 B). Moreover, while ANO4 and ORAI coimmunoprecipitated (Fig 2.3 C), no evidence was found for an interaction of ANO4 with IP3R or ANO4 with SERCA (data not shown). This result indeed suggests a differential interaction of ANO1 and ANO4 with IP3R/ORAI and suggests that ANO1 and ANO4 may control different Ca^{2+} sources. ANO1 may be activated only by store release Ca^{2+}, but not by SOCE, while ANO4 is activated by SOCE, and not by store release. Remarkably, and in contrast to Fura-2, store release induced by CPA or Ca^{2+} influx through SOCE after re-adding extracellular Ca^{2+} was not at all detected by GCAMP2 targeted to the IP3R/ANO1 compartment (not shown). Thus the data strongly suggest that in mammalian cells Ca^{2+} pools (store release Ca^{2+} and SOCE) are spatially separated, as demonstrated recently in experiments in *Xenopus* oocytes [127] (Fig 2.5 G).

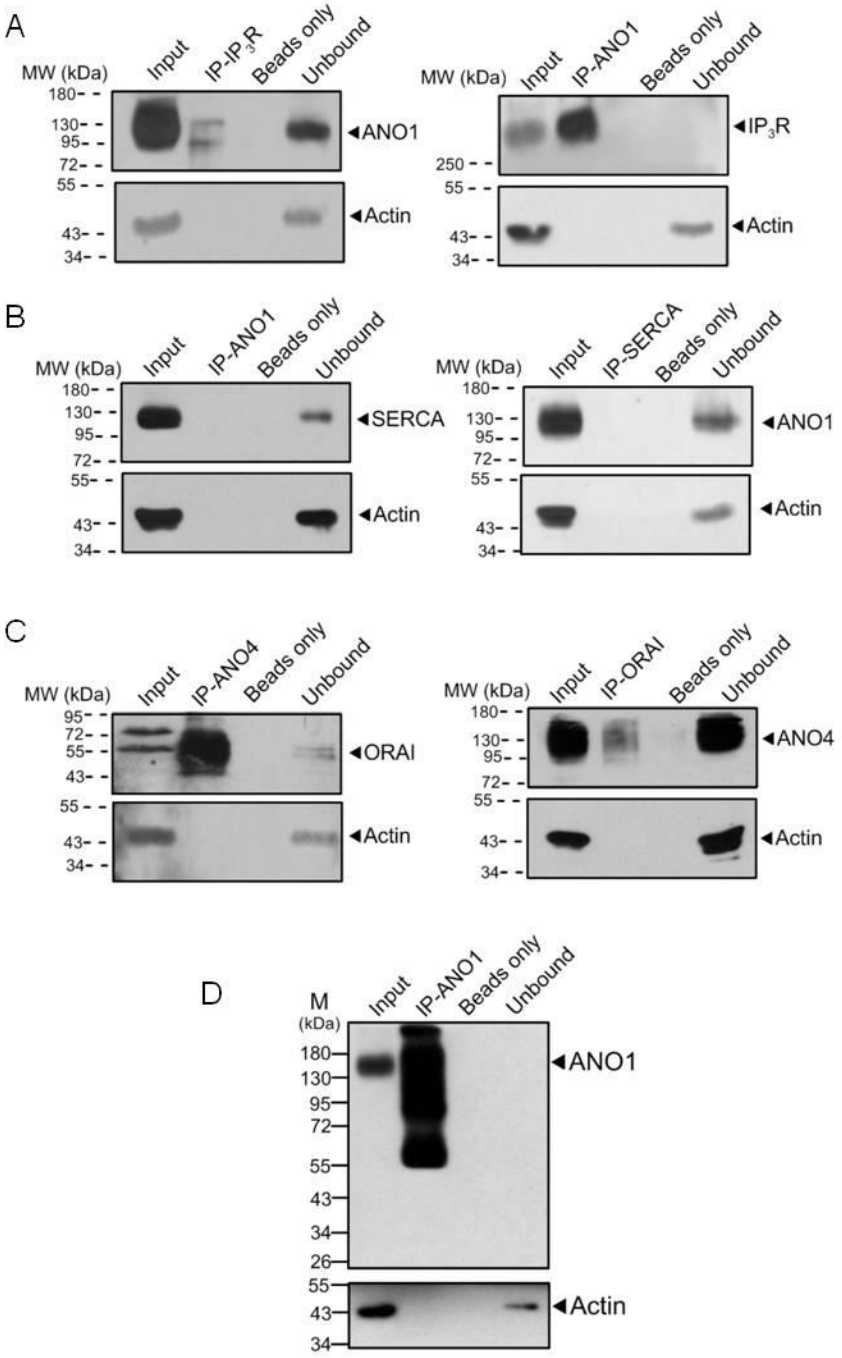

Fig 2.3 *Coimmunoprecipitation of ANO1 and ANO4 with IP3 receptor and SERCA in HeLa cells.*
A) ANO1 was coimmunoprecipitated with IP3R, while IP3R was pulled down with ANO1. B) Immunoprecipitation of ANO1 did not pull down SERCA, and no pull down of ANO4 was seen by immunoprecipitation of SERCA. C) ORAI was coimmunoprecipitated with ANO4, while immunoprecipitation of ORAI pulled down ANO4. D) Control experiment in which ANO1 was pulled down and the pulled down protein was detected by ANO1 Western blotting. Experiments were performed in triplicates.

We demonstrated earlier that ANO4, similar to ANO1, induces Ca^{2+} activated Cl^- currents when overexpressed in HEK293 cells [114]. Also in the present study we found that whole cell

currents were activated by ATP in ANO1 and in ANO4 expressing HEK293 cells, but not in mock transfected cells (Fig 2.4 A-D, I, J). Currents were strongly inhibited by removal of extracellular Cl^- indicating activation of Cl^- currents. Remarkably, ATP-induced Ca^{2+} increase activated ANO1 instantaneously (fast Ca^{2+} store release), while activation of ANO4 was slow (delayed SOCE). This suggests an exclusive crosstalk of store release Ca^{2+} and ANO1 (Fig 2.4 E). But how is it possible that expression of ANO4 leads to delayed-activated whole cell Cl^- currents although ANO4 is expressed in an intracellular compartment? It is known from earlier studies that ANO6 is expressed in the plasma membrane and produces delayed Ca^{2+} activated Cl^- currents [114, 140, 141]. ANO6 has also been shown to be activated through Ca^{2+} influx [140]. We therefore speculated that ANO4 may facilitate activation of ANO6 by emptying the ER store or by inhibiting filling of the ER store and thereby enhancing Ca^{2+} influx (SOCE), which activates ANO6. We examined mock transfected cells or ANO4-expressing cells without or with simultaneous siRNA-knockdown of endogenous ANO6. In mock transfected cells (no ANO4), ATP did not activate a current and simultaneous siRNA-knockdown of ANO6 had only a minor effect. In ANO4-overexpressing cells, a whole cell current was activated by ATP, which was largely suppressed by simultaneous knockdown of ANO6. The data indicate that expression of ANO4 (intracellular) induces an ATP-induced whole cell current that requires plasma membrane localized ANO6 (Supplementary Fig 2.5 D, F, G, H).

ANO6 is obviously activated by SOCE, while ANO1 is activated by IP3R-mediated Ca^{2+} release. In fact, removal of extracellular Ca^{2+} did not compromise activation of ANO1, but completely abolished activation of ANO6 (in ANO4 expressing cells) (Fig 2.4F). Vice versa, inhibition of IP3R with Xestospongin C [142] (IP_3R-inhibitor A in Fig 2.4G) or low molecular weight heparin (IP_3R-inhibitor B in Fig 2.4 G) [143] blocked activation of ANO1 but had no effect on ANO4-induced currents (Fig 2.4). Finally, inhibition of ORAI by YM8483 (ORAI-inh. A)[144] or GSK-7975A (ORAI-inh. B) [145] completely blocked ANO4 activation, without affecting ANO1. These results were validated by performing comparable experiments in HeLa cells, which produced essentially identical results (Supplementary Fig 2.2A-D). Taken together, these results strongly suggest differential coupling of ANO1 and ANO6 to IP3R and ORAI,

respectively (Fig 2.4).

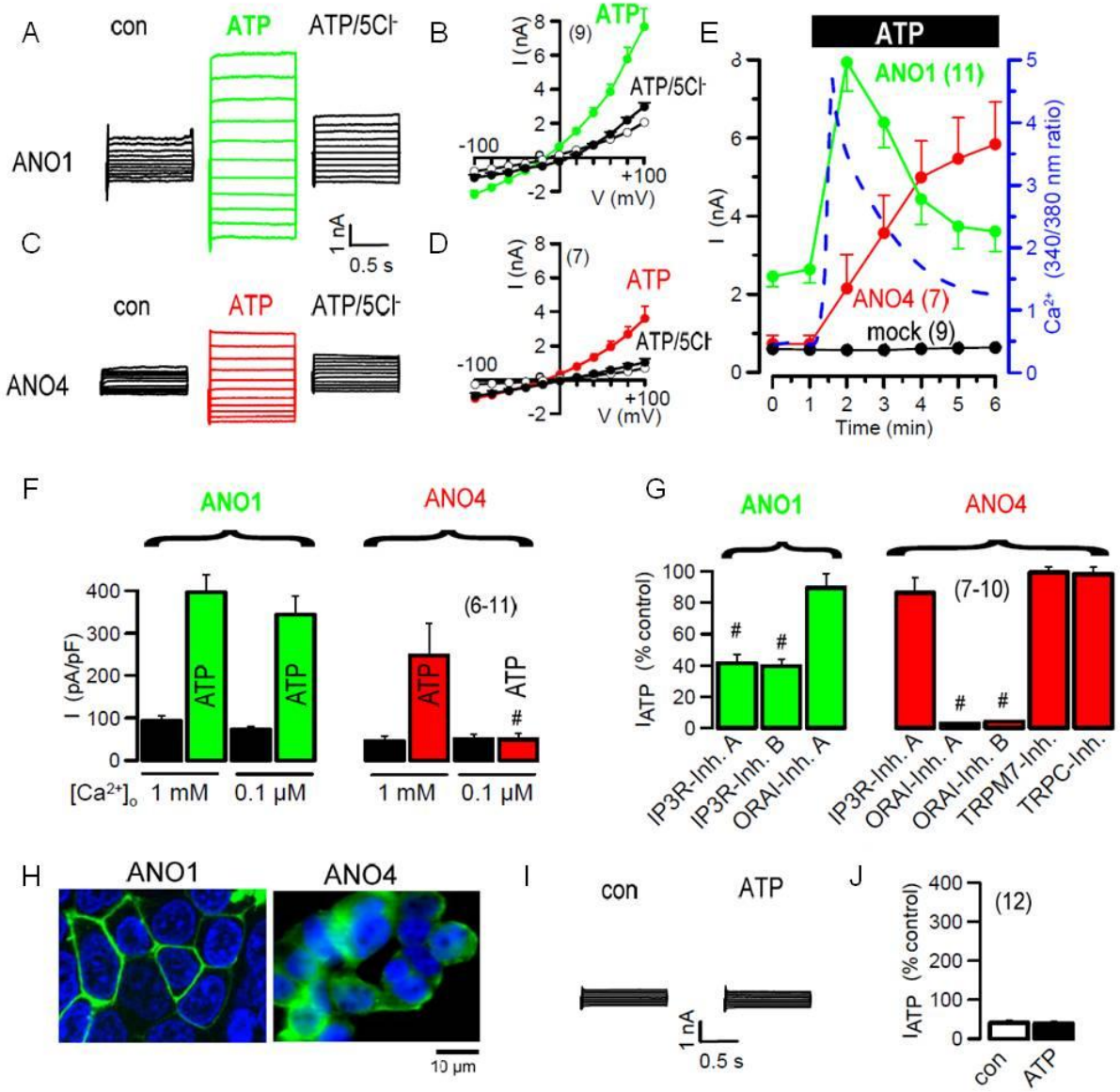

Fig 2.4 *ANO1 and ANO4 Cl^- currents are activated by different Ca^{2+} sources.*

A) Patch clamp recording of ATP (100 µM) activated whole cell currents in an ANO1-expressing HEK293 cells. Inhibition of currents by removal of extracellular Cl^- ($5Cl^-$). B) Corresponding current/voltage relationships. C) Patch clamp recording of ATP activated whole cell currents in an ANO4-expressing HEK293 cell. Inhibition of currents by removal of extracellular Cl^- ($5Cl^-$). D) Corresponding current/voltage relationships. E) Current activation during Ca^{2+} peak and plateau. Time course for ATP-activation of whole cell currents: Fast activation of ANO1, but delayed activation of ANO4. F) Activation of whole cell currents by ATP in ANO1 and ANO4 expressing cells, in the presence of high (1 mM) or low (0.1 µM) extracellular Ca^{2+} concentration. Activation of ANO4 requires influx of extracellular Ca^{2+} while activation of ANO1 is independent of the extracellular Ca^{2+} concentration. G) Effects of compounds inhibiting Ca^{2+} signaling and activation of ANO1 and ANO4. Activation of ANO1 is suppressed by inhibition of IP3R with xestospongin C (1 µM/30 min; IP3R-Inh. A) and low molecular

weight heparin (1 mM/30 min; IP3R-Inh. B), but not by the ORAI inhibitor YM8483 (5 µM; ORAI-Inh. A). In contrast activation of ANO6 (in ANO4-expressing cells) is abolished with YM8483 and GSK-7975A (5 µM; ORAI-Inh. B), but not by Xestospongin C. The TRPM7 inhibitor NS8593 (10 µM) and the TRPC inhibitor SKF-96365 (100 µM) had no effects on activation of ANO4. ORAI inhibitors, NS8593, and SKF-96365 were applied acutely, cells were pre-incubated with Xestospongin C and heparin for 10 min. H) Demonstration of expression of ANO1 (plasma membrane) and ANO4 (intracellular) in HEK293 cells. I, J) Control experiments in mock transfected cells. ATP did not activate any whole cell currents. Mean ± SEM (number of cells). # significant inhibition by low extracellular Ca^{2+} and inhibitors, respectively (unpaired t-test and ANOVA).

ANO4, 8, 9 probably lower filling of the ER Ca^{2+} store.

ATP-induced Ca^{2+} peaks and plateau were larger in ANO1-expressing cells, but were small and very transient in ANO4 expressing cells, which might be due to reduced store Ca^{2+} in ANO4 expressing cells (Supplementary Fig 2.2 E). In the presence of extracellular Ca^{2+} free solution, the SERCA inhibitor CPA emptied ER Ca^{2+} stores, leading to a transient Ca^{2+} increase. The results from this store release protocol suggested that expression of ANO4, 8 and 9 lowered Ca^{2+} store content, as Ca^{2+} release was small and quickly collapsing, while expression of ANO1, 5, 6 and 10 did not affect store content (Supplementary Fig 2.2 F, G). These results are supported by several additional Ca^{2+} store release protocols described above. Taken together, the results suggest that ANO1, 5, 6, and 10 facilitate local ER Ca^{2+} release in close proximity to the plasma membrane. In contrast ANO4, 8, and 9 seem to lower the Ca^{2+} store content. It is likely that localization of ANO4 (and maybe ANO8, 9) in the ER membrane leads to a Ca^{2+} leakage out of the ER, thereby reducing ER store content. In fact ANO4 (and other anoctamins) have been described as leaky Cl^- channels that are also permeable for cations such as Ca^{2+} [114, 146]. Remarkably, augmented ATP-induced Ca^{2+} signals in ANO1-expressing cells, and reduced ATP-induced Ca^{2+} signals in ANO4 or ANO9 expressing cells could also be monitored by expression of the Ca^{2+} activated K^+ channel hSK4 (KCNN4). ATP-activated hSK4 currents were strongly attenuated in cells expressing either ANO4 or ANO9, while expression of ANO1 augmented ATP-activation of hSK4 (Supplementary Fig 2.2 H-K).

Ca^{2+} signaling is attenuated in epithelial cells from $Ano10^{-/-}$ mice.

It appears essential to demonstrate the role of anoctamins for Ca^{2+} signaling also in original tissues. This has been shown already for Ano1 in intestinal epithelial cells from Ano1 knockout mice [128]. We found a pronounced inhibition of ATP induced Ca^{2+} signals after siRNA knockdown of endogenous ANO10 and, inversely, a strong augmentation of Ca^{2+} signals in ANO10 overexpressing cells (Fig 2.2). Moreover, our earlier study indicated a role of ANO10 for Ca^{2+} signaling also in macrophages [122]. We therefore further validated the effects of Ano10 on intracellular Ca^{2+} signaling by generating renal tubular specific Ano10 knockout mice (Fig 2.5 A, B). Ano10 was found to be localized in an intracellular compartment below the brush boarder membrane (Fig 2.5 C). This compartment is likely to correspond with the endoplasmic reticulum, as localization of ANO10 in the ER has been demonstrated earlier [122]. Proximal tubular epithelial cells were isolated from $Ano10^{+/+}$ and $Ano10^{-/-}$ mice, primary cultured and loaded with Fura-2. Cells were stimulated with ATP, which induced the typical peak/plateau response. In $Ano10^{-/-}$ cells, baseline Ca^{2+} as well as ATP-induced peak and plateau responses were attenuated (Fig 2.5 D-F). Despite the changes in Ca^{2+} signaling, we did not observe any overt phenotype in renal Ano10 null mice, and renal serum and urine parameters were not different to wt animals (Supplementary Figs. 2.3,2.4). However, we noticed an upregulation of ANO6 expression in tubular epithelial cells from Ano10 null mice, which could somehow compensate for the lack of ANO10 (Supplementary Fig 2.4 D).

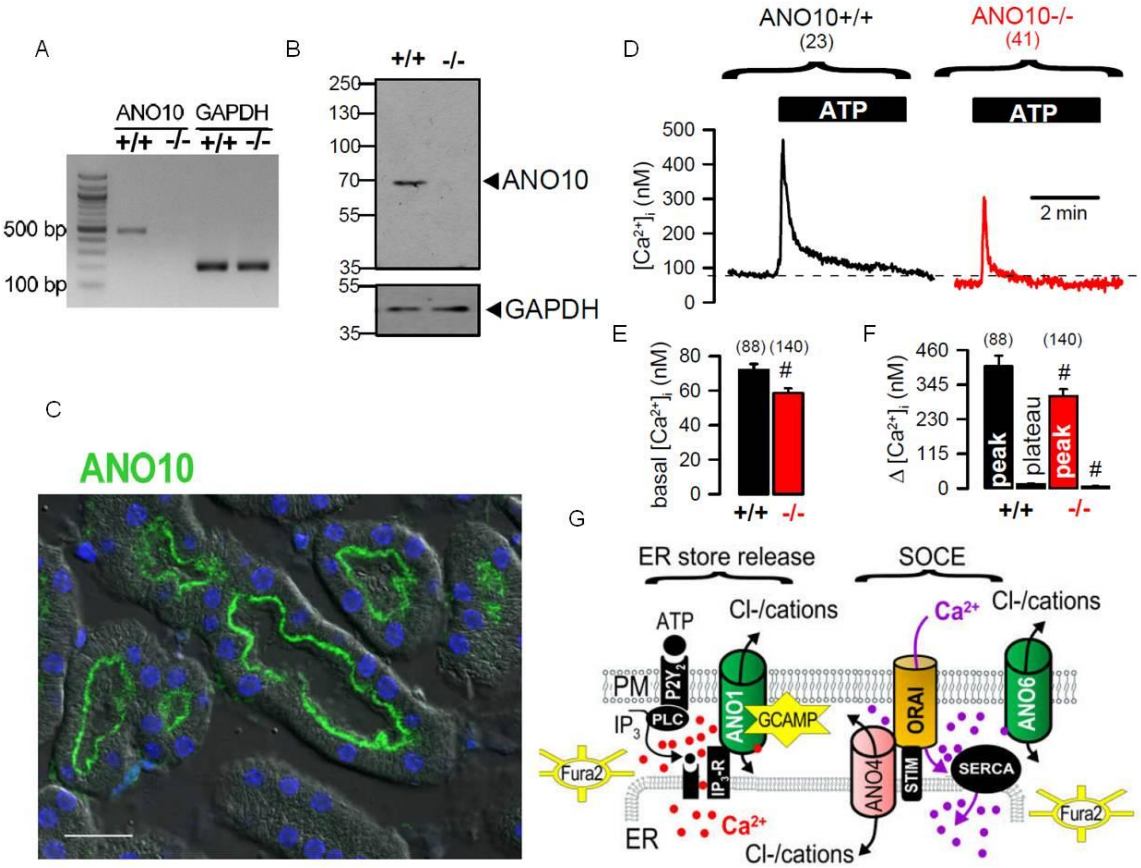

Fig 2.5 *Attenuated Ca^{2+} signals in isolated epithelial cells from Ano10$^{-/-}$ mice.*
RT-PCR A) and Western blotting B) demonstrating lack of expression of Ano10 in proximal tubular epithelial cells from ANO10$^{-/-}$ mice. C) Immunohistochemistry of Ano10 in proximal tubular epithelial cells. Ano10 is located underneath the brush boarder membrane in a cytosolic compartment. Bar indicates 50 µm. d) ATP (100 µM) induced Ca^{2+} increase measured by Fura-2 in mouse primary cultured proximal tubular epithelial cells. Summary traces showing reduced basal Ca^{2+} and attenuated ATP-induced Ca^{2+} peak and plateau in cells isolated from Ano10$^{-/-}$ mice. Summaries for basal Ca^{2+} E) and ATP-induced Ca^{2+} peak and plateau F) in cells from wt ($^{+/+}$) and Ano10 knockout ($^{-/-}$) mice. # significantly reduced Ca^{2+} plateau and Ca^{2+} increase in Ano10 knockout cells (unpaired t-test). Mean ± SEM (number of cells). G) Model for the differential effects of ANO1 and ANO4 on receptor operated Ca^{2+} signaling. Two well-separated cytosolic Ca^{2+} pools exist in mammalian cells, caused by store release (red dots) and Ca^{2+} entry (violet dots). Plasma membrane localized ANO1 tethers ER Ca^{2+} stores to raft compartments and augments compartmentalized Ca^{2+} signals and activation of ANO1 (or other Ca^{2+} dependent channels such as SK4). This compartment also contains the Ca^{2+} sensor PI-G-CaMP2. ER-localized ANO4 possibly operates as a Ca^{2+} leakage channel, thereby reducing Ca^{2+} store filling which activates/augments ORAI-mediated Ca^{2+} influx. Ca^{2+} entry activates ANO6 whole cell currents. This compartment does not contain the Ca^{2+} sensor PI-G-CaMP2. Fura-2 detects global Ca^{2+} signals throughout the cell.

Discussion

TMEM16A/ANO1 has been reported as a protein that confers receptor-activated calcium-dependent chloride conductance [113]. In their paper the authors showed data indicating that ANO1 is much more activated through phospholipase C coupled GPCRs than through direct large Ca^{2+} rises induced by Ca^{2+} ionophores [113]. These results suggest a cellular compartment containing GPCR, ANO1, and components of intracellular Ca^{2+} signaling that allow efficient activation of ANO1. Notably, an inhibitory role of PIP2 on TMEM16A encoded calcium-activated chloride channels has been demonstrated in rat pulmonary artery, which further substantiates the functional coupling of Ano1 to GPCRs [147]. This functional coupling leads to augmented Ca^{2+} store release via IP3R. Apart from the ER-store/plasma membrane tethering function the present data also suggest that chloride transport through ANO1 is crucial for this effect, as suggested by the use of ANO1 inhibitors. Although currently unclear, Cl^- exit and change of local submembranous Cl^- concentrations may determinate store release. As an alternative ANO1 may be partially located in the ER where it may function as a counter ion channel, facilitating electroneutrality during Ca^{2+} exit [148]. Clearly more work will be required to fully understand the effects of ANO1 on Ca^{2+} signaling.

Subsequent reports supported the existence of such functional compartments in *Xenopus* oocytes as well as dorsal root ganglia [126, 127, 149]. These signaling compartments are essential for efficient activation of ANO1, and may allow local Ca^{2+} concentrations that are much higher than global cytosolic Ca^{2+} levels detected by standard (Fura-2) fluorescence techniques [79]. Tethering of the ER to the plasma membrane by means of ANO1/IP3R interactions is therefore an essential mechanism to concentrate Ca^{2+} signals at the plasma membrane. ER tethering has also been well described for the yeast ANO1 homologue Ist2 [150]. In contrast to ANO1, the present data support the concept that ANO6 (through expression of ANO4, which lowers ER Ca^{2+} and thereby facilitates capacitive Ca^{2+} entry) is activated by SOCE through ORAI and maybe other Ca^{2+} influx channels [140] (Fig 1 G). Moreover, earlier studies showed that ANO6 is only weakly activated through GPCRs, but strongly activated by ionomycin [114].

In intact cells ANO1 requires Ca^{2+} concentrations in the higher µmolar range to be fully activated, because the negative membrane voltage interferes with binding of Ca^{2+} to the

channel [79]. These signaling compartments appear to be well shielded, as Ca^{2+} influx through voltage gated Ca^{2+} channels or store operated channels does not reach these compartments and therefore does not activate ANO1 [126]. The present results directly demonstrate the role of ANO1 (and ANO5, 6, 10) for GPCR-activated local Ca^{2+} signaling and suggested a different role for ANO4, 8, 9. ANO4, 8, 9 lower ER store Ca^{2+}, possibly as Cl^- bypass channels to allow Ca^{2+} leakage out of the ER or by operating directly as ER Ca^{2+} leakage channels, thereby activating Ca^{2+} influx and thus activation of plasma membrane localized Ca^{2+} sensitive Cl^- channels (ANO6) or K^+ channels (SK4) (Figs. S2.1F, S2.2, 2.4). Cytosolic Ca^{2+} increase by ATP, CPA or ionomycin-induced ER-store release was reduced in ANO4 expressing cells, while store filling was attenuated when measured by the ER Ca^{2+} sensor ER-LAR-GECO1, pointing to store depletion by ANO4 (and ANO8, 9) (data not shown).

The physiological role of ANO1 Cl^- currents in the context of Ca^{2+} signaling has been demonstrated in small nociceptive neurons from rat dorsal root ganglia [151]. Stimulation by the pain-inducing hormone bradykinin activates ANO1, which depolarizes the membrane voltage thus increasing firing of action potentials. In airway and intestinal smooth muscles, ANO1 maintains baseline contraction, muscle tone and coordinated intestinal contraction by very similar mechanisms [152-155]. Inhibitors of ANO1 lower airway smooth muscle tone and intracellular calcium, which has a large therapeutic potential in asthma. Pharmacological modulation of ANO1 changes contractile activity and intestinal fluid secretion [68, 156]. A functional interaction has been demonstrated between ANO1 and TRPV4 in epithelial cells from the choroid plexus [157]. The microdomains in which Ano1 functionally interacts with Ca^{2+} channels and transporters may be therefore cell specific. E.g., in intestinal epithelial cells ANO1 is predominantly in the basolateral membrane, while in renal proximal tubule, pancreatic and salivary gland acini or in airway epithelial cells, ANO1 is resides in the apical membrane. Finally, regulation of ANO1 by store operated Ca^{2+} entry in eccrine sweat glands was reported recently [158]. Thus ANO1 may couple to different Ca^{2+} transporting proteins in a tissue specific manner. Notably, attenuated agonist-induced Ca^{2+} signaling has also been demonstrated recently in large intestine of $ANO10^{-/-}$ mice [159].

Notably, in intestinal epithelial cells where ANO1 is expressed on the basolateral side of the epithelium, it augments Ca^{2+} signals that activate Ca^{2+} sensitive hSK4 K^+ channels [128]. These K^+ channels maintain a negative membrane voltage that is required to drive Cl^- secretion at the apical side of the epithelium. Thus ANO1 supports Cl^- secretion not as a secretory Cl^- channel, but indirectly by activating K^+ channels. In airway epithelial cells ANO1 may have a similar role by facilitating Ca^{2+} signals in close proximity of the Cystic Fibrosis transmembrane conductance regulator (CFTR) Cl^- channel[160]. CFTR is known as protein kinase A and ATP regulated Cl^- channel, but it requires also Ca^{2+} dependent kinases to be fully activated [161]. In fact, most of the apparent Ca^{2+} activated Cl^- secretion may actually occur through CFTR [162]. Thus anoctamins control physiological functions through compartmentalized Ca^{2+} signaling, which may explain their role in many cellular functions and diseases [160] (Fig 2.5 G).

Acknowledgements

Supported by DFG SFB699-A7/A12, DFG KU756/12-1, and Cystic Fibrosis Trust SRC 003, INOVCF. The excellent technical assistance by Mss. B. Wild, P. Seeberger, and E. Tartler is gratefully acknowledged.

Supplementary material

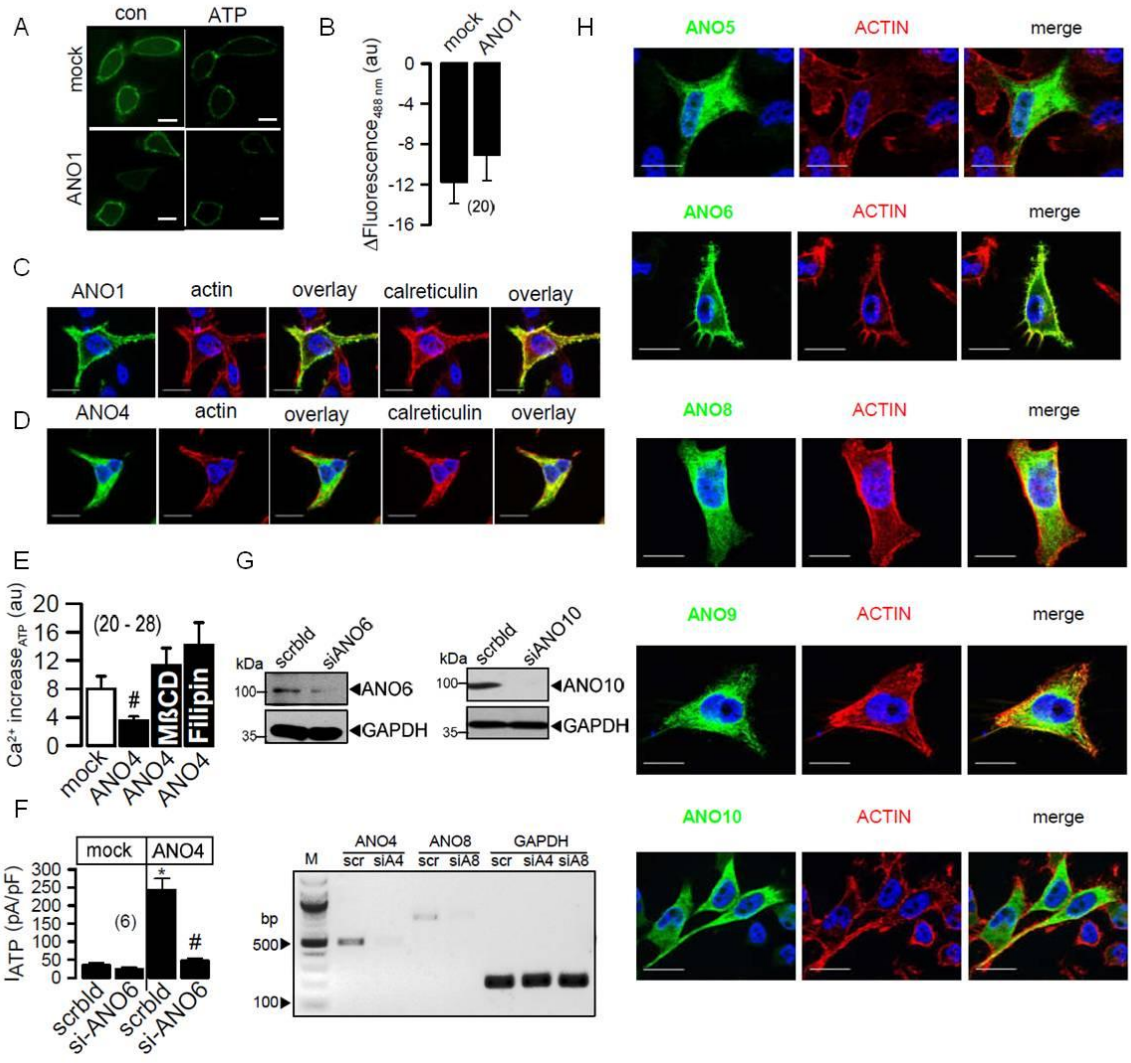

Supplementary Figure 2.1 *Role of ANO1, ANO4, and ANO6 for Ca^{2+} signaling and whole cell currents.*

A) HeLa cells expressing PLCδ1PH-GFP to monitor PIP2 hydrolysis by stimulation with ATP (100 µM, 20 min) in the absence or presence of ANO1. ATP reduced membrane binding of PLCδ1PH-GFP and thus decreased membrane GFP fluorescence by ATP-induced PIP2 hydrolysis. Typical examples out of 20 measured cells are shown. Bar indicates 10 µm. B) Decrease in membrane fluorescence was comparable in mock transfected and ANO1 expressing cells. C) Predominant membrane expression of ANO1-GFP in HeLa cells and colocalization with cortical actin. D) Predominant intracellular expression of ANO4. The endoplasmic reticulum (ER) is demonstrated using the ER marker calreticulin. Bars indicate 10 µm. E) HeLa cells were incubated with 1 mM methyl-ß-cyclodextrin (MβCD) at 37 °C/2-4 hrs to remove cholesterol from the plasma membrane, or treated with the membrane disrupter filipin (37 °C/30') to dissolve lipid rafts. Summary of the ATP induced Ca^{2+} increase in mock transfected control cells, and ANO4 expressing cells in the absence or presence of MβCD or Filipin. The results suggest that the inhibitory effect of ANO4 on Ca^{2+} signaling requires intact rafts. F) Whole cell currents in ANO4 expressing cells are due to activation of endogenous ANO6. Activation of whole cell currents

by ATP (100 µM) in ANO4 expressing cells was almost abolished by simultaneous siRNA knockdown of endogenous ANO6. No currents were activated in the absence of ANO4. G) Western blots indicating knockdown of ANO6 and ANO10 by siRNA. For ANO4 and ANO8 knockdown is shown by quantitative RT-PCR, which was 80.1% ± 7.9 % (n = 8, siANO4) and 74.1 ± 5.3 % (n = 6, siANO8). H) Expression of GFP-tagged ANO5, 6, 8, 9, and 10 in Hela cells. Bars indicate 10 µm. Mean ± SEM (number of cells). $^{\#}$ significant inhibition by ANO4 or siANO6 (ANOVA). * significant increase by ATP (paired t-test).

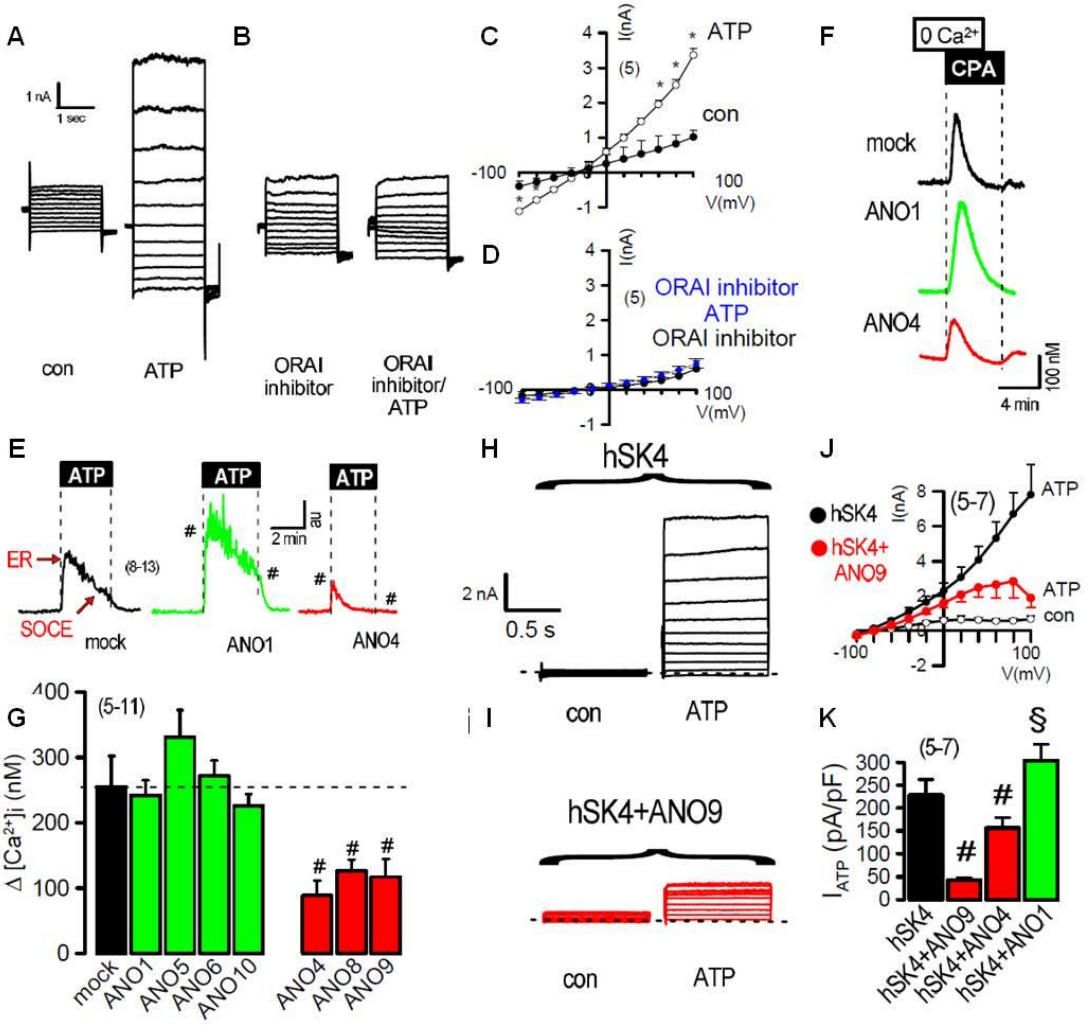

Supplementary Figure 2.2 *Anoctamins control activation of ion channels through regulation of* Ca^{2+} *levels.*

A) Whole cell currents activated by ATP (100 µM) in ANO4 expressing HeLa cells. B) Complete suppression of activation of whole cell currents by the ORAI inhibitor YM8483 (5 µM). C,D) Summary current / voltage relationships of the experiments shown in a,b. E) ATP (100 µM) induced Ca^{2+} increase measured by Fura-2. Summary recordings for Ca^{2+} store release (ER) and store operated Ca^{2+} entry (SOCE) indicate an increase by ANO1 but decrease by ANO4. F) Ca^{2+} stores emptying by inhibition of SERCA with cyclopiazonic acid (CPA; 10 µM) in the presence of Ca^{2+} free extracellular buffer. G) Ca^{2+} store content was not affected by overexpression of ANO1, 5, 6, 10, but was significantly reduced by overexpression of ANO4, 8, 9. H,I) Whole cell patch clamp currents in HeLa cells overexpressing hSK4 or coexpressing hSK4 with ANO9. Activation of hSK4 by ATP was much reduced in the presence of ANO9. J) Current voltage relationships indicate reduced activation of hSK4 in cells coexpressing ANO9. K) Current densities indicating inhibition or amplification of Ba^{2+} sensitive ATP-activated currents, by coexpression of ANO9/ANO4 or ANO1, respectively. Mean ± SEM (number of cells). * significant activation ATP (paired t-test). # significantly different from mock and hSK4 (ANOVA).

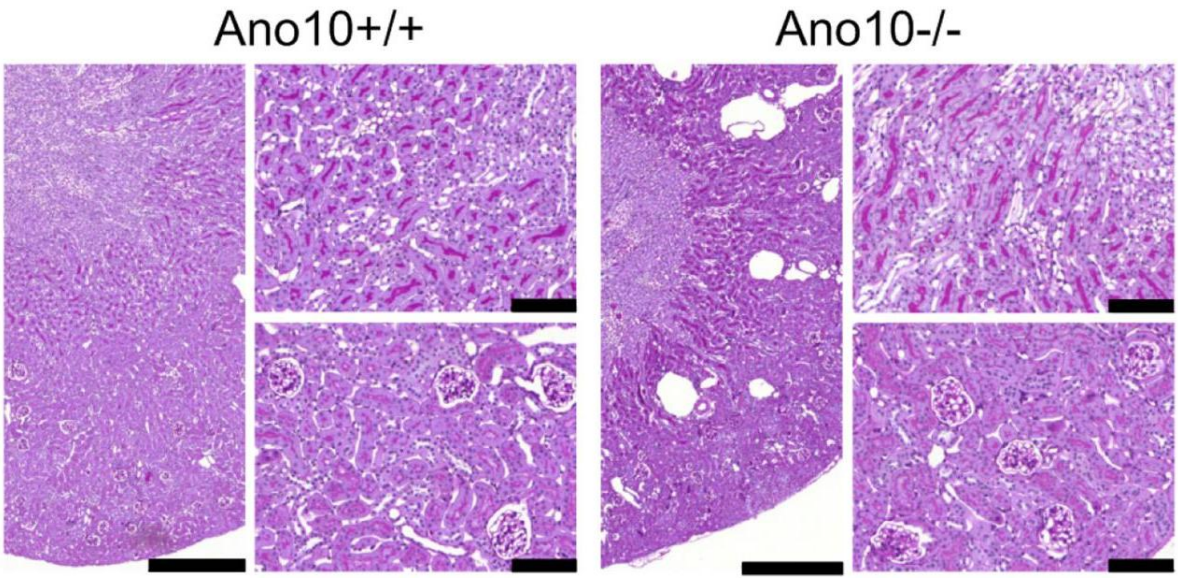

Supplementary Figure 2.3 *Representative periodic acid-Schiff stainings of kidneys from Ano10$^{+/+}$ and Ano10$^{-/-}$ animals.*

Scale bars indicating 500 µm in overview and 100 µm in detailed view. Mean ± SEM (n = 8-9).

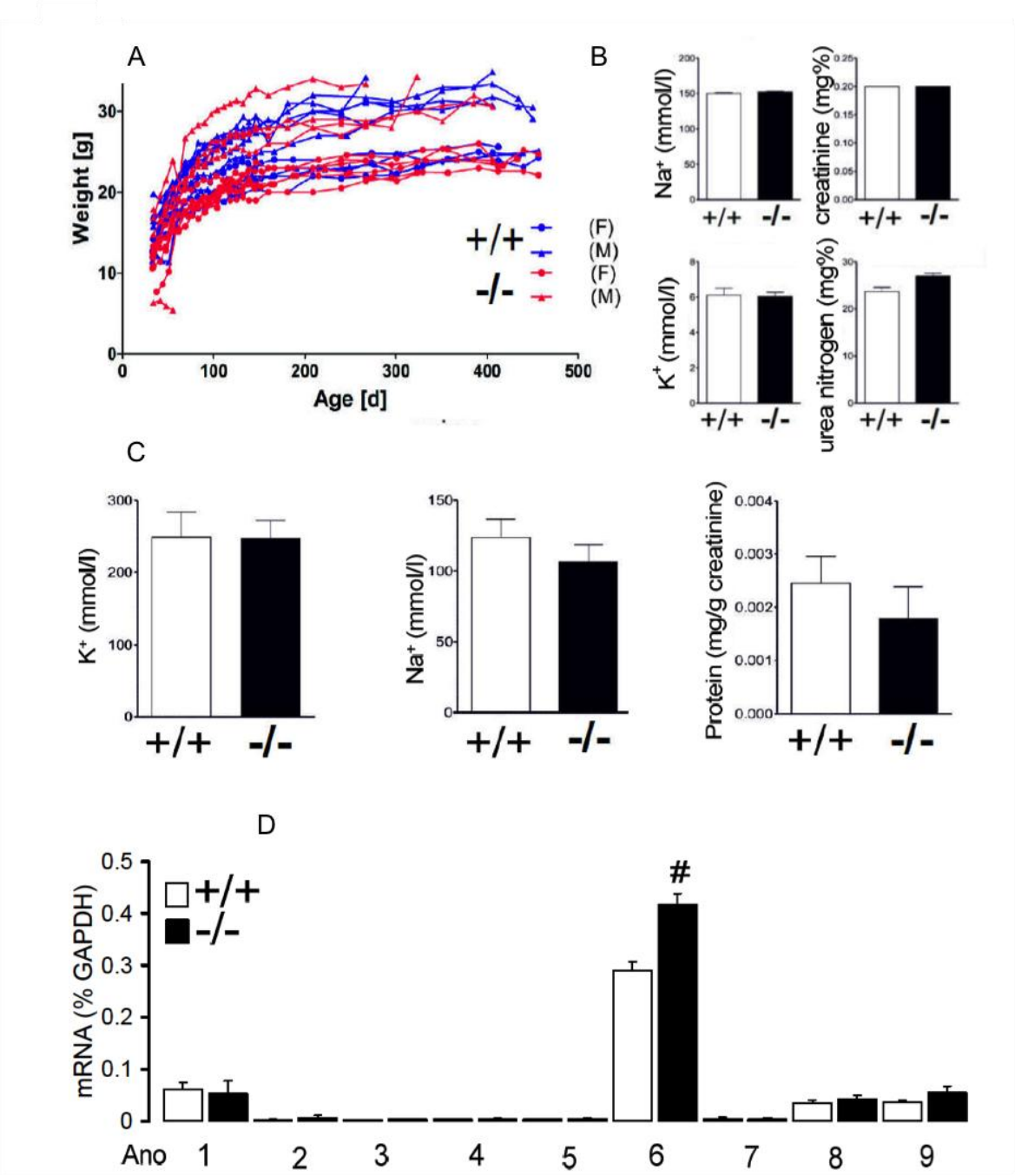

Supplementary Figure 2.4 *Phenotypic characterization of mice with renal tubular specific Ano10 knockout.*

Nephron-specific knockout was achieved by crossbreeding Ano10$^{loxp/loxp}$ with Six2Cre mice. Knockout mice ($^{-/-}$) were compared to their Cre-negative littermate controls (+/+). A) Individual weight gain of $^{+/+}$ (blue) and $^{-/-}$ (red), (circles, female; triangles, male). B) Serum concentrations for sodium, potassium, creatinine and urea nitrogen (each n = 3). C) Urine concentrations for potassium, sodium and normalized protein in spontaneous urine (each n = 10). D) RT-PCR analysis of anoctamin expression in tubular epithelial cells isolated from kidneys of +/+ and -/- animals. Mean ± SEM (n = 8-9), $^{\#}$indicates statistical significance ($p<0.05$).

Chapter 3

Epithelial chloride transport by CFTR requires TMEM16A

Abstract

Cystic Fibrosis Transmembrane Conductance Regulator (CFTR) is the secretory chloride/bicarbonate channel in airways and intestine that is activated through ATP binding and phosphorylation by protein kinase A, but fails to operate in Cystic Fibrosis (CF). TMEM16A (also known as Anoctamin 1, ANO1) is thought to function as the Ca^{2+} activated secretory chloride channel independent of CFTR. Here we report that tissue specific knockout of the TMEM16A gene in mouse intestine and airways not only eliminates Ca^{2+} activated Cl^- currents, but unexpectedly also abrogates CFTR-mediated Cl^- secretion and completely abolishes cAMP-activated whole cell currents. The data demonstrate fundamentally new roles of TMEM16A in differentiated epithelial cells: TMEM16A provides a mechanism for enhanced ER Ca^{2+} store release, possibly engaging Store Operated cAMP Signaling (SOcAMPS) and activating Ca^{2+} regulated adenylyl cyclases. TMEM16A is shown to be essential for proper activation and membrane expression of CFTR. This intimate regulatory relationship is the cause for the functional overlap of CFTR and Ca^{2+} dependent chloride transport.

Keywords: Cystic Fibrosis transmembrane conductance regulator (CFTR); TMEM16A, anoctamin 1, airway transport; intestinal transport

Published in: Roberta Benedetto, Jiraporn Ousingsawat, Podchanart Wanitchakool, Yong

Zhang, Michael J. Holtzman, Margarida Amaral, Jason R. Rock, Rainer Schreiber, Karl Kunzelmann. Sci Rep. 2017 Sept; 7(1): 12397.

Own experimental contribution: All patch clamping, Ussing Chamber experiments, Immunocytochemistry.

Own written contribution: Methods, Results, Parts of Introduction and Discussion. Designed experiments and analyzed data.

Other contributions: Designed experiments and analyzed data.

Introduction

The Cystic Fibrosis transmembrane conductance regulator (CFTR) and the calcium-activated chloride channel TMEM16A (Anoctamin 1) are the two major secretory anion channels in intestinal and airway epithelia and therefore provide the critical regulation of mucus hydration at these sites[8, 112, 163, 164]. TMEM16A and a third anion channel, SLC26A9, have been shown to be upregulated and particularly relevant during airway inflammation and asthma[152,165]. TMEM16A and SLC26A9 attenuate airway inflammation in Cystic Fibrosis (CF)[166] , prevent mucus obstruction during airway inflammation and attenuate the intestinal obstructive phenotype in CF mice[165, 167]. In CF, TMEM16A and its regulator CLCA1 have been proposed as potential drug targets to compensate for the abrogated CFTR function in CF patients, while in asthma it may help to solubilize excess inflammatory mucus which may otherwise lead to airway obstruction[168, 169]. Previous *in vitro* studies suggested a functional relationship between calcium-activated TMEM16A and cAMP-regulated CFTR by some unknown mechanism[170-172]. Inhibition of TMEM16A by activated CFTR was suggested, while others reported similar pharmacological and functional properties for both Ca^{2+} and cAMP-activated Cl^- currents[173-175]. A recent study in human airway epithelial cells suggested CFTR as the principal chloride secretory pathway for both cAMP and purinergic (i.e. Ca^{2+} enhancing) agonists[162]. Similarly, muscarinic stimulation was shown to activate CFTR via increase in intracellular cAMP, and both Src and Pyk2 tyrosine kinases[176]. Collectively, these data suggest that CFTR may function as a chloride channel that is activated by both cAMP and Ca^{2+}.

Earlier work showed that mice lacking expression of TMEM16A in the airways present with a CF-like lung phenotype, suggesting that TMEM16A is essential for chloride secretion and maintenance of the airway surface liquid in mouse airways[164, 177]. However, these results were obtained in conventional TMEM16A-deficient mice that exhibit multiple organ failures, requiring studies being performed on compromised newborn pups. We therefore generated mouse lines in which TMEM16A expression was selectively deleted in intestinal villus and crypt epithelial cells (using *Vil1-Cre-TMEM16A$^{flox/flox}$* mice) or ciliated airway epithelial cells (using *FOXJ1-Cre-TMEM16A$^{flox/flox}$* mice). This approach allowed for the first studies of adult mice with TMEM16A deficiency and demonstrated that TMEM16A expression is responsible

for the calcium-activated chloride anion current in the intestine and lower respiratory airways and is essential for CFTR function at both of these mucosal sites.

Material and Methods

Animals, cells, isolation of crypts. All animal experiments were approved by the local ethics committee of the Government of Unterfranken/Würzburg (AZ: 55.2-2532-2-328) and were conducted according to the guidelines of the American Physiologic Society and the German law for the welfare of animals. Generation of *Vil1-Cre-TMEM16A$^{flox/flox}$* mice and isolation of intestinal epithelial cells have been described earlier[128]. Knockout of TMEM16A in mouse airways way achieved by crossbreeding *Vil1-Cre-TMEM16A$^{flox/flox}$* mice with FOXJ1-Cre transgenic mice generated as described previously[178]. Generation and culture of human Cystic Fibrosis bronchial epithelial cell lines (CFBE) is also described in previous reports[179, 180]. CFBE cells have been originally generated by Dr. D.C. Gruenert (Cardiovascular Research Institute, UCSF, San Francisco, USA) in accordance with the local guidelines and regulations. Cells were grown in minimum essential medium supplemented with 2 mM glutamine and 2.5 µg/ml puromycin. For Ussing chamber measurements, the cells were grown on permeable supports (Corning® Costar® Snapwell™, Life Science, Tewksbury, MA). Respiratory epithelial cells were isolated from mice as described[181] and were grown in AECGM plus supplement (Promocell, Heidelberg, Germany) that contained bovine pituitary extract 13 mg/ml, EGF 10 ng/ml, epinephrine 0.5 µg/ml, hydrocortisone 0.5 µg/ml, retinoic acid 0.1 ng/ml, transferrin 10 µg/ml, and triiodo-l-thyroxine 6.7 ng/ml. Media were further supplemented with 100 U/ml penicillin, 100 µg/ml streptomycin, 3 µg/ml fungizone, 50 µg/ml chloramphenicol, 0.1 mg/ml kanamycin. All media were supplemented with 10% fetal calf serum. Cells were incubated in 5% CO_2 at pH 7.4. siRNA for hTMEM16A was transfected into CFBE cells using standard methods (Lipofectamine, Invitrogen, Darmstadt, Germany). Cells were studied 48h after transfection. *cDNAs and RT-PCR.* For semi-quantitative RT-PCR, total RNA from mouse tracheal epithelial cells, crypts from mouse jejunum, proximal and distal colon and CFBE cells were isolated using NucleoSpin RNA II columns (Macherey-Nagel, Düren, Germany). Total RNA (1µg/50µl reaction) was reverse-transcribed using random

primer (Promega, Mannheim, Germany) and M-MLV Reverse Transcriptase RNase H Minus (Promega, Mannheim, Germany). Each RT-PCR reaction contained sense and antisense primer (0.5 µM, see supplementary table 1), 0.5 µl cDNA and GoTaq Polymerase (Promega, Mannheim, Germany). After 2 min at 95°C cDNA was amplified 30 cycles for 30 s at 95°C, 30 s at 57°C and 1 min at 72°C. PCR products were visualized by loading on peqGREEN (Peqlab,VWR, Germany) containing agarose gels and analysed using Meta Morph Vers. 6.2 (Molecular Devices, USA). Human and mouse Primers for RT-PCR were (5´-3´, s-as):

hTMEM16A CGACTACGTGTACATTTTCCG, GATTCCGATGTCTTTGGCTC;

hCFTR CATCTTTGGTGTTTCCTATG, GGAGTCTTTTGCACAATGG;

mTMEM16A GTGACAAGACCTGCAGCTAC, GCTGCAGCTGTGGAGATTC;

mCFTR GAATCCCCAGCTTATCCACG, CTTCACCATCATCTTCCCTAG;

GAPDH GTATTGGGCGCCTGGTCAC, CTCCTGGAAGATGGTGATGG.

Ussing chamber experiments. Isolated tracheas were put into ice cold bath solution containing (in mM/l) 145 NaCl, 0.4 KH_2PO_4, 1.6 K_2HPO, 4.6 D-glucose, 1 $MgCl_2$ 1.3 Ca^{2+} gluconate; pH 7.4). After isolation of tracheas connective tissue was removed. Tissues were mounted into an Ussing chamber with a circular aperture of 0.785 mm^2. Luminal and basolateral sides of the epithelium were perfused continuously at a rate of 5 ml/min. Luminal and basolateral solutions were heated to 37 °C, using a water jacket. Experiments were carried out under open-circuit conditions. Data were collected continuously using PowerLab (AD Instruments, Spechbach, Germany). Values for transepithelial voltages (Vte) were referred to the serosal side of the epithelium. Transepithelial resistances (Rte) were determined by applying short (1s) current pulses (ΔI = 0.5 µA). Rte and equivalent short circuit currents (Isc) were calculated according to Ohm's law (Rte = $\Delta Vte/\Delta I$, Isc = Vte/Rte).

Intestinal organoids. The protocol for the small intestinal organoids isolation and culture was adopted from[182]. In brief crypts from the small intestine were isolated in Ca^{2+} free chelating buffer, and the crypts pellet was resuspended in Advanced DMDM/F12 (Thermo Fisher Scientific, Waltham, MA, USA) supplemented with 2mM glutathione, 100 U/ml penicillin, 100

µg/ml streptomycin, 10mM Hepes and mixed with ice- cold Matrigel TM (Corning® Matrigel® Matrix, Life Sciences, Tewksbury, MA). The Matrigel TM was overlayed with basal minigut media supplemented with Noggin and recombinant Rspo-1 (PeproTech, Hamburg, Germany).

Patch Clamping. Primary-culture of mouse tracheal epithelial cells and CFBE cells were grown on coated glass cover slips for patch clamp experiments. Isolated intestinal crypts were immobilized on polylysine coated glass cover slips. If not indicated otherwise, patch pipettes were filled with a cytosolic-like solution containing in mM: KCl 30, K-gluconate 95, NaH_2PO_4 1.2, Na_2HPO_4 4.8, EGTA 1, Ca -gluconate 0.758, $MgCl_2$ 1.03, D - glucose 5, ATP 3, pH 7.2. The Ca^{2+} activity was 0.1 µM. Coverslips were mounted in a perfused bath chamber on the stage of an inverted microscope (IM35, Zeiss) and kept at 37 °C. Transfected cells were identified by cotransfection of pIRES and antibody bound beads (Sigma Taufkirchen, Germany). The bath was perfused continuously with Ringer solution at a rate of 8 ml/min. Patch clamp experiments were performed in the fast whole cell configuration. Patch pipettes had an input resistance of 2–4 MΩ when filled with cytosolic like solution. Currents were corrected for serial resistance. The access conductance was monitored continuously and was 60–140 nS. Currents (voltage clamp) and voltages (current clamp) were recorded using a patch clamp amplifier (EPC 7, List Medical Electronics, Darmstadt, Germany), the LIH1600 interface and PULSE software (HEKA, Lambrecht, Germany) as well as Chart software (AD Instruments, Spechbach, Germany). Data were stored continuously on a computer hard disc and analyzed using PULSE software. In regular intervals, membrane voltage (*V*c) was clamped in steps of 20 mV from -100 to +100 mV from a holding voltage of -100 mV. Current density was calculated by dividing whole cell currents by cell capacitance.

Measurement of [Ca^{2+}]$_i$. The plasma membrane bound calcium sensor GCaMP6 was fused to the N-terminus of CFTR. HEK293 cells grown on coated glass cover slips were transfected with GCaMP6-CFTR, and were mounted in a perfusion chamber 72h after transfection. Cells were perfused with ringer solution at a rate of 8 ml/min at 37˚C. Cell fluorescence was measured continuously with an inverted microscope Axiovert S100 (Zeiss) using a x40 objective (Fluar 40x/1.3 Oil, Zeiss) and a high speed polychromator system (VisiChrome, Visitron, Puchheim, Germany). GCaMP6-CFTR was excited at 485 nm and 405 nm. Emission

was recorded between 520 and 550 nm using a CCD-camera (CoolSnap HQ, Visitron). Control of experiments, imaging acquisition, and data analysis were done with the software package Meta-Fluor (Universal imaging, New York, USA). Alternatively, cells were loaded with Fura-2 and intracellular Ca^{2+} concentrations were determined as described earlier[134].

Western Blotting, COIP, biotinylation. Protein was isolated from parental CFBE cells and from CFBE cells expressing wt-CFTR or F508del-CFTR using a sample buffer containing 50 mM Tris-HCl, 150 mM NaCl, 50 mM Tris, 100 mM dithiothreitol, 1% Nonidet P-40, 0.5% deoxycholate sodium, and 1% protease inhibitor mixture (Sigma, Taufkirchen, Germany). For co-immunoprecipitation CFBE cells (wt and dF508) were collected and lysed in 0.5% CHAPs lysis buffer containing 1X protease inhibitor cocktail. Protein (500 µg) was incubated with 6 µg of antibody (North American CFF, #596) and pre-cleaned protein G agarose (60 µl) on a rotator at 4°C overnight. Afterward, beads were centrifuged and washed three times with 0.5% CHAPs lysis buffer containing 1X protease inhibitor cocktail. The immunocomplexes were eluted by 2x sample buffer. For biotinylation CFBE cells (90-100% confluent) in T75 cm^2 flasks were washed twice with ice-cold PBS ($+Ca^{2+}/Mg^{2+}$), followed by incubation with Sulfo-NHS-SS-Biotin (Thermo Scientific, Waltham, MA USA) at 4°C for 30 min according to the manufacturer's instructions. Cells were lysed and homogenized in lysis buffer containing complete protease inhibitor cocktail (Roche, Penzberg, Germany) on ice for 30 minutes and centrifuged at 10,000g at 4°C for 2 min. Biotin labeled surface proteins were captured on neutravidin agarose resin (Thermo Scientific, Waltham, MA USA) at room temperature for 1h. The resins were washed 5 times with wash buffer containing protease inhibitor. Proteins bound to the resin were eluted with SDS PAGE sample buffer, and analysed by western blotting. Sample was separated by 8.5 % SDS-PAGE and transferred to PVDF membrane (GE Healthcare, Munich, Germany). The membrane was blocked with 5 % NFM/TBST or 5 % NFM/PBST at RT for 1h and incubated overnight 4 °C with rabbit polyclonal anti-TMEM16A AB (1:1000, 1 % NFM/TBST), mouse monoclonal anti-CFTR AB (1:500, 3 % NFM/PBST), rabbit polyclonal anti-Na+/K+-ATPase α AB (1:1000, 1 % NFM/TBST) or mouse monoclonal anti β-actin AB (5 % NFM/PBST). Subsequently, the membrane was incubated with HRP-conjugated donkey anti-rabbit or goat-anti mouse IgG at RT for 2h. Immunoreactive signals

were visualized using supersignal chemiluminescence substrate detection kit (Pierce Biotechonology, Rockford, USA).

Chemiluminescence. CFBE wtCFTR and F508del-CFTR were tagged with an extracellular FLAG epitope and stably expression in CFBE cells using a doxycycline-inducible gene expression system. Surface CFTR expression was detected using monoclonal anti-FLAG M2-Peroxidase (Sigma, Taufkirchen, Germany) after 48 hr of doxycycline application. Cells were fixed in 4% paraformaldehyde, blocked in 5% BSA and incubated with anti-FLAG M2-Peroxidase (1:1000). Chemiluminescene was detected using a SuperSignal West Pico chemiluminescence substrate (Thermo Scientific, Darmstadt Germany) and measured using plate reader NOVOstar (BMG Labtach, Offenburg, Germany).

Immunocytochemistry. Mouse intestine, lungs and trachea were fixed by perfusion with 4 % paraformaldehyde (PFA) and post-fixed in 0.5 mol/l sucrose, 4 % PFA solution. Cryosections of 5 µm were incubated in 0.1 % SDS for 5 min, washed with PBS, and blocked with 5 % bovine serum albumin (BSA) and 0.04 % Triton X-100 in PBS for 30 min. Sections were incubated with primary antibodies (Alomone Labs, #ACl 006) in 0.5 % BSA and 0.04 % Triton X-100 overnight at 4 °C and with Alexa Fluor 488 labeled donkey anti rabbit IgG (Invitrogen). Sections were counterstained with Hoe33342 (0.1 µg/ml PBS, Aplichem, Darmstadt, Germany).

Immunofluorescence was detected using an Axiovert 200 microscope equipped with ApoTome and AxioVision (Zeiss, Germany). CFBE cells were grown on glass coverslips and fixed for 10 min with 4% (w/v) PFA at room temperature. After washing, the cells were permeabilized and blocked with 2% (w/v, PBS) bovine serum albumin and 0.04% (w/v, PBS) Triton-X-100 and incubated with primary anti-CFTR rabbit antibody (1:100, Alomone labs, # ACl^- 006) and anti-TMEM16A rabbit antibody (1:100, Geneway GWB-MP178G) over night at 4 °C. Binding of the primary antibody was visualized by incubation with a secondary antibody conjugated with Alexa 488 (Life Technologies, A-21206). Nuclei were stained with Hoe33342 (0.1 µg/ml PBS, Aplichem, Darmstadt, Germany). Cells were mounted on glass slides with fluorescent mounting medium (DAKO Cytomation, Hamburg, Germany) and examined with an ApoTome Axiovert 200 M fluorescence microscope (Zeiss, Göttingen, Germany).

Materials and statistical analysis. All animal experiments were approved by local authorities and were conducted according to the guidelines of the American Physiological Society and the German law for welfare of animals. All compounds used were of highest available grade of purity. Data are reported as mean ± SEM. Student's t-test (for paired or unpaired samples as appropriate) or ANOVA were used for statistical analysis. A p-value < 0.05 was accepted as significant difference.

Results

Intestinal epithelial cell knockout of TMEM16A eliminates CFTR currents.

An intestinal epithelial cell-specific *TMEM16A* gene knockout mouse (*Vil1-Cre–TMEM16A*$^{flox/flox}$) was generated from *Vil1-Cre* and *TMEM16A*$^{flox/flox}$ mice (Fig S3.1) to determine TMEM16A function in the adult mouse intestinal epithelium. In contrast to reports of conventional TMEM16A-defiicent mice[164, 177], the *Vil1-Cre–TMEM16A*$^{flox/flox}$ mice did not show any difference in birth rate or lifespan, or manifest any baseline intestinal abnormalities (including intestinal obstruction or change in faecal water content) compared to control TMEM16A wild-type (wt) mice (*Vil1-Cre–TMEM16A*$^{wt/wt}$) (Fig S3.2). Micro-perfused Ussing chamber experiments were used to assess ion transport of colonic epithelium by determining transepithelial voltage (V_{te}) under open circuit conditions and calculating equivalent currents (I_{sc}). Perhaps as expected, carbachol-stimulated Ca^{2+}-activated anion transport was no longer present in colonic epithelia from *Vil1-Cre–TMEM16A*$^{flox/flox}$ compared to *Vil1-Cre–TMEM16A*$^{wt/wt}$ control mice (Fig 3.1A,B). In addition, and rather unexpectedly, cAMP-activated anion transport was also markedly attenuated in intestinal epithelia from *Vil1-Cre–TMEM16A*$^{flox/flox}$ mice (Fig 3.1C,D). This decrease in transport function was not accompanied by any change in the level of CFTR expression in colonic epithelial cells based on TMEM16A western blotting (Fig S3.1D). In contrast, the pattern of CFTR expression in colonic epithelium of *Vil1-Cre–TMEM16A*$^{flox/flox}$ mice was different, with clearly compromised apical CFTR expression (Fig S3.1A). cAMP (IBMX and Forskolin) stimulation failed to expand the luminal cavity in intestinal organoids from *Vil1-Cre–TMEM16A*$^{flox/flox}$ mice compared to wild-type control mice, indicating that the defect in intestinal cAMP-activated anion transport in *Vil1-*

Cre–TMEM16A$^{flox/flox}$ mice was accompanied by decreased secretion (Fig 3.1E,F). Consistent with these results, both carbachol and cAMP stimulation of ion currents determined by whole cell patch clamping were lost in freshly isolated mouse colonic epithelial cells from *Vil1-Cre–TMEM16A*$^{flox/flox}$ mice compared to wild-type control mice (Fig 3.1G-R). Ca^{2+} and cAMP activated currents were identified by blockade with inhibitors for TMEM16A (CaCC-AO1) and CFTR (CFTRinh172)[156, 183] (Fig 3.1M,O-R; Fig 3.2G,H). However, as indicated below crosstalk of both, Ca^{2+} and cAMP signalling pathways may lead to a cross-inhibition by both inhibitors. Together, the results show that calcium-activated as well as cAMP-stimulated CFTR-dependent chloride secretion in mouse intestinal epithelial cells depends on TMEM16A expression.

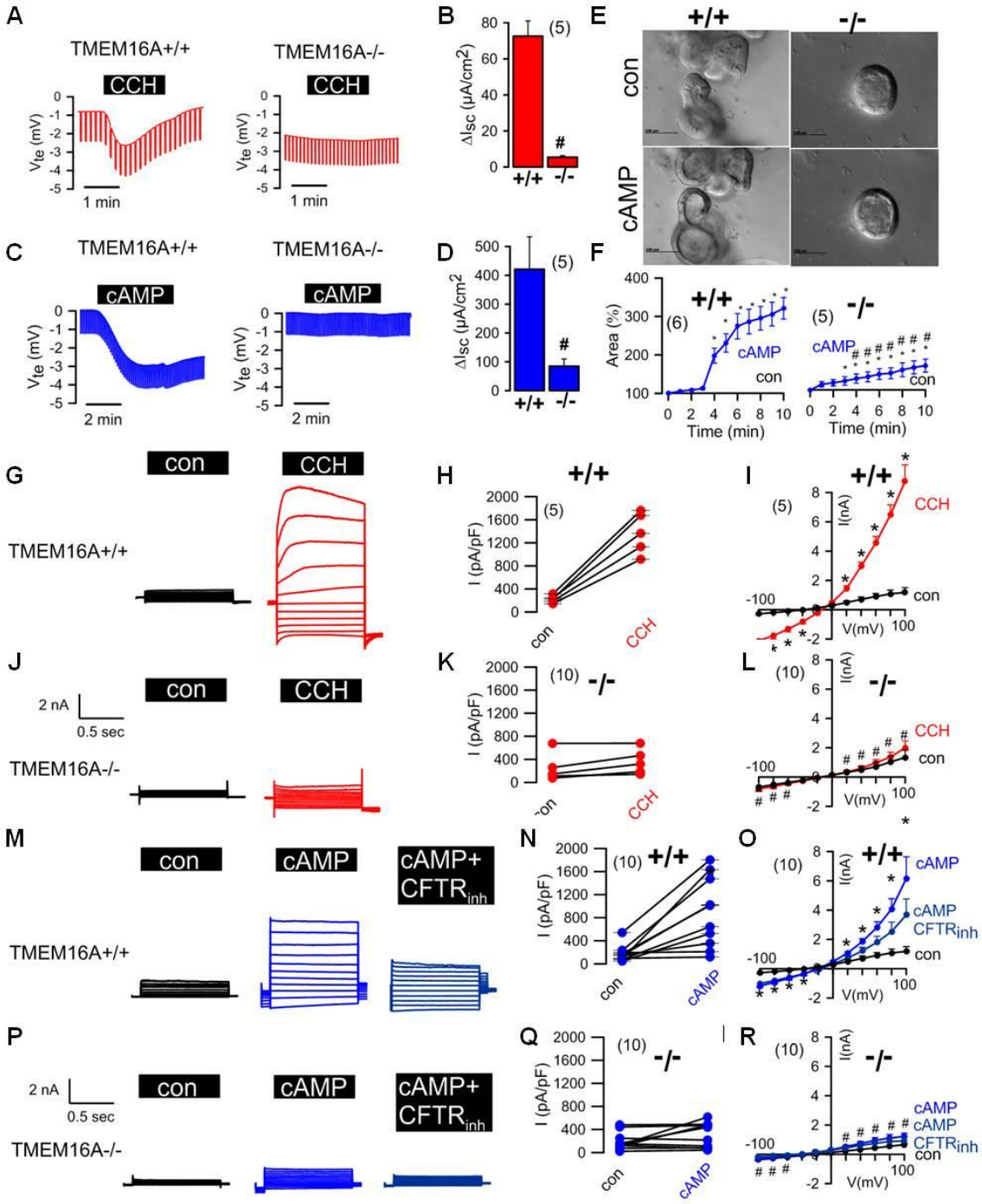

Fig 3.1 *Intestinal epithelial knockout of TMEM16A eliminates CFTR currents.*

A) Original recordings of the transepithelial voltage V_{te} and the effect of carbachol (CCH, 100 µM) in colonic epithelia from mice with intestinal epithelial knockout of TMEM16A (*Vil1-Cre–TMEM16A*$^{flox/flox}$; TMEM16A$^{-/-}$) and wild-type mice (TMEM16A$^{+/+}$). B) Summary of the calculated CCH-induced short circuit currents (ΔI_{sc}). C;D) Original recordings of V_{te} and summary of cAMP (IBMX 100 µM/Forskolin 2 µM)-induced ΔI_{sc} in +/+ and -/- colonic epithelia. E, F) cAMP-induced secretion in intestinal organoids from $^{+/+}$ and $^{-/-}$ intestines (upper panel) and summaries of luminal area increase (lower panel). (G-J) Activation of whole cell currents by CCH and inhibition by CaCCinhAO1 (AO1; 10 µM) in isolated intestinal epithelial cells from $^{+/+}$ mice. Original recordings (G), individual experiments (H) and current/voltage relationships (I). J-L) Corresponding experiments in intestinal epithelial cells from -/-

mice. (M-O) Activation of whole cell currents by cAMP and inhibition by CFTRinh172 (CFTRinh; 10 µM) in isolated intestinal epithelial cells from $^{+/+}$ mice. P-R) Corresponding experiments in intestinal epithelial cells from $^{-/-}$ mice. Mean ± SEM; * significant activation by cAMP or CCH (paired t-test). $^{\#}$ significant difference between $^{-/-}$ and $^{+/+}$ (unpaired t-test). (number of mice or cells, respectively).

Respiratory epithelial knockout of TMEM16A eliminates CFTR currents.

We next examined the effect of TMEM16A-deficiency in respiratory airway function by generating an epithelial ciliated cell-specific knockout of the *TMEM16A* gene (*FOXJ1-Cre-TMEM16A$^{flox/flox}$* mice) derived from *FOXJ1-Cre* and *TMEM16A$^{loxp/loxp}$* mice (Fig 3.2,S3.3 A-C). TMEM16A was partially colocalized with CFTR in ciliated epithelial cells, but was absent in knockout airways (Fig S3.3 D,E). Notably, the TMEM16A antibody may have only detected larger expression levels. Like *Vil1-Cre-TMEM16A$^{flox/flox}$* mice, the *FOXJ1-Cre-TMEM16A$^{flox/flox}$* mice developed normally with birth rates and lifespans similar to wild-type control mice. Particle transport was assessed in isolated mouse tracheas as an index of mucociliary clearance (MCC)[164]. It was not compromised, but unexpectedly even enhanced under basal conditions in tracheas from *FOXJ1-Cre-TMEM16A$^{flox/flox}$* mice, compared to wild-type control tracheas. However, stimulation by ATP or carbachol did not further enhance MC in *FOXJ1-Cre-TMEM16A$^{flox/flox}$* cells, in contrast to wild-type control cells (Fig S3.2 E). No mucus plugging was observed in the lungs of *FOXJ1-Cre-TMEM16A$^{flox/flox}$* mice or wild-type control mice. Experiments with micro-perfused Ussing chambers showed that luminal ATP- or basolateral CCH-induced voltage deflections (ΔV_{te}) and calculated ΔI_{sc} were both attenuated in tracheas from *FOXJ1-Cre-TMEM16A$^{flox/flox}$* mice compared to wild-type control mice (Fig 3.2A-D). As observed in cells from *Vil1-Cre-TMEM16A$^{flox/flox}$* mice, also in tracheas from *FOXJ1-Cre-TMEM16A$^{flox/flox}$* mice cAMP activated transport was inhibited (Fig 3.2 E,F). Moreover, whole cell patch clamp experiments on primary-cultured mouse tracheal epithelial cells demonstrated large ATP-activated Cl^- currents in cells from wild-type tracheas, which were absent in cells from *FOXJ1-Cre-TMEM16A$^{flox/flox}$* tracheas, indicating that Ca^{2+} dependent Cl^- currents in mouse respiratory epithelial cells are entirely due to TMEM16A (Fig 3.2 G, H). cAMP activated whole cell Cl^- currents were small but detectable in wild-type airway cells, and were significantly inhibited by CFTRinh172. In contrast, in cells from *FOXJ1-Cre-*

TMEM16A$^{flox/flox}$ tracheas no currents were activated by cAMP, and CFTRinh172 had no effects (Fig 3.2 I, J). Taken together, in both intestine and airways knockdown of TMEM16A strongly inhibited cAMP-activated, i.e. CFTR-related Cl^- transport in addition to the abolished Ca^{2+} dependent chloride secretion.

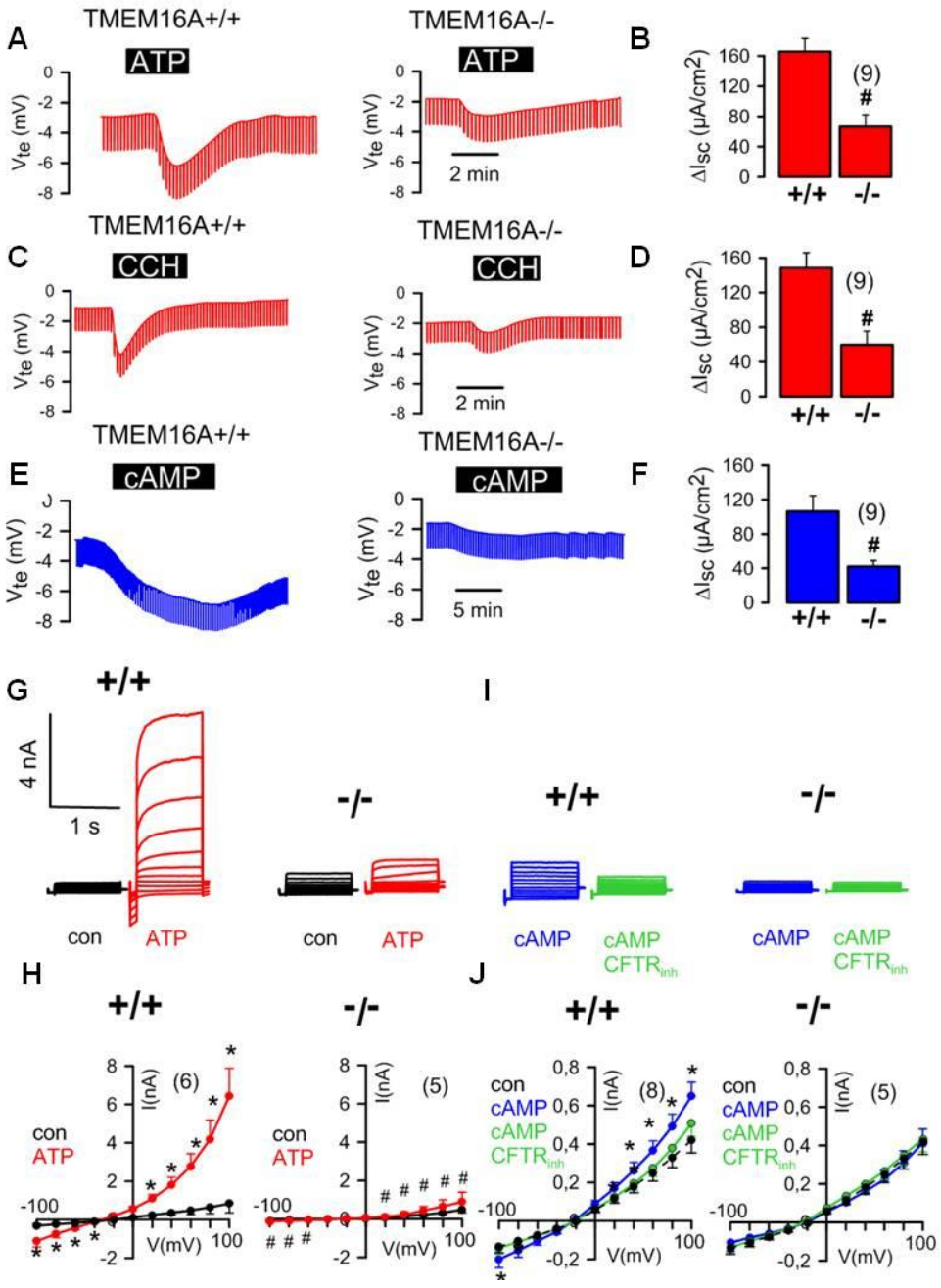

Fig 3. 2 *Respiratory epithelial knockout of TMEM16A eliminates CFTR currents.*
A) Original recordings of the transepithelial voltage V_{te} and the effect of ATP (100 µM) in tracheas from *FOXJ1-Cre-TMEM16A*$^{wt/wt}$ ($^{+/+}$) and *FOXJ1-Cre-TMEM16A*$^{flox/flox}$ ($^{-/-}$) mice. B) Summary of the calculated ATP-induced short circuit currents (ΔI_{sc}). C, D) Original recordings of V_{te} and summary of CCH-induced ΔI_{sc} in +/+ and -/- tracheas. E, F) Original recordings of V_{te} and summary of cAMP (IBMX

100 µM/Forskolin 2 µM)-induced ΔI_{sc} in +/+ and -/- tracheas. G) Original recordings of whole cell currents activated by ATP in primary-cultured tracheal epithelial cells from TMEM16A$^{+/+}$ and TMEM16A$^{-/-}$ mice. Experiments were performed in the presence of an inhibitor of Ca^{2+} activated K^+ channels, TRAM-34 (100 nM). H) Corresponding current/voltage relationships of whole cell currents activated by ATP in TMEM16A$^{+/+}$ and TMEM16A$^{-/-}$ cells. I) Original recordings of whole cell currents activated by cAMP in primary cultured respiratory epithelial cells from TMEM16A$^{+/+}$ and TMEM16A$^{-/-}$ mice. J) Corresponding current/voltage relationships of whole cell currents activated by cAMP in TMEM16A$^{+/+}$ and TMEM16A$^{-/-}$ cells. Mean ± SEM; *significant activation by cAMP or ATP (paired t-test). $^{\#}$significant difference between $^{-/-}$ and $^{+/+}$ (unpaired t-test). (number of mice or cells, respectively).

Cl^- currents by CFTR and TMEM16A in human airway epithelial cells are linked.

To translate the results obtained in mouse airways to humans, we studied Cystic Fibrosis bronchial epithelial (CFBE) cell lines engineered to stably express wt-CFTR or the most frequent mutant form F508del-CFTR, when compared to the parental cell line that does not express CFTR (Fig 3.3 A, Fig S3.5 A) [180]. Although all three cell lines expressed comparable levels of TMEM16A (Fig 3.3 A, Fig S3.5 A), the Ca^{2+}-dependent whole cell currents activated by ATP were large in CFBE/wt-CFTR cells, but were small for CFBE/F508del-CFTR and parental cells (Fig 3.3 B,C). As expected, cAMP-dependent currents were large in CFBE/wt-CFTR, but were essentially absent in CFBE/F508del-CFTR cells (Fig 3.3 D, E). Because large cAMP-dependent (CFTR) currents were paralleled by large TMEM16A currents, we knocked down *TMEM16A* gene expression in CFBE/wt-CFTR cells to see whether this affects CFTR currents (Fig 3.3 F). Strikingly, elimination of ATP-activated TMEM16A whole cell currents (Fig 3.3 G, upper panel), also abolished cAMP-activated CFTRinh172-inhibitable currents, despite expression of CFTR remained unaffected by TMEM16A-knockdown (Fig 3.3 G, lower panel, Fig S3.5 B). The results reproduce the functional interaction between TMEM16A and CFTR, and identify TMEM16A as the Ca^{2+} activated anion channel in human airway epithelial cells. There was also a considerable pharmacological overlap between CFTR and TMEM16A, as both currents were inhibited by the TMEM16A inhibitor AO1 and the CFTR blocker CFTRinh172 (Fg. 3.3 H). Finally, when CFBE/wt-CFTR and CFBE/F508del-CFTR cells were grown to polarized epithelia on permeable supports and examined in Ussing chambers, the results were analogous: V_{te} and I_{sc} induced by either cAMP or ATP were large in CFBE/wt-CFTR epithelia, but were almost absent in CFBE/F508del-CFTR tissues.

Moreover, CFTRinh172 blocked both CFTR (cAMP) and CaCC (ATP)-induced transport (Fig 12i-k).

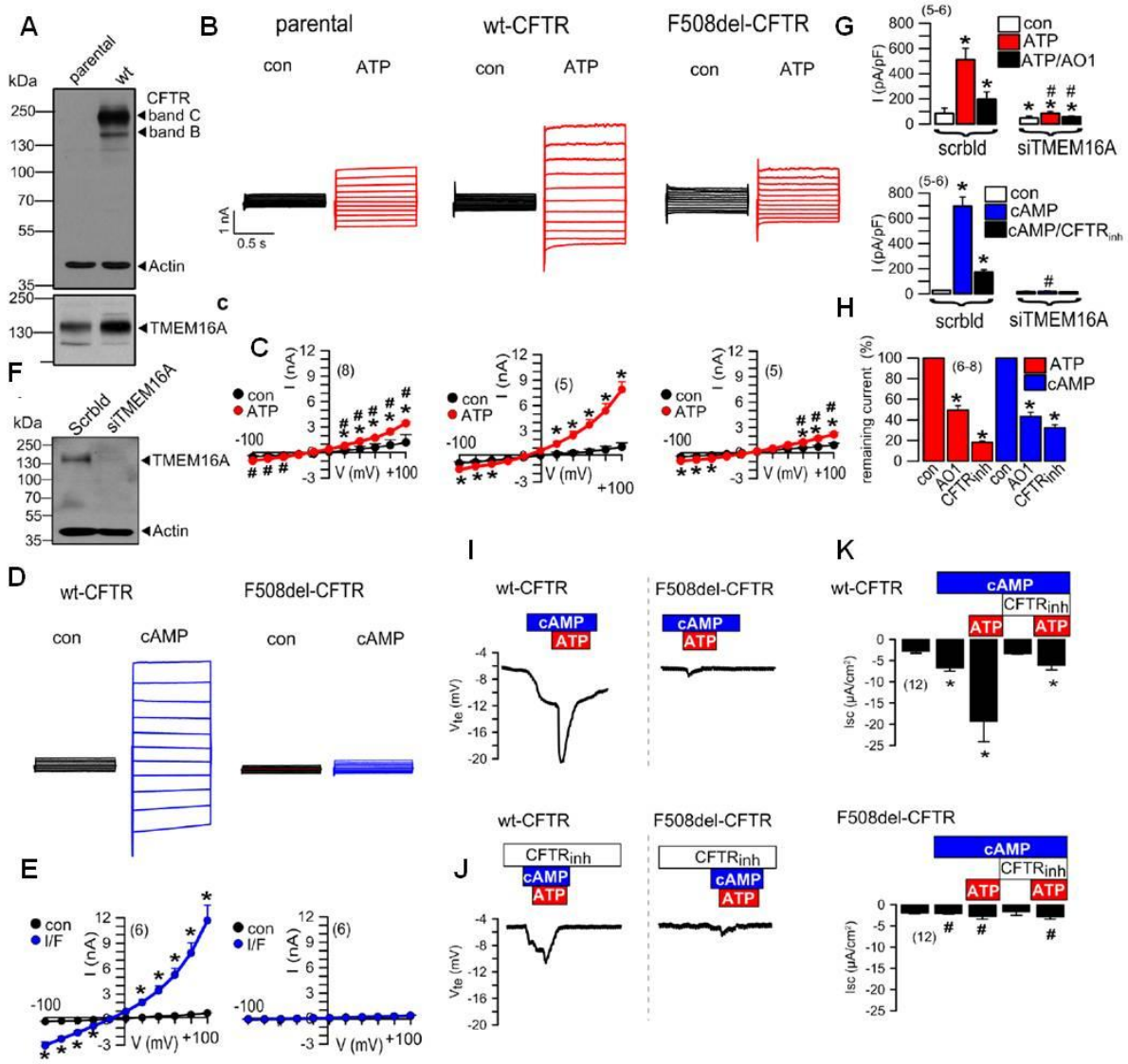

Fig 3.3 *Cl⁻ currents by CFTR and TMEM16A in human airway epithelial cells cannot be strictly separated.*

A) Western blot demonstrating wt-CFTR expression in CFBE/wt-CFTR cells, but not in CFBE parental cells. Both cells lines express similar levels of TMEM16A. B) ATP (100 µM) -activated whole cell currents in CFBE parental cells and CFBE cells expressing wt-CFTR or F508del-CFTR. C) Corresponding current / voltage relationships. D) Whole cell currents activated by cAMP (100 µM IBMX/2 µM Forskolin) in CFBE cells expressing wt-CFTR or F508del-CFTR. E) Corresponding current / voltage relationships. F) Western blot indicating suppression of TMEM16A in CFBE/wt-CFTR cells by siRNA G) Summary of ATP (100 µM) -activated whole cell currents in CFBE/wt-CFTR cells treated with scrambled RNA or after siRNA-knockdown of TMEM16A (upper panel). Inhibition by CaCCinh-AO1 (10 µM). Summary of cAMP-activated whole cell currents in control (scrambled) and TMEM16A-knockdown cells, and effect of CFTRinh172 (10 µM). H) Remaining currents after inhibition with

CaCCinh_AO1 and CFTRinh172. Both blockers inhibit ATP- and cAMP-activated whole cell currents. I) Transepithelial voltages recorded in polarized grown CFBE/wt-CFTR and CFBE/F508del-CFTR cells. Voltage deflections induced by cAMP or ATP. J) Transepithelial voltages recorded in the presence of CFTRinh172 (10 µM). K) Summaries of the corresponding calculated short circuit currents (I_{sc}). Mean ± SEM; * significant activation by ATP and cAMP, or currents inhibition by AO1 and CFTRinh, respectively (paired t-test). # significant difference between scrambled and siTMEM16A or between wt-CFTR and F508del-CFTR, respectively (paired t-test). (number of cells).

TMEM16A activates CFTR by enhancing Ca^{2+} store release.

The present results establish that CFTR and TMEM16A currents are functionally linked and interdependent. To determine the mechanism for TMEM16A enhancement of CFTR activity, we analysed the effect of additional (exogenous) TMEM16A expression on CFTR function in CFBE/wt-CFTR cells. We found that additional TMEM16A enhanced ATP-activated TMEM16A currents in parental cells as expected, but in addition also enhanced cAMP-activated CFTR currents in CFBE/wt-CFTR and even in CFBE/F508del-CFTR cells (Fig 3.4 A). To determine the molecular mechanism for TMEM16A regulation of CFTR, we examined whether TMEM16A-driven release of ER store calcium might be responsible since TMEM16A is reported to enhance ER calcium store release[79, 80, 160]. This mechanism may cause CFTR activation in response to stimulation of purinergic and other phospholipase C coupled receptors[162, 176]. We found that activation of wt-CFTR was markedly decreased when Ca^{2+} was chelated by BAPTA-AM (Fig 3.4 B). Moreover, release of Ca^{2+} from the ER store (peak) was significantly reduced in tracheal epithelial cells from *FOXJ1-Cre-TMEM16A$^{flox/flox}$* mice (Fig 3.4 C,D). Correspondingly, ATP-induced Ca^{2+} store release was inhibited with siRNA-mediated knockdown of TMEM16A in airway epithelial cells (Fig 3.4 E, F). Notably, after knockdown of TMEM16A, a whole cell current could only be activated by cAMP in the presence of the Ca^{2+} ionophore ionomycin, confirming the role of Ca^{2+} and/or ER store release for activation of CFTR (Fig S3.5 C, D). To measure Ca^{2+} signals in close proximity of CFTR, the Ca^{2+} sensor GCAMP6 was fused to the C-terminus of CFTR and was expressed in HEK293 cells. TMEM16A enhanced ATP-stimulated Ca^{2+} release under control conditions and in the presence of cAMP (Fig 3.4 G, H).

Role of Ca^{2+} regulated adenylate cyclases.

Enhanced Ca^{2+} store release in the presence of TMEM16A may support activation of CFTR through Ca^{2+} dependent adenylate cyclases[161, 162]. In support of this, we found that the IP_3 receptor inhibitor Xestospongin C markedly inhibited activation of CFTR by IBMX and Forskolin (Fig S3.5 E), while the TMEM16A inhibitor CaCCinhAO1 (AO1) blocked basal and ATP-induced Ca^{2+} increase (Fig S3.5 F). AO1 also blocked cAMP-induced fluid secretion in organoids from T84 intestinal epithelial cells (Fig S3.5 G, H). Moreover, ST034307 and KH7, both inhibitors of Ca^{2+} dependent adenylate cyclases, potently inhibited ATP-activated Cl^- currents in CFBE/wt-CFTR cells (Fig 3.5 J). Because TMEM16A enhances ER Ca^{2+} store release, it is possible that compartmentalized increase in intracellular cAMP is induced by a mechanism recently identified as store operated cAMP signaling (SOcAMPs)[184]. SOcAMPs, i.e. increase of cAMP by ER store emptying, was shown to contribute to Ca^{2+}-dependent activation of Cl^- secretion in T84 colonic epithelial cells[185]. Ca^{2+}-refill of ER stores, was shown to terminate SOcAMPs, and occurs through store operated Ca^{2+} entry (SOCE) via ORAI channels. Remarkably, the ORAI channel blocker YM58483 or Ca^{2+} removal caused prolonged activation of Cl^- currents activated by ATP, which strongly suggests a contribution of SOcAMPs to activation of Cl^- secretion (Fig 3,5 K).

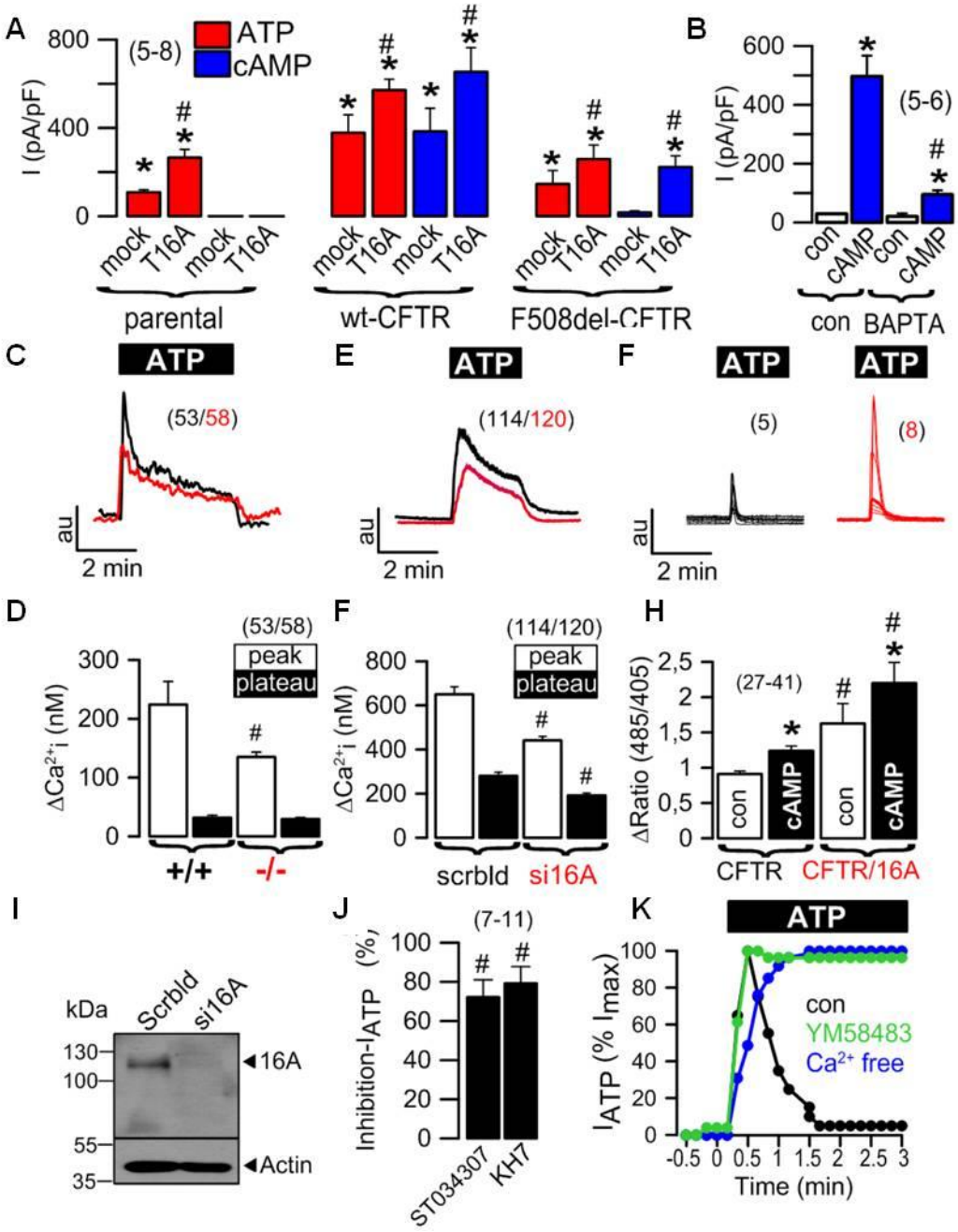

Fig 3.4 *TMEM16A provides Ca^{2+} for activation of CFTR.*

A) Summary of whole cell currents activated by increase in intracellular Ca^{2+} (ATP; 100 µM) and cAMP (IBMX 100 µM/Forskolin 2 µM) in parental cells, CFBE/wt-CFTR and CFBE/F508del-CFTR cells, with or without (mock) additional expression of exogenous TMEM16A. Additional TMEM16A augments ATP-induced currents in all cell lines, enhances cAMP-activated currents in CFBE/wt-CFTR cells, and induces cAMP-activated currents in CFBE/F508del-CFTR cells B) cAMP-activated whole cell currents in CFBE/wt-CFTR cells were inhibited by the Ca^{2+} chelator BAPTA-AM. C, D) Mean recordings of ATP-induced rise in intracellular Ca^{2+} (Fura-2) in primary airway epithelial cells form $TMEM16A^{+/+}$ (black) and $TMEM16A^{-/-}$ (red) mice (upper panel). Summary of peak and plateau Ca^{2+} increase (lower panel). E, F) Mean recordings of ATP-induced rise in intracellular Ca^{2+} (Fura-2) in CFBE/wt-CFTR cells (upper panel) and summary of peak and plateau Ca^{2+}, which were reduced after siRNA-knockout (red) of TMEM16A (lower panel). G, H) Recordings of ATP-induced Ca^{2+} peaks in HEK293 cells expressing

GCAMP2-tagged CFTR. The ATP-induced Ca^{2+} peaks are larger in cells TMEM16A (red) coexpressing cells (upper panel). Summaries of Ca^{2+} peaks in the absence or presence of cAMP (lower panel). J) Western blot indicating knockdown of TMEM16A expression by siRNA. (J) Inhibition (in %) of ATP-activated Cl^- currents by two different inhibitors of Ca^{2+}-dependent adenylate cyclases, ST034307 (30 µM) and KH7 (10 µM). K) Time courses for activation of whole cell currents by ATP (100 µM) under control conditions, in the presence of the ORAI-inhibitor YM58483, and in the absence of extracellular Ca^{2+}. Mean ± SEM; *significant activation by ATP or cAMP (paired t-test). # significant difference when compared to mock, +/+, scrambled, absence of TMEM16A, or con, respectively (unpaired t-test). (number of cells or assays).

Control of CFTR membrane expression by TMEM16A.

To further define the mechanisms for regulation of CFTR by TMEM16A, we examined membrane expression of CFTR. The results suggested a cellular mislocalization of CFTR in TMEM16A knockout tissues (Fig S3.1 A, B). We quantified the amount of plasma membrane CFTR in CFBE cells by chemiluminescence, using an extracellular FLAG epitope. Very little background luminescence was found in non-expressing parental cells (con), while a robust signal was detected in CFBE/wt-CFTR-FLAG cells (Fig 3.5 A). siRNA knockdown of TMEM16A (si16A) lowered membrane expression of CFTR (Fig 3.5 A), while additional expression of TMEM16A further enhanced luminescence (Fig 3.5 B). Cellular distribution of CFTR was analysed in CFBE cells in the presence or absence of TMEM16A. Membrane and cytosolic expression were quantified by analysing fluorescence intensities in the regions of interests (ROI) and are shown as proportions of membrane versus cytoplasmic fluorescence. CFTR was detected either by cherry fluorescence (Cherry-CFTR) in live imaging (Fig 3.5 C,D), or by using an anti-CFTR antibody in fixed cells (Fig 3.5 E, F). Both methods supplied comparable results and showed a shift of CFTR from the cell membrane towards a cytosolic perinuclear localization. Using cell membrane surface biotinylation, we found membrane expression of CFTR and TMEM16A in CFBE/wt-CFTR cells, while neither CFTR nor TMEM16A could be biotinylated in CFBE/F508del-CFTR cells (Fig 3.5 G). Knockdown of TMEM16A in CFBE/wt-CFTR cells attenuated membrane expression of CFTR (Fig 14h).

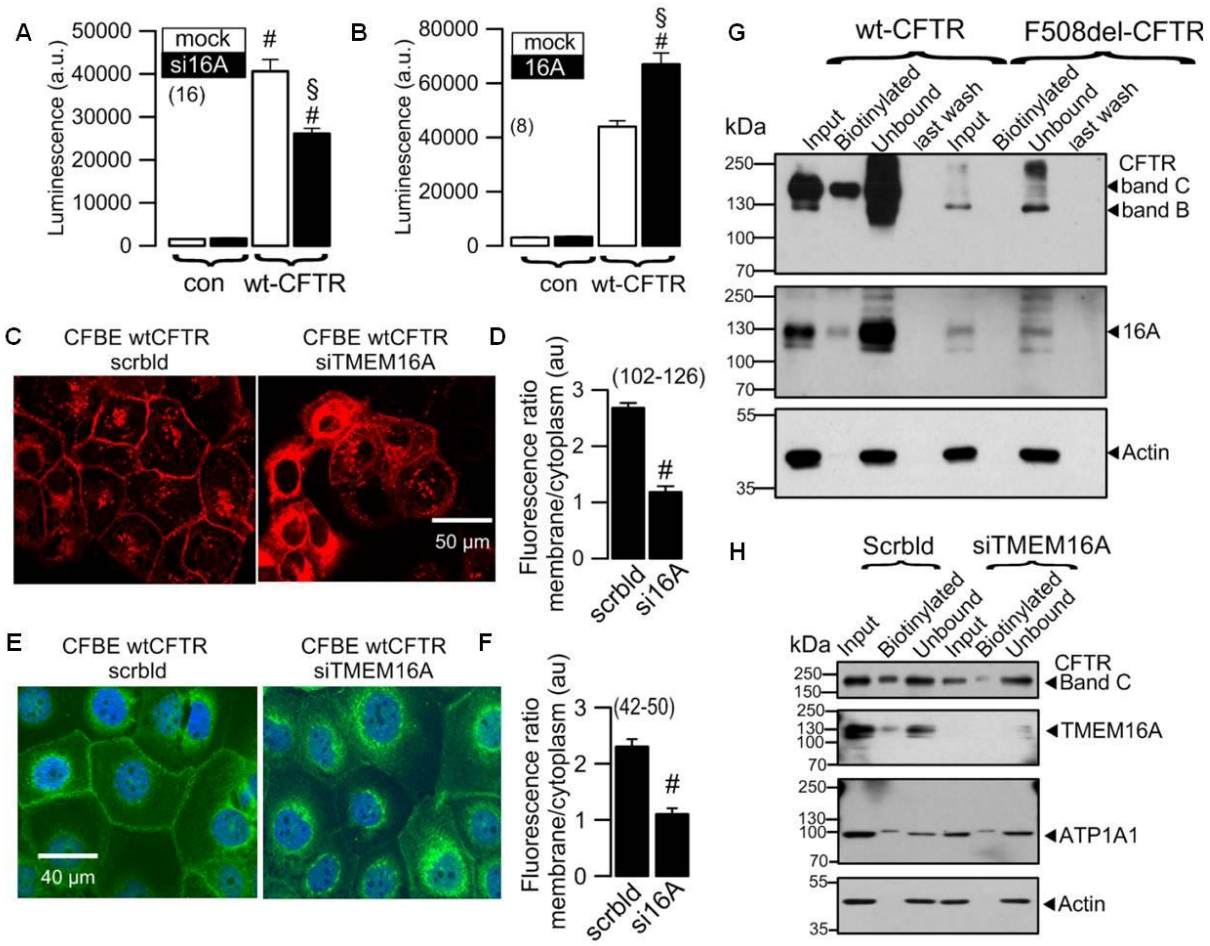

Fig 3.5 *TMEM16A enhances membrane expression of CFTR.*

A, B) Membrane expression of CFTR detected by chemiluminescence in CFBE/wt-CFTR cells expressing CFTR containing a FLAG tag in the first extracellular loop and a N-terminal cherry tag. Cells were exposed to a primary FLAG antibody (Sigma Taufkirchen, Germany, # F3165) and a secondary peroxidase-conjugated antibody. Luminescence was detected in CFBE/wt-CFTR cells but not in control parental cells (con). siRNA-knockdown of endogenous TMEM16A reduced chemiluminescence in CFBE/wt-CFTR cells A), while additional expression of exogenous TMEM16A enhanced chemiluminescence B). Very little background chemiluminescence was observed in the absence of CFTR (con). Mean ± SEM, (n) number of assays. #significant difference when compared to mock (unpaired t-test). C,D) Life imaging of cherry-CFTR in CFBE/wt-CFTR cells with and without siRNA-knockdown of TMEM16A, as detected by cherry fluorescence. Summary of fluorescence intensity ratios (plasma membrane/cytosolic fluorescence) indicating redistribution of the fluorescence towards cytoplasm by siRNA-TMEM16A. E, F) Antibody-staining of CFTR in CFBE/wt-CFTR cells with and without siRNA-knockdown of TMEM16A. Summary of fluorescence intensity ratios (plasma membrane/cytosolic fluorescence) indicating redistribution of the fluorescence towards cytoplasm by siRNA-TMEM16A. G) Membrane biotinylation of CFBE/wt-CFTR and CFBE/F508del-CFTR cells, and detection of membrane and cytosolic fractions of CFTR and TMEM16A using Western blot. H) Effect of TMEM16A-knockdown on biotinylation (membrane expression) of CFTR and TMEM16A. Mean ± SEM; #significant difference when compared to scrambled (paired t-test). (Number of cells). Assays were performed in triplicates.

Molecular interaction of CFTR and TMEM16A and a possible role of PDZ-interacting motifs.

The present results show a functional interaction of CFTR and TMEM16A. Both proteins may therefore be colocalized in a functional compartment or may even physically interact, possibly through adapter proteins like post-synaptic density protein/Drosophila disc large tumour suppressor/zonula occludens (PDZ) proteins [172]. In support of this, we found that wt-CFTR and F508del-CFTR could be coimmunoprecipitated with TMEM16A in CFBE cells (Fig 3.6 A,B). Notably, TMEM16A pulled down the fully glycosylated form of wt-CFTR (band C), and the core glycosylated form of F508del-CFTR (band B). Coimmunoprecipitation was not observed for wt-CFTR and the TMEM16A-paralogue TMEM16F (Fig 3,6 C, D). Molecular interaction may require the PDZ-interacting motifs present at C-terminus of CFTR and TMEM16A[186, 187]. In support of this we found that deletion of PDZ-interacting motifs in either CFTR or TMEM16A reduced membrane expression of each protein (Fig S3.5 A,B). Membrane expression of both proteins was further inhibited by simultaneous deletion of both PDZ-interacting motifs (Fig S3.9 C). Taken together, control of CFTR through TMEM16A appears largely Ca^{2+} dependent, which also affects membrane expression of CFTR and may require anchoring of these proteins in a functional compartment by the help of PDZ proteins.

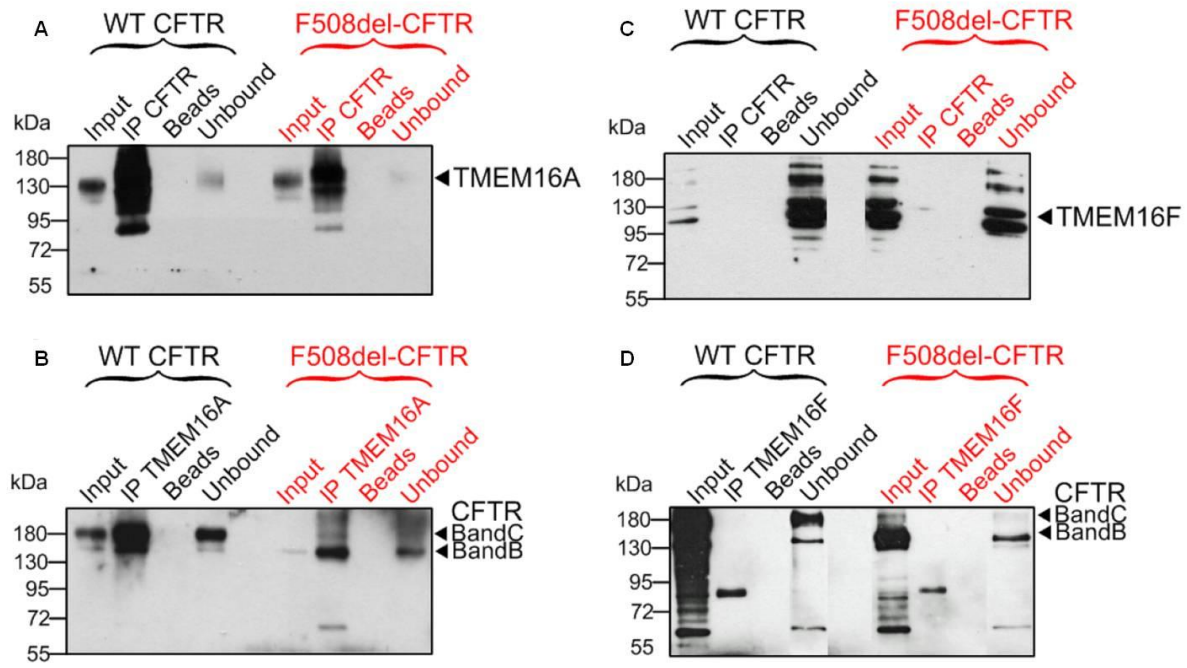

Fig 3.6 *Molecular interaction of TMEM16A and CFTR.*

A, B) Coimmunoprecipitation of CFTR and TMEM16A overexpressed in HEK293 cells. CFTR was pulled down by anti-CFTR antibody (Alomone labs, # ACl 006), while TMEM16A was pulled down by mouse monoclonal TMEM16A-antibody (Geneway GWB-MP178G). Both wt-CFTR and F508del-CFTR were found to interact with TMEM16A. Assays were performed in triplicates. C, D) No coimmunoprecipitation was detected for CFTR and TMEM16F when experiments were performed under identical conditions using a TMEM16F antibody (Davids technology, Regensburg). White lines in the right blot indicate that lanes for unbound protein present on the same gel, have been relocated. Mean +/- SEM; #indicates significant difference ($p<0.05$; unpaired t-test). (number of experiments).

Discussion

We demonstrate a complete absence of cAMP-activated Cl^- transport and a lack of Ca^{2+}-dependent Cl^- secretion in large intestine and trachea from adult conditional TMEM16A knockout mice. A disturbed cAMP-dependent transport was not found in airways of conventional TMEM16A knockout pups[164, 177], confirming the somewhat different physiology of neonatal vs. adult airways[188]. Somewhat surprising the complete absence of Cl^- currents in TMEM16A knockout tissues did not cause any overt phenotype. Mouse airways lacking TMEM16A did not show any mucus accumulation, which may support the concept that airway Na^+ transport is physiologically more relevant than Cl^- secretion in mouse airways[188]. The data show that most (Ca^{2+} and cAMP-dependent) murine airway Cl^- secretion depends on TMEM16A, with little contribution of CFTR[175, 188]. This is somewhat surprising since TMEM16A is expressed at very low levels in (non-inflamed) murine airways[152, 189].

Ruffin and coworkers found reduced TMEM16A-currents in mouse and human CF bronchial epithelium[190]. Our data obtained in human CFBE cells demonstrate a pronounced inter-dependence between CFTR and TMEM16A, in terms of membrane expression as well as activation of ion currents (Figs. 3.4,3.5,). Moreover, we were not able to discriminate clearly between CFTR and TMEM16A current based on ion channel inhibitors. The data demonstrate a remarkable overlap of cAMP and Ca^{2+}-dependent signaling and are in line with studies reporting Ca^{2+}-activated secretion through CFTR[161, 162, 176, 191] and cAMP-depending Ca^{2+} signaling controlling CFTR-mediated serous cell fluid secretion in porcine and human airways[192].

Although ATP might be released during activation of CFTR and may activate $P2Y_2$ receptors, this is unlikely to explain the present results, as activation of CFTR was not inhibited by the

$P2Y_2$ blocker suramin (100 µM), or by hydrolyzing extracellular ATP with apyrase (2 U/ml) (data not shown). In fact, the present data demonstrate a mechanism through which TMEM16A facilitates local Ca^{2+} signals that are required for activation of apical CFTR (and probably basolateral K^+ channels) [79, 80, 160]. Because TMEM16A facilitates ER Ca^{2+} store release, it may induce store-operated cAMP signaling[184], which has been shown to control Ca^{2+} activated Cl^- secretion in T84 colonic epithelial cells[185] (Fig 4j). Moreover, further evidence is provided for a central role of Ca^{2+} activated adenylate cyclases[162] (Fig 3.4 K).

In contrast to mouse airways expression of CFTR is pronounced in mouse large intestine, where it was found to be fully dependent on the presence of TMEM16A. Intestinal knockout of TMEM16A eliminated cAMP and Ca^{2+} activated Cl^- currents in colonic epithelial cells, again without causing intestinal obstructions. This is explained by the fact that cAMP-activated Cl^- currents were still present in the jejunum. Jejunal epithelial cells do not express TMEM16A and do not produce Ca^{2+} dependent, i.e. CCH induced Cl^- currents (Fig S3.6) [188]. Jejunal epithelial cells obviously do not require TMEM16A for activation or membrane insertion of CFTR, which may suggest the role of another TMEM16 protein. Noteworthy, cAMP-activated currents were found to be reduced in jejunal epithelial cells from TMEM16K-/- mice[193]. Our results also explain Ca^{2+} dependent Cl^- and HCO_3^- transport by CFTR in mouse intestine and other tissues[194-197].

The present data suggest that TMEM16A is required for proper expression of CFTR in the plasma membrane (Fig 3.5, Fig S3.1, 3.3). Interaction of TMEM16A and CFTR in a functional signaling compartment at the plasma membrane may require the help of PDZ-proteins[198] (Fig S3.5 C-F). TMEM16A has been shown to interact with IP3 receptors in a functional compartment also containing G-protein coupled receptors [80, 126]. The present data add CFTR to such a compartment as it may be colocalized and interact directly or through PDZ proteins with TMEM16A. Due to the functional interaction of both proteins and cAMP/Ca^{2+}-crosstalk, inhibitors for TMEM16A (e.g. CaCC-AO1) and CFTR (e.g. CFTRinh172) may be of limited use to dissect signaling pathways and the contribution of each channel to Cl^- transport in highly differentiated tissues[162, 199].

Acknowledgements

Supported by DFG SFB699-A7/A12, DFG KU756/12-1, and Cystic Fibrosis Trust SRC 003, INOVCF (to K.K.) and NIH UH2-HL123429, U19-AI070412, and R01-HL121791 (to M.J.H.).

Supplementary material

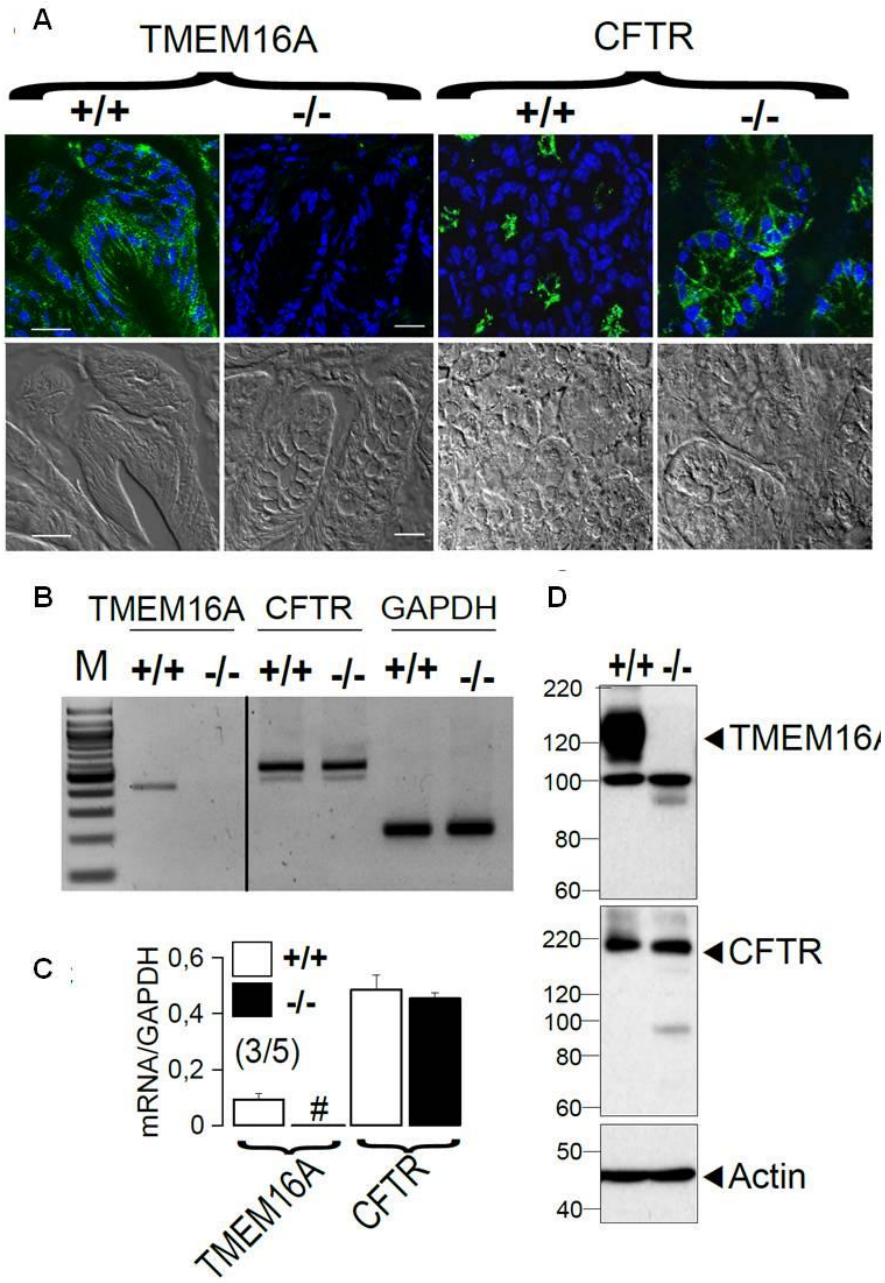

Supplementary Figure 3.1 *Expression of TMEM16A and CFTR in intestinal epithelial cells from Vil1-Cre-TMEM16A$^{wt/wt}$ ($^{+/+}$) and Vil1-Cre-TMEM16A$^{flox/flox}$ ($^{-/-}$) mice.*

A) Immunocytochemistry of TMEM16A and CFTR in large intestinal epithelial cells from wild type mice ($^{+/+}$) and mice with an epithelial cell specific knockout of TMEM16A ($^{-/-}$) (upper panel). Differential interference contrast images of the tissues (lower panels). Note that deletion of TMEM16A caused a cellular redistribution of CFTR away from the apical and towards the lateral plasma membrane and cytosolic compartments. Bar indicates 20 µm. B) RT-PCR analysis of expression of TMEM16A and CFTR in isolated large intestinal epithelial cells. C) Semiquantitative analysis of mRNA expression (relative to GABDH). D) Western blots of TMEM16A and CFTR from isolated intestinal crypts of ($^{+/+}$) and ($^{-/-}$) mice. Mean ± SEM, (n) number of animals (wt/KO). # significant difference when compared to +/+ (unpaired t-test).

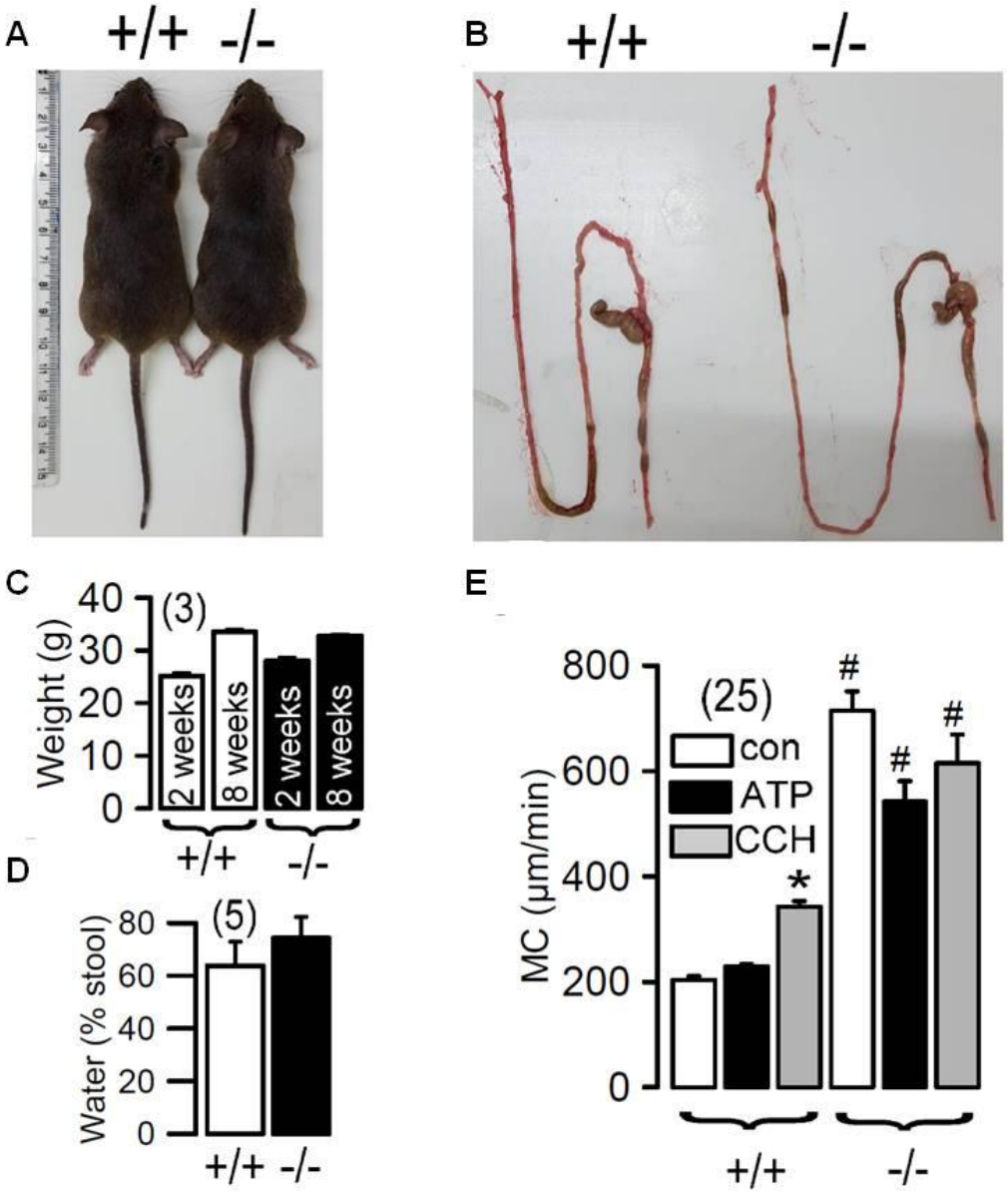

Supplementary Figure 3.2 *Lack of pathology in Vil1-Cre–TMEM16A$^{wt/wt}$ ($^{+/+}$) and Vil1-Cre–TMEM16A$^{flox/flox}$ ($^{-/-}$) mice.*

A) Size of wild-type mice ($^{+/+}$) and mice with an intestinal epithelial specific knockout of TMEM16A ($^{-/-}$). B) Overall appearance of the intestine without obvious abnormalities in -/- mice. C) Weight increase in *($^{+/+}$)* and *($^{-/-}$)* mice. D) Percentage stool water content in samples from *($^{+/+}$)* and *($^{-/-}$) mice*. E) Mucociliary clearance (MC) measured by particle transport in isolated mouse tracheas placed in humidified chambers, as described earlier [131]. MC was assessed under control conditions and after stimulation with 100 µM ATP (luminal) or 100 µM carbachol (basolateral). Mean ± SEM, (n) number of animals. * significant increase by CCH (paired t-test). $^{\#}$ significant difference when compared to ($^{+/+}$) mice.

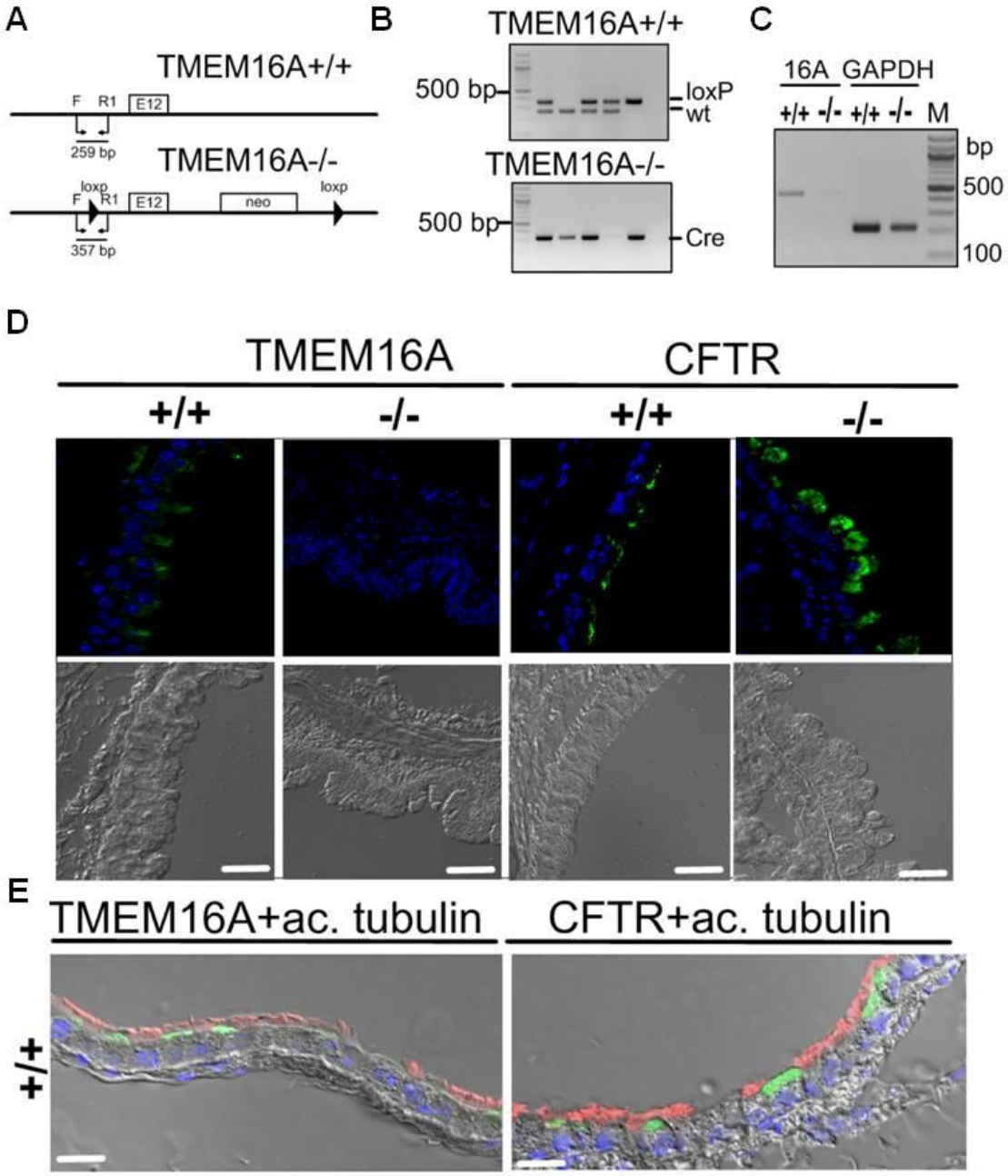

Supplementary Figure 3.3 *Expression of TMEM16A and CFTR in airway epithelial cells from TMEM16A$^{+/+}$ and TMEM16A$^{-/-}$ mice.*

A) Scheme indicating the loxP sites to generate $^{-/-}$ mice. B, C) Genotyping protocol and RT-PCR analysis of TMEM16A (16A) expression in epithelial cells. D) Immunocytochemistry of TMEM16A and CFTR in TMEM16A$^{+/+}$ and TMEM16A$^{-/-}$ mice. Note the more diffuse staining of CFTR in TMEM16A$^{-/-}$. E) Immunocytochemistry of TMEM16A/CFTR and acetylated tubulin suggesting heterogeneous expression of TMEM16A and CFTR and partial colocalization. Bar indicates 20 µm.

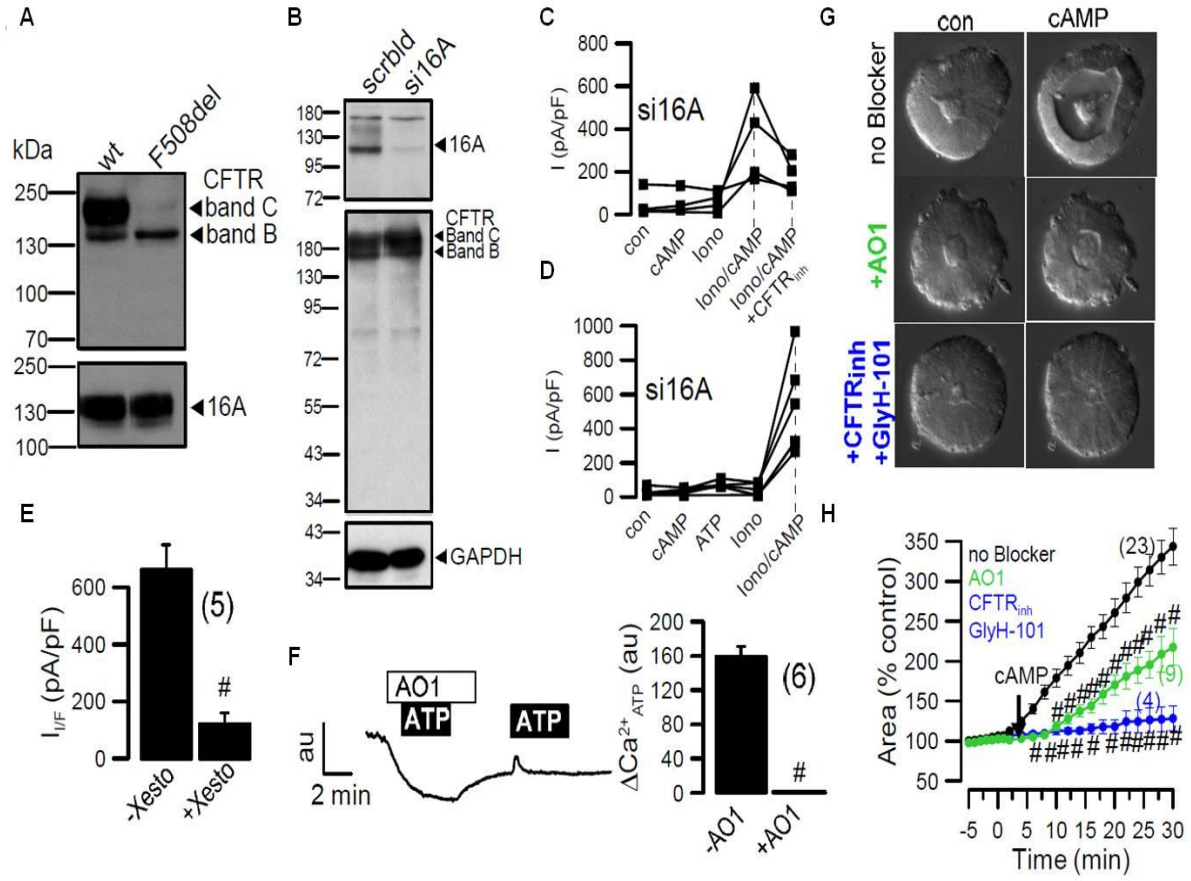

Supplementary Figure 3.4 *CFTR and TMEM16A (16A) dependent Cl⁻ transport cannot be separated.* A) Western blots of 16A and wt-CFTR or F508del-CFTR in stably expressing bronchial epithelial cells (CFBE). Expression levels for 16A are similar in both wt-CFTR or F508del-CFTR expressing cells. B) siRNA-knockdown of 16A (si16A) in CFBE cells does not affect expression of CFTR as shown by Western blotting. C, D) Continuous recording of whole cell current density in CFBE cells with siRNA-knockdown of 16A (si16A). Note that both IBMX/Forskolin (100 µM/2 µM; cAMP) and ionomycin (C, 1 µM; Iono) or ATP (D, 100 µM) induced currents are inhibited by knockdown of TMEM16A (16A). In the presence of ionomycin, cAMP is able to activate whole cell currents, which are inhibited by $CFTR_{inh}172$. E) IBMX/Forskolin (100 µM/2 µM) activated CFTR currents are inhibited by the IP_3R-inhibitor Xestospongin (50 µM; Xesto). F) ATP (100 µM) induced Ca^{2+} transients as measured by GCAMP6 fused to CFTR, were completely suppressed by TMEM16A inhibitor AO1 (10 µM). Original recording (left) and summary of ATP induced Ca^{2+} changes (right). G, H) Organoids grown from T84 colonic epithelial cells demonstrate secretion upon stimulation with cAMP. Secretion is inhibited by AO1 (10 µM) as well as $CFTR_{inh}172$ (10 µM). Mean ± SEM, (n) number of cells. # significant difference when compared to absence of blocker (unpaired t-test).

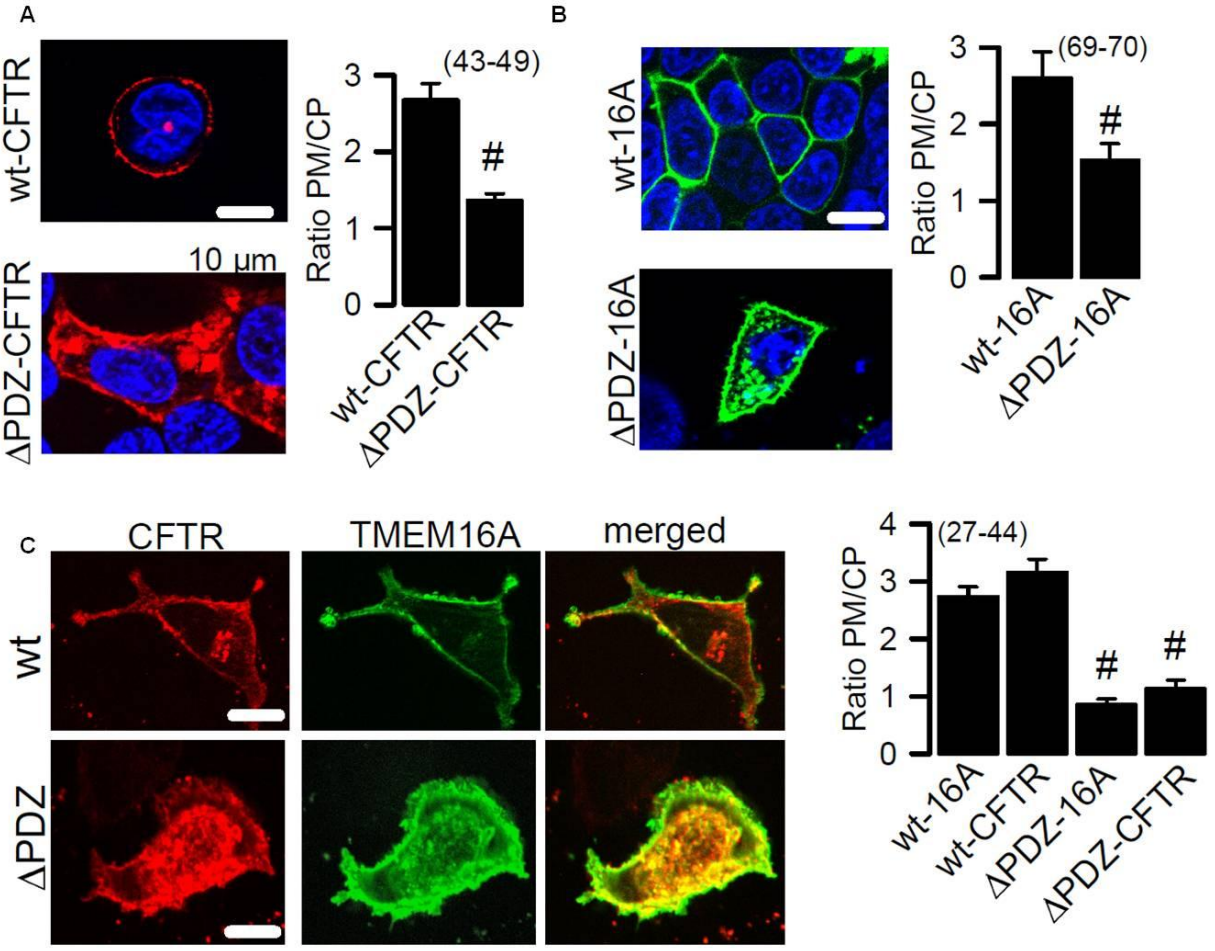

Supplementary Figure 3.5 *Plasma membrane expression of CFTR depends on TMEM16A (16A) containing a PDZ-binding domain***.**

A, B) Immunocytochemistry of Cherry-CFTR and GFP-TMEM16A (16A) expressed in CFBE parental cells. Expression of wild type CFTR and TMEM16A (16A), respectively, or expression of truncated proteins, in which the C-terminal PDZ-binding motifs DTRL (ΔPDZ-CFTR) and GGVL (ΔPDZ-16A) were removed. Plasma membrane expression (PM) and cytoplasmic expression (CP) of wt and truncated proteins (ΔPDZ) were quantified by measuring fluorescence intensities in the region of interest, and ratios (PM/CP) were calculated. Plasma membrane expression of ΔPDZ-CFTR and ΔPDZ-16A were significantly reduced when compared to wt-proteins containing PDZ-binding motifs. C) Coexpression of ΔPDZ-CFTR and ΔPDZ-16A leads to further decrease in membrane expression of CFTR and TMEM16A. Mean +/- SEM; #indicates significant difference compared to wt ($p<0.05$; unpaired t-test). (number of experiments).

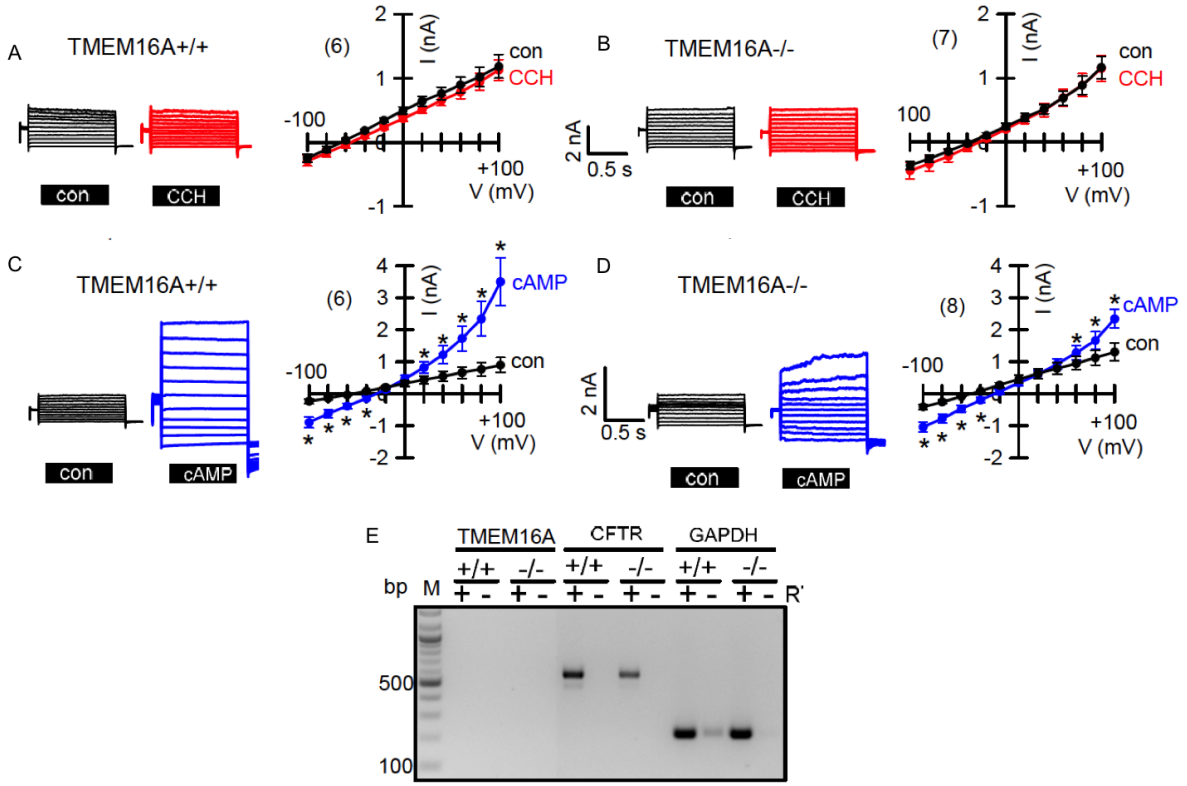

Supplementary Figure 3. 6 *TMEM16A and CFTR in jejunum of Vil1-Cre–TMEM16A$^{wt/wt}$ ($^{+/+}$) and Vil1-Cre–TMEM16A$^{flox/flox}$ ($^{-/-}$) mice.*

A, B) Whole cell patch clamp recordings with isolated jejunal epithelial cells. Carbachol (CCH, 100 µM) does not activate Cl^- currents in cells from wt or ($^{-/-}$) mice in the presence of TRAM-34 (50 nM), an inhibitor of Ca^{2+} activated K^+ currents. C, D) Activation of whole cell currents by increase in intracellular cAMP (100 µM IBMX, 2 µM Forskolin) in jejunal epithelial cells. Mean ± SEM, (n) number of assays. *indicates significant activation by cAMP (paired t-test). E) RT-PCR analysis in isolated jejunal epithelial cells indicating the absence of TMEM16A mRNA in $^{+/+}$ and $^{-/-}$ cells. The somewhat reduced cAMP-activated currents in $^{-/-}$ cells might be explained by the lower levels of CFTR expression.

Chapter 4

Compartimentalized Crosstalk of CFTR and TMEM16A (ANO1)Through EPAC1 and ADCY1

Abstract

Airway epithelial cells express both Ca^{2+} activated TMEM16A/ANO1 and cAMP activated CFTR anion channels. Previous work suggested a significant crosstalk of intracellular Ca^{2+} and cAMP signaling pathways, leading to activation of both chloride channels. We demonstrate that in airway epithelial cells, stimulation of purinergic or muscarinic G-protein coupled receptors (GPCRs) activates TMEM16A and CFTR. Additional expression of $G_{q/11}$ and phospholipase C coupled GPCRs strongly enhanced the crosstalk between Ca^{2+}- and cAMP-dependent signaling. Knockdown of endogenous GRCRs attenuated crosstalk and functional coupling between TMEM16A and CFTR. The number of receptors did not affect expression or membrane localization of TMEM16A or CFTR, but controlled assembly of the local signalosome. GPCRs translocate Ca^{2+}-sensitive adenylate cyclase type 1 (ADCY1) and exchange protein directly activated by cAMP (EPAC1) to particular plasma membrane domains containing GPCRs, CFTR and TMEM16A, thereby producing compartmentalized Ca^{2+} and cAMP signals and significant crosstalk. While biosynthesis and membrane trafficking of CFTR requires a functional Golgi apparatus, maturation and membrane trafficking of TMEM16A may occur independent of the Golgi. Ca^{2+} activated TMEM16A currents are only transient. Thus, efficient Cl^- secretion by airway epithelial cells requires CFTR. The present data explain why receptor-dependent activation of TMEM16A is more efficient than direct stimulation by Ca^{2+}.

Key words: CFTR, TMEM16A, anoctamin 1, Ca^{2+} activated Cl^- channel, cAMP, Ca^{2+} sensitive adenylate cyclase 1, ADCY1, exchange protein directly activated by cAMP, EPAC1

Published in: Joana Lérias, Madalena Pinto, **Roberta Benedetto**, Rainer Schreiber, Margarida Amaral, MassimoAureli, Karl Kunzelmann. Compartmentalized Crosstalk of CFTR and TMEM16A (ANO1) Through EPAC1 and ADCY1. Cellular Signaling. 2018 Apr;44:10-19.
Own experimental contribution: Part of patch clamp experiments.
Own written contribution: Part of Methods and Results.
Other contributions: Designed experiments and analyzed data.

Introduction

TMEM16A (Anoctamin 1, ANO1) is a Ca^{2+} activated chloride (Cl^-) channel [55, 56, 113]. In their groundbreaking publication Yang et al. reported receptor-activated and Ca^{2+}-dependent Cl^- currents conferred by TMEM16A [113]. We regularly observed larger ATP-activated TMEM16A currents in the presence of additional purinergic $P2Y_2$ receptors, although ATP-induced increase in intracellular Ca^{2+} was not changed by additional receptors [149]. This suggests i) that ATP-induced Ca^{2+} signals take place within a well shielded plasma membrane domain/compartment and ii) that additional mechanisms for receptor-channel coupling may exist in such a compartment.

We reported earlier that in *Xenopus* oocytes the Cl^- ion channel Cystic Fibrosis transmembrane conductance regulator (CFTR) is activated through stimulation of purinergic $P2Y_2$ receptors [191]. Recent work also demonstrated activation of CFTR by purinergic stimulation of airway epithelial cells [162, 200]. Thus CFTR may serve as Cl^- secretory pathway for Ca^{2+} enhancing agonists, probably via Ca^{2+}-sensitive adenylate cyclase [162, 200]. Also other G-protein coupled receptors (GPCRs) such as muscarinic receptors can activate CFTR via increase in intracellular cAMP, by the help of tyrosine kinases [176]. An intimate relationship between TMEM16A and CFTR has been suggested earlier [172], and was demonstrated recently in TMEM16A-knockout mice, which exhibit both compromised Ca^{2+}-dependent and cAMP-activated Cl^- transport [200]. Here we provide for the first time evidence for a colocalization of GPCRs, CFTR and TMEM16A in functional membrane compartments/microdomains together with Ca^{2+}-sensitive adenylate cyclase type 1 (ADCY1) and exchange protein directly activated by cAMP (EPAC1). Compartmentalization of these signaling molecules will provide intense crosstalk between Ca^{2+} and cAMP signals, and explains parallel activation of the chloride channels CFTR and TMEM16A.

Materials and Methods

Cells, cDNA, transfection, RT-PCR. CFBE cells stably overexpressing WT-CFTR or F508del-CFTR and expressing endogenous TMEM16A were cultured in MEM-Eagle's

Minimum Essential Media with L-Glutamine supplemented with 10% (v/v) heat inactivated fetal bovine serum (FBS) and 2 µg/ml puromycin (Invitrogen).

Cells were transfected with cDNA for purinergic $P2Y_2$ receptors ($P2Y_2R$) or muscarinic M3 receptors (M3R) or siRNA for $P2Y_2R$ as described earlier. For semiquantitative RT-PCR, total RNA was isolated from CFBE cells using NucleoSpin RNA II columns (Macherey-Nagel, Düren, Germany). Total RNA (1 µg / 50 µl reaction) was reverse-transcribed using random primers and M-MLV reverse transcriptase (Promega, Mannheim, Germany). Each RT-PCR reaction contained sense and antisense primers for the respective gene (0.5 µM) or for GAPDH (0.5 µM), 0.5 µl cDNA and GoTaq Polymerase (Promega, Mannheim, Germany). After 2 min at 95°C cDNA was amplified during 30 cycles for 30 s at 95°C, 30 s at 56°C and 1 min at 72°C. PCR products were visualized by loading on agarose gels containing peqGREEN DNA/RNA Dye (Peqlab Biotech) and analysed using Meta Morph Vers. 6.2 (Molecular Devices, USA). Experiments were performed 48h or 72h after the transfection.

Immunocytochemistry. Transfected CFBE cells were fixed for 10 min with methanol/acetone (4:1) (v/v) at -20 ºC. Cells were washed 3 times with PBS and afterwards incubated for 30 min at 37ºC with PBS supplemented with 1% Bovine serum albumin (BSA) and 0.04% Triton-X to block and permeabilize the cells, respectively. Cells were incubated for 1h at room temperature with primary rabbit DOG1 antibody (Novus Biologicals, # NP_060513) diluted to 1:200 in PBS supplemented with 1% BSA. Cells were washed 3 times with PBS and incubated with the secondary antibody Alexa Fluor 488–conjugated donkey anti-rabbit IgG (1:300; Thermo Fisher Scientific) and 0.1 mg/ml Hoechst 33342 (1:200; Aplichem, Darmstadt, Germany) for 1h at room temperature. Coverslips were mounted with fluorescence mounting medium (Dako Cytomation, Hamburg, Germany). Immunofluorescence was detected with an Axiovert 200 microscope equipped with an ApoTome and analyzed with the profile measurement tool of AxioVision software (AxioVs40; V 4.8.2.0; Zeiss, Jena, Germany). For EPAC1 staining, a similar protocol was followed, though fixation was performed with PFA 4% (w/v) for 10 min at room temperature; cells were incubated overnight at 4ºC with primary antibody (Santa Cruz, # sc_28366) (1:100) and

incubated with the secondary antibody Alexa Fluor 546–conjugated donkey anti-mouse IgG (1:300; Thermo Fisher Scientific) and 0.1 mg/ml Hoechst 33342 (1:200; Aplichem, Darmstadt, Germany) for 1h at room temperature.

Western blotting. CFBE cells were collected and lysed in 0.5% (v/v) NP40 lysis buffer. Proteins were separated by 7% (w/v) SDS-PAGE and transferred into Nitrocellulose membranes (0,45 µm; BIORAD, # 162-0115). The membranes were blocked with 5% (w/v) nonfat milk powder (NFM) in Tris buffer saline with 0.1 % Tween 20 (TBS-T) for 1 h at room temperature and incubated overnight at 4°C with rabbit DOG1 antibody (Novus Biologicals, # NP_060513) (1:500 in 1% (w/v) NFM/TBS-T) and rabbit anti β-Actin (1:10000 in 1%NFM/TBS-T) (Sigma, A2066). The membranes were incubated with horseradish peroxidase (HRP)-conjugated goat anti-rabbit IgG (diluted 1:10000 in 1% NFM/TBS-T) for 2h at room temperature. Signals were detected using a SuperSignal West Pico chemiluminescence substrate (Thermo Fisher Scientific). Experiments were performed in triplicate.

***Immunoprecipitation*.** For immunoprecipitation (pull down) of TMEM16A by $P2Y_2R$ cell lysate was prepared using 1% Triton X100 in TNEV, followed by mechanical homogenization and centrifugation to eliminate nuclei and cellular debris. 20 µg loaded. Lysate was precleared by incubation of the input for 2h with Protein-A and Protein-G conjugated beads. 15 of 50 µl (~20 µg) were loaded onto gels. 500 µg protein was subjected to immunoprecipitation of TMEM16A using 6 µl of anti-TMEM16A (Dog1) overnight, 15 of 50 µl were loaded onto the gel. Unbound protein was detected by loading the supernatant (15 µl) remaining after IP.

Patch Clamping. Cells were grown on coated glass cover slips. Patch pipettes were filled with a cytosolic-like solution containing KCl 30, K-gluconate 95, NaH_2PO_4 1.2, Na_2HPO_4 4.8, EGTA 1, Ca-gluconate 0.758, $MgCl_2$ 1.03, D - glucose 5, ATP 3, pH 7.2. The intracellular (pipette) Ca^{2+} activity was 0.1 µM. Fast whole cell current recordings were performed as described recently [62]. The bath was perfused continuously with Ringer solution containing 50 nM TRAM34 (Abcam, ab141885) at a rate of 8 ml/min. Patch pipettes had an input resistance

of 2–4 MΩ and whole cell currents were corrected for serial resistance. Currents were recorded using a patch clamp amplifier (EPC 7, List Medical Electronics, Darmstadt, Germany), the LIH1600 interface and PULSE software (HEKA, Lambrecht, Germany) as well as Chart software (AD Instruments, Spechbach, Germany). In regular intervals, membrane voltage (*V*c) was clamped in steps of 20 mV from -100 to +100 mV from a holding voltage of -100 mV. Current density was calculated by dividing whole cell currents by cell capacitance.

Calcium measurements. CFBE cells were transfected on coated glass coverslips with pcDNA3.1-Pl-G-CaMP6 fused to the C-terminus of CFTR and were mounted in a perfusion chamber 72 h after transfection. Cells were perfused with Ringer solution at a rate of 8 ml/min at 37°C. Cell fluorescence was measured continuously with an inverted microscope Axiovert S100 (Zeiss) with a 340 objective (Fluar 340/1.3 oil; Zeiss) and a high-speed polychromator system (VisiChrome; Visitron, Puchheim, Germany). Pl-G-CaMP6 was excited at 485 and 405 nm. Emission was recorded between 520 and 550 nm with a CCD-camera (CoolSnap HQ; Visitron, Hauppauge, NY, USA). For Fura-2 experiments, CFBE cells were seeded on glass coverslips and loaded with 2 mM Fura-2-AM and 0.02% Pluronic F-127 (Life Technologies, Germany) in ringer solution (mmol l 1: NaCl 145; KH_2PO_4 0,4; K_2HPO_4 1,6; Glucose 5; $MgCl_2$ 1; Ca-Gluconat 1,3) for 1h at room temperature. Fluorescence was detected in cells perfused with Ringer's solution at 37ºC using an inverted microscope (Axiovert S100, Zeiss, Germany) and a highspeed polychromator system (VisiChrome, Germany). Fura-2 was excited at 340/380 nm, and emission was recorded between 470 and 550 nm using a CoolSnap camera (CoolSnap HQ, Visitron). Control of experiments, imaging acquisition, and data analysis were performed with the software package Meta-Fluor (Universal Imaging, New York, NY, USA). Measurements of global cytosolic Ca^{2+} concentrations by Fura-2 or measurements of compartmentalized Ca^{2+} levels in close proximity to the plasma membrane using GCAMP2, have been previously described in detail [80].

cAMP measurements. cAMP direct immunoassay Kit (abcam, ab138880) was used following the manufacturer's protocol. This assay is based on the competition between HRP-labeled cAMP and free cAMP present in the sample for cAMP antibody binding sites. Briefly,

F508del-CFTR/CFBE cells were treated either with IBMX (100µM)/ Forskolin (2µM) or ATP (100µM) and then, lysate and centrifuged in order to obtain the cAMP containing supernatant. The supernant was incubated in the cAMP antibody coated 96-well plate for 10 min and, after incubation; cAMP-HRP conjugated was added. The amount of cAMP-HRP bound to the plate was determined by reading HRP activity at OD450nm using a NOVOstar Microplate Reader (BMG LABTECH GmbH, Ortenberg, Germany). The intensity of OD450 nm is inversely proportional to the concentration of cAMP in samples and cAMP concentration was obtained using a standard curve with known cAMP-HRP concentrations.

Chemiluminescence measurements. For TMEM16A chemiluminescence, 3HA-TMEM16A-eGFP CFBE cells were seeded on coated black 96-well plates (Corning #3631) at a density of $8x10^3$ cells/well. On the following day, cells were induced with 1 µg/ml doxycycline and were transfected with the siRNAs targeting the genes of interest. 48h after the transfection, cells were washed once with ice cold PBS supplemented with 0.7 mM $CaCl_2$ and 1.1 mM $MgCl_2$. Then cells were incubated for 1h at 4˚C with monoclonal anti-HA (1:500). Then, cells were washed 3 times with ice cold PBS, incubated 10 min with 4% (w/v) paraformaldehyde (PFA) at 4°C and transferred to room temperature for the remaining staining procedure. Cells were then washed three times with PBS and incubated 1h at room temperature with a goat anti-mouse HRP-conjugated secondary antibody (1:5000). Signals were detected with SuperSignal West Pico chemiluminescence substrate (Thermo Fisher Scientific) using a NOVOstar Microplate Reader (BMG LABTECH GmbH, Ortenberg, Germany). All solutions were prepared in Dulbecco's PBS freshly supplemented with 0.7 mM $CaCl_2$ and 1.1 mM $MgCl_2$. Antibody solutions contained 1% (w/v) bovine serum albumin (BSA, Sigma-Aldrich #A9056). For F508del/WT-CFTR chemiluminescence, a similar protocol was followed. In this case, CFBE mCherry-flag-F508del/Wt-CFTR were used and incubated only with anti-flag-HRP conjugated (1:1000) for 1h at 4˚C before fixation with PFA 4% (w/v).

Statistical Analysis. Data are reported as means ± SEM. Student's *t* test (for paired or unpaired samples as appropriate) or ANOVA were used for statistical analysis. A value of $P<0.05$ was accepted as a significant difference.

Results

G-protein coupled receptors control activation of the Ca^{2+} dependent Cl^- channel TMEM16A.

In human airway epithelial cells expressing wild type CFTR (WT-CFTR/CFBE) stimulation of $P2Y_2$ receptors ($P2Y_2R$) with ATP (100 µM) activates whole cell currents (Fig 4.1 A, B). Expectedly, siRNA-knockdown of $P2Y_2R$ ($siP2Y_2$; Fig S 11A) inhibited activation of currents by ATP, but surprisingly also attenuated direct activation by the Ca^{2+} ionophore ionomycin (IONO) (Fig 4.1 C). However, increase in intracellular Ca^{2+} ($[Ca^{2+}]_i$) by IONO was not affected by $siP2Y_2R$, in contrast to ATP-induced $[Ca^{2+}]_i$ (Fig 4.1 D,E). Overexpression of $P2Y_2R$ in CFBE cells expressing WT-CFTR or F508del-CFTR, dramatically enhanced Cl^- currents activated by ATP as well as by IONO (Fig 4.1 F, G), while global cytosolic $[Ca^{2+}]_i$ increase by ATP and IONO were not affected (Fig 4.1 H, I). The effect of additional $P2Y_2R$ on current increase was remarkably bigger in cells expressing WT-CFTR than F508del-CFTR (Fig 4.1F, G). Very similar results were obtained by overexpressing muscarinic M3 receptors (M3R), which are not expressed endogenously in CFBE cells. Expression of M3R not only induced carbachol-activated whole cell currents, but unexpectedly also enhanced ATP-activated currents (Fig S4.1 B, C). Finally, stimulation of histamine H1 receptors, another type of phospholipase C (PLC)- coupled GPCR, activated larger whole cell currents in cells overexpressing $P2Y_2R$ (Fig S4.1 D). These experiments suggest that i) expression of $G_{q/11}$ and PLC-coupled GPCRs translocates additional signaling proteins to the plasma membrane (PM) to activate Cl^- currents, and that ii) Ca^{2+}-dependent whole cell current are strongly CFTR-dependent [200]. Additional proteins are probably required to assemble the signalosome, such a scaffold proteins. In further preliminary experiments we found that siRNA-knockdown of Na^+/H^+ Exchanger Regulatory Factor 1 (NHERF1) attenuated both CFTR and TMEM16A-related Cl^- currents [201].

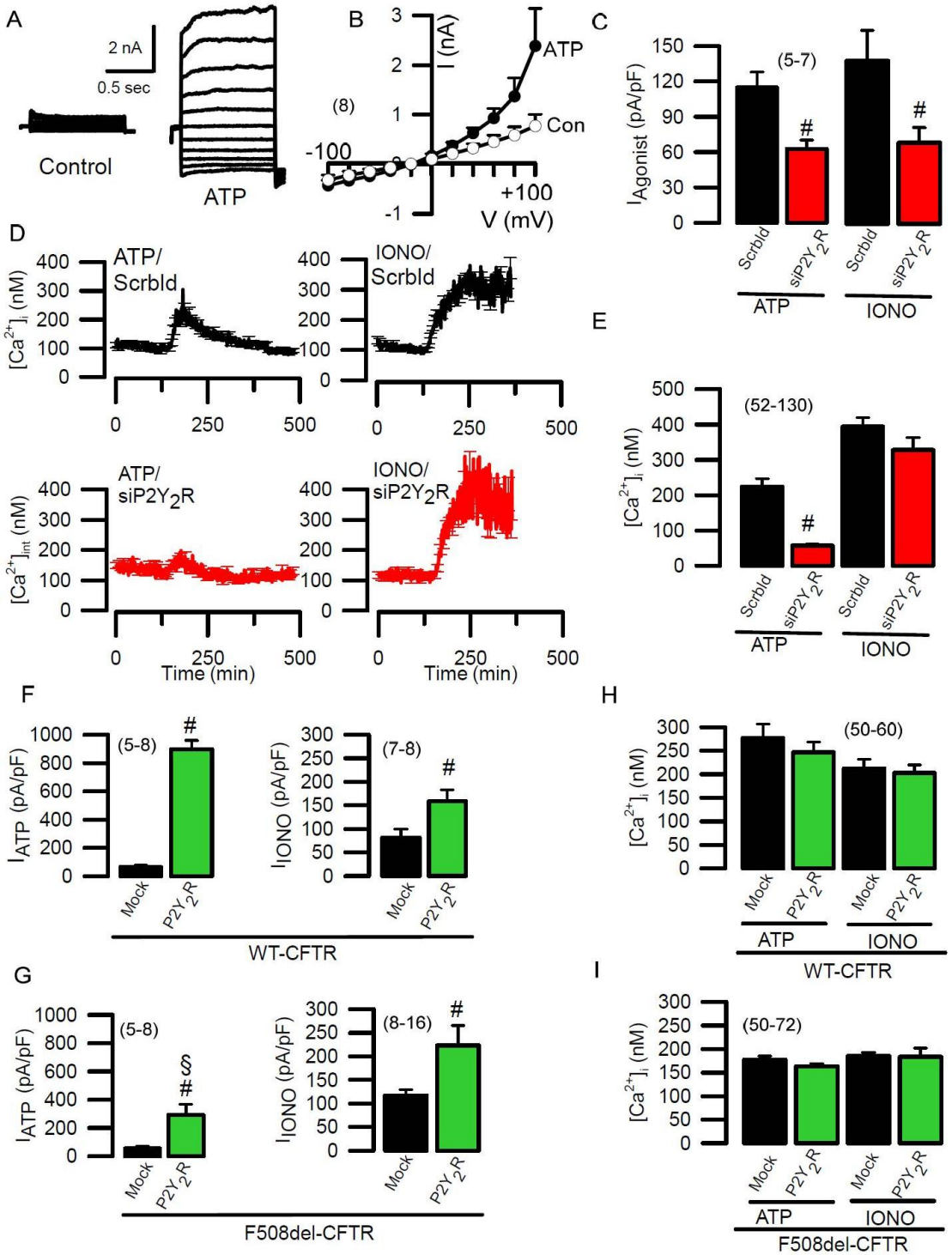

Fig 4.1 *$P2Y_2$ G-protein coupled receptors control activation of the Ca^{2+} dependent Cl^- channel TMEM16A.*

A) Whole cell currents activated by ATP (100 µM) in CFBE airway epithelial cells. B) Corresponding current/voltage relationships. C) Activation of TMEM16A by ATP (100 µM) or ionomycin (IONO; 0.1 µM). Summary of current densities in cells treated with scrambled RNA (Scrbld) or siRNA for P2Y2 receptors (siP2Y2R). ATP- and IONO-dependent activation of TMEM16A was inhibited by knockdown of $P2Y_2R$. D) Increase in intracellular Ca^{2+} ($[Ca^{2+}]i$) by stimulation with ATP or IONO, as measured by Fura-2 (mean curves ± SEM). E) Summary of $[Ca^{2+}]i$ indicates no inhibition of IONO-induced increase in $[Ca^{2+}]i$ by knockdown of P2Y2R. In contrast, ATP-induced $[Ca^{2+}]i$ increase was reduced. F)

Overexpression of P2Y2R largely augmented ATP (100 µM)-induced TMEM16A currents and doubled IONO-activated TMEM16A currents in WT-CFTR/CFBE cells. G) Overexpression of P2Y2R in F508del-CFTR/CFBE cells caused a smaller increase in ATP/IONO-activated whole cell currents. H, I) Expression of additional $P2Y_2R$ did not change intracellular Ca^{2+} signals in WT-CFTR/CFBE or F508del-CFTR/CFBE cells. Mean ± SEM (number of experiments). # significant difference when compared to Scrbld or Mock ($p < 0.05$, unpaired t-test). § significantly smaller than in WT-CFTR ($p < 0.05$, unpaired t-test).

CFTR but not GPCRs affect membrane expression of TMEM16A.

CFTR and/or $P2Y_2R$ may affect activation of whole cell currents by changing expression levels or PM localization of TMEM16A. However, similar levels of TMEM16A were found with knockdown or overexpression of $P2Y_2R$ in CFBE/WT-CFTR and F508del-CFTR/CFBE cells or in HEK293 cells (Fig 4.2 A, B, Fig S4.1 E). Moreover, membrane expression of TMEM16A was not affected by knockdown or overexpression of $P2Y_2R$, when analyzed by immunofluorescence or chemiluminescence (Fig 4.2 C-H, Fig S 4.1 F). Membrane expression of TMEM16A was also not changed by overexpression of M3R, but was generally lower in F508del-CFTR/CFBE cells (Fig 4.2 C-H, Fig S4.1 G).

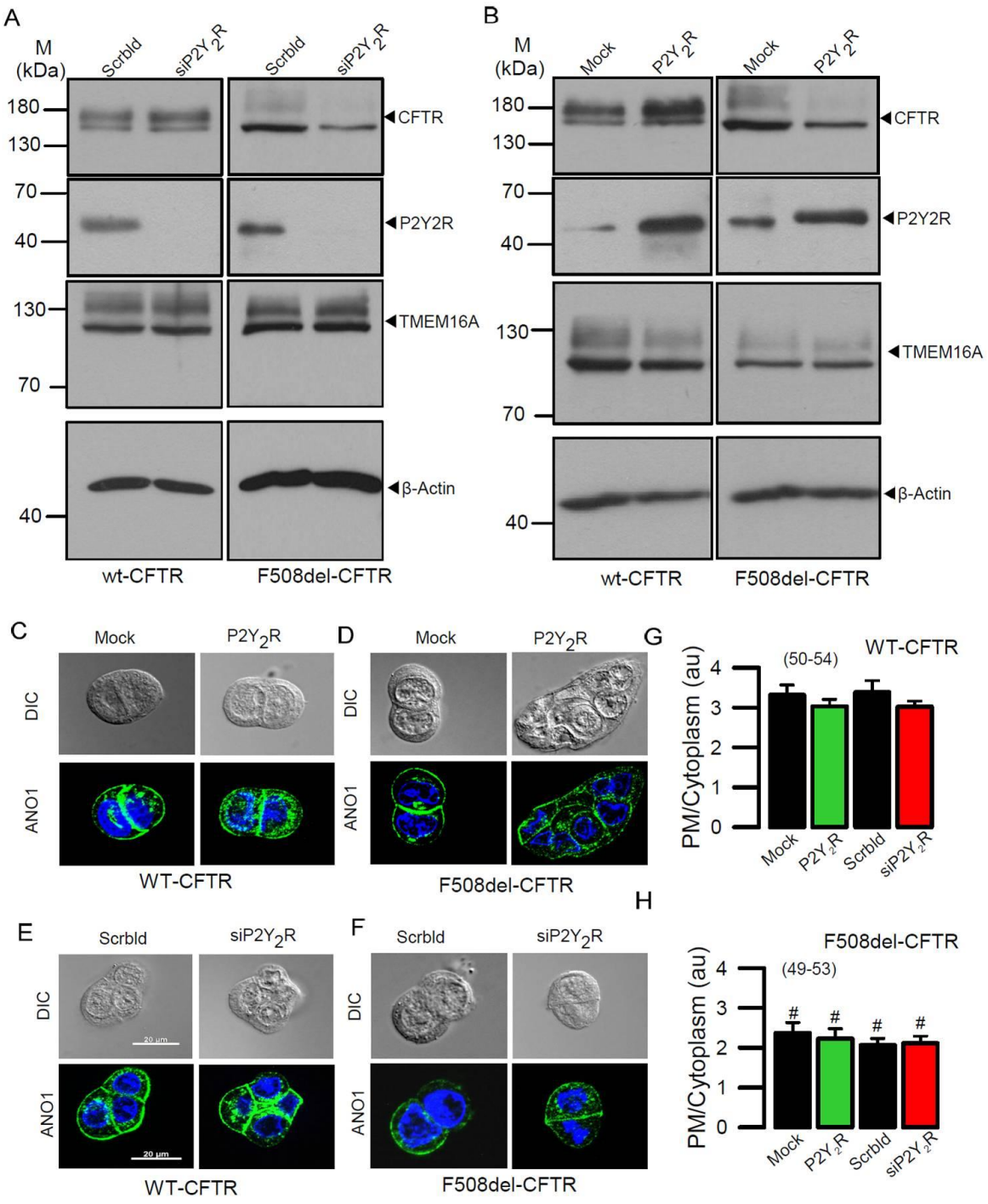

Fig 4.2 *$P2Y_2R$ do not change expression and localization of TMEM16A*.

A, B) Western blots showing expression of CFTR, $P2Y_2R$ and TMEM16A. ß-acting is shown as gel loading control. Similar expression levels were detected for TMEM16A in WT-CFTR/CFBE and F508del-CFTR/CFBE cells. siRNA-knockdown of $P2Y_2R$ or overexpression of $P2Y_2R$ had no clear effects on TMEM16A expression. C-F) Immunofluorescence of TMEM16A in WT-CFTR/CFBE and F508del-CFTR/CFBE cells. siRNA-knockdown of $P2Y_2R$ or overexpression of $P2Y_2R$ had no obvious effect on cellular localization of TMEM16A. G, H) Analysis of cellular distribution of TMEM16A in WT-CFTR/CFBE and F508de-CFTR/CFBE cells by quantitative assessment of fluorescence in plasma membrane/cytoplasm (au; arbitrary units). Bars indicate 10 µm. Mean ± SEM (number of experiments). # significant difference when compared to WT-CFTR ($p < 0.05$, unpaired t-test).

Purinergic receptors augment CFTR whole cell currents.

We found that the presence of $P2Y_2R$ not only enhances ATP- and IONO-activated Cl^- currents (Fig 4.1), but also CFTR Cl^- currents stimulated with IBMX and Forskolin (I/F) (Fig 4.3 A-D). Notably, significant I/F activated Cl^- currents could even be detected in CFBE cells expressing F508del-CFTR, upon additional expression of $P2Y_2R$ (Fig 4.3 C,D). Expression of WT-CFTR and F508del-CFTR were not affected by knockdown or overexpression of $P2Y_2R$, when analyzed by immunofluorescence and chemiluminescence (Fig 4.3 E-L). WT-CFTR is well expressed in the PM, but not F508del-CFTR, and thus I/F should be unable to activate F508del-CFTR. However, I/F activated a whole cell current in F508del-CFTR expressing cells (Fig 4.3 C,D). We found that WT-CFTR currents activated by membrane permeable 8-Br-cAMP were largely independent of $P2Y_2R$, in contrast to activation by I/F (Fig 4.4 A). This result suggests that Ca^{2+}-dependent adenylate cyclases are translocated to the plasma membrane by $P2Y_2R$. We also noticed that 8-Br-cAMP activated a small, albeit significant Cl^- current in CFBE cells expressing F508del-CFTR. This current demonstrated a TMEM16A-typical time dependent activation and outward rectification (inset in Fig 19A), and is therefore not a CFTR-current. Activation of this current by 8-Br-cAMP was abolished by knockdown of $P2Y_2R$ (Fig 4.4 A). These results strongly suggest that the 8-Br-cAMP signal has been converted most likely by EPAC1, into a Ca^{2+} signal, which activated TMEM16A. EPAC1 (also known as RAPGEF3) functions as a guanine nucleotide exchange factor (GEF) for both Rap1 and Rap2. EPAC1 may have been translocated to a plasma membrane compartment by $P2Y_2R$. In fact, 8-substituted cAMP derivatives such as 8-Br-cAMP or 8-pCPT-2-O-Me-cAMP (007-AM) are known to be potent activators of EPAC1 [199]. The current activated by 8-Br-cAMP or 8-pCPT-2-O-Me-cAMP (007-AM) was inhibited by the TMEM16A-inhibitor AO1 (Fig 4.4 C). As an earlier study was unable to demonstrate a direct relation of TMEM16A by cAMP/TMEM16A, it is unlikely that 8-Br-cAMP directly activated TMEM16A [202].

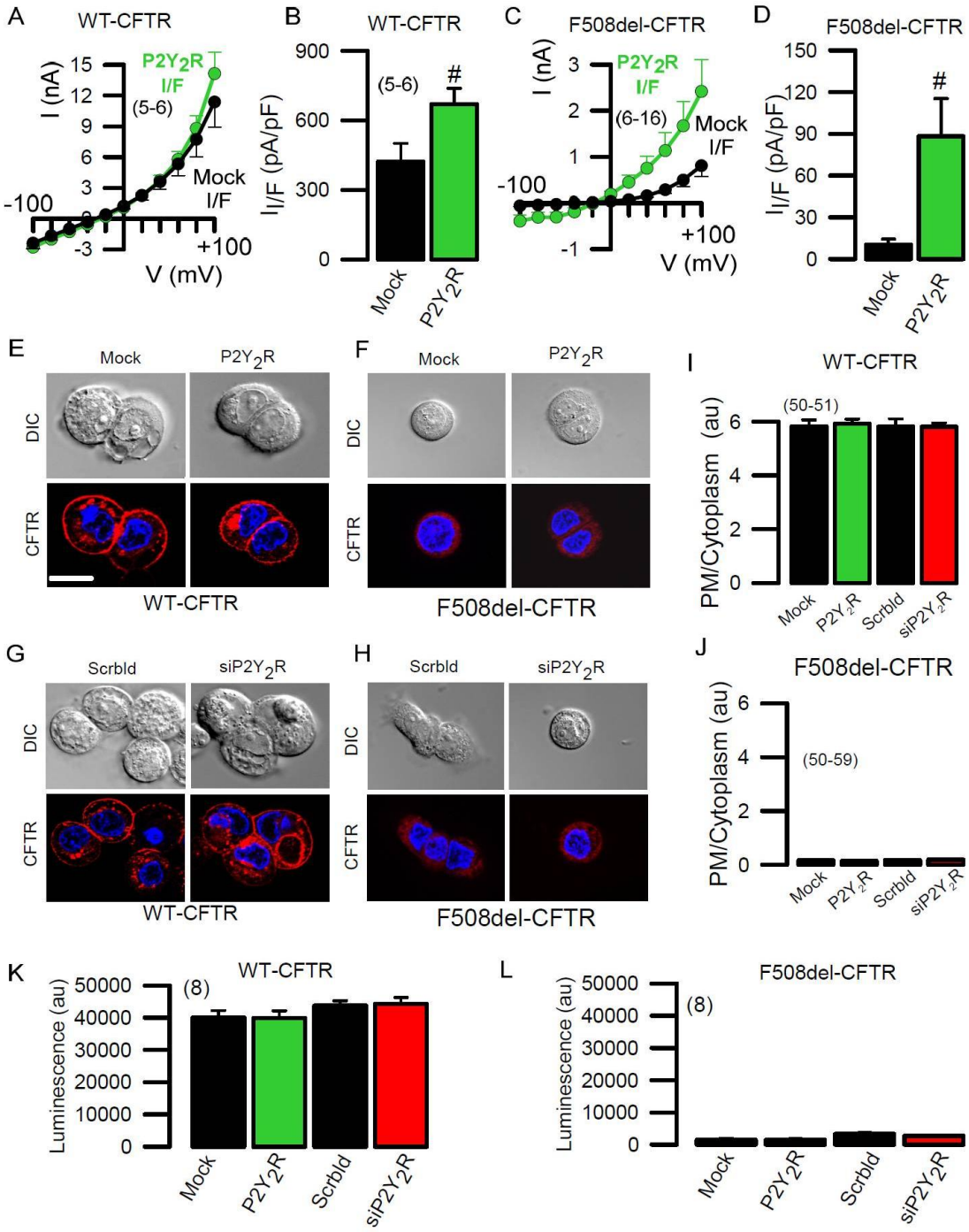

Fig 4.3 *P2Y$_2$R control activation of CFTR but not CFTR membrane expression.*

A-D) Current/voltage relationships and current densities from patch clamp experiments in mock transfected and P2Y$_2$R overexpressing wt-CFTR/CFBE cells and F508del-CFTR/CFBE cells. Cells were stimulated with 100 µM IBMX and 2 µM Forskolin (I/F). E, H) Expression of wt-CFTR and F508del-CFTR as detected by cherry-fluorescence (life imaging). P2Y$_2$R was overexpressed or endogenous P2Y$_2$R was knocked down by siP2Y$_2$R. I, J) Ratios for expression of wt-CFTR or F508del-CFTR in plasma membrane (PM) versus cytoplasm (au; arbitrary units). K, L) Membrane expression of wt-CFTR and F508del-CFTR as detected by chemiluminescence, using an extracellular FLAG tag inserted into the first extracellular loop of CFTR and an anti-FLAG antibody. Mean ± SEM (number of experiments). # significant difference when compared to mock ($p < 0.05$, unpaired t-test). Scale bar, 10

µm.

Role of EPAC1 for activation of Cl^- currents.

Expression of EPAC1 was well detected in CFBE cells (Fig 4.4 B). Using the EPAC1 activator 007-AM, whole cell Cl^- currents were activated in WT-CFTR/CFBE cells that were strongly inhibited by removal of extracellular Cl^- ($5Cl^-$). Both TMEM16-inhibitor $CaCC_{inh}AO1$ (AO1) and CFTR inhibitor $CFTR_{inh}172$ partially inhibited 007-AM-activated Cl^- currents, suggesting that both (CFTR and TMEM16A) Cl^- secretory pathways are activated by 007-AM (Fig 4.4 C). The role of EPAC1 for activation of TMEM16A and CFTR was further examined using the EPAC1-inhibitor ESI09. While ESI09 did not block stimulation of Cl^- currents by ATP or IONO in mock transfected wt-CFTR/CFBE and F508del-CFTR/CFBE cells, it inhibited ATP/IONO-activated Cl^- currents in cells overexpressing $P2Y_2R$. Inhibition by ESI09 was more pronounced in F508del-CFTR/CFBE cells (Fig 4.4 D). Moreover, I/F-induced currents in wt-CFTR and F508del-CFTR expressing cells were inhibited by ESI09 by about 50%. Additional currents in the presence of $P2Y_2R$ were completely inhibited by ESI09 (Fig 4.5 E). Immunocytochemistry detected localization of EPAC1 (in red) closer to the plasma membrane in cells expressing additional $P2Y_2R$ (in green) (Fig 4.5 F, G). Taken together, a significant portion of the I/F-activated Cl^- current is EPAC1-dependent and this portion is further enhanced by additional expression of GPCRs.

Role of ADCY1 for activation of Cl^- currents.

Because CFTR can be activated by ATP, we examined expression of the Ca^{2+}-sensitive adenylate cyclases (ADCYs). ADCY1 and ADCY3 (but not ADCY8 or ADCY10) are expressed in both WT-CFTR/CFBE and F508del-CFTR/CFBE at approximately similar levels (Fig 4.4 H). We found that activation of purinergic receptors with ATP increased intracellular cAMP, and cAMP-increase was further enhanced by additional expression of P2YR. Remarkably, in the presence of $P2Y_2R$, ATP-induced rise in intracellular cAMP was almost as high as with stimulation by I/F (Fig 4.4 J). Yet, expression levels for ADCY1 were not affected by additional

$P2Y_2R$ (Fig 4.4 I). Namkung et al. demonstrated the role of ADCY1 for ATP-activated and CFTR-dependent Cl^- secretion in airway epithelial cells [162]. We therefore used the ADCY1-specific inhibitor ST034307 (ST034) to further examine the role of ADCY1 for IONO activated Cl^- secretion. In the presence of additional $P2Y_2R$, Ca^{2+} activated Cl^- secretion by IONO was strongly inhibited by ST034 (Fig 4.4 K). Remarkably, ST034 potently blocked I/F-activated currents in WT-CFTR/CFBE cells and inhibited I/F-induced currents in $P2Y_2R$-expressing F508del-CFTR/CFBE cells, indicating the dominating role of ADCY1 for generation of cAMP (Fig 4.4 L, M). Taken together, an intensive crosstalk between cAMP- and Ca^{2+}-dependent signaling exists in airway epithelial cells due to EPAC1 and ADCY1, converting cAMP into Ca^{2+} signals and vice versa (Fig S4.2). Intensive crosstalk prevents clear discrimination between adrenergic/CFTR and purinergic/TMEM16A dependent chloride secretion. This is further indicated by the fact that specific inhibitors for CFTR (CFTRinh172) and TMEM16 (CACCinhAO1) inhibit both, Ca^{2+} and I/F-activated currents (Fig 4.4 N, O). Crosstalk and interaction between CFTR and TMEM16A amplify electrolyte secretion. This new insight is applicable to Cystic Fibrosis and the search for novel pathways to improve defective Cl^- secretion [200].

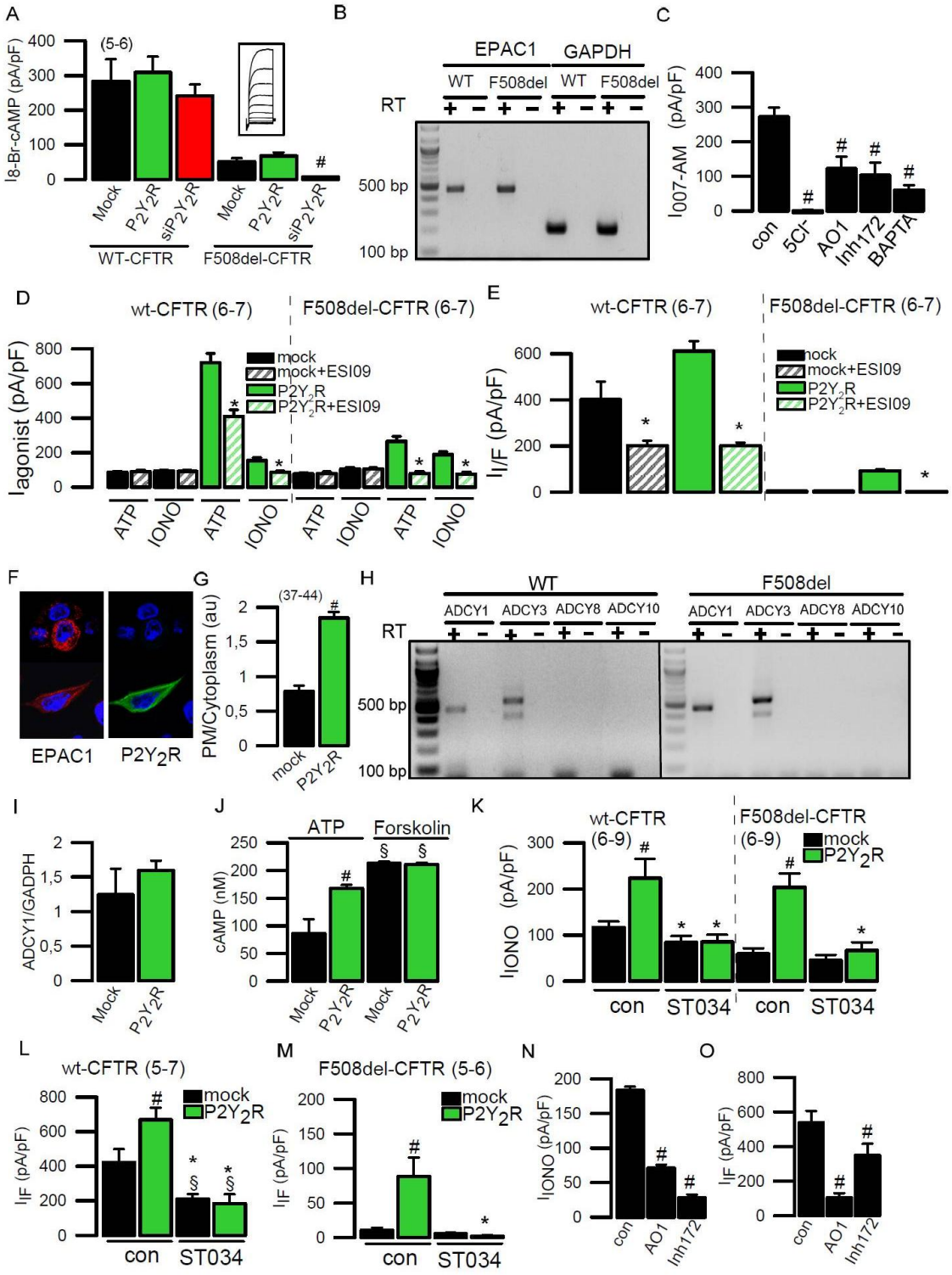

Fig 4.4 *EPAC1 and ADCY1 mediate cAMP/Ca^{2+} crosstalk and cross-activation of TMEM16A and CFTR.*

A) Summary of current densities obtained by stimulation of WT-CFTR/CFBE cells and F508del-CFTR/CFBE cells with 8-Bromo cAMP (25 µM). Cells overexpressed $P2Y_2R$ or endogenous $P2Y_2R$ was knocked-down by si$P2Y_2R$. B) RT-PCR demonstrating expression of EPAC1 in WT-CFTR/CFBE cells and F508del-CFTR/CFBE cells. C) Summary of current densities measured in cells stimulated with the EPAC1 activator 007-AM (30 µM). Replacement of extracellular **Cl^-** by impermeable gluconate

(5**Cl^-**), or application of the TMEM16A inhibitor CaCCinhAO1 (AO1; 20 µM), or application of the CFTR-inhibitor CFTRinh172 (Inh172; 20 µM) inhibited current densities. Ca^{2+} chelating by BAPTA-AM (50 µM) also inhibited activation by 007-AM. D) Currents densities activated by ATP (100 µM) and ionomycin (IONO; 0.1 µM), respectively, and inhibition by the EPAC1 inhibitor ESI09 (10 µM) in WT-CFTR/CFBE and F508del-CFTR/CFBE cells. E) Current densities activated by 100 µM IBMX and 2 µM Forskolin (I/F) in WT-CFTR/CFBE cells and F508del-CFTR/CFBE cells. Cells were mock transfected or overexpressed $P2Y_2R$. Effects of the EPAC1-inhibitor ESI09. F) Immunocytochemistry of EPAC1 and $P2Y_2R$ in WT-CFTR/CFBE cells. G) Ratio of EPAC1 expression in plasma membrane (PM) versus cytoplasm in mock transfected cells and cells overexpressing $P2Y_2R$ (arbitrary units; au). H) RT-PCR indicating expression of the Ca^{2+}-sensitive adenylate cyclases (ADCY) 1 and 3 but not 8 and 10. I) Relative expression of ADCY1-mRNA in mock transfected and $P2Y_2R$-overexpressing cells. J) Increase in intracellular cAMP levels induced by stimulation with ATP (100 µM) and 100 µM IBMX/2 µM Forskolin (I/F). K) Current densities activated by IONO (0.1 µM) in mock transfected and $P2Y_2R$-expressing WT-CFTR/CFBE and F508del-CFTR/CFBE cells, and inhibition by the ADCY1-inhibitor **ST034307 (**ST034; 30 µM). L, M) Current densities activated by I/F in mock and $P2Y_2R$-expressing WT-CFTR/CFBE L) and F508del-CFTR/CFBE M) cells, and inhibition by the ADCY1-inhibitor ST034. N,O) Inhibition of Cl^- currents (current densities) by $CaCC_{inh}AO1$ (AO1; 20 µM) and CFTR inhibitor $CFTR_{inh}172$ (20 µM). Mean ± SEM (number of experiments). $^{\#}$ significant difference when compared to con or mock ($p < 0.05$, unpaired t-test). § significant difference when compared to WT-CFTR expressing cells ($p < 0.05$, unpaired t-test). * significant inhibition by ST034 ($p<0.05$, paired t-test).

Discussion

The present data demonstrate the role of EPAC1 and ADCY1 for cross activation of CFTR and TMEM16A by cAMP and Ca^{2+}. Our previous study indicated an intimate functional relationship between CFTR and TMEM16A and demonstrated cAMP-activated transport being almost absent in epithelia from TMEM16A knockout mice [200]. TMEM16A was shown to be essential for proper activation as well as membrane expression of CFTR. We showed that TMEM16A causes ER Ca^{2+} store release, thereby engaging Store Operated cAMP Signaling (SOcAMPS) and activation of Ca^{2+} regulated adenylyl cyclases (ADCYs) [80]. Here we show that cAMP-dependent and Ca^{2+} activated Cl^- currents in airway epithelial cells strongly overlap due to the crosstalk of intracellular signaling molecules. The present results are in line with an earlier study that reported activation of CFTR via $P2Y_2R$ [191]. Notably, evidence was provided that TMEM16A can also be activated by a Ca^{2+} independent but G-protein-dependent mechanism [131]. Apart from the described crosstalk between TMEM16A and CFTR via Ca^{2+} dependent ADCY1 and cAMP-regulated EPAC1, additional crosstalk via calcium

dependent cAMP phosphodiesterase (PDE1), and possibly via PDE4 may take place. Such an additional regulatory circuit would further modulate the cooperativity between these channels. As our studies were performed in the presence of the PDE-inhibitor IBMX and non-hydrolysable analogues of cAMP, subsequent studies will have to clarify the contributions of PDEs.

Crosstalk of TMEM16A and CFTR is relevant in ciliated airway epithelial cells and intestinal epithelial cells, which are both Cl^- and fluid secreting. However, TMEM16A is expressed at higher levels in mucus producing club cells and goblet cells. Upregulation of TMEM16A during inflammation will therefore increase its impact on fluid and mucus secretion. As expression and upregulation of TMEM16A during inflammation is much more obvious in mucus producing cells, the effects on mucus secretion will be more relevant. This will be even more so in case of Cystic Fibrosis (CF), where functional CFTR is absence and thus the direct impact of TMEM16A on fluid secretion (which requires functional CFTR) might be negligible. Nevertheless, a direct small molecule opener of TMEM16A could be beneficial in CF.

This signaling/functional overlap is likely to take place in a shielded membrane compartment. Membrane bound ADCYs are known to colocalize with PLC-coupled GPCRs possibly in lipid raft-like membrane compartments [203]. TMEM16A and CFTR have been both located in lipid rafts [126, 204], while EPAC1 was shown to colocalize with CFTR [199]. EPAC1 is a known hub for cAMP/Ca^{2+} crosstalk [199, 205, 206]. We found enrichment of $P2Y_2R$ in an immunoprecipitate against TMEM16A, further supporting the existence of such functional membrane platforms (Fig 4.5). Signaling occurring in such functional compartments is well shielded. The EPAC1 activator 007-AM induced a whole cell Cl^- current. Activation of this current was suppressed by the Ca^{2+} chelator BAPTA-AM, demonstrating the role of intracellular Ca^{2+} (Fig 4.4 C). Moreover, 50-60% of the whole cell current activated by I/F were inhibited by the EPAC1-inhibior ESI09, indicating a central role of EPAC1 in regulating Cl^- secretion (Fig 4.4 E). However, I/F did not increase global intracellular Ca^{2+} levels measured by Fura-2 (Fig 4.5 B). In contrast, local compartmentalized Ca^{2+} was increased by I/F and 007-AM in close proximity

of CFTR, which was detected by the Ca^{2+} sensor G-CAMP6 fused to the C-terminus of CFTR (Fig 4.5 C-E).

We found earlier that extended synaptotagmins (ESYT1-3) strongly affect activation of TMEM16A through stimulation of $P2Y_2R$. ESYT1-3 tethers the endoplasmic reticulum (ER) close to plasma membrane thereby facilitating local Ca^{2+} signaling [207]. Thus ESYT1 stabilizes plasma membrane / ER microdomains to allow proper coupling of the Ca^{2+} sensor STIM1 to store operated Orai1 Ca^{2+} influx channels [208]. It seems noteworthy that I/F-activated currents were also found to be ESYT1-dependent: About 50 % of the I/F-activated whole cell current was inhibited siRNA knockdown of ESYT1 (388.1 ± 63.4; n = 5, scrambled RNA vs. 195.5 ± 49.3; n = 5, siESYT1). This corroborates the intimate relationship between TMEM16A and CFTR, and supports colocalization of signaling machines allowing Ca^{2+}/cAMP-crosstalk.

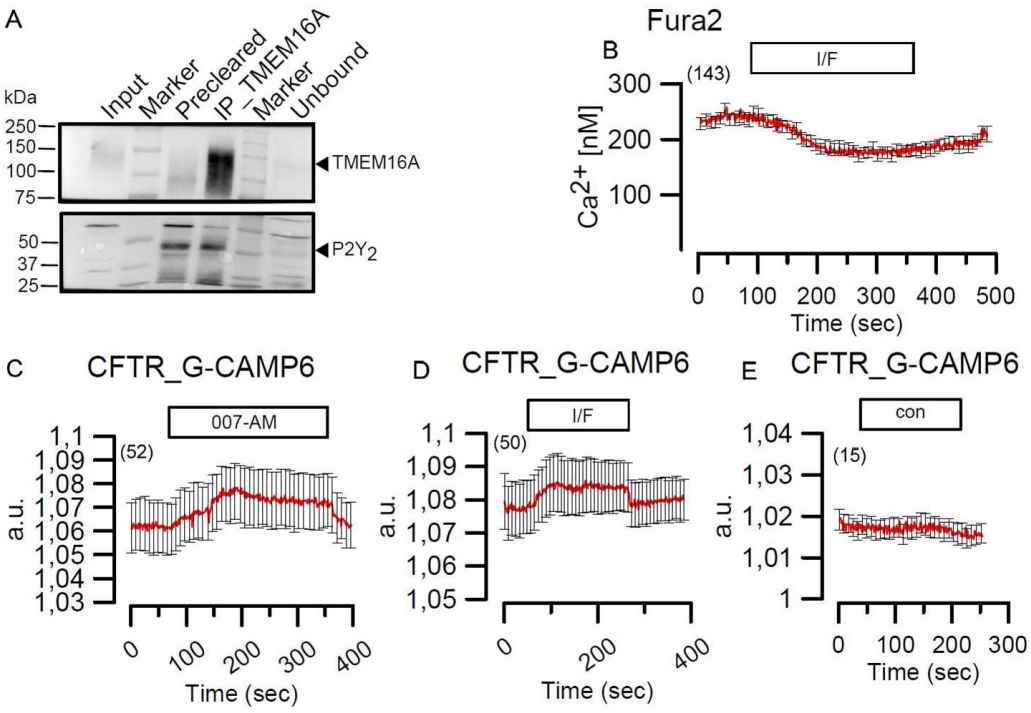

Fig 4.5 *Compartmentalized Ca^{2+} signaling.*

A) Immunoprecipitation of TMEM16A pulled down $P2Y_2R$. Input; cell lysate. Precleared; negative control obtained by incubation of Input for 2h with Protein-A and Protein-G conjugated beads. IP_TMEM16A; Immunoprecipitation of TMEME16A. Unbound; Supernatant remaining after IP. B) Global intracellular Ca^{2+} (mean ± SEM; n = 143), measured by Fura-2 in WT-CFTR/CFBE cells. I/F rather decreased than increased global intracellular Ca^{2+} levels. C, D) Intracellular compartmentalized Ca^{2+} levels close to the plasma membrane, as detected by the Ca^{2+} sensor G-CAMP6, which was fused to the C-terminal end of CFTR. Both I/F and the EPAC1-activator 007-AM slightly enhanced

compartmentalized intracellular Ca^{2+} in close proximity to CFTR. E) Control (con); absence of any stimulus. Mean ± SEM (number of experiments).

CFTR and TMEM16A are both glycosylated [113, 209, 210]. Indeed, collapsing the Golgi and thus blocking secretory traffic using BFA eliminated the glycosylated forms of CFTR and TMEM16A (Fig 4.6 A). Interestingly, membrane trafficking of CFTR was completely inhibited by BFA, while membrane trafficking of TMEM16A remained largely unchanged by BFA (Fig 4.6 B-E). Astonishingly, although CFTR was completely absent from the cell membrane in BFA-treated cells, whole cell currents activated by I/F were still considerable (about 50 %). In fact I/F-induced currents remained almost unaffected by BFA in cells overexpressing $P2Y_2R$ (Fig 4.6 F, G). Ca^{2+} (IONO) activated currents were not reduced by BFA (Fig 4.6 H,I). These rather surprising results confirm that a significant portion of the cAMP-activated Cl^- current is due to TMEM16A and that it appears well justified screening for more potent activators of TMEM16A to activate Cl^- secretion in Cystic Fibrosis. In summary, we demonstrate an intimate relationship between TMEM16A and CFTR, which is enabled by cAMP/Ca^{2+} crosstalk due to EPAC1 and ACDY1. Future studies may supply further details regarding the origin of the compartmentalized submembranous Ca^{2+} signal, and the possible contribution of Ca^{2+} -regulated phosphodiesterases.

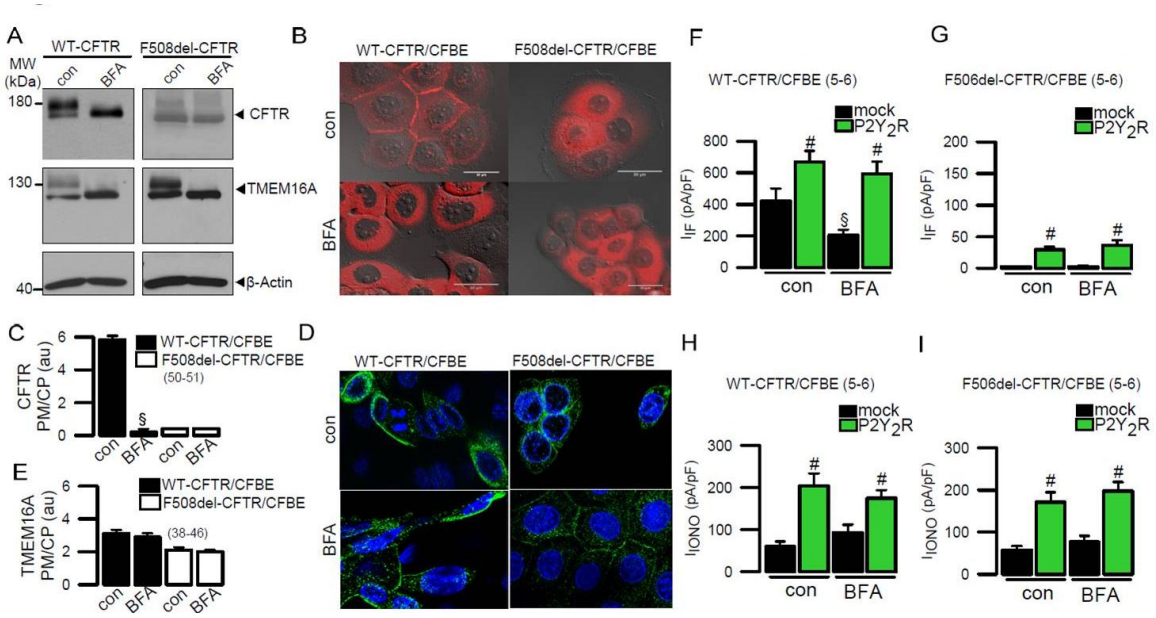

Fig 4.6 *TMEM16A can compensate for the lack of CFTR in BFA treated cells.*
A) Western blots of CFTR and TMEM16A in WT-CFTR/CFBE and F508del-CFTR/CFBE cells exposed to control solution (con) or the protein transport inhibitor brefeldin A (BFA; 10 µM/24h). BFA eliminated the glycosylated forms of CFTR (Band C) and TMEM16A (upper band at 130 kDa). B) Expression of CFTR (cherry fluorescence in living cells) indicating membrane localization of WT-CFTR (left upper panel), which was completely suppressed by BFA (left lower panel). F508del-CFTR (right panels) was located intracellularly, independent of BFA. C) Ratio of plasma membrane (PM) vs. cytoplasmic (CP) localization of CFTR, as analyzed by fluorescence intensities in regions of interest (ROI). D) Expression of TMEM16A (primary anti-TMEM16A (DOG1)-antibody; secondary fluorescent labeled antibody) indicating variable membrane localization that was not changed by BFA in either WT-CFTR/CFBE (left panels) or F508del-CFTR/CFBE (right panels) cells. E) Ratio of PM vs. CP localization of TMEM16A indicating no significant changes by BFA. In F508del-CFTR expressing cells, less TMEM16A was membrane localized. F) Whole cell currents activated by IBMX/Forskolin (I/F; 100 µM/2 µM) in wt-CFTR/CFBE and F508del-CFTR/CFBE cells. In WT-CFTR/CFBE cells, BFA inhibited only 50% of the I/F-activated current in mock transfected cells. BFA did not inhibit currents in cells overexpressing the purinergic receptors $P2Y_2R$. G) In F508del-CFTR/CFBE cells, additional currents produced by expression of $P2Y_2R$ were not affected by BFA. H,I) Whole cell currents activated by Ionomycin (IONO; 100 nM) in WT-CFTR/CFBE and F508del-CFTR/CFBE cells were not affected by BFA. Mean ± SEM (number of experiments). $^{\#}$ significant difference when compared to mock ($p<0.05$; unpaired Student's t test). § significant difference when compared to con ($p<0.05$; unpaired Student's t test).

Acknowledgements

Supported by DFG SFB699-A7/A12, DFG KU756/12-1, SFB877/A4 (to KK), and UK CF Trust SRC003 INOVCF (to KK and MDA) and by UID/MULTI/04046/2013 centre grant from FCT, Portugal (to BioISI). JRL and MFP are recipients of fellowships from BioSys PhD program (SFRH/BD52489/2014 and SFRH/PD/BD/114393/2016 respectively) from FCT (Portugal).

Supplementary material

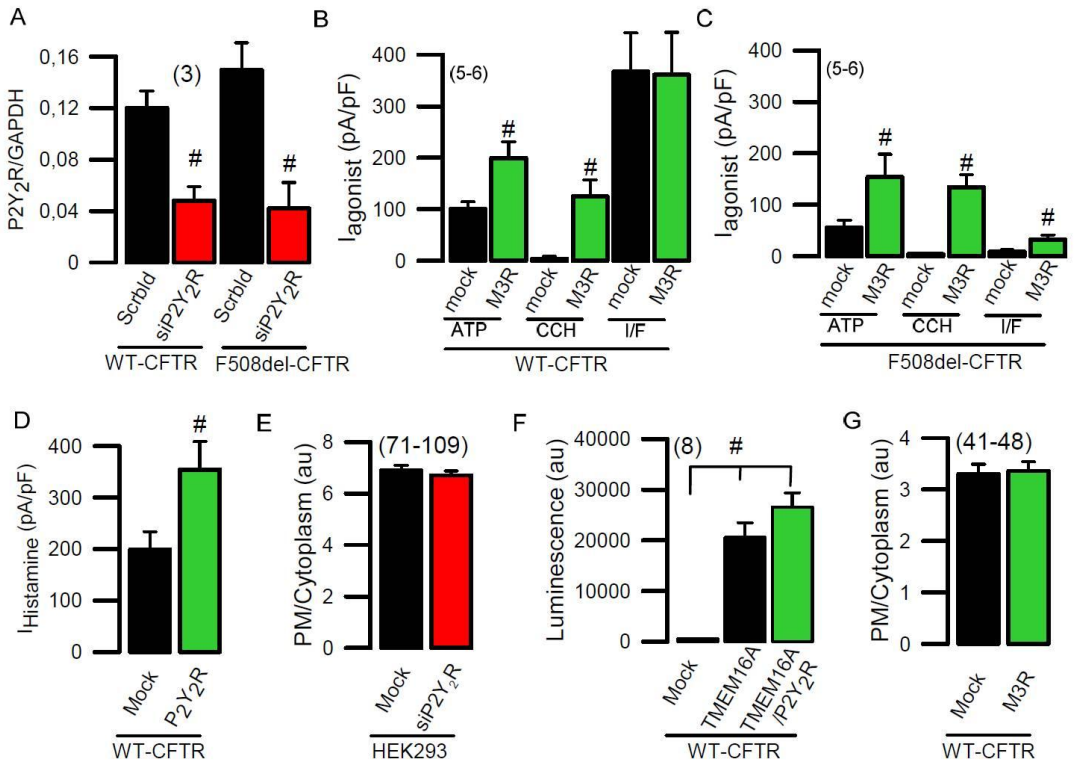

Supplementary Figure 4.1 *Activation of TMEM16A by GPCR.*

A) siRNA knockdown of $P2Y_2R$ detected by semiquantitative RT-PCR in WT-CFTR and F508del-CFTR expressing CFBE cells. B,C) Summary of whole cell currents activated by ATP (100 µM), carbachol (CCH; 100 µM) and IBMX/Forskolin (100 µM/2 µM). Summaries are shown for cells expressing empty plasmid (mock) or M3 receptors (M3R) in CFBE/WT-CFTR (B) and CFBE/F508del-CFTR (C) cells. D) Summary of current densities activated by histamine (50 µM) in mock transfected CFBE cells and cells overexpressing $P2Y_2R$. E) Ratio of plasma membrane to cytoplasmic expression of TMEM16A in HEK293 cells by analysis of fluorescence intensities in regions of interest. Knockdown of $P2Y_2$ receptors does not change membrane expression. F) Membrane expression of TMEM16A in CFBE cells measured by chemiluminescence. CFBE cells expressed a TMEM16A construct that contained an extracellularly accessible HA tag in the first extracellular loop of TMEM16A. Cells were labeled using an anti-HA antibody and a secondary horseradish peroxidase conjugated antibody. Additional expression of $P2Y_2R$ did not change membrane expression of TMEM16A. G) Ratio of plasma membrane to cytoplasmic expression of TMEM16A in CFBE cells. Expression of M3R does not change membrane expression. Mean ± SEM (number of experiments). # significant difference when compared to mock or scrambled RNA (Scrbld) or mock transfected cells (unpaired Student's t test).

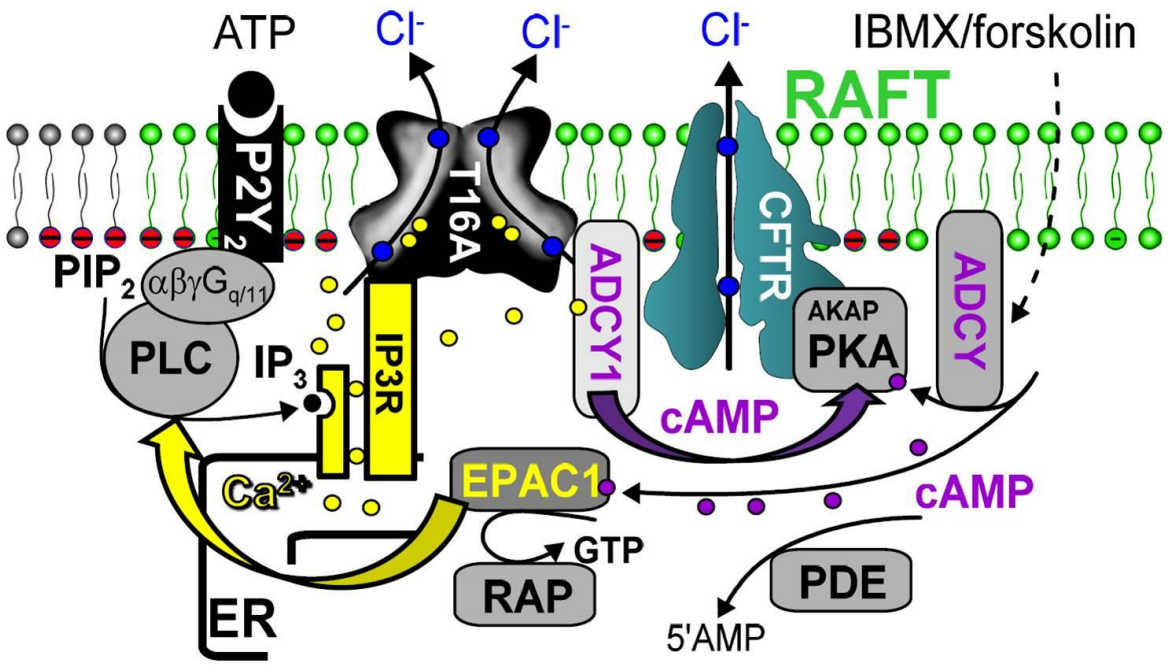

Supplementary Figure 4.2 *cAMP/Ca^{2+}-crosstalk activates CFTR and TMEM16.*
Stimulation of purinergic receptors leads to endoplasmic reticulum (ER) Ca^{2+} store release through IP3 receptors (IP_3R). Ca^{2+} not only activates TMEM16A (T16A) but also stimulates adenylate cyclase type 1 (ADCY1) to produce cAMP and to activate CFTR via protein kinase A (PKA). Vice versa, activation of adenylate cyclases by IBMX/Forskolin (or through ß-adrenergic stimulation) generates cAMP and activates not only CFTR but also TMEM16A via exchange protein directly activated by cAMP (EPAC1), the small GTP-binding protein RAP, phospholipase C (PLC) and local increase in intracellular Ca^{2+}. Receptor, TMEM16A, CFTR and signaling molecules are probably colocalized in a raft-like plasma membrane microdomain.

Chapter 5:

TMEM16A is indispensable for basal mucus secretion in airways and intestine

Abstract

TMEM16A is the Ca^{2+} activated chloride channel in airways and intestine and has been associated with goblet cell metaplasia. Expression of TMEM16A is strongly upregulated in CF and asthma during mucus hypersecretion. The role of TMEM16A for mucus production or mucus secretion remains obscure, and whether TMEM16A affects the function of intestinal goblet cells is entirely unknown. Basal (unregulated) mucus secretion occurs through low levels of ATP. Here we report for the first time that TMEM16A is essential for basal secretion of mucus in airways and intestine. Airway and intestinal epithelial specific knockout of TMEM16A (*FoxJ1-TMEM16A*$^{flox/flox}$*, Vil1-TMEM16A*$^{flox/flox}$) leads to accumulation of mucus in airway club (Clara) cells and large intestinal goblet cells. Acute ATP-induced mucus secretion by airway club cells and colonic goblet cells is strongly compromised in the absence of TMEM16A. Experiments in human Calu3 airway epithelial cells show similar TMEM16A-dependence of mucus release. In contrast, cholinergic mucus secretion due to compound exocytosis is independent of TMEM16A. The data demonstrate a previously unrecognized role of TMEM16A for membrane exocytosis and describe a novel ATP-driven pathway for intestinal mucus secretion. We conclude that ATP-dependent, i.e. constitutive mucus secretion in both airways and intestine requires TMEM16A. Providing similar regulation in human, the present results form the basis for a completely novel therapeutic approach for the treatment of mucus hypersecretion.

Key words: TMEM16A; anoctamin 1; mucus secretion, Cystic Fibrosis, asthma, COPD, Ca^{2+} signaling

Published as: Roberta Benedetto, Inês Cabrita, Rainer Schreiber, Karl Kunzelmann. TMEM16A is indispensable for basal mucus secretion in airways and intestine. Faseb J. 2018 Dec:fj201801333RRR.

Own experimental contribution: Patch clamping experiments, Ovalbumine sensitization, Histology, Mucociliary transport.

Own written contribution: Methods, Results, Parts of Introduction and Discussion.

Other contributions: Designed experiments and analyzed data.

Introduction

Mucus covers airways and intestine and represents the innate defense against pathogens. In the airways, mucus traps inhaled pathogens and particles, while intestinal mucus physically separates bacteria from epithelial cells and lubricates the intestinal content [211, 212]. In healthy lungs mucus is formed by secretion and hydration of gel forming mucins from surface goblet and club (Clara) cells producing MUC5AC and MUC5B, and from submucosal glands releasing MUC5B [213]. The major mucin in the gut is MUC2 [214]. Although clear differences exist between airway and intestinal goblet cells, they share common features such as low pH and high Ca^{2+} content in their secretory granules, which allows for tight packaging of the mucus [214]. Despite protective functions, mucus becomes a severe problem when hypersecreted upon mucous metaplasia during inflammatory lung diseases such as asthma, COPD and Cystic Fibrosis (CF) [215]. Mucus hyperproduction causes airway obstruction, reduced mucociliary clearance and chronic inflammation, the predominant problems in CF [213]. In CF, mucus is particularly viscous and adhesive due to compromised Cl^- and HCO_3^- secretion caused by defective Cystic Fibrosis transmembrane conductance regulator (CFTR) channels [216, 217]. Expression of the Ca^{2+} activated Cl^- channel TMEM16A (anoctamin 1) is strongly upregulated in CF by bacterial components and in asthma by Th2 cytokines. This parallels goblet cell metaplasia and mucus hypersecretion [152, 218, 219]. Upregulation of TMEM16A is predominant in mucus producing cells and to a lesser degree in ciliated epithelial cells [152, 189]. The role of TMEM16A for mucus production or mucus secretion remains obscure, although both is inhibited by Niflumic acid, an inhibitor of TMEM16A and other ion channels [220, 221]. Whether TMEM16A affects the function of intestinal mucus-producing cells is entirely unknown. The present study makes use of airway and intestinal selective epithelial knockout mice and demonstrates for the first time an indispensable role of TMEM16A for mucus secretion. TMEM16A provides a mechanism to enhance Ca^{2+} in the apical pole of mucus producing cells, which is essential for ATP-activated mucus release. ATP-dependent mucus release takes place continuously under basal conditions. TMEM16A therefore is a regulator of exocytosis and controls the release of proinflammatory mediators as well. The findings

presented here are probably correlated with the reported role of TMEM16A for cytoplasmic Cl^- homeostasis, controlling PtdIns (4,5)P2 microdomains and membrane remodeling [222].

Materials and Methods

Cells culture, RT-PCR. HEK293 cells were grown as previously described[223]. Calu3 cells were grown in DMEM-F12 media supplemented with 1% HEPES, 1% L-glutamine, 10% FBS at 37ºC in the absence of antibiotics in a humidified atmosphere with 5% CO_2. Total RNA was isolated from lungs and was reverse-transcribed using random primer (Promega, Mannheim, Germany) and M-MLV Reverse Transcriptase RNase H Minus (Promega, Mannheim, Germany). Primers used were: 5´-GTGACAAGACCTGCAGCTAC and 5´-GCTGCAGCTGTGGAGATTC.

TMEM16A knockout animals, ovalbumin challenge, preparation of tissues. Generation of mice with intestinal epithelial knockout of TMEM16A (*TMEM16A$^{flox/flox}$Vil1-Cre; fl/fl-Vil1*) has been described earlier [128]. Tissue specific knockout of TMEM16A in ciliated airway epithelial cells was achieved by crossbreeding *TMEM16A$^{flox/flox}$* (*fl/fl*) mice with *FOXJ1-Cre* mice *(TMEM16A$^{flox/flox}$FoxJ1-Cre;*) and is outlined in [200]. Allergen challenge of mice has been described earlier [224]. In brief: Mice were sensitized to ovalbumin (OVA, Sigma) by i.p. injection of 100 µg OVA with 1 mg aluminum hydroxide gel (Sigma) on days 0 and 14. At days 21 and 24, mice were anaesthetized (ketamine 90–120 mg/kg, xylazine 6–8 mg/kg) and challenged to OVA by intratracheal instillation of 50 µg OVA in 20 µl saline. Control mice were sham sensitized with saline and aluminum hydroxide gel (Sigma) and challenged to 20 µl saline by intratracheal instillation. All animal experiments complied with the ARRIVE guidelines and were carried out in accordance with the U.K. Animals Act, 1986 and associated guidelines, EU Directive 2010/63/EU for animal experiments. All animal experiments were approved by the local ethics committee of the Government of Unterfranken/Würzburg (AZ: 55.2-2532-2-328) and were conducted according to the guidelines of the American Physiologic Society and the German law for the welfare of animals.

Histological analysis. Intestinal sections were saved for histological analyses. Mouse

airways were fixed by transcardial fixation and were embedded in paraffin or were used as cryosections. For paraffin sections, tissues were fixed in 4% paraformaldehyde (PFA), 0.2% picric acid and 3.4% sucrose in PBS, and were washed in methanol before embedding in paraffin. Sections were stained according to standard Periodic acid-Schiff (PAS) or Alcian Blue methods and assessed by light microscopy. Sections were analyzed using an Axiovert 200 microscope equipped with AxioCam ICc 1 and ApoTome (Zeiss, Germany). Cross sectional areas were determined using AxioVision Software and an Axiovert 200 microscope equipped with AxionCam.

In vitro perfused intestine. Mice were sacrificed and excised intestines were placed immediately in ice-cold Ringer solution and carefully flushed to remove residual luminal contents. The intestinal segments were mounted and perfused vertically in a custom-designed perfusion chamber with a constant temperature, similar to [93].

Patch Clamping. Patch pipettes were filled with a cytosolic-like solution containing in mM: KCl 30, K-gluconate 95, NaH_2PO_4 1.2, Na_2HPO_4 4.8, EGTA 1, Ca -gluconate 0.758, $MgCl_2$ 1.03, D - glucose 5, ATP 3, pH 7.2. TMEM16A was activated by high pipette Ca^{2+} (1 µM). Extracellular Cl^- (145 mM) was replaced by gluconate, HCO_3^- or I^-. Experiments were performed as described earlier[200].

Electron microscopy. For transmission electron microscopy of mouse airways, deeply anesthetized mice were sacrificed and fixed by intracardial perfusion with 2.5% glutaraldehyde in 0.1 M cacodylate buffer (pH 7.4). Lungs were treated with 1% OsO_4, 0.8% $K_4[Fe(CN)_6]$ in 0.1 M cacodylate buffer for 1.5 h, dehydrated with graded ethanol solutions and embedded in Epon (Roth, Karlsruhe, Germany). Semi-thin sections were stained with Richardson's stain. Ultrathin sections were stained with uranyl acetate and lead citrate, and analyzed on a transmission electron microscope (Libra, Zeiss).

Analysis of mucus, IL-8 release, leukocytes. Tissues were fixed using 4 % paraformaldehyde (PFA), 0.2% picric acid and 3.4% sucrose in PBS and washed in methanol before embedding in paraffin. Mucus was analyzed using standard Periodic acid-Schiff (PAS) or alcian blue staining. MUC5AC was stained using anti-MUC5AC mouse antibody (1:200, Abcam, ab3649) (1h at 37°) and a secondary antibody conjugated with Alexa 488 (Life

Technologies, A-21206). Nuclei were stained with Hoe33342 (0.1 µg/ml PBS, Aplichem, Darmstadt, Germany). To measure secretion of the cytokine IL-8 by Calu3 cells Quantikine ELISA kits (R&D systems) were used.

Mucociliary transport ex vivo. Tracheas were removed, fixed with insect needles onto extra thick blot paper (Bio-Rad, Germany) and transferred into a chamber with water-saturated atmosphere at 37°C. Transport was measured as described recently [200].

***CD8, luminescence, FM 4-64*.** Coverslips were mounted in a chamber and continuously perfused at 37 °C with Ringer solution containing 2 µg/ml FM 4-64. After 30 s, the cells were stimulated with 1 µM ionomycin for 3 min following washout. FM4-64 was excited at 546 ± 6 nm and emission was recorded at 575/640 nm.

Measurement of [Ca^{2+}***]$_i$.*** Crypts were isolated from inverted proximal mouse colon using Ca^{2+}-free Ringer solution with 1 mM DTT and 1 µM indomethacin for 20 min at 37°C. Crypts were loaded with 10 µM Fura-2-AM (Biotum, USA) and 1 mg/ml BSA (Sigma-Aldrich) in ringer solution for 1h at RT. Intracellular Ca^{2+} was measured as outlined in [80].

Materials and statistical analysis. Data are reported as Mean ± SEM Student's t-test (for paired or unpaired samples as appropriate) or ANOVA were used for statistical analysis. A p-value < 0.05 was accepted as significant difference. Tissues/cells from 3 - 7 *TMEM16A$^{flox/flox}$, TMEM16A$^{flox/flox}$FoxJ1, and TMEM16A$^{flox/flox}$Vil1* mice, respectively, were examined in each series of experiments.

Results

Inhibition of basal airway mucus secretion in the absence of TMEM16A.

Airways lacking epithelial cell specific expression of TMEM16A [200] demonstrated an impressive accumulation of mucus, which was not due to an increased fraction of nonciliated club (Clara) cells (Fig 5.1 A-C; Fig S5.1 A). *TMEM16A$^{flox/flox}$FoxJ1* airways did not show signs of inflammation, as no infiltration by CD45 positive leukocytes was detected. Moreover, analysis of airway cross-sections did not provide evidence for airway constriction (Fig 5.1 D,E). No mucus was found in the lumen of *TMEM16A$^{flox/flox}$FoxJ1* airways. Basal mucociliary

particle transport measured in isolated *TMEM16A*$^{flox/flox}$*FoxJ1* tracheas *in vitro* was enhanced, but was not further stimulated by ATP (Fig 5.1 F). We therefore suspected a defective basal mucus secretion in the absence of TMEM16A. Earlier work had shown that basal mucus secretion occurs at the rate of production, so that mucus does not accumulate in airway club cells [225]. Notably, the phenotype of *TMEM16A*$^{flox/flox}$*FoxJ1* airways was strikingly similar to that found in Munc2-/- knockout mice, which have a defect in basal mucus secretion [226]. We examined if mucus accumulating in airways of *TMEM16A*$^{flox/flox}$*FoxJ1* mice can be released by aerosolized carbachol (CCH) or ATP (both 100 µM). We found that CCH induced mucus secretion, while ATP-induced mucus release was strongly compromised (Fig 5.1 F,G).

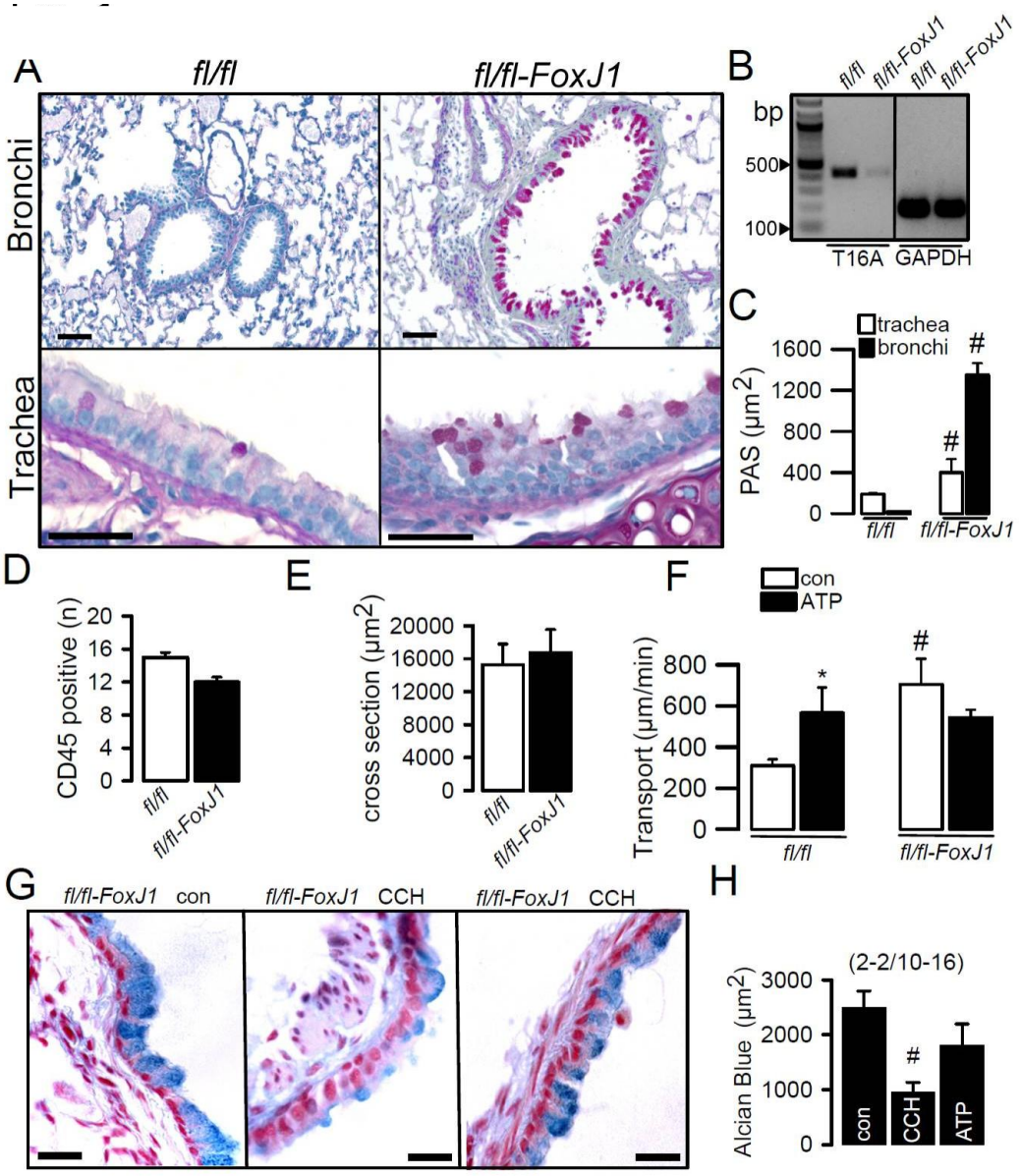

Fig 5.1 *Accumulation of mucus in airways of TMEM16A$^{flox/flox}$FoxJ1 mice.*
A) Mucus staining by PAS in bronchi and tracheas of *TMEM16A$^{flox/flox}$* (*fl/fl*) and *TMEM16A$^{flox/flox}$FoxJ1* (*fl/fl-FoxJ1*) mice, indicating accumulation of mucus in airways of *fl/fl-FoxJ1* mice. Bars indicate 20 µm. B) RT-PCR analysis of TMEM16A in isolated respiratory epithelial cells from *fl/fl* and *fl/fl-FoxJ1* mice. C) PAS positive staining in *fl/fl* and *fl/fl-FoxJ1* airways (n = 29). D) Number of CD45 positive cells (airways) in *fl/fl* and *fl/fl-FoxJ1* airways (n = 20). E) Cross sectional area of airways from *fl/fl* and *fl/fl* mice (n = 20). F) Mucociliary clearance and effect of carbachol (CCH) or ATP (both 100 µM) assessed by particle tracking *ex vivo* in tracheas from *fl/fl* and *fl/fl-FoxJ1* animals (n = 17). G,F) Alcian blue staining and quantification of mucus in *fl/fl-FoxJ1* airways under control conditions and after aerosol application of carbachol (CCH) or ATP (both 100 µM). Mean ± SEM; *significant difference when compared to *fl/fl* (paired t-test). #significant difference when compared to *fl/fl-FoxJ1* (unpaired t-test).

Electron microscopy images of *TMEM16A$^{flox/flox}$FoxJ1* airways showed protruded club cells that accumulated secretory granules in the apical pole (Fig 5.2 A,B). Both the number of

granules per cell and their size were enhanced (Fig S5.1 B,C). Clara cell specific protein (CCSP) positive cells were not enhanced in *TMEM16A*$^{flox/flox}$*FoxJ1* airways. Thus, metaplastic STAT-6/SPDEF pathways do not seem to be activated [227] (Fig 5.2C). Mucus accumulated apparently in club cells, while TMEM16A was knocked-down in FoxJ1-expressing ciliated epithelial cells. It is unlikely that mucus accumulates in ciliated cells, which therefore asks for the link between ciliated and mucus producing cells (Fig S5.1 D). The number of CCSP-positive cells was not enhanced in fl/fl-FoxJ1, thus lack of TMEM16A is unlikely to induce a transdifferentiation towards mucus producing cells. We were unable to co-localize clearly CCSP and FoxJ1 or CCSP and acetylated tubulin in airway cells (Fig S5.1 E). As described further down, it is possible that ciliated cells secrete a factor that is required to release mucus from club cells. This could be ATP itself. However, external application of high concentrations (100 µM) of ATP (via aerosol) induced only little mucus secretion, suggesting a secretory defect in club cells. Interestingly, not only mucus accumulated in club cells from *fl/fl-FoxJ1* mice, but also CCSP itself (Fig S5.1 F). Preliminary data also suggest an accumulation of CLCA3 in club cells, a protein that controls membrane expression and activity of TMEM16A [228] (not shown). Subsequent experiments will have to unmask the precise functional crosstalk between ciliated and club cells needed for basal mucus release.

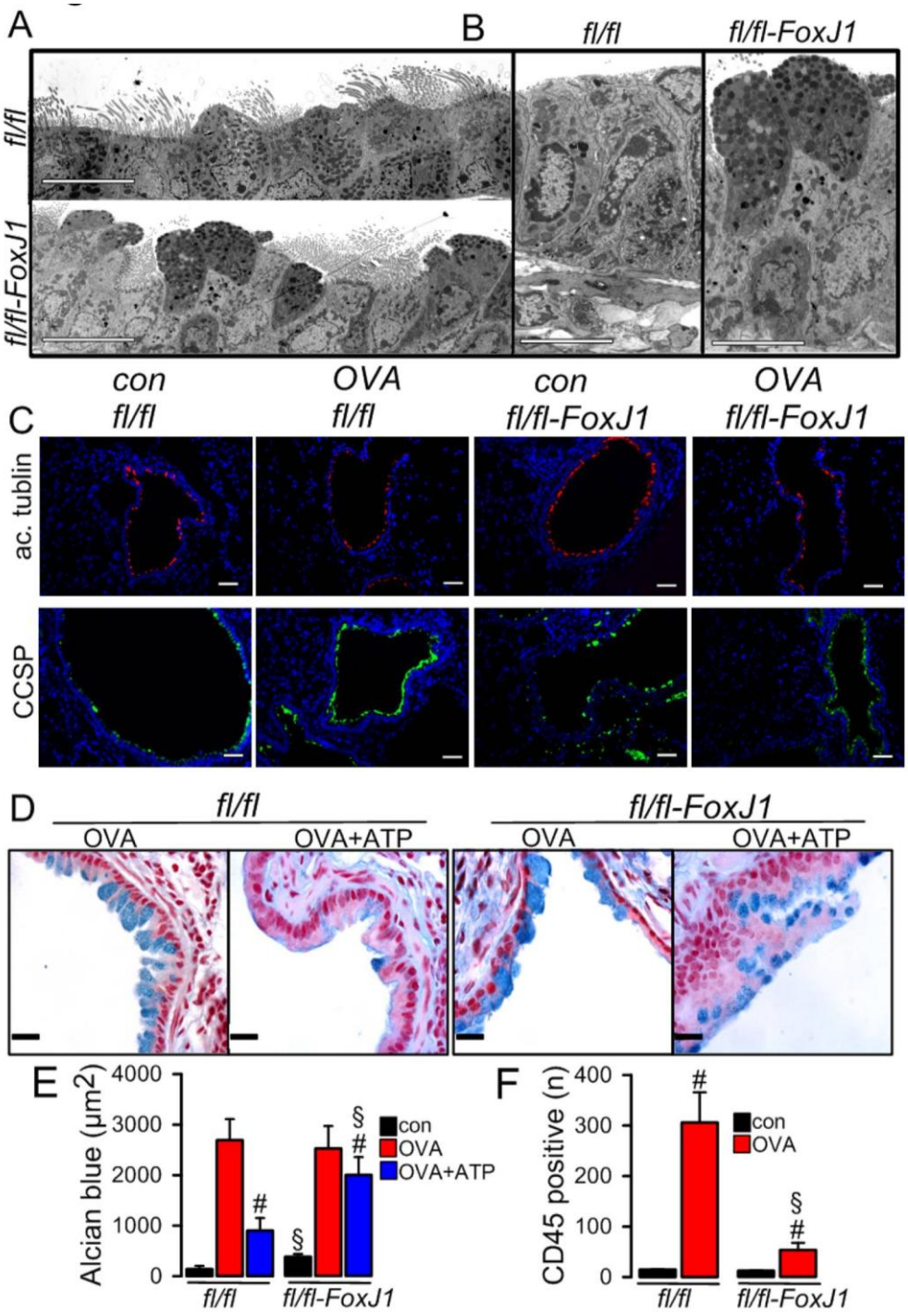

Fig 5.2 *Defective mucus secretion in airways of TMEM16A$^{flox/flox}$FoxJ1 mice.*

A,B) Electron microscopic panorama (A) and higher resolution images (B) indicating accumulation of granules in club cells of *TMEM16A$^{flox/flox}$FoxJ1* (*fl/fl-FoxJ1*) airways. Bars 5 µm. C) CCSP and acetylated tubulin staining in *TMEM16A$^{flox/flox}$* (*fl/fl*) and *fl/fl-FoxJ1* airways in control and OVA-sensitized animals. Bars 50 µm. D) Mucus induced by OVA-sensitization in airways of *fl/fl* and *fl/fl-Fox* animals, as detected by alcian blue staining. Exposure to ATP (100 µM) induced release of mucus in *fl/fl* airways, which was attenuated in *fl/fl-Fox* mice. Bars 20 µm. E) Quantification of alcian blue stainings (n = 10 - 16). F) Number of CD45 positive cells in lungs from control and OVA-sensitized animals (n = 10 - 16). Mean ± SEM; $^{\#}$significant effect of ATP or OVA, respectively (unpaired t-test); §significant difference when compared to *fl/fl* (unpaired t-test).

ATP-dependent but not muscarinic mucus secretion is compromised in TMEM16A$^{flox/flox}$FoxJ1 airways.

When exposed to ovalbumin, Th2-dependent goblet cell metaplasia and accumulation of mucus was observed in both *TMEM16A$^{flox/flox}$* and *TMEM16A$^{flox/flox}$FoxJ1* airways, suggesting that TMEM16A is not required for mucus production in mouse airways (Fig 5.2 D, Fig S5.1 A). In *TMEM16A$^{flox/flox}$* airways, pronounced mucus secretion was induced by nebulized ATP, which was significantly reduced in *TMEM16A$^{flox/flox}$FoxJ1* mice (Fig 5.2 D,E). Accumulation of CD45 positive leucocytes in lungs of OVA-treated *TMEM16A$^{flox/flox}$FoxJ1* animals was strongly reduced, suggesting attenuated airway inflammation in the absence of TMEM16A (Fig 5.2 F, Fig S5.2). In *TMEM16A$^{flox/flox}$* airways, ovalbumin-sensitization upregulated expression of TMEM16A in epithelial and smooth muscle (ASM) cells, as described earlier [68, 152, 218, 229] (Fig S5.3). In *TMEM16A$^{flox/flox}$FoxJ1* mice, upregulation of TMEM16A in ASM was much less evident, and the ASM layer was thinner (Fig S5.3, Fig 5.3A). We speculate that the release of mediators from epithelial cells that drive airway hyperreactivity and remodeling, could occur in a TMEM16A-dependent fashion [230]. In contrast to ATP (Fig 5.2), cholinergic stimulation of mucus secretion by nebulized carbachol was uncompromised in OVA-sensitized *TMEM16A$^{flox/flox}$FoxJ1* mice. Also muscarinic airway constriction when measured as airway cross-section was not different in *TMEM16A$^{flox/flox}$FoxJ1* mice [231] (Fig 5.3). Thus ATP but not cholinergic mucus secretion requires TMEM16A.

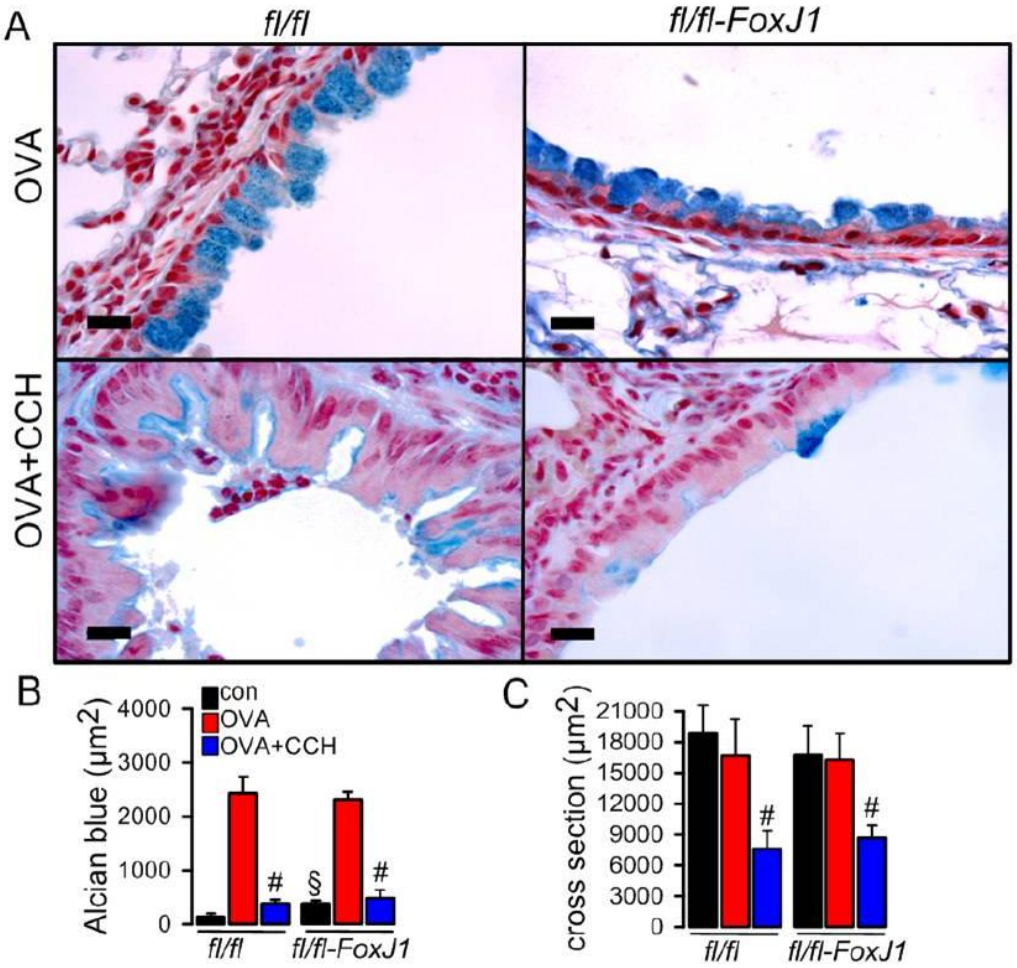

Fig 5.3 *Compromised mucus secretion in airways of OVA-sensitized TMEM16A$^{flox/flox}$FoxJ1 mice.*
A) Mucus production induced by OVA-sensitization in airways from *TMEM16A$^{flox/flox}$* (*fl/fl*) and *TMEM16A$^{flox/flox}$FoxJ1* (*fl/fl-FoxJ1*) mice and carbachol (CCH; 100 µM) induced mucus release. Bars indicate 10 µm. B) Summary of alcian blue staining indicating strong increase of mucus production by OVA-sensitization and release of mucus by stimulation with CCH (n = 23). C) Effect of OVA-sensitization and CCH on cross sectional area of airways from *fl/fl* and *fl/fl-FoxJ1* mice (n = 23). Mean ± SEM; $^{\#}$significant difference when compared to OVA (unpaired t-test). §significant difference when compared to *fl/fl* (unpaired t-test).

***Basal and ATP-dependent intestinal mucus release, but not cholinergic goblet cell secretion requires* TMEM16A.**

In mice with intestinal epithelial specific knockout of TMEM16A (*TMEM16A$^{flox/flox}$Vil1)* [200] we observed accumulation of mucus in both large and small intestinal goblet cells (Fig 5.4, Fig S 5.4 A). In goblet cells from *TMEM16A$^{flox/flox}$Vil1* mice, the mucus content per cell was enhanced, while the number of goblet cells per crypt remained unchanged from wt (Fig 5.4). Mucus covering the intestinal epithelium appeared thinner and more irregular in

TMEM16A$^{flox/flox}$*Vil1* mice (Fig S5.4 A,B). While cellular mucus content was enhanced Muc2 mRNA-expression was not upregulated in *TMEM16A*$^{flox/flox}$*Vil1* intestine, suggesting a secretory defect (Fig S 5.4 C). Goblet cells from *TMEM16A*$^{flox/flox}$ but not from *TMEM16A*$^{flox/flox}$*Vil1* expressed TMEM16A (Fig 5.4 D,E). Mucus accumulation in *TMEM16A*$^{flox/flox}$*Vil1* intestine corresponds well to accumulation of intestinal mucus observed in Munc13-2 deficient mice, therefore suggesting defective basal mucus secretion [226]. Cholinergic stimulation released mucus equally well from freshly isolated *TMEM16A*$^{flox/flox}$ and *TMEM16A*$^{flox/flox}$*Vil1* intestine (Fig 5.4 D-F). This was examined in more detail by perfusing freshly excised colon *in vitro* and by collecting released mucus. We found that stimulation with methacholine or luminal ATP induced acute mucus secretion in *TMEM16A*$^{flox/flox}$ colon. Costimulation with prostaglandin E2 was required to flush mucus out of the crypts. Identical results were obtained in intact (unstripped) and stripped (removal of submucosal tissue) colon, suggesting direct stimulation of goblet cells rather than indirect mechanisms (Fig S5.5 A-C). Due to compromised basal secretion, mucus accumulated in goblet cells of *TMEM16A*$^{flox/flox}$*Vil1* colon, which was nearly completely released upon cholinergic (MCh) stimulation. Thus MCh-induced mucus release was much larger in *TMEM16A*$^{flox/flox}$ when compared to *TMEM16A*$^{flox/flox}$*Vil1* colon (Fig 5.5 A, left). Stimulation with luminal ATP also released mucus in *TMEM16A*$^{flox/flox}$ colon (Fig 5.5 A, right). To our knowledge this is the first observation of purinergic mucus release in naïve colon, which occurs via activation of luminal $P2Y_2$ or $P2Y_4$ receptors [232].

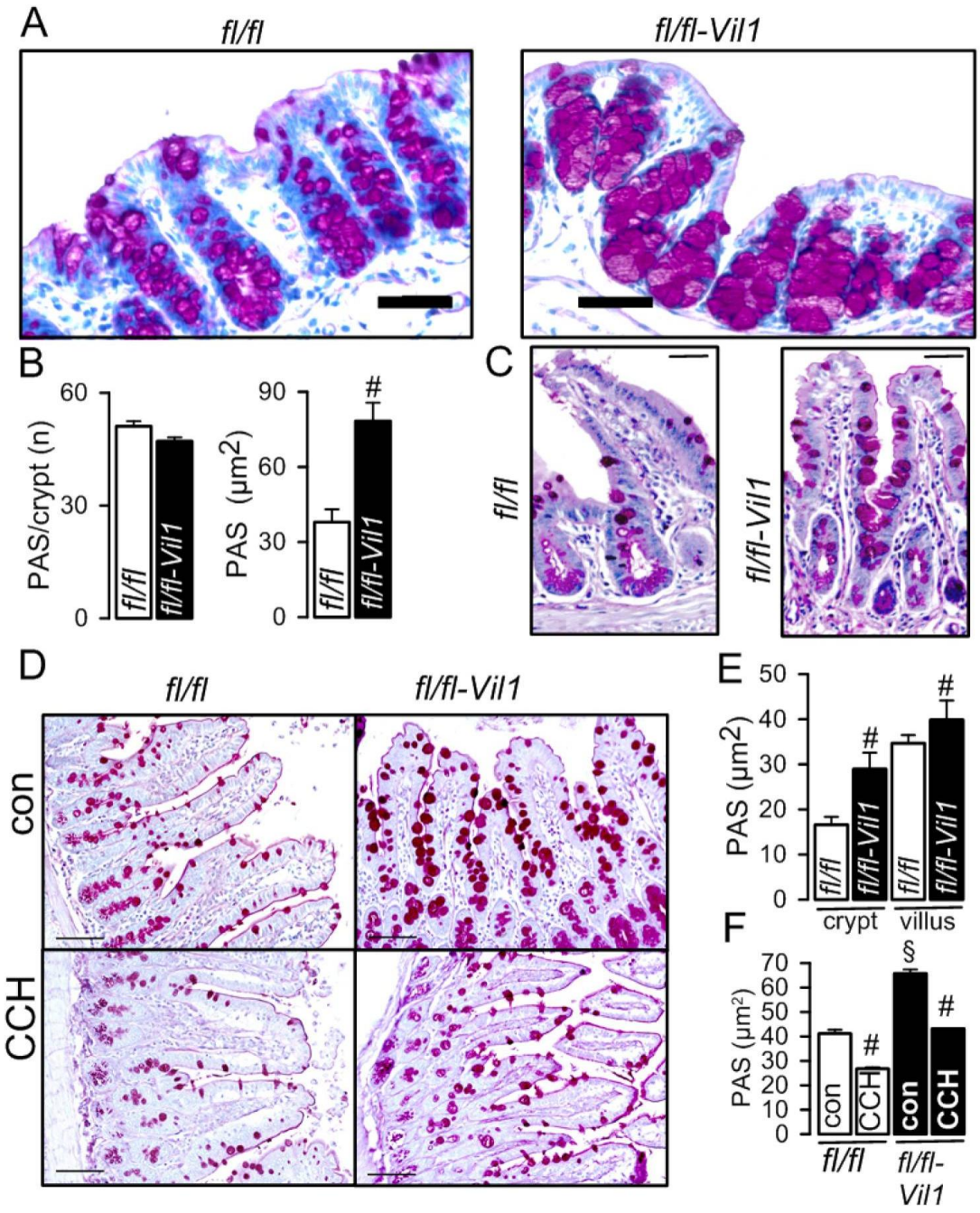

Fig 5.4 *Mucus accumulates in intestinal goblet cells of TMEM16A$^{flox/flox}$Vil1 mice.*
A) PAS-staining of large intestinal goblet cells from *TMEM16A$^{flox/flox}$* (*fl/fl*) and *TMEM16A$^{flox/flox}$Vil1* (*fl/fl-Vil1*) mice. B) Number of PAS-positive cells in mucus accumulation in crypts from *fl/fl* and *fl/fl-Vil1* mice (n = 40). C,D) PAS staining in small intestine of *fl/fl* and *fl/fl-Vil1* mice (C) and effect of CCH (100 µM) on mucus release (D). E) Quantification of PAS staining in crypts and villi of *fl/fl* and *fl/fl-Vil1* mice (n = 550 – 750). F) Effect of CCH on PAS staining in *fl/fl* and *fl/fl-Vil1* mice (n = 550 – 750). Mean ± SEM; #significant difference when compared to *fl/fl* or control, respectively (unpaired t-test).

In contrast to *TMEM16A$^{flox/flox}$* colon, no mucus was released by ATP in *TMEM16A$^{flox/flox}$Vil1* colon (Fig 5.5 A, right). While expression of $P2Y_2$ was unchanged, $P2Y_4$ was upregulated in *TMEM16A$^{flox/flox}$Vil1* colon, which could be a compensatory upregulation (data not shown).

Thus basal and ATP-mediated mucus release in both airways and intestine are TMEM16A-dependent.

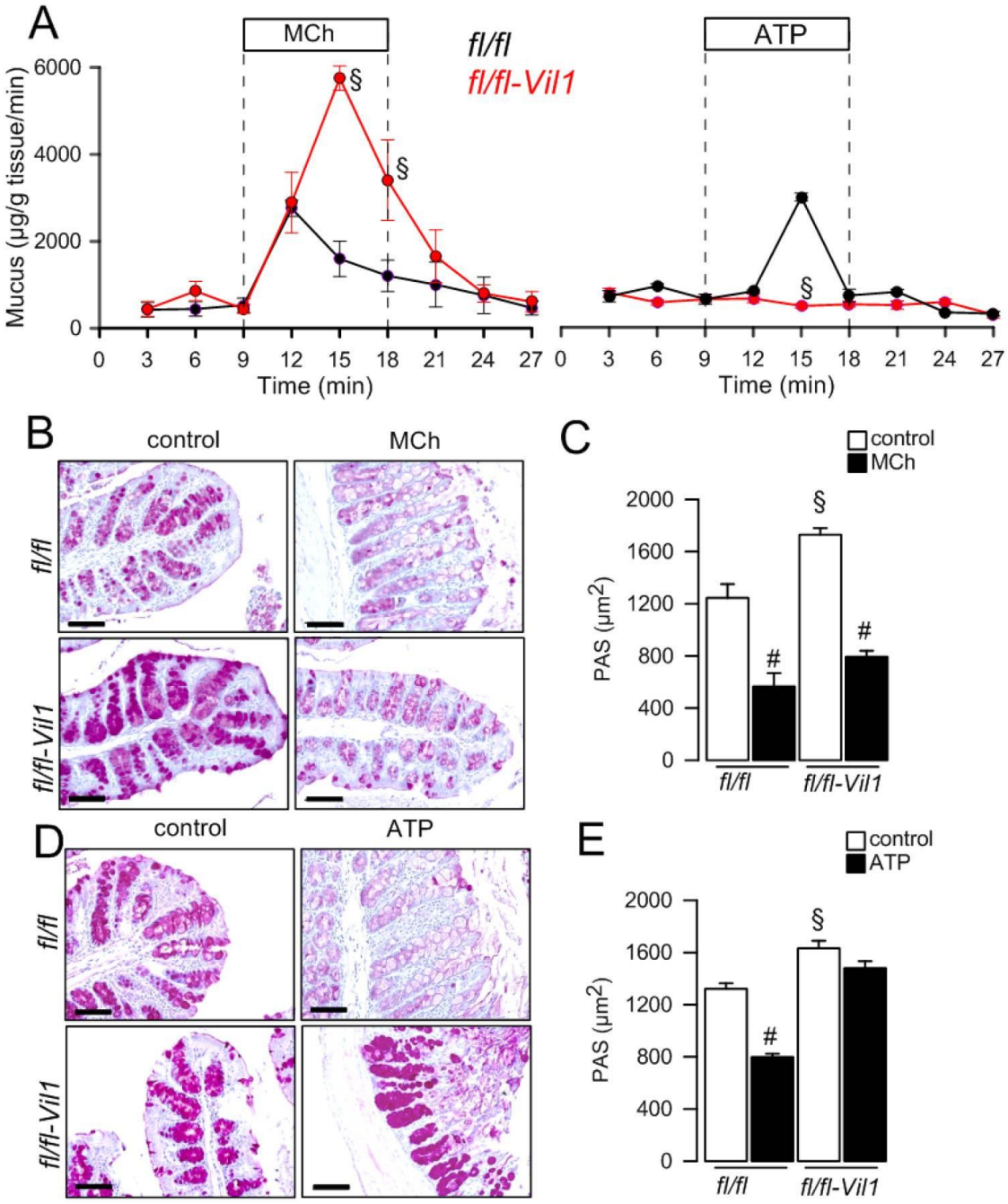

Fig 5.5 *Compromised mucus release in TMEM16A$^{flox/flox}$Vil1 intestine.*

A) Acute mucus secretion in perfused colon from *TMEM16A$^{flox/flox}$* (*fl/fl*) (black curve) and *TMEM16A$^{flox/flox}$Vil1* (*fl/fl-Vil1*) (red curve) animals. Mucus release was induced by luminal/basolateral perfusion with ATP (100 µM) and methacholine (MCh; 100 µM), respectively (n = 4 – 6). B,D) PAS stainings before and after application of MCh or ATP. Bars 50 µm. C,E) Quantification of PAS before and after stimulation with MCh or ATP (n = 19 – 34). Mean ± SEM; $^{\#}$significant difference when compared to control (unpaired t-test). §significant difference when compared to *fl/fl* (unpaired t-test).

TMEM16A controls intracellular Ca^{2+} signals and membrane exocytosis.

TMEM16A controls ATP-induced compartmentalized Ca^{2+} signals by enhancing Ca^{2+} store release and store operated Ca^{2+} influx (SOCE). Both was shown to be reduced in airways and intestine of *TMEM16A$^{flox/flox}$FoxJ1* and *TMEM16A$^{flox/flox}$Vil1* mice, respectively [80, 128, 200]. In the present study we found that intestinal mucus release by ATP requires luminal Ca^{2+} which is, however, not needed for MCh-induced secretion (Fig S5.5 E,F). Ca^{2+} increase stimulated by ATP was much reduced in goblet cells of freshly isolated *TMEM16A$^{flox/flox}$Vil1* crypts, while Ca^{2+} increase induced by basolateral cholinergic stimulation was only slightly compromised in the absence of TMEM16A (Fig S5.6). Apical intracellular Ca^{2+} prepares granules for release by the exocytic machinery via the Ca^{2+} sensors Munc13 and Doc2B [94, 102, 233]. Thus TMEM16A appears essential for exocytosis. A role of different TMEM16 paralogues for synaptic transmission has been proposed recently [67, 234, 235]. We examined TMEM16A-expressing HEK293 cells and noticed that this enhanced membrane capacitance. Membrane capacitance is proportional to membrane surface and was found to be further enhanced by stimulation with the Ca^{2+} ionophore ionomycin (Fig 5.6 A-C). Using the surface marker CD8, we found enhanced membrane expression in the presence of TMEM16A (Fig 5.6 D,E). We analyzed plasma membrane lipid content using the lipophilic dye FM4-64 and found enhanced staining in the presence of TMEM16A. This was inhibited by the TMEM16A blocker CaCCinhAO1 and by the exocytosis-inhibitor tetanus toxin[236] (Fig 5.6 F-J). The present data therefore suggest that TMEM16A controls exocytosis of mucus-filled granules by providing Ca^{2+} to an apical signaling compartment. TMEM16A is thus indispensable for basal and ATP-controlled mucus secretion in airways and intestine.

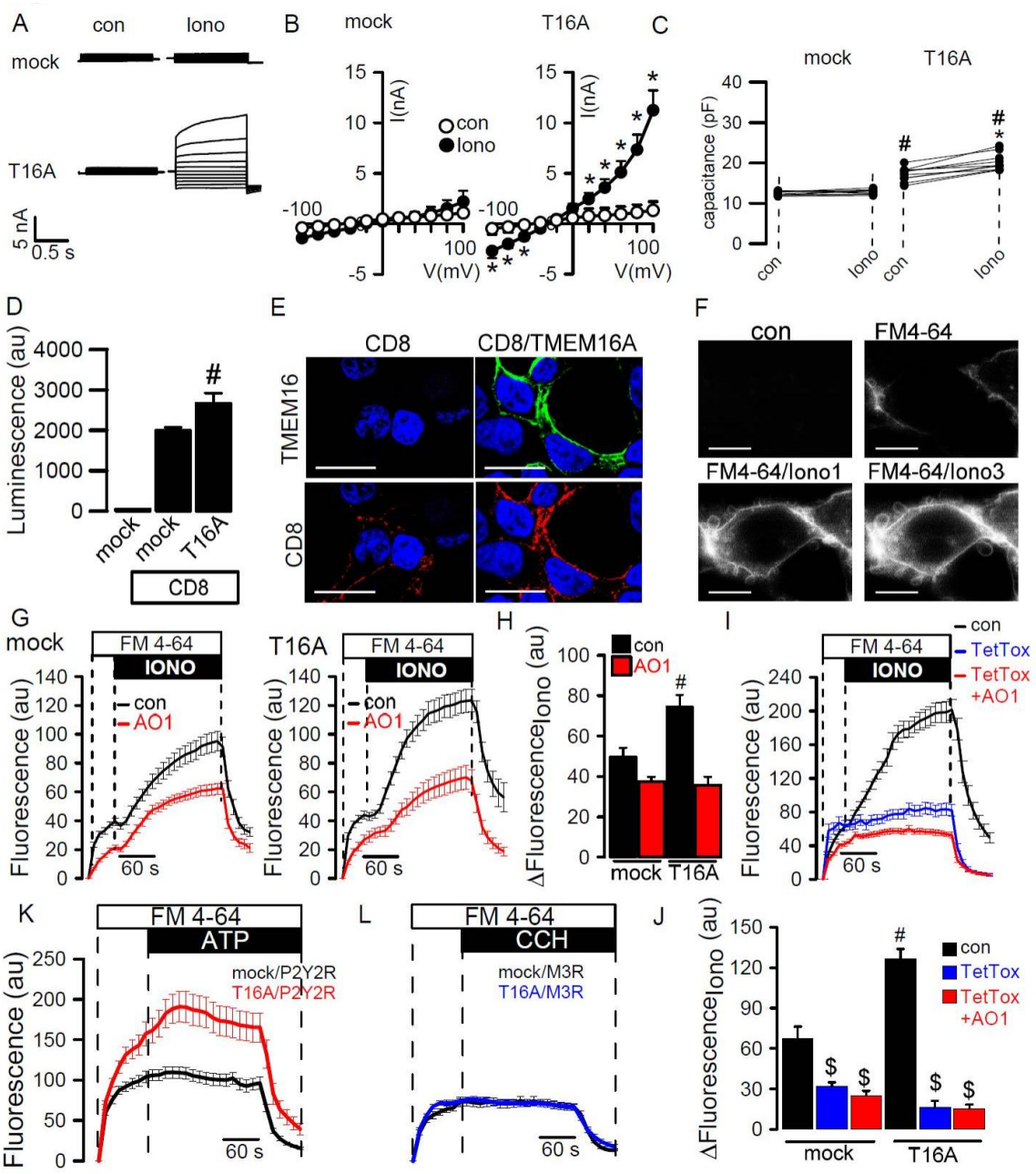

Fig 5.6 *TMEM16A controls exocytosis.*

A,B) Whole cell currents and current/voltage relationships obtained in mock transfected and TMEM16A (T16A) expressing HEK293 cells. Stimulation with the Ca^{2+} ionophore ionomycin (Iono; 1 µM) activated whole cell currents in TMEM16A-expressing cells (n = 12). C) Enhanced membrane capacitance in TMEM16A-expressing cells under control conditions and after stimulation with ionomycin (n = 12). D) Chemiluminescence measured in HEK293 cells expressing the surface receptor cluster of differentiation 8 (CD8) (n = 8 – 16). E) Membrane expression of CD8 detected by anti-CD8-AB and secondary fluorescence-labeled AB in CD8 and CD8/TMEM16A coexpressing cells. F) Plasma membrane staining in HEK293 cells exposed to the fluorescent lipid dye FM4-64. Staining was enhanced by 1 and 3 min stimulation with ionomycin (Iono, 1 µM). G) Time dependent increase of FM4-64 fluorescence upon stimulation with ionomycin in mock-transfected and TMEM16A-expressing cells, and inhibition by CaCCinhAO1 (AO1; 10 µM) (n = 30). H) Summary of fluorescence increase induced by ionomycin (n = 30). I) Iono-induced FM4-64 fluorescence and inhibition by tetanus toxin

(TetTox; 20 nM) and combined application of TetTox/AO1 (n = 12). J) FM4-64 fluorescence in mock and TMEM16A-expressing cells (n = 50). K,L) Effect of ATP or CCH (both 100 µM) on FM4-64 fluorescence in cells expressing $P2Y_2$ or M3 receptors (n = 30). Mean ± SEM. *significant increase by Iono (paired t-test). #significant difference when compared to mock (unpaired t-test). §significant difference when compared to control (unpaired t-test). Bars indicate 20 µm.

Discussion

Excessive airway mucus is a problem in CF, COPD, and asthma, while intestinal mucus can be enhanced in CF, ulcerative colitis and irritable bowel syndrome. Thus, there is a demand for novel drugs controlling excessive mucus secretion [237]. As suggested by the present results, inhibitors of TMEM16A may represent a new class of drugs that reduce mucus secretion under basal conditions and upon stimulation by apical ATP. Notably, basal mucus secretion may clearly exceed stimulated (cholinergic) secretion, which is blocked by inhibitors of TMEM16A [225]. In fact, the nonspecific inhibitor Niflumic acid (NFA) blocked mucus secretion and mucus production in earlier studies [220]. However, inhibition of mucus synthesis by NFA also occurs in the absence of TMEM16A, suggesting inhibition of other channels. TMEM16A could contribute to mucus release by providing a secretory pathway for HCO_3^-, which helps to unfold and solubilize mucus [217, 238]. We found only a weak HCO_3^- permeability of TMEM16A in patch clamp experiments at a cytosolic Ca^{2+} concentration of 1 µM (Fig 5.7 A). However, at higher intracellular Ca^{2+} levels the channel has been demonstrated to be well permeable for HCO_3^-[239].

Our data point out to an essential new role of TMEM16A for exocytosis. This function may not be limited to mucus release, but may also control the release of inflammatory mediators and secretory proteins such as CLCAs (Chloride Channel Accessory). In support of this, we found that LPS-induced release of IL-8 by Calu3 airway epithelial cells was significantly reduced by knockdown of TMEM16A (Fig S5.7 B). Attenuated release of inflammatory and chemotactic cytokines by airway epithelial cells lacking TMEM16A could explain the reduced leukocytic infiltration observed in OVA-challenged animals (Fig 5.2 F). It may also explain why expression of TMEM16A in ASM is lower in OVA-challenged *Vil1-TMEM16A$^{flox/flox}$* mice (Fig S5.3). Upregulated TMEM16A in airways smooth muscles (ASM) strongly supports bronchoconstriction [68, 152, 240]. Thus, blockade of TMEM16A will inhibit release of mucus and

cytokines, and will induce bronchodilation, which should be all beneficial in inflammatory airway disease [152, 241]. In contrast, activation of TMEM16A should have adverse effects. We found in OVA-sensitized mice that activation of TMEM16A by E_{act} [156] induced massive mucus release and airway contraction (Fig S5.8).

The present data also provide a novel regulation of basal ATP-mediated mucus release by intestinal goblet cells and demonstrate the crucial role of TMEM16A. In both airways and intestine, compound exocytosis induced by cholinergic stimulation was not compromised in *Vil1-TMEM16A*$^{flox/flox}$mice. Compound exocytosis is characterized by a fusion of secretory granules to a large mucin-filled vacuole, which is very different to apical single granule fusion triggered by ATP. It provides a mechanism for the release of deeper granules [214, 242-244]. Muscarinic stimulation induced mucus release was independent of extracellular Ca^{2+}, and did not induce exocytosis in HEK293 cells (Fig S5.5 F, Fig 5.6K). In contrast, ATP-dependent secretion is characterized by Ca^{2+} dependent single granule docking to the apical membrane that requires Munc13 proteins and the SNARE (soluble N-ethylmaleimide–sensitive factor attachment protein receptor) machinery [213]. To our knowledge, this is the first report on ATP-controlled mucus release by native intestinal goblet cells, which share similar regulatory properties with mucus producing airway cells.

Knockdown of TMEM16A in airway epithelial cells eliminated both TMEM16A and CFTR dependent Cl^- secretion [200], and abrogated mucus release. It was rather unexpected that these mice with complete absence of Cl^- secretion did not show any signs of compromised mucociliary clearance or lung disease [200]. We propose that mucus hypersecretion is the leading cause for CF lung disease, more so than the lack of Cl^- secretion. Further studies are needed to examine if the present findings obtained in mice are applicable to human airways. In Calu3 human airway epithelial cells, we found that IL-13 induced production of Muc5AC is inhibited by the TMEM16A-blocker Niclosamide and by siRNA-knockdown of TMEM16A, and mucus release appeared compromised (Fig 5.7).

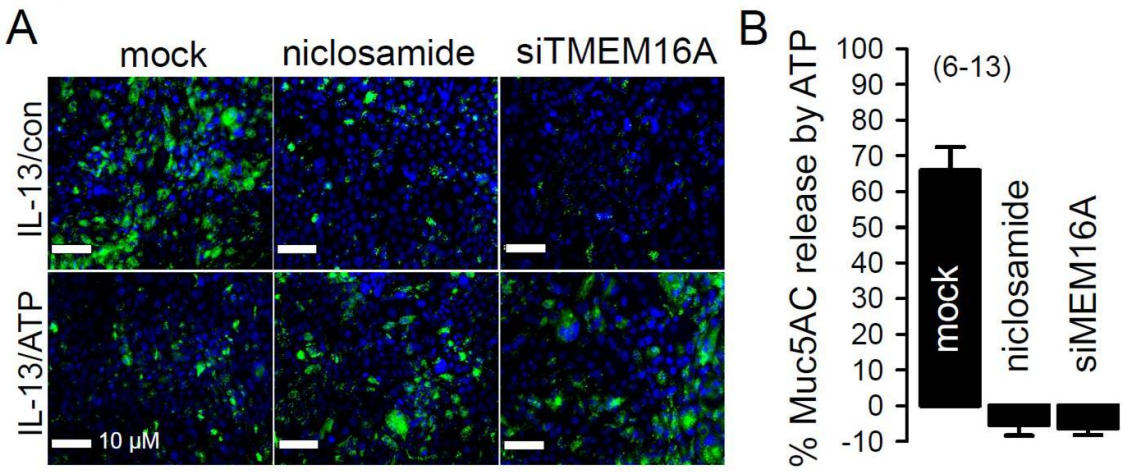

Fig 5.7 *TMEM16A controls basal mucus secretion in human airway epithelial cells.*
A) Immunocytochemistry of Muc5AC in Calu3 human airway epithelial cells. Mucus production was induced by the Th2 cytokine IL-13. In the presence of Niclosamide (1 µM) or after siRNA knockdown of TMEM16A, IL-13 induced Muc5AC was reduced and secretion was not detectable. B) Summary of ATP-induced Muc5AC release. Mean ± SEM. (number of experiments). Bars indicate 20 µm.

The present and previous [200] data somewhat question the role of active Cl^- secretion for maintenance of the airway surface fluid layer. Boucher and coworkers along with other teams provided evidence that human airways are primarily a reabsorptive tissue. Regulation of ASL height might be primarily dependent on Na^+ absorption by epithelial Na^+ channels [43, 44, 245-247]. Thus, control of Na^+ absorption by CFTR and particularly by purinergic receptors may affect ASL height more than electrogenic Cl^- secretion.

Blocking mucus secretion in CF by inhibiting TMEM16A may appear counterintuitive, since epithelial Cl^- secretion will be blocked. Moreover, Cl^- secretion via CFTR might also be compromised by inhibitors of TMEM16A, because of the known regulation of CFTR by TMEM16A [200]. However, net secretory Cl^- flux through TMEM16A is probably transient and rather small [248]. Moreover, Cl^- secretion through CFTR is already compromised in CF. Thus; the benefit through inhibition of mucus secretion (and probably mucus production [218, 221]) may well exceed potential drawbacks due to inhibition of Cl^- secretion. In fact, mice completely lacking airway Cl^- secretion did not exhibit airway plugging [80]. Clinical pilot studies may provide better insight towards the potential use of TMEM16A blockers in CF.

Acknowledgements

Supported by Cystic Fibrosis Trust, SRC 003, INOVCF, DFG SFB699-A7/A12, DFG KU756/12-1. The excellent technical assistance by Ms. P. Seeberger and Ms. E. Tartler is gratefully acknowledged. We thank Prof. Dr. Ernst Tamm and Ms. Margit Schimmel (Institute for Anatomy, University of Regensburg) for providing EM images. The supply of mice with a floxed *TMEM16A* gene by Prof. Jason R. Rock (Boston University School of Medicine) and Foxj1-Cre mice by Prof. Michael J. Holtzman and Dr. Y. Zhang (Washington University School of Medicine) is gratefully acknowledged.

Supplementary material

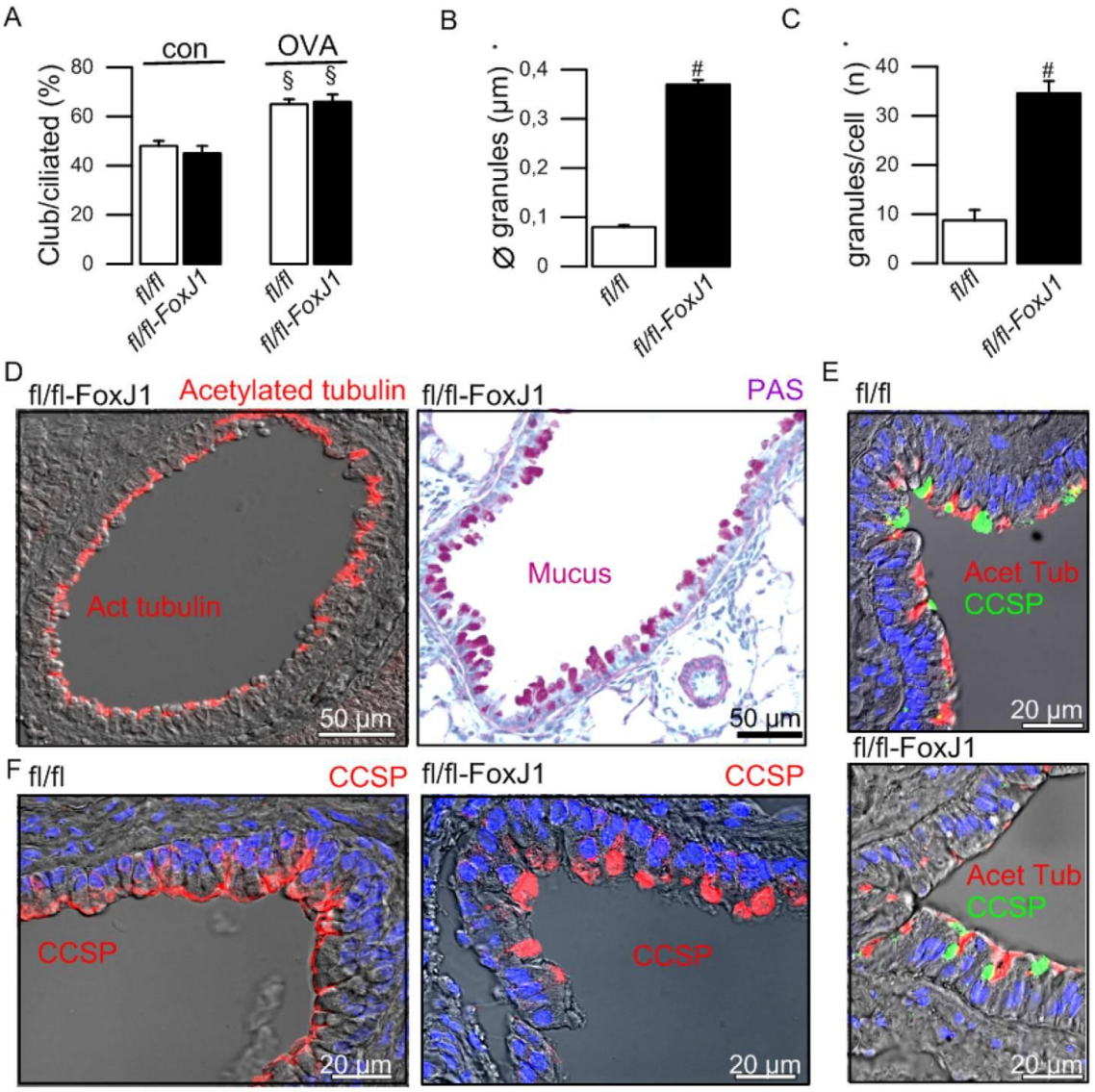

Supplementary Figure 5.1 *Airways of TMEM16A$^{flox/flox}$ (fl/fl) and TMEM16A$^{flox/flox}$-FoxJ1Cre (fl/fl-FoxJ1) mice.*

A) Ratio of club cells (CCSP positivity) versus ciliated (acetylated tubulin positivity) cells in small airways. No enhanced number of club cells in *fl/fl-FoxJ1* under control conditions. OVA-sensitization enhanced number of club cells in both *fl/fl* and *fl/fl-FoxJ1* mice. B,C) Diameter of secretory granules in club cells from *fl/fl and fl/fl-FoxJ1*, and number of granules per cell. D) Acetylated tubulin and mucus in *fl/fl-FoxJ1* under control conditions. E) Acetylated tubulin and CCSP in *fl/fl and fl/fl*-FoxJ1 airways. F) CCSP in *fl/fl and fl/fl*-FoxJ1 under control conditions. Mean ± SEM (1799 cells counted in 3 *fl/fl* and 3 *fl/fl-FoxJ1* animals). $^{\#}$indicates significant difference between *fl/fl* and *fl/fl-FoxJ1* ($p<0.05$; unpaired t-test). §indicates significant difference between control and OVA-treated animals ($p<0.05$; unpaired t-test).

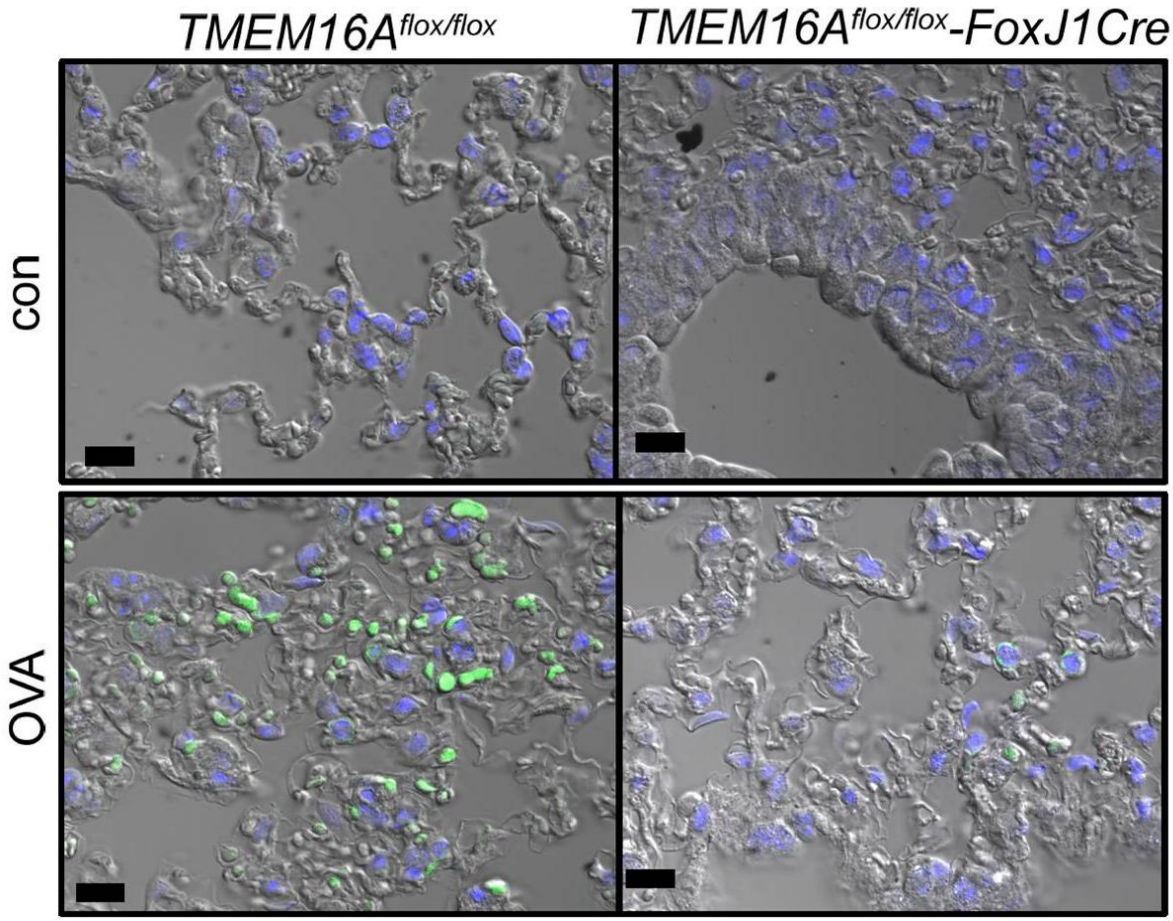

Supplementary Figure 5.2 *Accumulation of CD45-positive leucocytes is reduced in OVA-sensitized lungs of TMEM16A$^{flox/flox}$-FoxJ1Cre mice.*

Immunocytochemistry of CD45-positive cells in lungs of control and OVA-sensitized *TMEM16A$^{flox/flox}$* and *FoxJ1Cre-TMEM16A$^{flox/flox}$* mice. Images are representatives of n = 3 animals. Bars indicate 20 µm.

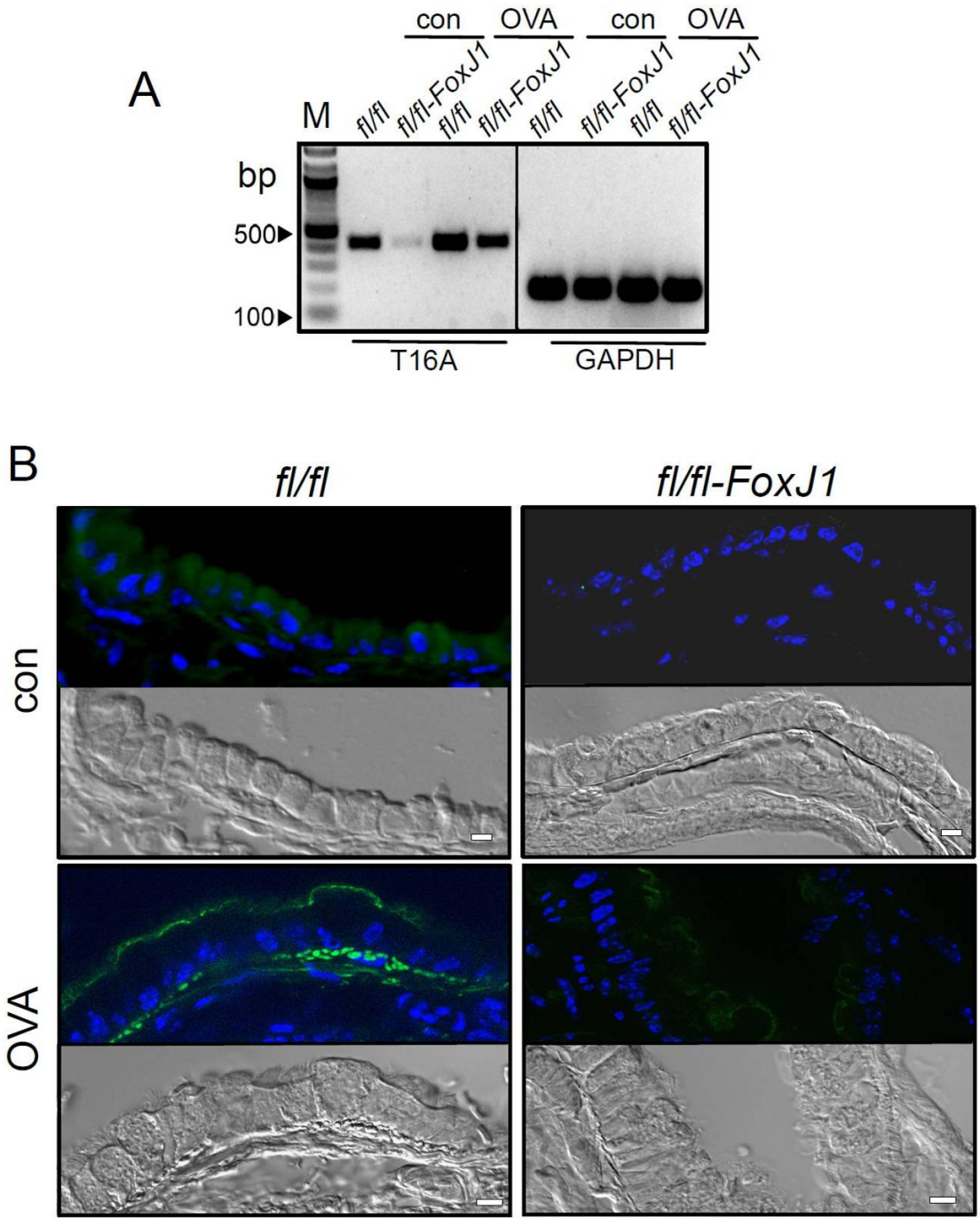

Supplementary Figure 5.3 *Effect of OVA on expression of TMEM16A in airways of TMEM16A$^{+/+}$ and TMEM16A$^{-/-}$ mice.*

A) RT-PCR from whole lung of TMEM16A+/+ and TMEM16A-/- mice. Expression of TMEM16A was upregulated by OVA-sensitization in TMEM16A+/+ and TMEM16A-/- lungs. GAPDH served as a control. Representatives of n = 3 separate reactions. B) Expression of TMEM16A in TMEM16A+/+ and TMEM16A-/- airways under control conditions and after OVA sensitization. In control TMEM16A+/+ airways, TMEM16A is very weakly expressed. After OVA-sensitization, expression is reduced in airway smooth muscle of TMEM16A$^{-/-}$ mice, when compared to TMEM16A$^{+/+}$. Bars indicating 10 µm.

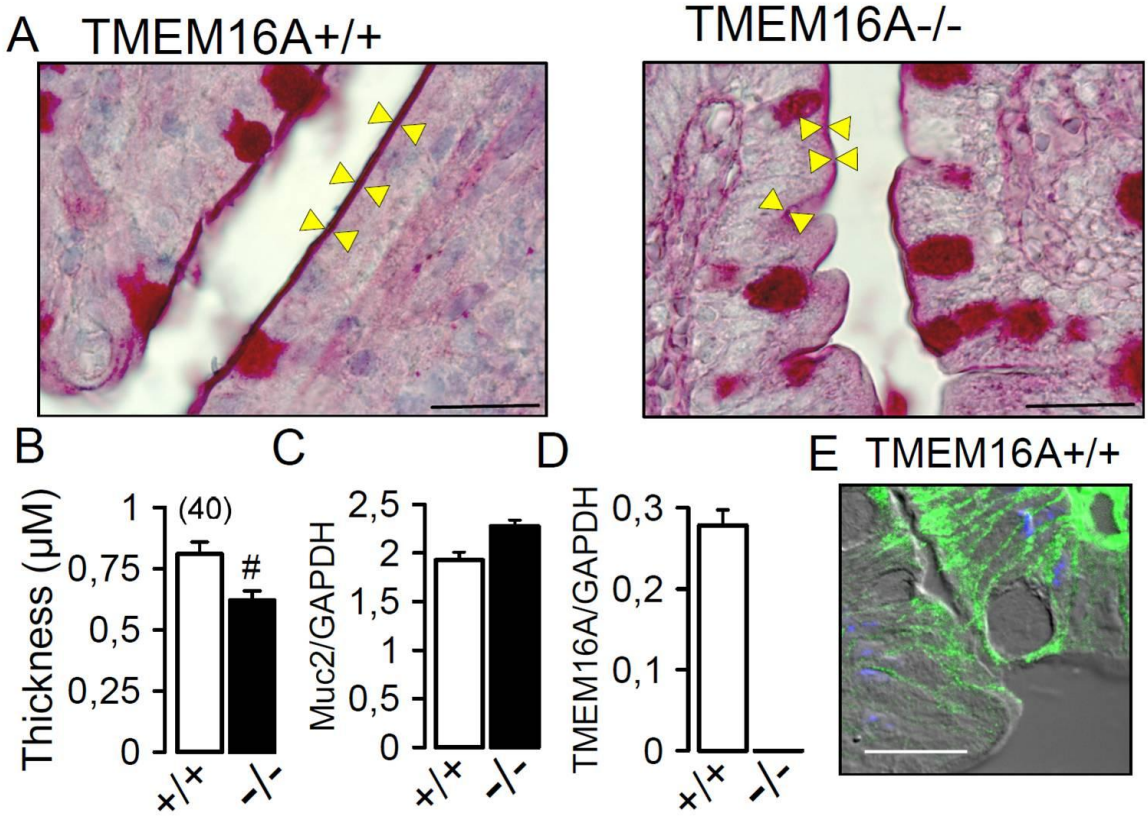

Supplementary Figure 5.4 *Defective mucus secretion in small intestine of TMEM16A$^{flox/flox}$Vil1 mice.* A, B) PAS staining of mucus covering jejunal mucosa of *TMEM16A$^{flox/flox}$* (*fl/fl*) and *TMEM16A$^{flox/flox}$Vil1 (fl/fl-Vil1)* mice. The mucus layer in *fl/fl-Vil1* intestine appeared thinner and more irregular. C, D) mRNA levels of Muc2 and TMEM16A in *fl/fl* and *fl/fl-Vil1* colon as assessed by semiquantitative RT-PCR. E) Differential interference contrast image and expression of TMEM16A detected by immunofluorescence (green) in enterocytes and goblet cells. Bars indicating 20 µm. Mean ± SEM (n = 40 crypts analysed in n=3 *fl/fl* and n=3 *fl/fl-Vil1* mice).

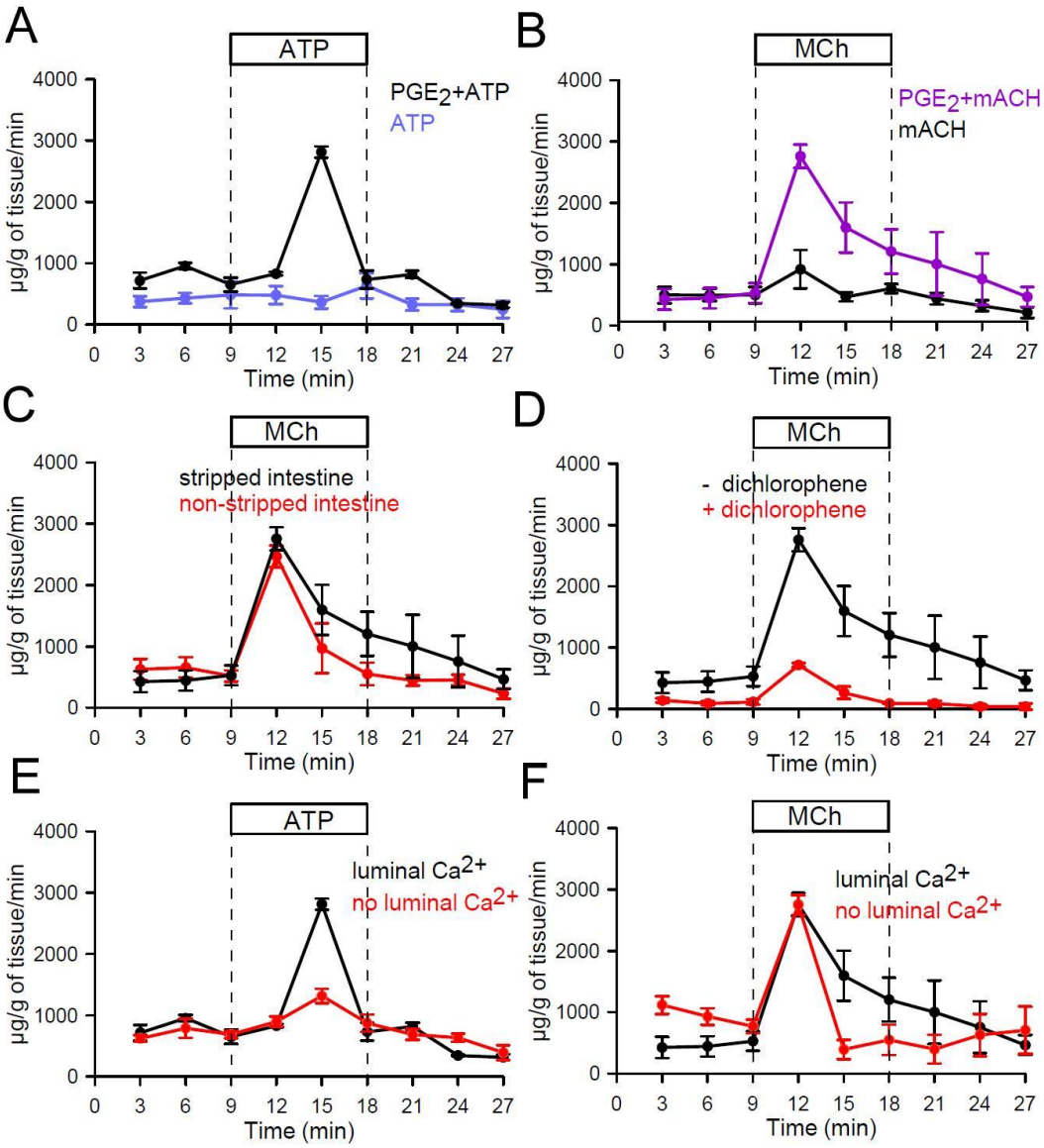

Supplementary Figure 5. 5 *Induction of mucus secretion in vitro perfused colon.*

A, B) Mucus secretion induced by ATP (100 µM) or methacholine (MCh; 100 µM) requires co-stimulation with PGE_2 (1 µM) to activate CFTR dependent fluid secretion and to flush mucus out of the crypts. PGE_2 alone did not induce mucus secretion. C) Mucus release by MCh was equal in non-stripped and stripped (removal of serosal and submucosal layers) colon, suggesting direct stimulation of goblet cells by MCh. D) Dichlorophene (30 µM), an inhibitor of TMEM16A, suppressed acute MCh-induced mucus secretion. E, F) Removal of apical Ca^{2+} in the perfusion solution inhibited mucus secretion by ATP but not by MCh. (n = 3 - 5 mice for each series).

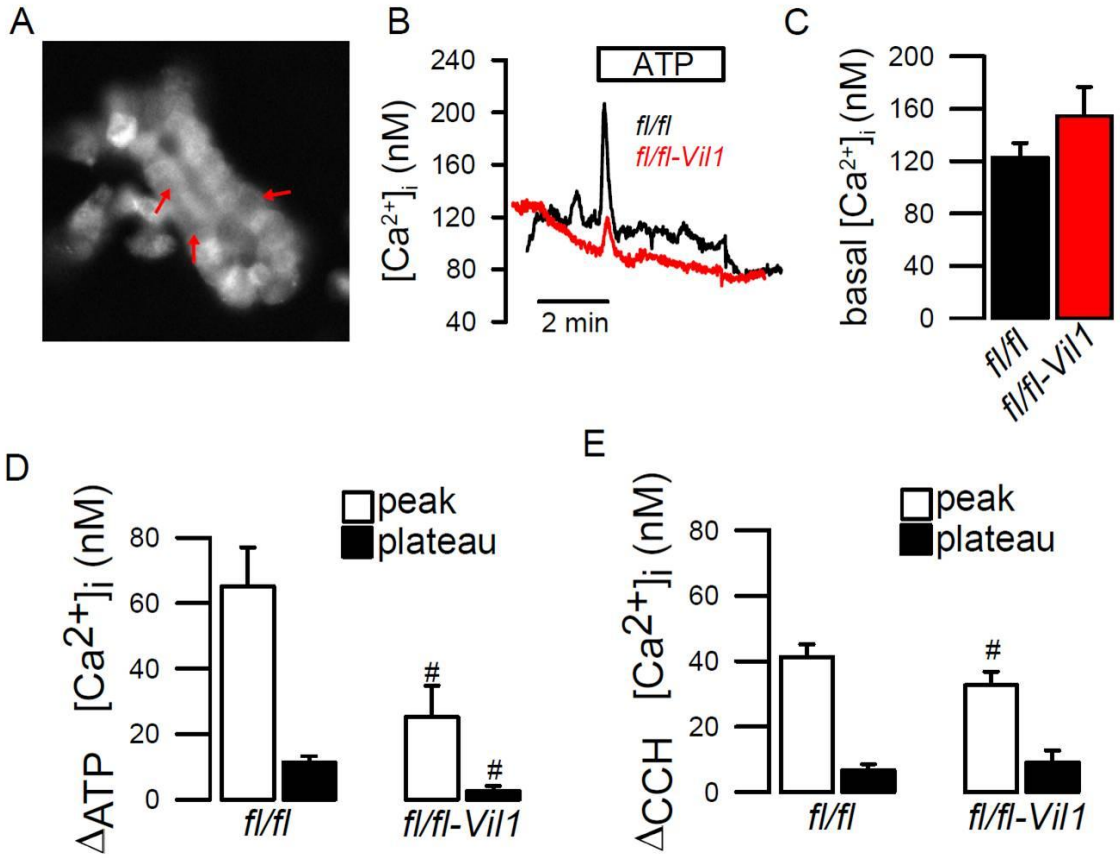

Supplementary Figure 5.6 *Purinergic Ca^{2+} signals are compromised in goblet cells from TMEM16A$^{flox/flox}$Vil1 colon.*

A) Isolated crypt loaded with the Ca^{2+} dye Fura-2. Arrows indicate goblet cells used for measurement of intracellular Ca^{2+}. B) Original recordings of Ca^{2+} concentrations in goblet cells from *TMEM16A$^{flox/flox}$ (fl/fl)* and *TMEM16A$^{flox/flox}$Vil1 (fl/fl-Vil1)* mice. Activation of Ca^{2+} signals by ATP (100 µM). C) Summary of basal Ca^{2+} levels in *fl/fl* and *fl/fl-Vil1* cells (n = 14). D, E) ATP induced Ca^{2+} increase (peak and plateau) were strongly reduced in goblet cells from *fl/fl-Vil1* mice. Ca^{2+} peaks induced by carbachol (CCH; 100 µM) were only slightly reduced in *fl/fl-Vil1* cells and plateau Ca^{2+} was indistinguishable from *fl/fl* (n = 111-126). $^{\#}$ indicates significant difference from *fl/fl* (n) number of goblet cells examined for each series.

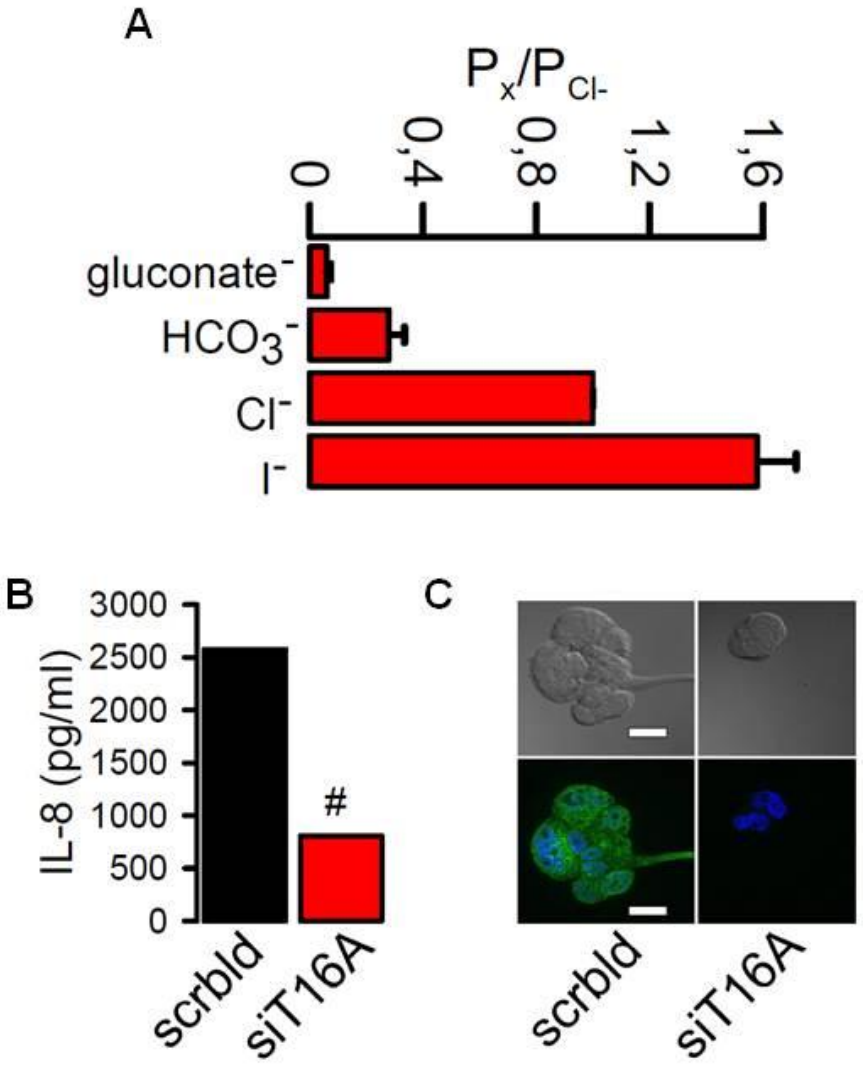

Supplementary Figure 5.7 *TMEM16A is limitedly permeable to HCO_3^-, TMEM16A downregulation reduces IL-8 release.*

A) Anion permeability ratios for TMEM16A overexpressed in HEK293 cells (n = 7). TMEM16A was activated by high pipette Ca^{2+} (1 µM). Extracellular Cl^- (145 mM) was replaced by gluconate, HCO_3^-, or I-. Shifts in the reversal potentials detected in current voltage relationships were used to calculate permeability ratios. (Pipette solution 145 mM NaCl). TMEM16A shows only a limited permeability for HCO_3^-. B) IL-8 release from Calu3 human airway submucosal cells. Exposure of the cells to LPS (10 µg/ml; 48 hrs) induced a pronounced IL-8 release that was markedly reduced upon knockout of TMEM16A with siRNA for TMEM16A (n = 3). C) Immunocytochemistry of TMEM16A (DOG1-antibody, 1:200) in Calu3 cells treated with siRNA for TMEM16A or scrambled RNA, respectively. Mean ± SEM (number of experiments). $^{\#}$ significant IL-8 release, §significant difference to scrambled ($p<0.05$, unpaired t-tests). Bar = 20 µm.

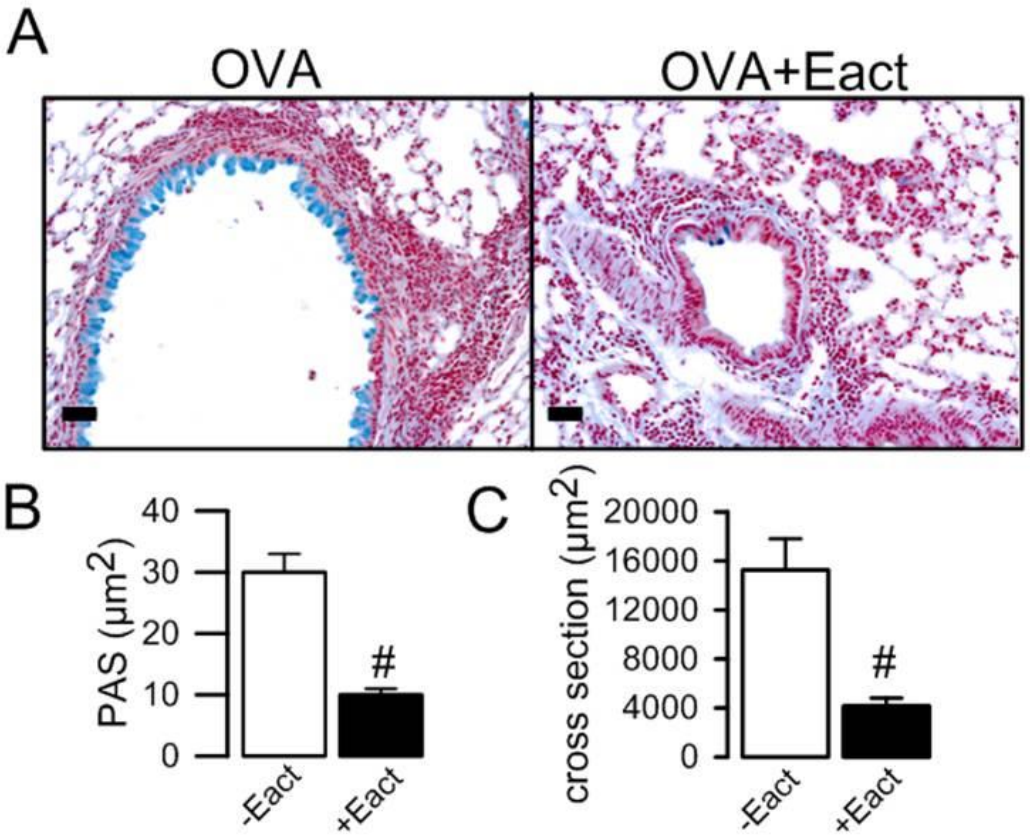

Supplementary Figure 5.8 *Effect of E_{ACT} on mucus release and airway contraction.*
A) Airways from OVA-sensitized mice show pronounced mucus accumulation as demonstrated by alcian blue staining. Acute exposure to the known activator of TMEM16A, Eact, (4.8 µg, tracheal instillation) induced a rapid mucus release and airway contraction. B) PAS positive staining in control airways (OVA) and after application of Eact (n = 14 - 26). C) Airway cross sectional area in control airways and after application of Eact (n = 20 – 34). Mean ± SEM. #indicates significant effect of Eact. Bars indicate 10 µm.

Chapter 6

Niclosamide repurposed for the treatment of inflammatory airway disease

Abstract

Inflammatory airway diseases such as asthma, Cystic Fibrosis (CF) and COPD are characterized by airway restriction and mucus hypersecretion. CF and asthma exhibit enhanced expression of the Ca^{2+} activated Cl^- channel TMEM16A in metaplastic club cells and airway smooth muscle, and contributes strongly to mucus hypersecretion and bronchoconstriction. Nonspecific inhibitors of TMEM16 proteins like Niflumic acid (NFA), inhibit mucus production and bronchoconstriction. Here we demonstrate that the FDA-approved drug Niclosamide is a highly potent inhibitor of TMEM16A and TMEM16F. In asthmatic mice, Niclosamide inhibited mucus production and secretion, as well as bronchoconstriction, and showed an anti-inflammatory effect. Both TMEM16A and TMEM16F are essential for mucus production/secretion that is explained by augmentation of intracellular Ca^{2+} signals. TMEM16A/F supported exocytic release of mucus and inflammatory mediators, and are inhibited by Niclosamide. The present results unmask TMEM16A/F as pathogenic factors during inflammatory airway disease, and suggest Niclosamide as a potent drug for the treatment of asthma, CF, and COPD.

Key words: Niclosamide, TMEM16A; TMEM16F; anoctamin 1; anoctamin 6; mucus, Cystic Fibrosis, asthma, COPD, Ca^{2+} signaling, repurposing

Submitted for publication: Inês Cabrita, **Roberta Benedetto**, Rainer Schreiber, Karl

Kunzelmann. Niclosamide repurposed for the treatment of inflammatory airway disease. JCI.
Own experimental contribution: Patch clamping experiments, Ovalbumine sensitization, Histology
Own written contribution: Methods, Results, Parts of Introduction and Discussion.
Other contributions: Designed experiments and analyzed data.

Introduction

Inflammatory airway diseases such as asthma, Cystic Fibrosis (CF), and COPD are characterized by airway obstruction due to mucus hypersecretion, mucus plugging and bronchoconstriction [152, 213, 218, 229, 249, 250]. The Cystic Fibrosis transmembrane conductance regulator (CFTR) chloride channel is dysfunctional in CF, leading to attenuated fluid and bicarbonate secretion, along with Na^+ hyperabsorption and dehydration of the airway surface liquid (periciliary fluid layer; ASL) covering the airway epithelium [217, 251]. The consequence is dehydrated airway mucus with abnormal rheological properties that occludes smaller airways. Local hypoxia, neutrophilic infiltration, accumulation of reactive oxygen species and bacterial superinfection cause destructive pulmonary inflammation. Whether an acidic ASL-pH further attenuates antimicrobial defense, and thus contributes to lung pathology, is still a matter of debate [252, 253]. Because of the obvious lack of apical CFTR Cl^- conductance in CF airways, alternative chloride channels were proposed to fill the gap. Thus, research focused on SLC26A9 and particularly on Ca^{2+} activated TMEM16A Cl^- channels [254].

A recent study on adult TMEM16A airway epithelial knockout (*FoxJ1-Cre-TMEM16A*$^{flox/flox}$) mice provided rather surprising results. Mice lacking airway epithelial expression of TMEM16A have no discernible apical airway epithelial Cl^- conductance; i.e. they neither exhibit Ca^{2+} activated Cl^- currents (CaCC) nor cAMP-activated CFTR Cl^- currents, yet the animals do not develop a CF-like phenotype, and do not show attenuated mucociliary clearance [200]. TMEM16A is expressed at low levels in ciliated cells, and at higher levels in mucus producing club (Clara) cells. It is strongly upregulated under inflammatory conditions such as CF and asthma [152, 213, 218, 229, 249, 250, 255]. Our previous report demonstrates that TMEM16A is essential for basal secretion of mucus in both airways and intestine [255]. The data demonstrate a previously unrecognized role of TMEM16A for membrane exocytosis and describe a novel ATP-driven pathway for intestinal mucus secretion. Moreover, TMEM16A is expressed in airway smooth muscle (ASM), where it supports contraction. TMEM16A therefore mediates a number of adverse events in inflammatory airway disease, which suggests that in CF the channel should be inhibited rather than activated.

TMEM16A is also weakly expressed in ciliated epithelial cells, where it may support Cl^- secretion. However, its prosecretory effect is mainly through activation of CFTR. In the CF lung, where CFTR is dysfunctional, inhibition of TMEM16A is therefore predicated to have little or no impact on Cl^- secretion [161, 162, 200]. In tissue specific airway and intestinal epithelial TMEM16F knockout mice, we find that both TMEM16A [255] and TMEM16F are in charge of mucus production and secretion. We demonstrate potent inhibition of mucus secretion in airways and intestine by the well-known anthelminthic drug Niclosamide, which has been shown recently to be a potent inhibitor of TMEM16A [241]. We suggest repurposing of Niclosamide for the use in inflammatory obstructive airway disease. Inhibition of mucus production/secretion along with bronchodilation is likely to be the most effective treatment of CF lung disease. It will normalize the imbalance between excessive mucus secretion and reduced ASL, and it will therefore counteract airway plugging.

Materials and methods

Animals, OVA*-induced *asthma. All animal experiments complied with the ARRIVE guidelines and were carried out in accordance with the U.K. Animals Act, 1986 and associated guidelines, EU Directive 2010/63/EU for animal experiments. Knockout of TMEM16A in ciliated airway epithelial cells (*TMEM16A$^{flox/flox}$FoxJ1Cre*) has been described elsewhere [200]. Generation of mice with a floxed TMEM16F allele was described in [256]. For knockout of TMEM16F in ciliated epithelial and intestinal epithelial cells, *TMEM16F$^{flox/flox}$* mice were crossed with *FoxJ1-Cre* and *Vil1-Cre* mice to obtained *TMEM16F$^{flox/flox}$FoxJ1Cre* and *TMEM16A$^{flox/flox}$Vil1Cre*, respectively. Mice were sensitized to ovalbumin (OVA, Sigma-Aldrich, Germany) by intraperitoneal (ip) injection of 100 µg OVA with 1 mg aluminum hydroxide gel (Sigma) on days 0 and 14. At days 21, 22 and 23, mice were anaesthetized and challenged to OVA by intratracheal instillation of 50 µg OVA in 100 µl saline. Control mice were sham sensitized with saline and aluminum hydroxide gel (Sigma-Aldrich, Germany) and challenged to 100 µl saline by intratracheal instillation [224]. NFA (0.5 mg/kg/day for three days, dissolved in Corn Oil (Sigma-Aldrich, Germany)) and Niclosamide (13 mg/kg/day for three days, dissolved

in Corn Oil) were administered via ip injections. In addition, Niclosamide (13mg/kg/day, dissolved in Corn Oil) was received via gavage. For control treatment vehicle were used.

Cells culture, cDNA, siRNA, RT-PCR. HEK293 cells were cultured in DMEM media (GIBCO, Germany) supplemented with 10% FBS (Capricorn, Germany). Calu3 cells were grown in DMEM-F12 media (GIBCO, Germany) supplemented with 1% HEPES, 1% L-glutamine, 10% FBS (Capricorn, Germany). All cells where grown at 37ºC in the absence of antibiotics in a humidified atmosphere with 5% CO_2.

***RT-PCR, siRNA*.** RT-PCR has been performed using RNA isolated from lungs of *wt* and TMEM16A and TMEM16F KO mice using NucleoSpin RNA columns (Macherey-Nagel, Germany). Total RNA (1 µg/50 µl reaction) was reverse-transcribed using random primer (Promega, Germany) and M-MLV Reverse Transcriptase RNase H Minus (Promega, Germany). Each RT-PCR reaction contained sense and antisense primer (table 1), 0.5 µl cDNA, and GoTaq Polymerase (Promega, Germany). After 2 min at 95 °C cDNA was amplified for 30 cycles for 30 s at 95 °C, 30 s at 57 °C and 1 min at 72 °C, followed by 10 min at 72°. PCR products were visualized by loading on peqGREEN (Peqlab,VWR, Germany) containing agarose gels and were analyzed using ImageJ. TMEM16F was downregulated by human siRNA transfection into Calu3 cells using standard methods (Lipofectamine, Invitrogen, Germany).

Western blotting. Cells were collected and lysed in 1% NP40 lysis buffer containing protease inhibitor cocktail and DTT (Sigma-Aldrich, Germany). Protein (30–50 µg) was separated by 8.5% SDS-PAGE and transferred to nitrocellulose membranes. Membranes were blocked with 5% NFM/TBST at RT for 1 h and were incubated overnight at 4 °C with rabbit polyclonal anti-TMEM16F (diluted 1:5000 in 5% NFM/TBST, Thermo Fisher Scientific, USA) or rabbit polyclonal anti-actin (diluted 1:10000 in 5% NFM/TBST, Sigma-Aldrich, Germany). Subsequently, membranes were incubated with secondary antibody at RT for 2 h. Immunoreactive signals were visualized using supersignal chemiluminescence substrate detection kit (Pierce Biotechonology, USA).

IL-8 assay. To measure secretion of the cytokine IL-8 (Peprotech, Germany), Calu3 cells

were rinsed twice with PBS (Capricorn, Germany), placed in OPTIMEM (GIBCO, Germany) and exposed to LPS (10 µg/ml48h). After 48 hours, the conditioned medium was collected and used to quantify IL-8 using Quantikine ELISA kits (R&D systems, Germany) according to the manufacturer's instructions.

In vitro perfusion of intestine. Mice were sacrificed by cervical dislocation and excised intestines were placed immediately in ice-cold Ringer solution and carefully flushed to remove residual luminal contents. The intestinal segments were mounted and perfused vertically in a custom-designed perfusion chamber with a constant temperature, similar to [93, 255]. After mounting, the serosal side was exposed to Ringer solution (NaCl 120 mM, KH_2PO_4 0.4 mM, K_2HPO_4 1.6 mM, D-glucose 5 mM, $MgSO_4$ 1 mM, Ca-gluconate 1.5 mM and $NaHCO_3$ 25 mM, pH 7.4, continuously gassed with 95% O_2 and 5% CO_2) and perfused luminally with glucose-free mannitol-replaced Ringer. Perfusates were collected at a rate of 0.5 ml/min at 3 min intervals for an additional 27 min. Tissues were stimulated with methacholine (MCh; 100 µM) or ATP (100 µM) for 9 min, always in the presence of 1 µM Prostaglandin E2 (PGE2) if not mentioned otherwise. In luminal Ca^{2+} free solution, Ca^{2+} was substituted with equimolar EGTA. The amount of mucus secretion was analyzed using a periodic acid-Schiff (PAS) assay (Sigma-Aldrich, Germany). In brief, 50 mM dithiothreitol was pipetted into each sample and incubated for 1h at 37º under continuous shaking. 0.2 ml periodic acid (0.1%) was added, incubated for 2 hours at 37°C, and additional 30 min at 20°C after adding 0.2 ml Schiff´s reagent (Sigma-Aldrich, Germany). Samples were centrifuged at 500 g/5 min and OD of the resulting solution was measured at 540 nm. The amount of mucus per tissue and minute was calculated using a calibration curve from defined pig gastric mucin (Sigma-Aldrich, Germany).

Histology, mucus staining by alcian blue and PAS, quantification. Mice were sacrificed by cervical dislocation. Small and large intestine were removed and cut in two sections. One section was kept in Ringer solution, the other section was exposed to 100 µM ATP (ROTH, Germany) or 100 µM CCH (carbachol; Sigma-Aldrich, Germany). Before and after each experiment, intestinal sections were fixed for further histological analyses. Mouse airways were fixed by transcardial fixation and were embedded in paraffin or frozen in liquid N_2. For

paraffin sections, tissues were fixed in 4% paraformaldehyde (PFA), 0.2% picric acid and 3.4% sucrose in PBS, and were washed in methanol before embedding in paraffin. For mucus analysis sections were stained according to standard Periodic acid-Schiff (PAS) or Alcian Blue methods and examined by light microscopy. A minimum of nine random images for each embedded tissue were acquired from a minimum of three animals (*TMEM16A$^{flox/flox}$, TMEM16F$^{flox/flox}$,TMEM16A$^{flox/flox}$FoxJ1Cre, TMEM16F$^{flox/flox}$FoxJ1Cre, TMEM16F$^{flox/flox}$Vil1Cre*). Sections were analyzed using an Axiovert 200 microscope equipped with AxioCam ICc 1 and ApoTome (Zeiss, Germany) and analysed using AxioVision (Zeiss, Germany).

Patch Clamping. Crypts from jejunum and distal colon were isolated in Ca^{2+}-free Ringer solution and immobilized on poly-lysine coated glass cover slips. HEK293 cells were grown on glass-coated cover slips and were mounted on the stage of an inverted microscope (Zeiss, Germany). Experimental procedures are described in detail in [200].

Measurement of intracellular Ca^{2+}***concentration.*** All measurements of intracellular Ca^{2+} concentration [Ca^{2+}] of cell lines and isolated goblet cells have been performed using the Ca^{2+} sensitive dye Fura-2-AM (TOCRIS, Germany), as described earlier [80].

YFP-Quencing. Quenching of the intracellular fluorescence generated by the iodide-sensitive enhanced yellow fluorescent protein (YFP) was used to measure anion conductance. YFP fluorescence was excited at 490 nm using a semi-automatic Novostar plate reader (BMG-Labtech, Offenburg, Germany). I− influx was induced by replacing 20 mM extracellular Cl− with 20 mM I− in the presence of 1µM Ionomycin (Enzo Life Science). Background fluorescence was subtracted and autofluorescence was negligible. Changes in fluorescence induced by I− are expressed as initial rates of fluorescence decrease (arbitrary units/sec) and analyzed using MARS data analyzing program (BMG-Labtech, Offenburg, Germany).

Materials and statistical analysis. All compounds used were of highest available grade of purity: Niclosamide, Eact, OVA, MCh, NFA, Dichlorophene, (Sigma-Aldrich, Germany). Niclosamide-ETHO, Nitazoxanide, tizoxanide (Caymann-Chemicals, USA), CaCCinhAO1 (Tocris; Germany) IL-8, IL-13 (Peprotech, Germany). Antibodies used were purchased from Thermo Fisher Scientific (USA) for TMEM16F and from Bioss (USA) (MUC5AC (41M)). Data

are reported as mean ± SEM. Student's t-test (for paired or unpaired samples as appropriate) or ANOVA were used for statistical analysis. A p-value < 0.05 was accepted as significant difference.

Results

Niflumic acid (NFA) is an inhibitor of TMEM16 and blocks airway mucus secretion.

OVA-induced allergic asthma in mice caused pronounced airway goblet cell metaplasia. Exposure of asthmatic lungs to aerosolized carbachol (CCH) induced massive release of mucus as well as airway contraction (Fig 6.1 A-C). Pretreatment of sensitized animals for three days with Niflumic acid (NFA; ip and tracheal instillation), a well-known inhibitor of Ca^{2+} activated chloride currents, abolished production so that no mucus could be released by CCH. Moreover, airway contraction was completely inhibited as judged from airway cross sections. We expressed in HEK293 cells the two main TMEM16 paralogs expressed in airway epithelial and smooth muscle cells [257], TMEM16A and TMEM16F, and measured whole cell currents upon activation by the Ca^{2+} ionophore ionomycin (Iono). Large whole cell currents were activated by simulation of TMEM16A and TMEM16F with Iono, and current activation was potently suppressed by NFA (Fig 6.1 D-F). The data suggest TMEM16A/F being in charge of both mucus production and contraction of airway smooth muscle (ASM). Novel therapeutic strategies for the treatment of inflammatory airway diseases such as asthma, CF, and COPD may therefore consider the use of inhibitors of TMEM16.

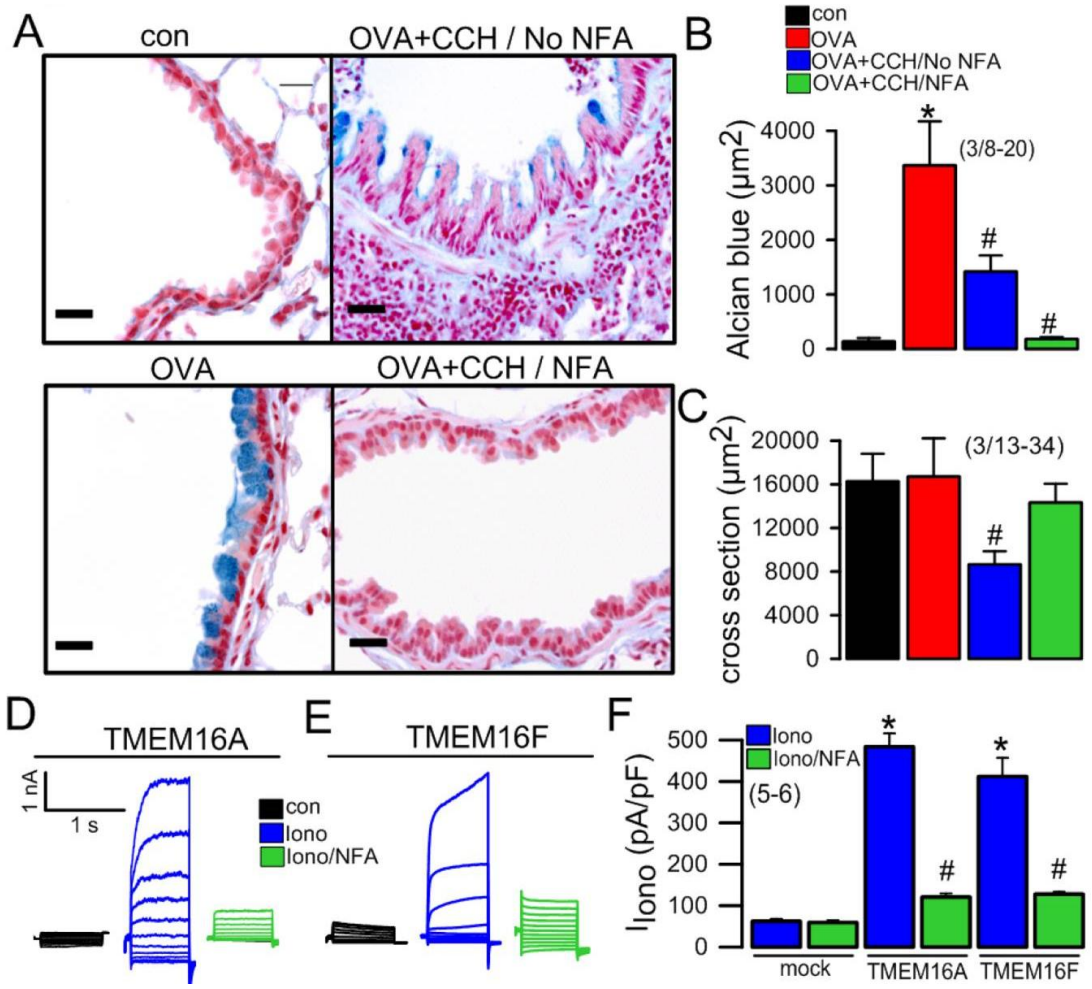

Fig 6.1 *The TMEM16-inhibitor Niflumic acid attenuates inflammatory airway disease.*
A, B) OVA-sensitization induced pronounced goblet cell metaplasia as indicated by alcian blue positivity. Exposure to carbachol (CCH, 25 mg/ml, nebulizer) induced release of mucus and airway contraction. Bars indicate 10 µm. Pre-exposure to the TMEM16A-inhibitor Niflumic acid (NFA, 0.5 mg/kg/day) by intratracheal and intra peritoneal application for three days, strongly attenuated mucus production and CCH-induced airway contraction (A-C). C) Cross section of airways under the different conditions indicating airway relaxation by NFA. D-F) Whole cell currents obtained in HEK293 cells expressing TMEM16A or TMEM16F after stimulation with 1 µM ionomycin (Iono), and inhibition by NFA (20 µM). Mean ± SEM; *significant inhibition by NFA (paired t-test). # significant difference when compared to OVA (unpaired t-test). (n) number of airways analysed or number of cells examined.

Niclosamide and derivatives: Potent inhibitors of anoctamins and Ca^{2+} signaling.

NFA is a broadly acting and non-specific compound, which may not be appropriate for the use in human. The anthelmintic drug Niclosamide has been recently reported to be a potent inhibitor of TMEM16A that fully bronchodilates airways [241]. In patch clamp experiments, we confirmed the inhibitory effect of Niclosamide on TMEM16A outward currents activated by

purinergic stimulation of HEK293 cells (Fig 6.2 A-C). Similar to TMEM16A, overexpressed TMEM16F was also inhibited by Niclosamide (Fig 6.2 D). We also examined the effect of Niclosamide on endogenous TMEM16A expressed in HT_{29} colonic carcinoma cells, which were stably transfected with iodide-sensitive yellow fluorescent protein (YFP). TMEM16A was activated by ionomycin and TMEM16A currents were measured as iodide quenching. Niclosamide and the related compounds Niclosamide-ETHO, tizoxanide, and nitazoxanide inhibited endogenous TMEM16A in the low nanomolar range, and were more potent than the well-known inhibitors CaCCinhAO1 or dichlorophen (Fig 6.2 E).

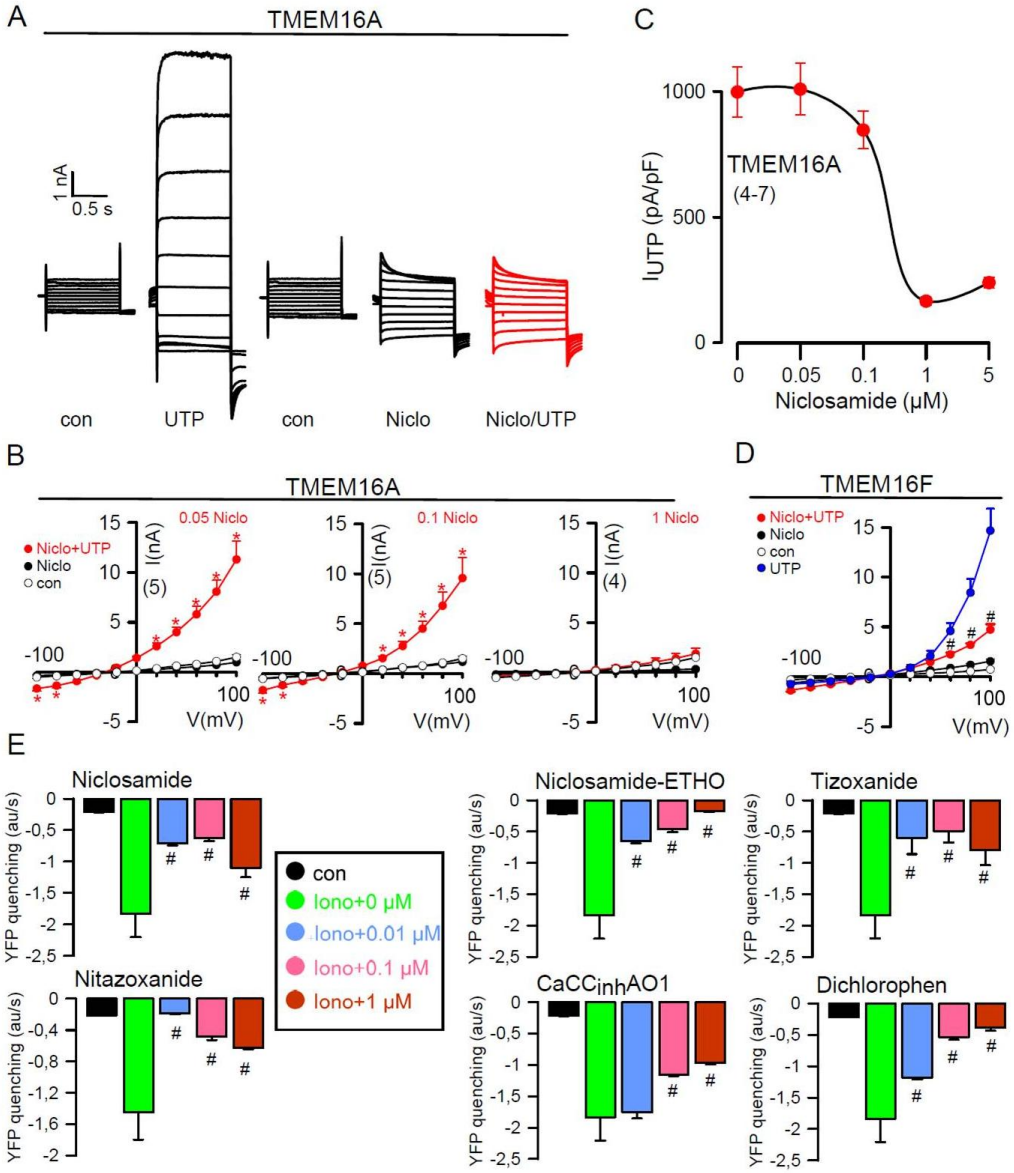

Fig 6.2 *Inhibition of TMEM16A and TMEM16F by Niclosamide.*

A) TMEM16A whole cell currents in overexpressing HEK293 cells. The purinergic agonist UTP was used to activate TMEM16A (100 μM). B, C) Concentration-dependent inhibition of TMEM16A by

Niclosamide (Niclo). D) Current/voltage relationship showing inhibition of TMEM16F by Niclosamide (1 µM). E) Inhibition of endogenous TMEM16A/F expressed in HT_{29} cells, as shown by iodide quenching. Rate of YFP quenching (arbitrary units (au/second), when applying 20 mM iodide to the extracellular bath solution. HT_{29} cells stably overexpressing YFP were stimulated with 1 µM ionomycin. 100.000 cells were seeded/well. Mean ± SEM; (number of experiments) #significant inhibition when compared to the absence of the inhibitor ($p<0.05$; unpaired t-test). * significant activation by UTP (paired t-test).

Earlier studies demonstrated that expression of TMEM16 proteins augment intracellular Ca^{2+} signals, which are attenuated by the inhibitors CaCCinhAO1, NFA, and others [80]. Here we show that Niclosamide also blocks Ca^{2+} signals elicited by ATP or by the TMEM16-activator Eact [156] (Fig S6.1). Niclosamide had also a marked effect on Ca^{2+} signals in freshly isolated goblet cells, which suggests an inhibitory effect on mucus production and secretion.

Niclosamide inhibits mucus production and mucus secretion, ASM contraction, and inflammation.

In fact, OVA-induced mucus production was strongly reduced by both NFA and Niclosamide (Fig 6.3 A, B). We reported earlier that airway epithelial knockout of TMEM16A caused a defect in basal, i.e. ATP-mediated mucus secretion. This resulted in an accumulation of mucus under control (non-inflammatory) conditions [255]. Mucus synthesis under inflammatory (OVA) conditions and mucus release upon cholinergic stimulation, however, were not compromised [255] (Fig 6.3 C). In wt (*TMEM16A*$^{flox/flox}$) mice and mice with knockout of TMEM16A in ciliated epithelial cells (TMEM16A$^{flox/flox}$FoxJ1Cre) airways, application of Niclosamide three days before applying CCH strongly reduced mucus synthesis, so that little mucus was left to be secreted by CCH (Fig 6.3 C-E). Because mucus production occurs in the absence of TMEM16A, other TMEM16 paralogs may also be in charge of mucus synthesis. We analyzed expression of the three main TMEM16 paralogs in isolated airway epithelial cells [257], and found that TMEM16A, also TMEM16F and TMEM16K, are upregulated through Th2 driven goblet cell metaplasia and mucus hyperproduction after OVA – sensitization (Fig 6.3 F). Thus, it is likely that TMEM16F/K control mucus production, because they are inhibited by Niclosamide and other TMEM16-inhibitors [140]. Interestingly, knockdown of TMEM16A in *fl/fl-FoxJ1* mice way paralleled by reduced expression of TMEM16F/K,

suggesting a co-regulation of TMEM16 proteins as suggested earlier [258].

In the presence of Niclosamide, not only mucus production/secretion was strongly attenuated, but also airways appeared much less contracted after acute application of CCH (Figs. 6.1 A, 6.3 C). We analyzed cross sections of small airways and similar to NFA we found inhibition of the cholinergic reduction of the cross sectional area by Niclosamide (Fig 6.3 G). This corresponds well to the findings by Miner *et al*., who described bronchodilation by Niclosamide [241]. Of note were also the peribronchial infiltrations by immune cells, observed after OVA treatment, which were strongly attenuated by Niclosamide (Fig 6.3 H). An attenuation of allergic lung inflammation by Benzbromarone, another TMEM16-inhibitor, has been reported earlier [259].

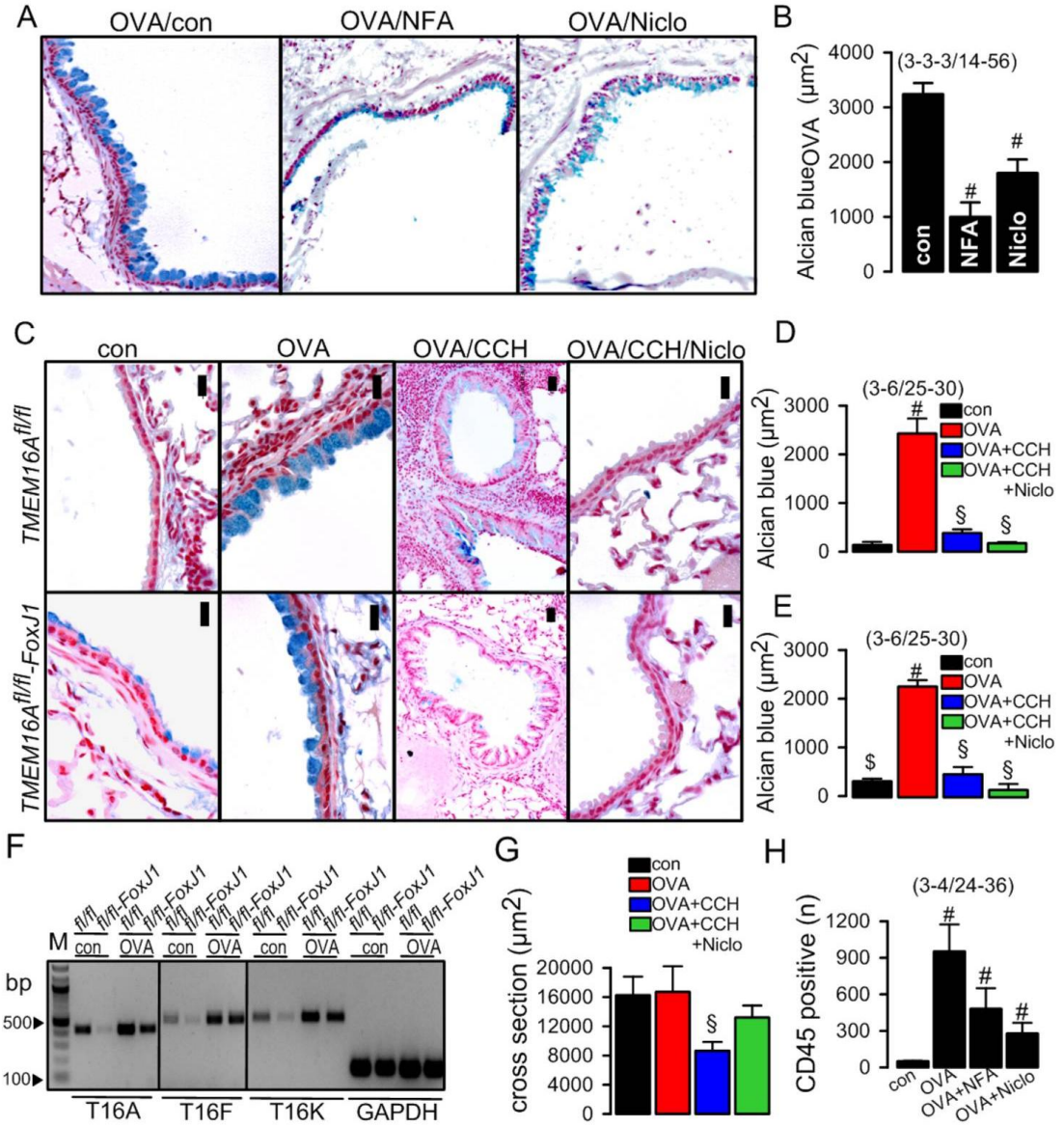

Fig 6.3 *Niclosamide attenuates inflammatory airway disease.*

A, B) OVA-sensitization of wt mice induced pronounced goblet cell metaplasia as indicated by alcian blue staining. Tracheal instillation of Niflumic acid (NFA; 0.5 mg/kg/day) or Niclosamide (Niclo; 13mg/kg/day) significantly reduced mucus production. C-E) OVA-sensitization of *TMEM16A*$^{flox/flox}$ (*fl/fl*) and *TMEM16A*$^{flox/flox}$*FoxJ1Cre* (*fl/fl-FoxJ1*) mice induced goblet cell metaplasia. Exposure of *fl/fl* and *fl/fl-FoxJ1* mice to carbachol (CCH, 25 mg/ml, nebulizer) induced release of mucus and pronounced airway contraction. Pre-exposure to Niclosamide by intratracheal application for three days strongly attenuated mucus production and CCH-induced airway contraction. F) Expression of the three main TMEM16 paralogs (A, F, K) in mouse airways before and after OVA-sensitization. Bars indicate 10 µm. G) Airway cross section indicating airway contraction by muscarinic stimulation (aerosol) and inhibition of contraction by Niclosamide. H) Number of CD45 positive cells (airways) under different conditions. Mean ± SEM; (number of experiments) $^{\#}$ significant effect of NFA, Niclo, and OVA, respectively ($p<0.05$; ANOVA). §significant difference when compared to OVA (unpaired t-test). $^{\$}$ significant difference when compared to *fl/fl* (unpaired t-test).

Attenuation of airway inflammation by Niclosamide suggests inhibition of inflammatory mediators, which has been recently demonstrated for other tissues [260, 261]. We exposed Calu3 airway epithelial cells to LPS for 48h and measured release of the neutrophil attractor interleukin 8 (IL-8). IL-8 release was enhanced by LPS-exposure and the release was clearly inhibited in the presence of Niclosamide (Fig 6.4 A). Upon stimulation with the Th2 cytokine IL-13, Calu3 cells produced MUC5AC (Fig 6.4 B, C). IL-13 induced synthesis of Muc5AC was clearly inhibited when TMEM16F-expression was knocked down by siRNA (Fig 6.4 C, E). As observed for mouse airways, incubation with Niclosamide also largely reduced Muc5AC-expression in Calu3 human airway epithelial cells (Figs. 6.4 B, C, Fig 6.3). Niclosamide did not change expression of either TMEM16A or TMEM16F (Fig 6.4D). As shown earlier, airway epithelial knockout of TMEM16A caused a defect in mucus secretion while mucus production was retained [255]. In summary, Niclosamide is a potent inhibitor of both TMEM16A and TMEM16F, and inhibits production and secretion of mucus. Niclosamid does not affect expression of TMEM16A/F. We therefore suggested that TMEM16F is required for mucus production in mouse airways.

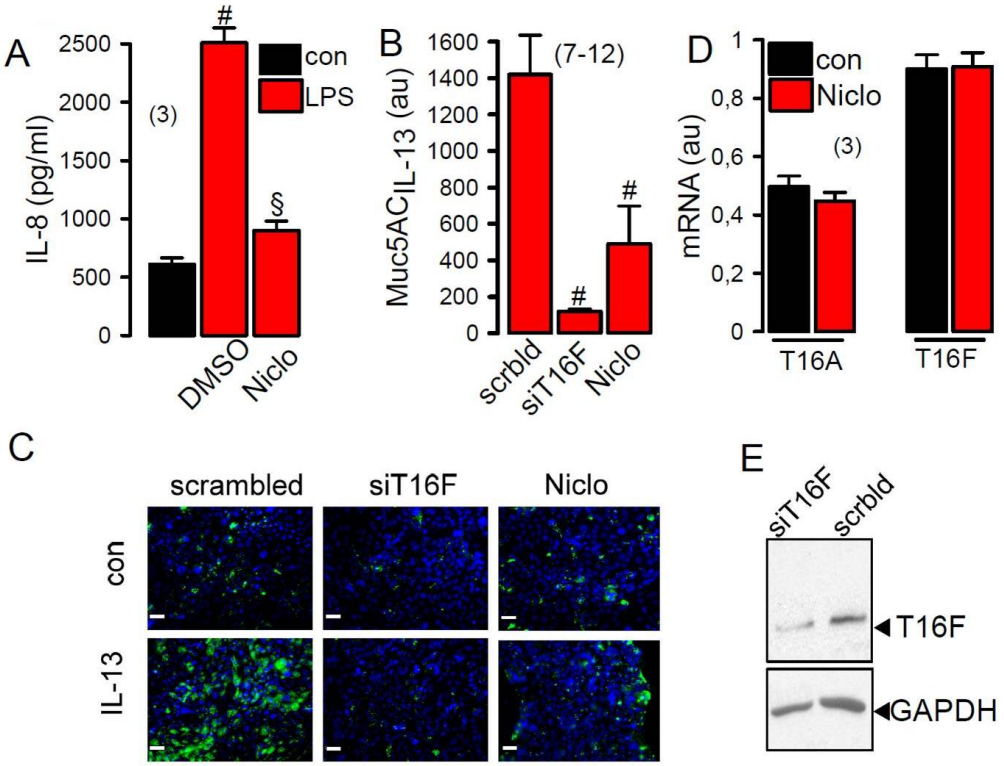

Fig 6.4 *Niclosamide attenuates inflammatory airway response.*
A) Effect of Niclosamide (1 µM) on LPS (10 µg/ml) induced release of IL-8 in Calu3 cells. B, C) IL-13 – induced MUC5AC release and inhibition by siRNA-TMEM16F and Niclosamide (1 µM). D) Effect of Niclosamide on mRNA-expression for TMEM16A and TMEM16F (semiquantitative RT-PCR). E) Western blot indicating knockdown of TMEM16F by siRNA. Mean ± SEM; [#] significant difference when compared to control or scrambled RNA (scrbld) (unpaired t-test). [§] significant difference when compared to DMSO (unpaired t-test).

Airway epithelial knockout of TMEM16F attenuates mucus production and release

We generated mice with a knockout of TMEM16F in ciliated epithelial cells *(TMEM16F$^{flox/flox}$FoxJ1Cre)* to examine further the role of TMEM16F for mucus production and mucus release in mouse. Alcian blue staining indicated accumulation of mucus in airways of *TMEM16F$^{flox/flox}$FoxJ1Cre* mice, which was not observed in *TMEM16F$^{flox/flox}$* littermate controls (Fig 6.5 A). This suggests a role of TMEM16F for basal mucus secretion in mouse airways, similar to TMEM16A [255]. OVA-sensitization induced pronounced goblet cell metaplasia and mucus production, which was attenuated in the *TMEM16F$^{flox/flox}$FoxJ1Cre* mice when compared to *TMEM16F$^{flox/flox}$*. Acute muscarinic stimulation with aerosolized CCH released mucus from both *TMEM16F$^{flox/flox}$FoxJ1Cre* and *TMEM16F$^{flox/flox}$* mice (Fig 6.5 A, B). However,

the amount of mucus released was clearly less in *TMEM16F*$^{flox/flox}$*FoxJ1Cre* mice. The data suggest role of TMEM16F for basal mucus release similar to that of TMEM16A, and a role of TMEM16F for mucus production.

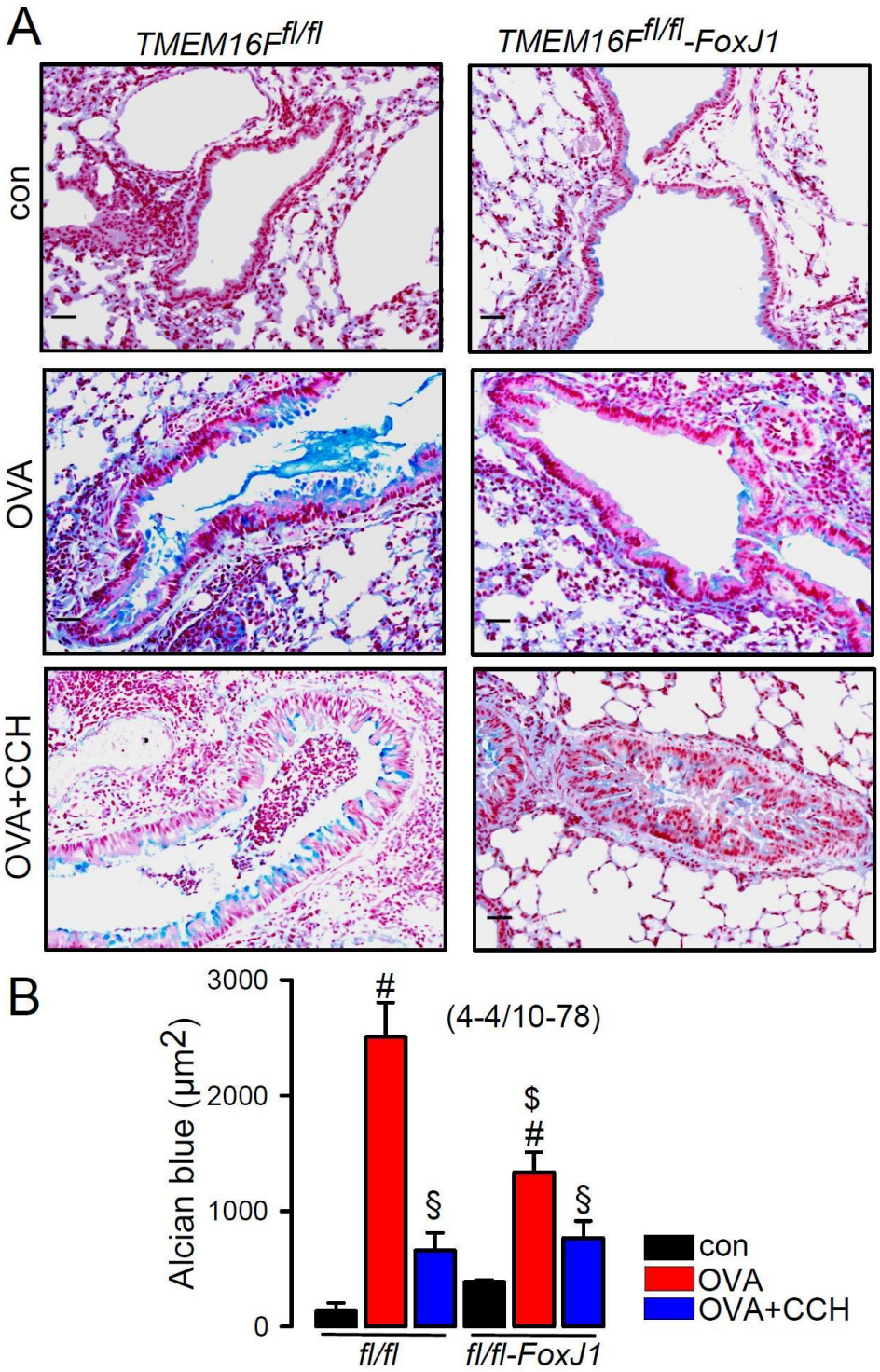

Fig 6.5 *TMEM16F controls mucus production.*

A) Mucus in mouse *TMEM16F*$^{flox/flox}$ (*fl/fl*) and *TMEM16F*$^{flox/flox}$*FoxJ1Cre* (*fl/fl-FoxJ1*) airways under control conditions, after OVA sensitization and after exposure to carbachol (CCH, 25 mg/ml, nebulizer). Bars indicate 10 µm. B) Summary alcian blue staining in *fl/fl* and *fl/fl-FoxJ1* animals. Mean ± SEM;

[#]significant difference when compared to con (unpaired t-test). [§]significant mucus release by CCH (unpaired t-test). [$]significant difference when compared to *fl/fl* (unpaired t-test). (n) number of airways analyzed.

TMEM16F is required for intestinal mucus production and secretion.

We examined whether TMEM16F is also important for intestinal mucus secretion and measured acute mucus release in freshly excised colonic segments mounted in a vertical custom-designed perfusion chamber at 37 °C and 24 mmol/l HCO_3^-/5 % CO_2 [255]. Secretion of mucus was induced by basolateral perfusion with methacholine (MCh) and by luminal perfusion of ATP [255]. Both, MCh and ATP induced secretion of mucus in colon from *TMEM16F*$^{flox/flox}$ and *TMEM16F*$^{flox/flox}$*Vil1Cre* mice (Fig 6.6 A).

Although acute perfusion with ATP induced mucus release in *TMEM16F*$^{flox/flox}$*Vil1Cre* mice (Fig 6.6 A), a milder defect in mucus release might be present in the colon of these mice because i) ATP-induced mucus release was attenuated according to PAS stainings (Fig 6.6 D,E) and ii) MCh induced release was augmented, suggesting an accumulation of mucus (Fig 6.6 A). These data suggest a defect in basal, i.e. ATP-driven mucus secretion, upon intestinal epithelial knockout of TMEM16F. Albeit being milder, the effect is similar to the secretory defect described recently in mice lacking intestinal epithelial expression of TMEM16A (*TMEM16A*$^{flox/flox}$*Vil1Cre)* [255]. Of note, *TMEM16F*$^{flox/flox}$*FoxJ1Cre* mice showed normal expression of purinergic or muscarinic receptors (not shown). Like in *TMEM16A*$^{flox/flox}$*Vil1Cre* mice, cholinergic mucus secretion was uncompromised in *TMEM16F*$^{flox/flox}$*Vil11Cre mice.*

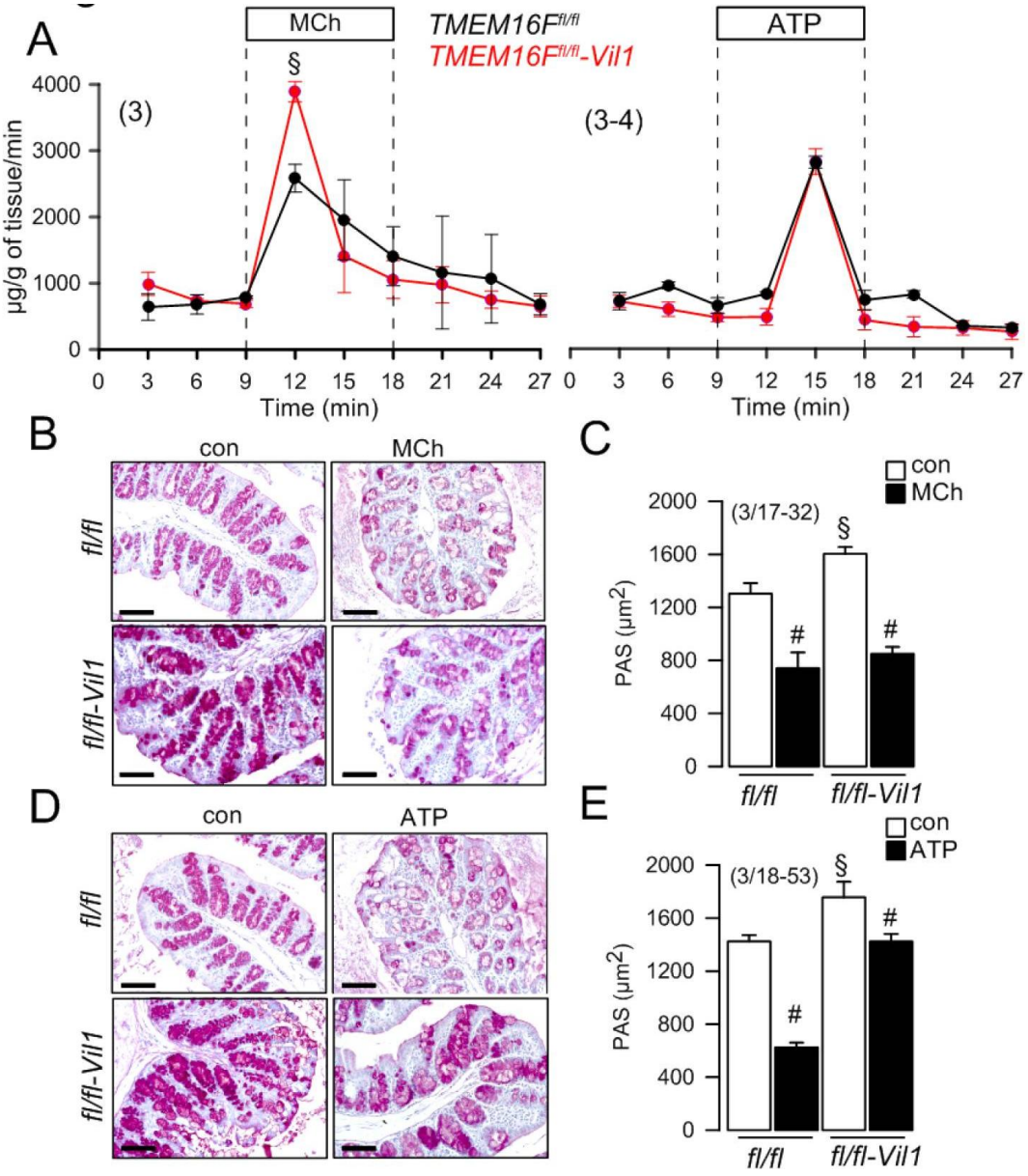

Fig 6.6 *Production of mucus but not release is affected in TMEM16F$^{flox/flox}$CreVil1 intestine.*
A) Acute mucus secretion in excised colon from *TMEM16F$^{flox/flox}$* (*fl/fl*) and *TMEM16F$^{flox/flox}$CreVil1* (*fl/fl-Vil1*) animals. Mucus release was assessed in *in vitro* perfused colon and was induced perfusion with methacholine (100 µM) or ATP (100 µM) respectively. B-E) PAS staining of proximal colon before and after stimulation with methacholine (100 M) (B, C) or ATP (100 µM) (D, E). Bars indicate 50 µm. Mean ± SEM; $^{\#}$significant difference when compared to control (unpaired t-test). § significant difference when compared to *TMEM16A$^{flox/flox}$* (unpaired t-test). (n) number of perfused colons and PAS stainings, respectively.

Niclosamide blocks mucus secretion and inhibits intestinal Ca^{2+} *signals.*

We examined whether Niclosamide inhibits intestinal mucus secretion. To this end, Niclosamide was added to the perfusate. This clearly inhibited mucus secretion activated by

luminal ATP but not basolateral MCh (Fig 6.7 A). Niclosamide was applied *in vivo* by intraperitoneal (ip) injection for three days, or was applied orally by gavage for seven days before intestinal perfusion. Both ip and oral application of Niclosamide completely inhibited ATP-induced release of mucus. Although mucus release was inhibited by Niclosamide, mucus did not accumulate in goblet cells, indicating again inhibition of mucus production by Niclosamide (Fig 6.7 B-E).

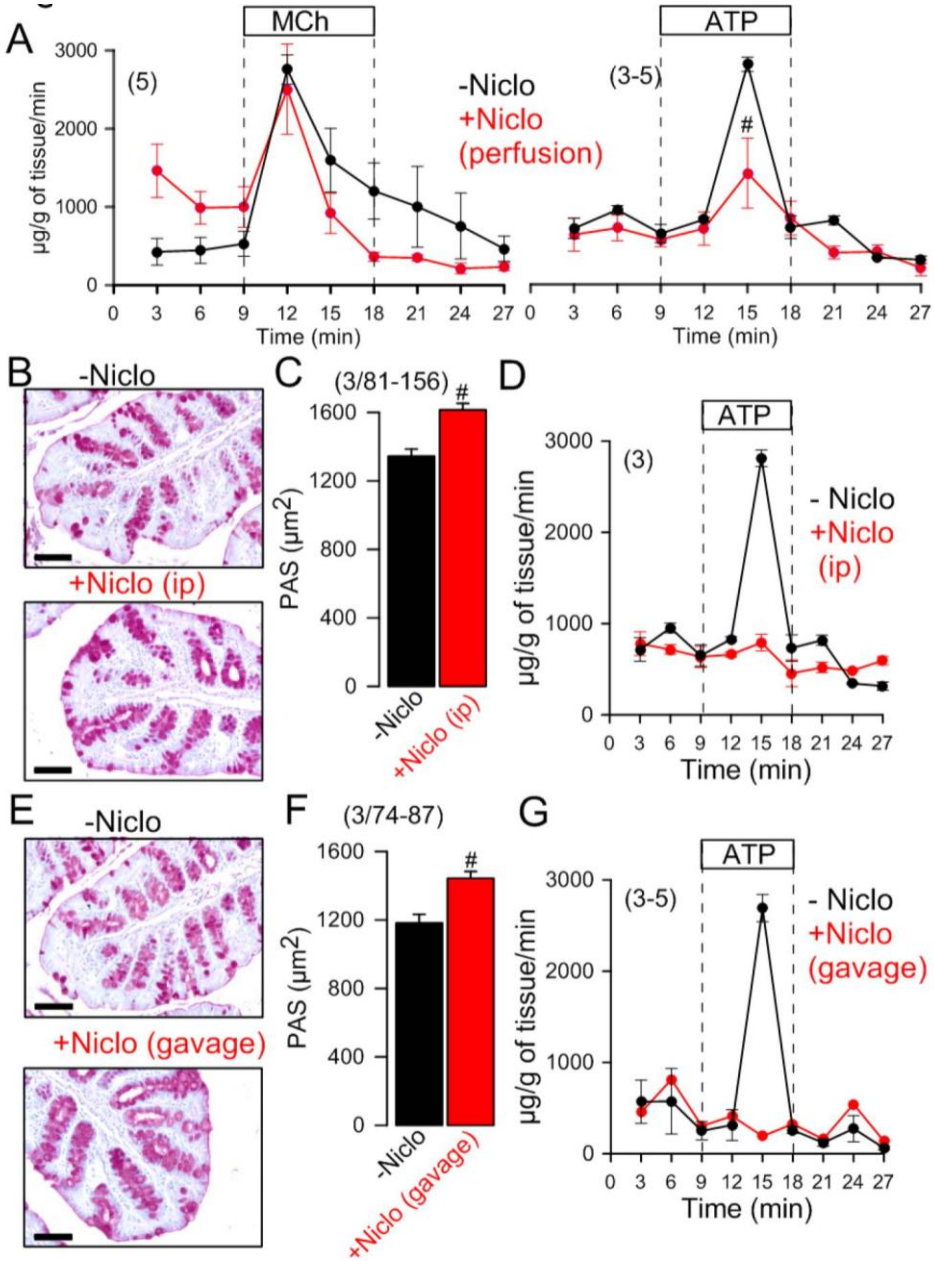

Fig 6.7 *Effect of Niclosamide on intestinal mucus release.*

A) Acute mucus secretion in excised wt colon activated by methacholine or ATP, respectively, and inhibition by acute perfusion with Niclosamide (Niclosamide; 10 µM). B-D) Effect of intraperitoneal injection of Niclosamide (13 mg/kg/day) on PAS staining (B, C) and acute mucus discharge induced by perfusion with 100 µM ATP (D). E-G) Effect of application of Niclosamide by gavage (13 mg/kg/day) on

PAS staining (E, F) and acute mucus discharge induced by perfusion with 100 µM ATP (G). Bars indicate 50 µm. Mean ± SEM; # significant difference when compared to Niclosamide (unpaired t-test). (n) number of perfused colons and PAS stainings analyzed, respectively.

We reported earlier the role of TMEM16F for intracellular Ca^{2+} signaling [80]. Here we found reduced Ca^{2+} increase upon ATP-stimulation of freshly isolated crypt cells from *TMEM16F$^{flox/flox}$Vil1Cre* (Fig S6.2 A-C). In contrast, CCH-induced Ca^{2+} rise was not affected. It shows that TMEM16F is relevant for purinergic (luminal) but not cholinergic (basolateral) receptor signaling (Fig S6.2 D). ATP-induced Ca^{2+} rise was potently inhibited by low concentrations of Niclosamide (Fig S6.2 E). Comparable results were obtained in cells from large intestine (Fig 6.2 F,G). As demonstrated recently, increase in FM4-64 fluorescence in the plasma membrane is a marker for membrane exocytosis [255]. We found that ATP-stimulation (but not cholinergic stimulation) of HEK293 cells expressing TMEM16F, induced FM4-64 fluorescence, i.e. exocytosis (Fig S3). Taken together, the data demonstrate that both airway and intestinal mucus production and secretion depend on TMEM16F, and are potently inhibited by Niclosamide.

Discussion

Role of TMEM16A/F in inflammatory airway diseases.

The present paper shows the importance of TMEM16F for mucus production and mucus secretion and identifies TMEM16F *in vivo* as a target of the anthelmintic drug Niclosamide. We may therefore propose TMEM16 inhibitors, and particularly Niclosamide, as a novel pharmacological tool to treat diseases with excessive mucus secretion, such as the inflammatory airway diseases asthma, COPD and CF, as well as intestinal mucus hypersecretion in CF. Mucus hypersecretion in airways results in mucus plugging, causing reduced mucociliary clearance, the predominant problem in CF lung disease [213]. Pronounced upregulation of TMEM16A was observed in asthma during Th2-driven goblet cell metaplasia and mucus hypersecretion, but it was unclear if TMEM16A is required for mucus production or release [189]. TMEM16A expression is driven via IL4/IL-13/STAT6 and by bacterial antigens [219, 262].

Using T16Ainh-AO1 inhibitor, regulation of MUC5AC-expression by TMEM16A via STAT6/Erk1,2 was proposed [263]. However, TMEM16A inhibitors, including T16AinhAO1, are non-specific and inhibit other TMEM16 proteins as well [140]. The present results show that in the absence of TMEM16A goblet cell metaplasia is uncompromised (Fig 6.3 C). In contrast, SAM pointed domain-containing ETS transcription factor (SPDEF) activated via STAT6 is an essential regulator of Th2-dependent mucus production and goblet cell hyperplasia [227]. The data shown here demonstrate a role of TMEM16F for mucus production in airways and intestine. Like TMEM16A, also TMEM16F (along with TMEM16K) are upregulated during Th2-dependent goblet cell metaplasia (Fig 6.3 F). These three proteins are among the three main TMEM16 paralogs expressed in human and mouse airway epithelium [130, 257]. They are inhibited by TMEM16 blockers such as NPPB, NS3728, T16inhAO1, or NFA [122, 140].

TMEM16A/F control intracellular Ca^{2+} signals and exocytosis.

TMEM16A, F, K augment intracellular Ca^{2+} signals induced by stimulation of G-protein coupled receptors. This has been demonstrated in naïve mouse epithelial cells from airways, intestine and kidney, as well as macrophages, sensory neurons, and a number of different cell lines [80, 126, 128, 134, 160, 193, 200]. It is also shown in the present study (Fig S6.2). Enhanced GPCR-triggered intracellular Ca^{2+} signaling induced exocytosis of mucus and increases plasma membrane localized signaling and membrane expression of CFTR [222, 255 200]. In epithelial cells, TMEM16 proteins are located in apical membranes, in subapical compartments, in the basolateral membrane, or in intracellular compartments [80, 128, 130]. Thus, they affect Ca^{2+} signals at different cellular locations and therefore have an impact on different cellular functions, causing various tissue defects and symptoms when mutated [52]. Intracellular Ca^{2+} signals may be enhanced through tethering of the endoplasmic reticulum to the plasma membrane by TMEM16A, or by Ca^{2+} influx through TMEM16F [63, 80].

However, He *et al*. described another interesting link between expression/activation of TMEM16A and the intracellular Cl^- concentration [222]. The team demonstrated that activation of TMEM16A affects localization of phosphatidylinositol-4,5-bisphosphate (PIP_2) in the plasma

membrane, by changing the intracellular Cl^- concentration. Plasma membrane PIP_2 is required for proper recycling of endosomes, increase in plasma membrane surface area and exocytosis [222]. Such a scenario would also explain enhanced purinergic Ca^{2+} signals and mucus exocytosis in the presence of TMEM16A and TMEM16F. Moreover, it could be the reason for the pleiotropic cellular effects induced by expression of TMEM16 and the pathology observed in knockout mice or patients [264].

Not activation, but Inhibition of TMEM16 may improve CF lung disease

Pharmacological activation of TMEM16A and induction of Cl^- secretion is currently thought to improve CF lung disease [169]. However, in CF activation of Cl^- secretion through stimulation of TMEM16A may be ineffective because i) maturation/function of TMEM16A in CF tissues is compromised [190, 200], and ii) Ca^{2+} activated Cl^- secretion is essentially through CFTR and not through transient CaCC [161, 200]. Related to this, earlier trials using stabilized purinergic ligands (denufosol) to restore Ca^{2+} dependent Cl^- secretion in CF, failed to demonstrate any benefit [51, 265].

Using Niclosamide as a potent inhibitor of TMEM16 may have a number of beneficial effects in CF: i) It is a potent inhibitor of excessive mucus secretion as shown in the present study. ii) It relaxes airways and thereby reduces bronchoconstriction [241] (and present study). iii) It is a commonly used FDA-approved drug, which is well tolerated [266]. iv) It was shown to inhibit *Pseudomonas aeruginosa* quorum sensing [267]. v) Inhalable formulations of Niclosamide have been developed for the treatment of *Pseudomonas* lung infections [268]. vi) It was shown to have broad antimicrobial effects directed against hospital-acquired bacterial infections [269]. vii) It is anti-inflammatory [270] (and present study). viii) It has additional anti-cancer effects [271]. Taken together all reported positive effects of Niclosamide, additional preclinical studies and subsequent clinical pilot studies appear indicated.

Acknowledgements

Supported by Cystic Fibrosis Trust SRC 003, INOVCF, Gilead Stiftung, DFG KU756/14-1. The excellent technical assistance by Miss. B. Wild, P. Seeberger, E. Tartler, is gratefully acknowledged. We gratefully acknowledge the supply of mice with a floxed *TMEM16A* allele by Prof. Jason R. Rock (Boston University School of Medicine), and the FOXJ1-Cre mice by Prof. Michael J. Holtzman and Dr. Y. Zhang (Washington University School of Medicine).

Supplementary material

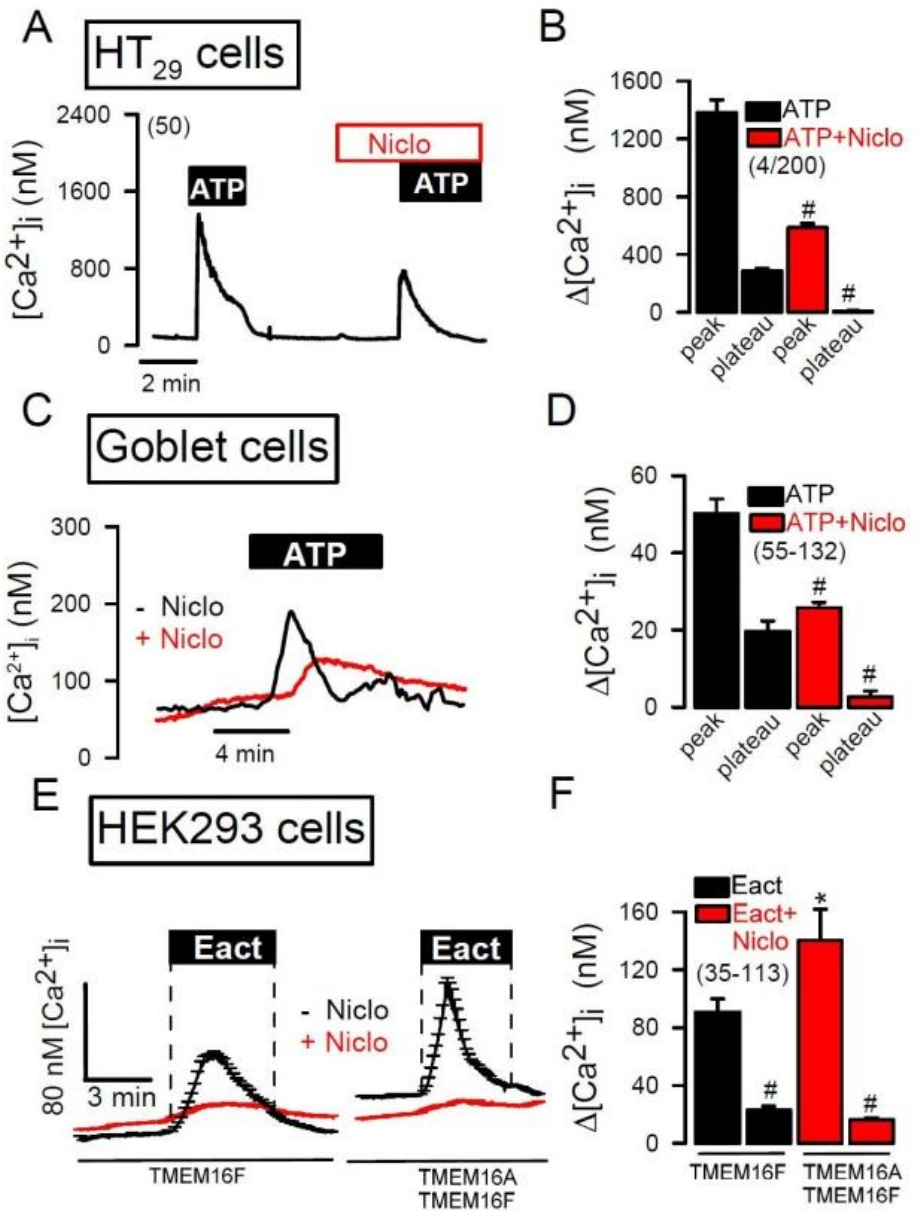

Supplementary Fig 6.1 *Inhibition of Ca^{2+} signaling by Niclosamide in different cell types.*
A-B) HT_{29} cells were loaded with the Ca^{2+}-sensitive dye Fura-2 (5 µM/30 min). 10 µM ATP was applied to stimulate purinergic receptors, which increased intracellular Ca^{2+} and activated TMEM16A. Activation of TMEM16A was inhibited in the presence of Niclosamide (Niclo, 5 µM), which also inhibited ATP-induced Ca^{2+}-release from the endoplasmic reticulum (peak) and blocked store operated Ca^{2+} influx (plateau). C-D) ATP-induced Ca^{2+} increase in goblet cells of freshly isolated colonic crypts. ATP (100 µM) was applied in the absence (black curve) or presence (red curve) of Niclo (100 nM). D) Summary of ATP-induced Ca^{2+} changes in goblet cells, indicating inhibition of peak and plateau Ca^{2+} increase by Niclo. E-F) Ca^{2+} increase in HEK293 cells expressing endogenous TMEM16F only, or overexpressing TMEM16A together with endogenous TMEM16F. Ca^{2+}-rise by the activator of TMEM16A, E_{ACT} (50 µM), was inhibited by Niclo (1 µM) (n=60-70). Mean ± SEM; (number of experiments) #significant inhibition by Niclo ($p<0.05$; unpaired t-test).

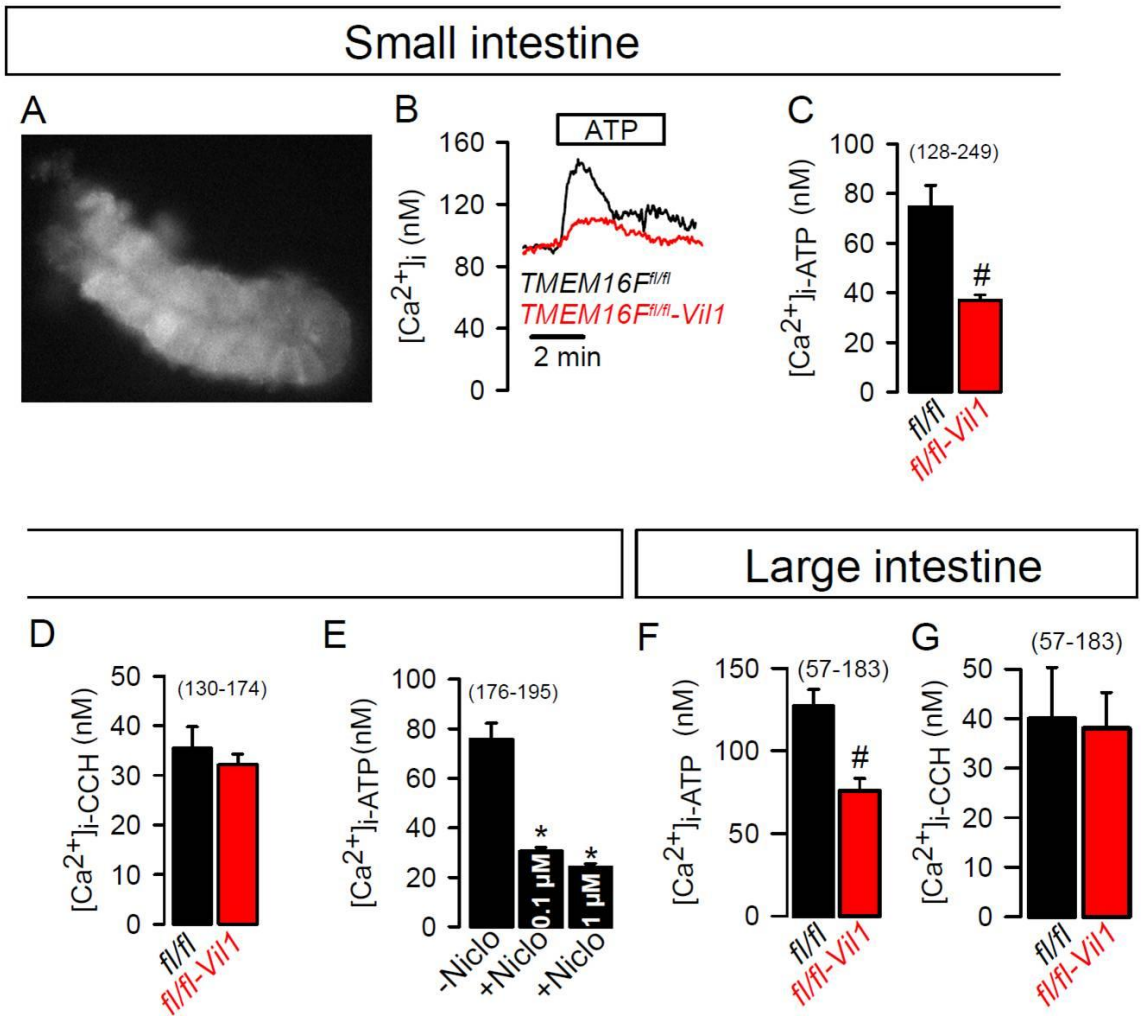

Supplementary Fig 6.2 *Inhibition of intestinal Ca^{2+} signals in the absence of TMEM16F, and by Niclosamide.*

A) Crypt from small intestine (jejunum) loaded with the Ca^{2+} dye Fura-2 (5 µM/30 min). B) ATP (100 µM) induced Ca^{2+} signals in crypt cells from *TMEM16F$^{flox/flox}$* (*fl/fl*) and *TMEM16F$^{flox/flox}$ Vil1Cre* (*fl/fl-Vil1*) littermates. C, D) Summary of ATP (100 µM) and carbachol (CCH, 100 µM) induced Ca^{2+} peaks, respectively. E) Inhibition of ATP-induced Ca^{2+} increase by two different concentrations of Niclosamide (Niclo). F, G) Summary of ATP (100 µM) and carbachol (CCH, 100 µM) induced Ca^{2+} peaks in colonic crypt cells from *fl/fl* and *fl/fl-Vil1* littermates. Mean ± SEM; (number of experiments) #significant difference when compared to *fl/fl* ($p<0.05$; unpaired t-test). * significant effect of Niclosamide (Niclo; $p<0.05$; paired t-test).

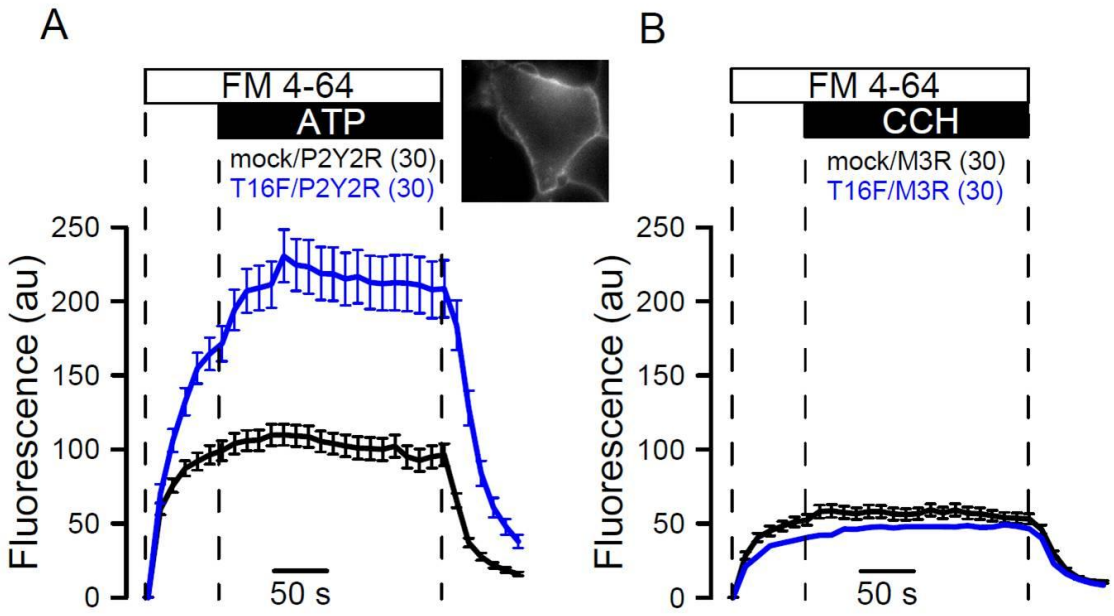

Supplementary Fig 6.3 *Coupling of $P2Y_2$ receptors but not muscarinic M3 receptors with TMEM16F.*
A) Effect of ATP (100 µM) on plasma membrane insertion of the lipid dye FM4-64, present in the extracellular bath solution. Increase in FM4-64 fluorescence in the plasma membrane of HEK293 cells can be taken as a measure for endosomal recycling/exocytosis. Cells expressing TMEM16F in addition to $P2Y_2$ receptors, show stronger basal FM4-64 fluorescence, which is further enhanced by stimulation with ATP. Inset: FM4-64 labeled HEK293 cell. B) Effect of CCH (carbachol; 100 µM) on FM4-64 insertion and staining of the plasma membrane in HEK293 cells expressing mock/M3R or TMEM16F/M3R. Lower basal FM6-64 fluorescence and lack of muscarinic stimulation of membrane exocytosis was observed in these cells. Mean ±SEM; (n) number of experiments.

Discussion

TMEM16 proteins control cellular functions by modulating *Ca^{2+}* signaling in microdomains

Function of TMEM16A in smooth muscles

We show that TMEM16A augments Ca^{2+} signals induced by stimulation of phospholipase C coupled GPCRs, release of 1,4,5-trisphosphate (IP_3) (Chapter 2, Fig 1 I/J. Fig 2A/B). Our findings correlate with studies conducted in dorsal root ganglia [79] and in yeast [125]. In the gastrointestinal tract, TMEM16A is expressed in interstitial cells of Cajal, [272] where it modulates their pacemaker activity. Cajal cells regulate intestinal smooth muscle contraction by calcium oscillation, which is an IP_3 receptor mediated process [273]. This mechanism is triggered by adrenergic induced Ca^{2+} store release and leads to CaCC activation [274]. Activation of CaCC leads to membrane depolarization and activation of voltage dependent calcium channels (L-type), and to further calcium influx [273]. A mouse model for total knockout of TMEM16A showed defective smooth muscle contraction, confirming a physiological role for TMEM16A for proper gastric motility [229].

In the airways and reproductive tract, TMEM16A is also found in the smooth muscle cells [152]. Contraction of airway smooth muscles (ASM) is under the control of a number of stimuli. The agonist binding to the receptor triggers a signaling cascade that involves the activation of the Gq/11 proteins and Phospholipase C (PLC). PLC catalyzes the hydrolysis of PIP_2 in IP_3 and DAG. IP_3 binding to its receptor in the ER triggers Ca^{2+} store release. Emptying of the Ca^{2+} store is followed by Ca^{2+} influx and finally by airway contraction (Fig 7.1). Ca^{2+} influx can occur by several mechanisms. Firstly, by opening of L-type voltage gated Ca^{2+} channels (VGCCs) activated through membrane depolarization [275]. Secondly, Ca^{2+} can enter the cell via receptor-operated channels (ROCs), which are activated upon binding of the agonist [276, 277]. A third mechanism for Ca^{2+} entry involves store operated Ca^{2+} entry (SOCE) triggered by emptying of the Ca^{2+} store. This concept is defined as pharmacomechanical coupling. It is a

mechanism for Ca^{2+} entry that is independent of membrane depolarization. SOCE is considered the predominant regulatory system in vascular smooth muscle contraction [278]. In asthmatic patients SOCE has been shown to cause narrowing of the airways, airway hyperresponsiveness and hyperplasia of smooth muscle mass [279]. The role of TMEM16A in excitable cells as a modulator of calcium signals, thereby supporting airway smooth muscle contraction is fascinating. But how does TMEM16A modulate Ca^{2+} signaling in excitable cells?

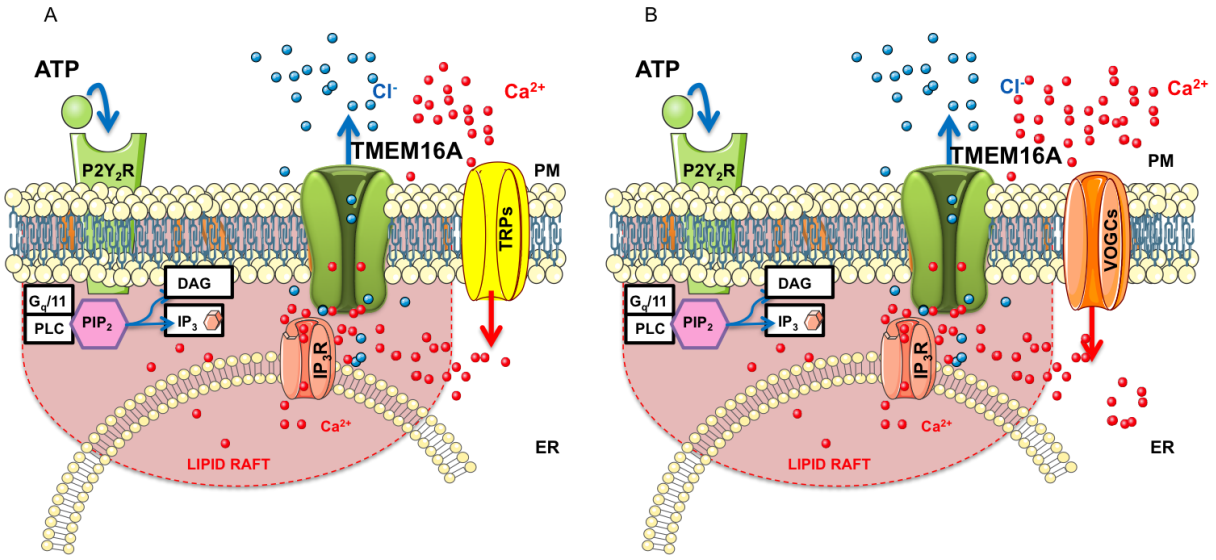

Fig 7.1: *TMEM16 proteins control cellular functions by modulating* Ca^{2+} *signaling in microdomains.* Model proposing separation of Ca^{2+} pools, and colocalization of TMEM16A with IP_3 in a lipid raft A) TMEM16A tethers the ER to the plasma membrane thereby forming a functional microdomain. Release of Ca^{2+} from endoplasmic reticulum (ER) store, is followed by Ca^{2+} influx through store operated Orai1 and Orai1/TRP (Transient Receptor Potential Channels) Ca^{2+} influx channels. B) Ca^{2+} activated TMEM16A secrets Cl^- (blue) and causes depolarization of the membrane voltage, which activates VGCCs (voltage gated Ca^{2+} channels) and Ca^{2+} influx.

Our findings show that TMEM16A forms microdomains by tethering the ER to the plasma membrane through interaction with IP_3 receptors (Fig 1 and Chapter 2, Fig 1E/F). Noteworthy, the yeast homologue of TMEM16A, Ist2, was shown to tether the cortical endoplasmic reticulum to the plasma membrane. In these apical microdomains, Ca^{2+} release from the Ca^{2+} store is facilitated by activation of TMEM16A. TMEM16A mediated Cl^- secretion causes plasma membrane depolarization; this activates the voltage operated Ca^{2+} channels, leading to further calcium influx and augmented contraction of smooth muscle cells.

Function of TMEM16A in airway epithelial cells

We show that TMEM16A is essential for membrane insertion and activation of CFTR. Thus, TMEM16A and CFTR demonstrate a tight functional and molecular relationship. The relationship between these two proteins and its role in CF has been observed for quite some time, but the results were somewhat controversial. The Boucher group and other research laboratories reported enhanced Ca^{2+} activated Cl^- currents in airways cells from CF patients [280]. Along these results it was reported from the Kunzelmann lab that F508del-CFTR increases intracellular Ca^{2+} signalling, leading to increased CaCC activation[281, 282]. However, other studies suggested a rather inhibitory effect of CFTR on TMEM16A [170, 171].

Our results from Chapters 3 and 4 suggest that CFTR and TMEM16A are functionally coupled. TMEM16A facilitates purinergic Ca^{2+} release in microdomains, thereby engaging Store Operated cAMP Signaling (SOcAMPS). The localized Ca^{2+} rise activates the Ca^{2+} sensitive Adenylate Cyclase type 1 leading to cAMP production and activation of CFTR. In other word; increase in intracellular cAMP activates TMEM16A through activation of the exchange factor directly activated by cAMP 1 (EPAC1) (Fig 2).

Ca^{2+} depletion from ER stores triggers aggregation of stromal interaction molecule 1 (STIM1; an ER membrane localized Ca^{2+} sensor [283]) in multiple plasma membrane puncta. STIM1 translocates to the junctions between ER and the plasma membrane, where it binds to the Ca^{2+} channel protein ORAI1 to activate Store Operated Calcium Entry (SOCE). Calcium influx mediated refilling of the stores inhibits SOcAMPs [284]. We show that TMEM16A is a major player within this process; it provides the Ca^{2+} required for activation of ADCY1 and for production of cAMP, which will then activate CFTR. Similar findings related to our results were reported elsewhere and it was shown that CFTR is colocalized with EPAC1 in membrane lipid rafts [203] [204].

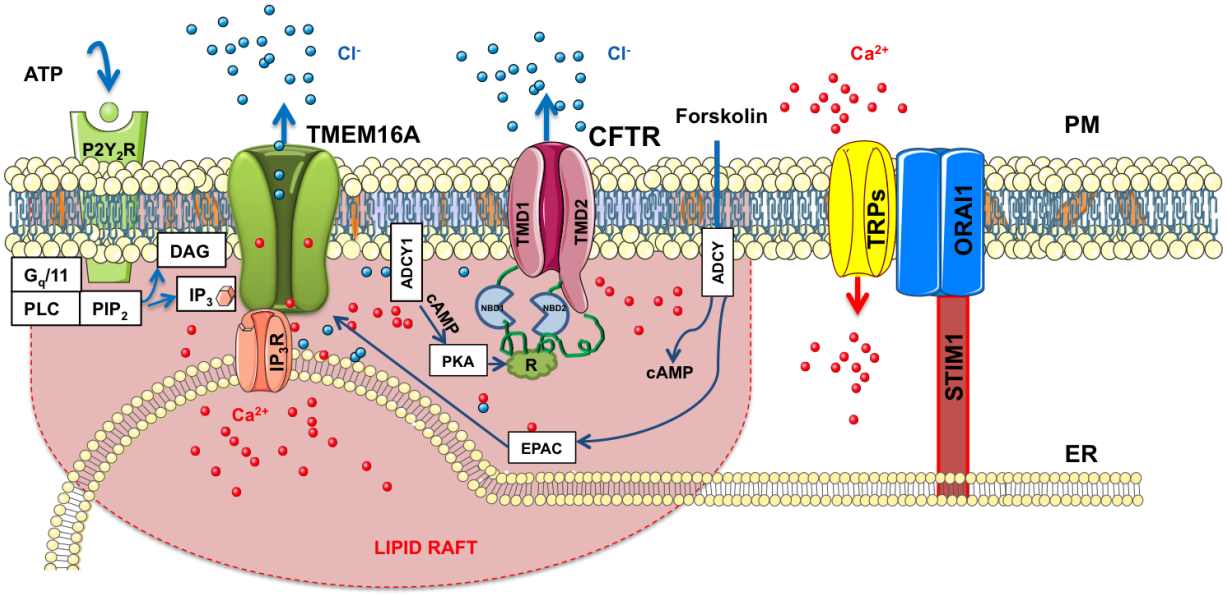

Fig 7.2 *TMEM16A and CFTR are functionally dependent and interact through EPAC1 and ADCY1.* Purinergic stimulation induces Ca^{2+} release from the ER store. Ca^{2+} not only activate TMEM16A but stimulates also ADCY1 (Adenylate Cyclase type 1), which produces cAMP. The intracellular messenger cAMP activates CFTR via protein kinase A (PKA). Activation of ADCYs (Adenylate Cyclases) by Forskolin generates cAMP and activates not only CFTR, but also TMEM16A via EPAC1 (Exchange Factor Directly Activated by cAMP 1).

These findings confirm what was reported previously in primary human bronchial cells, namely that CFTR also mediates chloride currents induced by purinergic stimuli [162]. Interestingly purinergic activation of CFTR was independent of protein kinase C, calmodulin dependent kinase and intracellular calcium, but was suppressed by inhibition of phospholipase C [191]. These observations together with our results suggest that purinergic activation of CFTR is mediated mainly through TMEM16A (Chapters 3 and 4).

We show a functional overlap between CFTR and TMEM16A in terms of both membrane expression and activation of ion currents. (Chapter 3, Fig 4, Fig 5, Fig 6). Functional studies in the TMEM16A knockout animals revealed that CFTR is fully dependent on the presence of TMEM16A in the intestine (Chapter 3, Fig 2). The fact that no intestinal obstructions where observed in the knockout models could be explained by the fact that cAMP activated Cl^- currents were still present in the jejunum. It appears that jejunal epithelial cell do not require TMEM16A for activation or membrane insertion of CFTR. We speculated that another membrane localized TMEM16 paralog might be expressed in the jejunal epithelial to

compensate for the lack of TMEM16A. In unpublished data we could show that TMEM16F, which is expressed in jejunal epithelium, can replace the function of TMEM16A. Another proof for the functional link between CFTR and TMEM16 proteins was obtained in experiments, in which trafficking of CFTR to the membrane was disrupted. CFTR accumulated in the Golgi and no longer reached the plasma membrane, whereas TMEM16A traffic was undisturbed. Under these conditions, cAMP induced Cl^- currents were still detectable even in the absence of CFTR from the plasma membrane, and it was shown that cAMP activated TMEM16A via ADCY1 (Chapter 4, Fig 6H). Our results confirm that in CF, a significant portion of the cAMP-activated Cl^- current is due to activation of TMEM16A. Therefore screening for more potent activators of TMEM16A to treat CF appears well justified. However, the impact of TMEM16A on fluid secretion is probably negligible, because Ca^{2+} activated chloride secretion by TMEM16A is very transient. For functionally appropriate chloride secretion, a sustained activation of a chloride current by CFTR is needed.

TMEM16A is also expressed in salivary glands [285], in pancreatic islets [286] and in neurons [126] in both mouse and human tissues. Huang *et al* reported in 2009 that TMEM16A is expressed in the apical membrane of tracheal epithelial cells [229]. Surprisingly and although expressed rather sparsely TMEM16A mediates large Ca^{2+} activated chloride currents in bronchial epithelial cells and in CFBE41o– cells [189].

Our results confirm expression of TMEM16A together with CFTR in airway epithelia cells (Chapter 3, Supplementary Fig 3E). Very recently, co-localization of TMEM16A, CFTR and ENaC in non ciliated cells was reported [287]. The authors studied a possible compensatory system through TMEM16A in a *cftr* $^{-/-}$ mouse and in a Scnn1b-overexpressing mouse. In the absence of CFTR expression, the authors found no changes in either expression or function of TMEM16A [287]. However, this could be explained by the lack of mucus plugging in these CF models. At any rate, there is consensus that TMEM16A is upregulated in asthma and in other inflammatory conditions. Treatment of bronchial epithelial cells with IL-4 increased both expression and function of TMEM16A [189]. Other inflammatory stimuli can trigger upregulation of TMEM16A, such as bacterial peptides [219], Th2 cytokines, IL-13, as well as IFN-γ [288]. In

addition, under inflammatory conditions TMEM16A is predominantly upregulated in mucus producing cells [152, 189] and submucosal glands [152] when compared to ciliated cells. This strongly suggests that the role of TMEM16A in mucus producing cells is dominating.

TMEM16A plays an essential role in mucus secretion

Functionally, airways epithelia are characterized by the presence of fluid secreting ciliated cells and ionocytes that promote mucus transport through coordinated action of motile cilia and maintenance of the ASL layer. This operates in concert with mucus producing club and submucosal goblet cells. The rare Foxi1-positive ionocytes have been described only recently as high CFTR expressing cells [289]. Under healthy conditions, mucins are continuously synthesized and released from the club cells. Airways specific knockout for TMEM16A (TMEM16A-FoxJCre$^{flox/flox}$) shows intracellular mucus accumulation in club cells without signs of inflammation (Chapter 5, Fig 1A). Mucus accumulation suggests an imbalance between mucus production and mucus secretion. We therefore concluded a defect in mucus secretion by airway club cells form TMEM16A-FoxJCre$^{flox/flox}$ mice.

The striking finding was that mucus accumulated in club cells, although the TMEM16A was knocked out in ciliated cells. In the airways the ratio between ciliated and secretory cells is slightly shifted towards more ciliated cells (60% ciliated cells versus 40% club cells). Under inflammatory conditions, this ratio is shifted towards more club cells [290]. We therefore wondered whether knockout of TMEM16A could have produced an inflammatory state or a genetic differentiation of ciliated cells towards club cells. We labeled club cells using the CCSP (Clara Cell Secretory Protein) antibody and ciliated cells using acetylated tubulin. We observed that the number of CCSP positive cells was not increased in mice lacking TMEM16A (Chapter 5, Fig 2C and Supplementary Fig 1A). This suggests that knockout of TMEM16A did not produce an inflammation and the normal proportion between ciliated and secretory cells is maintained. Several studies have reported that IL-13 increases the number of goblet cells in cultured epithelia, while suppressing the number of ciliated cells [291, 292]. A study that made use of a lentiviral-mediated lineage–tagging approach using the human

FoxJ1 promoter, proved that goblet cells in response to IL-13 treatment derived from progenitor cells expressing FoxJ1 cells [293]. However, we did not observe colocalization between CCSP and FoxJ1 or CCSP and acetylated tubulin (Chapter 5, Supplementary Fig 1 D-F). TMEM16A knockout in ciliated cells may therefore cause a defect in the paracrine signaling that is normally required to drive mucus secretion by club cells. Possible molecules involved are ATP or Clca3, which corresponds to CLCA1 in humans (Fig 3). CLCA1 is a human zinc-metalloproteinase reported to be upregulated during airway inflammation [294]. Matrix metalloproteinases (MMP) are a family of zinc-dependent endopeptidase. They are broadly expressed and modulate inflammation by regulating bioavailability and activity of cytokines, chemokines, and growth factors. CLCA1 was regarded a tumor suppressor and reported as such in breast cancer and melanomas [295]. CLCA proteins are linked to the development of mucous cell metaplasia and possibly airway hyperactivity in experimental models and in humans [296]. Several studies reported that Niflumic acid (NFA) blocks mucus secretion caused by CLCA3 [297] and reduced ATP induced exocytosis of mucin granules[298]. In addition, NFA and MSI-2216 (both CaCC inhibitors) were shown to reduce the TNFalpha-induced mucin expression and have a strong anti-inflammatory effect [299]. An earlier study showed that Talniflumate, a precursor of NFA, reduces intestinal mucus obstruction in a CF mouse model [300]. Talniflumate was shown to be nontoxic in phase II of a clinical trial and was considered for the treatment of asthma and COPD [301]. CLCA1 was reported recently to stabilize TMEM16A in the plasma membrane, thereby increasing the number of channels at the cell surface and increasing the Ca^{2+} activated current. Despite these interesting findings, several questions are still unanswered: Is CLCA1 involved in the inflammatory process mediated by TMEM16A, and if so, what is the link between TMEM16A and CLCA1. Does knockout of TMEM16A in the ciliated cells in the mouse cause defective release of CLCA3 from ciliated cells, which in turn causes mucus accumulation in club cells?

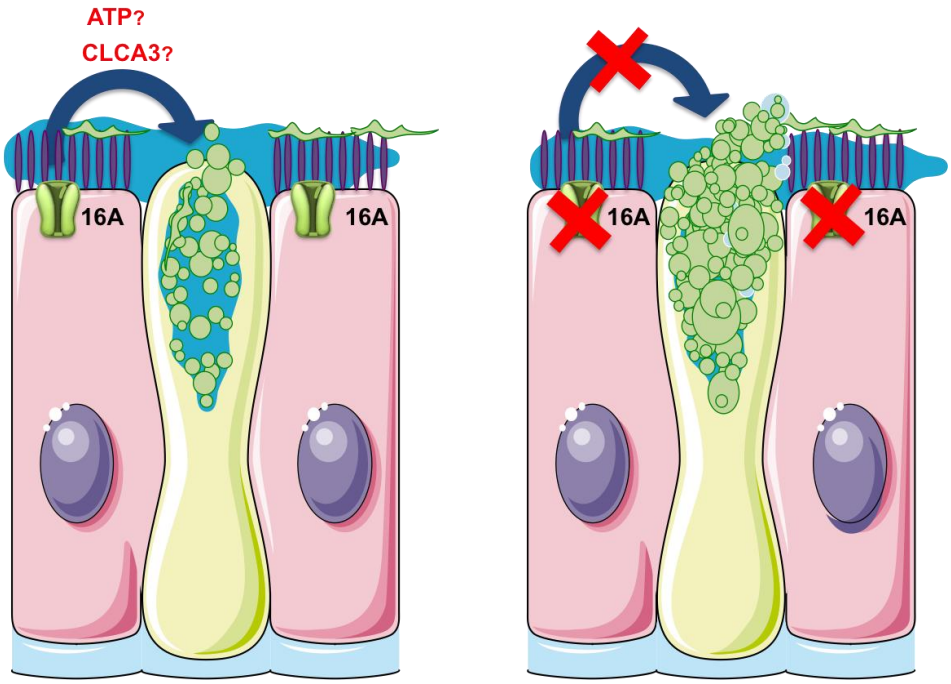

Fig 7. 3: *Role of TMEM16A in airway epithelial cells.*
TMEM16A mediated secretion of paracrine factors by ciliated cells, acting as secretagogues for mucus exocytosis/secretion by club cells. TMEM16A knockout leads to accumulation of mucus intracellularly due to impaired constitutive exocytosis.

Apart from this indirect effect of TMEM16A on mucus secretion, studies on intestinal goblet cells lacking expression of TMEM16A demonstrate also a direct role of TMEM16A for exocytosis and mucus release. We observed that TMEM16A-Vil1$^{flox/flox}$ mice also showed enhanced intracellular mucus content in goblet cells. In addition, in both airway and intestinal secretory cells, knockout of TMEM16A did not compromise cholinergic mucus secretion, i.e. compound exocytosis. Only apical ATP-induced mucus release was found to be TMEM16A dependent. These data reveal a novel function of TMEM16A in regulation of ATP-mediated mucus release by secretory cells.

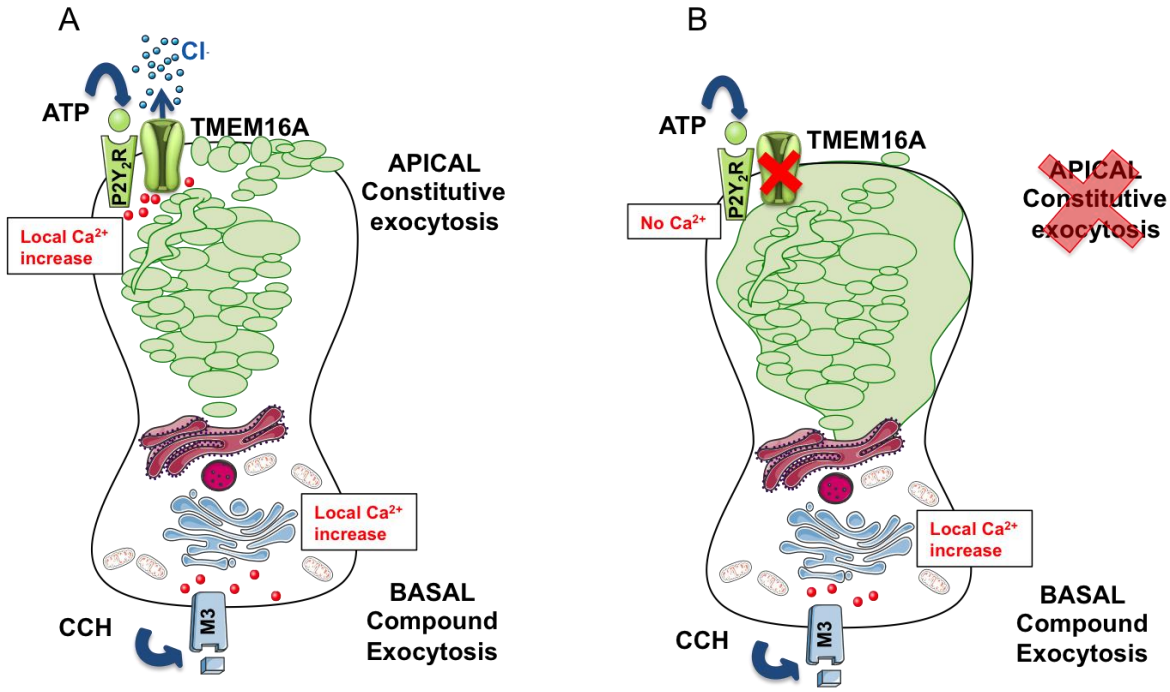

Fig 7. 4 *TMEM16A mediates ATP dependent constitutive exocytosis in the apical side of goblet cells.* A) Model elucidating TMEM16A mediated constitutive exocytosis of mucus in granules on the apical side, and cholinergic dependent compound exocytosis on the basolateral side. B) Colinergic (CCH) mediated compound exocytosis occurs independently of TMEM16A from the basolateral side, while constitutive exocytosis is impaired.

TMEM16A mediates not only mucus secretion, but also the release of inflammatory mediators. In fact our data show that in inflammatory airways of TMEM16A knockout mice CD45 positive leukocytes accumulation and contraction of the airway smooth muscle layer (ASM) was strongly reduced (Chapter 5, Fig 5.2F and Fig S5.2, and [152]). These data replicate the findings of several other studies in which downregulation of TMEM16A reduced inflammation and neuropathy-induced hyperalgesia [302-304]. Similar data were recapitulated in Calu-3 cells, where we found that LPS-induced release of IL-8 was significantly reduced by knockdown of TMEM16A (Chapter 5 Fig 5.7 A-B). In addition, we observed that IL-13 induced Muc5AC production was inhibited by the TMEM16A-blocker Niclosamide (Chapter 6, Fig 6.4 A-C).

Targeting TMEM16 proteins to treat CF?

Excessive mucus secretion represents one of the main clinical hallmarks in respiratory

diseases, as well as in ulcerative colitis and irritable bowel syndrome [305, 306]. Therefore, the need for novel drugs to control mucus hyperproduction is compelling. We investigated the effect of two compounds: Niclosamide, a FDA approved drug used as anthelmintic, that was found to be a potent bronchodilator [241] and NFA, a known CaCC inhibitor. Niclosamide and NFA inhibited purinergic Cl^- currents in HEK293 cells expressing TMEM16A or TMEM16F (Chapter 6, Fig1 A-C and Fig 2A-D). In addition, both drugs showed a marked effect on Ca^{2+} signals in in freshly isolated intestinal cells (Chapter 6, Supplementary Fig 1A-D). In asthmatic mice, Niclosamide and NFA reduced mucus production and attenuated bronchoconstriction after acute application of cholinergic stimuli (Chapter 6, Fig 3 C-E). Moreover, both inhibitors reduced the inflammation in asthmatic mice (Chapter 6, Fig 3H).

Th2-induced goblet cell metaplasia occurs at the same rate in both normal asthmatic mice and asthmatic mice lacking expression of TMEM16A. Therefore, we speculated that not TMEM16A, but other members of TMEM16 family are in charge of mucus production. Deletion of TMEM16A in the airways (TMEM16F-FoxJCre $^{flox/flox}$) displayed mucus accumulation similar to TMEM16A-FoxJCre $^{flox/flox}$ mice but showed attenuated mucus accumulation when compared to wild type mice (Chapter 6, Fig 5 A-B). Acute cholinergic stimulation induced mucus release in wt and TMEM16F-FOXJCre $^{flox/flox}$ mice. However, the amount of mucus release was clearly less in the tissue specific TMEM16F knockout mice. Taken together the results suggest a predominant role of TMEM16A for mucus secretion, and a role for TMEM16F in both mucus production and secretion.

In the intestine, ATP induced mucus secretion was also attenuated in TMEM16F-Vil1$^{flox/flox}$ mice similarly to the TMEM16A-Vil1$^{flox/flox}$ mice, while, cholinergic release was augmented compared to wt mice (Chapter 6, Fig 6A). Interestingly, pretreatment of the mice with Niclosamide inhibited apical ATP-induced release, but not basolateral cholinergic induced mucus secretion. Since mucus accumulation was not observed, these results suggested inhibition of both mucus production and mucus secretion by Niclosamide (Chapter 6, Fig 7 A-G). Freshly isolated colonic crypt from TMEM16F-Vil1$^{flox/flox}$ mice showed a reduced ATP induced Ca^{2+} rise while the CCH-induced increase of intracellular Ca^{2+} concentration was

unaffected (Chapter 6, Supplementary Fig 2 A-G). Taken together these results indicate a role for TMEM16F in mucus production and mucus secretion. We also show that TMEM16F is involved in purinergic (luminal) but not cholinergic (basolateral) receptor signaling. Taken together both TMEM16A and TMEM16F are inhibited by Niclosamide, which appears suitable to treat excessive mucus secretion *in vivo*.

Upregulation of TMEM16A during inflammation strongly supports bronchoconstriction. The role of TMEM16A in provoking bronchoconstriction was further shown in asthmatic mice, by activating TMEM16A directly using the activator E_{ACT}. E_{ACT} induced massive mucus release and airway contraction (Chapter 5, Supplementary Fig 8 A-C).

Therefore, blocking of TMEM16A activity will not only inhibit the release of mucus and cytokines, but will also promote bronchorelaxation. Inhibition of TMEM16A will block the release of inflammatory mediators and therefore which is likely to provide an additional beneficial effect in inflammatory airway and intestinal disease. Given the tight regulatory relationship between TMEM16A and CFTR, blocking TMEM16A and mucus secretion in CF may appear counterintuitive, because residual epithelial Cl^- secretion via TMEM16A and mutated CFTR will also be blocked. However, we reported that the net secretory Cl^- flux through TMEM16A is rather small and mostly occurs though CFTR. Moreover, Cl^- secretion occurring through CFTR is already compromised in CF. Thus, the benefit through inhibition of mucus secretion may well exceed potential drawbacks due to potential inhibition of Cl^- secretion. Our studies suggest that both TMEM16A and TMEM16F might play major roles in mucus secretion and production. Both proteins can be used as pharmacologic targets in CF therapy. We therefore propose inhibitors of TMEM16A as a new class of drugs that reduce mucus secretion in inflammatory airway diseases (an overview of TMEM16 inhibitors and activators is given in Table1 and Table 2 of Appendix II).

Conclusions and further perspectives

Development of new drugs is a challenging, time consuming and expensive process. Re-profiling of approved drugs is cost-effective, fast and saves resources. Niclosamide is a FDA approved drug already in use against the tapeworm *Hymenolepis* infestations, and is used in several clinical trials to treat colonic cancer and prostatic cancer. We report that Niclosamide is a potent inhibitor of TMEM16 proteins and may have a number of beneficial effects in CF. As we show in the present study it inhibits excessive mucus secretion and is a potent bronchorelaxant. In addition, several studies have proposed Niclosamide for the treatment of *Pseudomonas aeruginosa* lung infections. Niclosamide was proved to be a strong inhibitor of *P. aeruginosa* quorum sensing (QS) response and inhibits the production of acyl-homoserine lactones QS signal molecules [307]. Moreover, it was reported to combat existing biofilms of several relevant Gram-positive bacteria, namely strains of *Staphylococcus aureus*, including methicillin MRSA, and *Staphylococcus epidermidis*, all common causes of hospital-acquired and device-associated infections [269]. Taken together all reported positive effects of Niclosamide strongly suggest its use in inflammatory airway and intestinal disease.

Considering the role of TMEM16A in exocytosis, it will be interesting to look into the role of TMEM16A in activation of immune cells and neutrophil degranulation. Exocytosis of granules in neutrophils requires increase in intracellular Ca^{2+} [308] likewise other secretory processes. We may therefore examine the release of neutrophil elastase and the release of other proinflammatory factors.

Niflumic acid is a known COX-2 inhibitor. COX-2 (cyclooxygenase-2) is an enzyme involved in the conversion of arachidonic acid toprostaglandins. COX-2 is upregulated during inflammation and in cancer. It was shown that in pancreactic ductal adenocarcinoma (PDA), COX-2 upregulation is under the influence of MUC1. MUC1 upregulation increases COX-2 and vice versa, downregulation of MUC1 attenuates COX-2. In addition, upregulation of COX-2 via Interleukin 1β upregulates MUC5AC and MUC2 by a mechanism that dependents on mitogen-activated protein kinase (MAPK) [309]. It is known that TMEM16A is involved in tumor

progression, and that this involves induction of the RAS-RAF-MEK-ERK1/2 pathway[310]. Therefore, a link between TMEM16A and COX-2 during mucus production should be further examined. In particular it will be interesting to learn about their role in inflammation and whether COX-2 is responsible for TMEM16A-mediated inflammation. In addition, recent studies showed that reactive oxygen species (ROS) also activate the TAK1-MAPKs/NF-κB pathway. This leads to induction of COX-2 and therefore MUC5AC and MUC2 accumulation. Along this line, ROS was shown to induce lipid peroxidation and activation of TMEM16F during chronic inflammation[65]. Along this line, a role of fatty acids during exacerbation of *P. aeruginosa* infection has been shown recently [311]. It appears attractive to speculate on a functional role of TMEM16A and TMEM16F in modulating airways inflammation and lung remodeling.

Appendix I

TMEM16 PROTEINS	LOCALIZATION	PATHOLOGY
TMEM16A/ANO1	Broadly expressed in secretory epithelia[312] and skeletal muscles[313].	Upregulated in renal cancer,head and neck cancer, pancreatic cancer and lung cancer[314, 315].
TMEM16B/ANO2	Mainly expressed in chemosensory neurons.	Upregulated in colorectal cancer.
TMEM16C/ANO3	Expressed mainly in the brain, particularly in the *putamen* [316].	Mutation of this protein have been associated with dominant craniocervical dystonia [316] due to disturbances in the Ca^{2+} signaling. Hypersensitivity to high temperature. Na^{+} and K^{+} currents largely reduced.
TMEM16D/ANO4	Neuronal tissue.	Upregulated in patients with aldosterone adenomas and pheochromocytoma in the *zona glomerulosa* of the human adrenal gland.
TMEM16E/ANO5	Skeletal muscles and the tyroid.	Responsible for the bone-related late-onset disease gnathodiaphyseal dysplasia (GDD) [317], in the Limb-girdle muscular dystrophy type 2L (LGMD2L) [318].
TMEM16F/ANO6	Broadly expressed.	Upregulated in breast cancer and cervical cancer
TMEM16G/ANO7	Epithelial tissues.	Prostate cancer.
TMEM16H/ANO8	Upregulated in the *substanzia nigra* and in the *cerebellum.*	Upregulated in a variety of cancer.
TMEM16I/ANO9	Gastro intestinal tract and pancreatic cells [319, 320].	Upregulated in Head and Neck cancer.
TMEM16K/ANO10	Broadly expressed in human, while in the mouse is preferentially expressed in the pancreas and in the thyroid [53].	A coding variant of Tmem16K (ANO10-R263H) was shown to have an impact on the human immune response against *Borrelia.* Mutations of TMEM16K are also causing recessive cerebellar ataxia[123], epilepsy, cognitive impairment and coenzyme Q10 deficiency[123].

Table 1 Appendix 1 *Members of the TMEM16 family and their significance in diseases.*

Appendix II

INHIBITORS	IC50 (μM)
5F (Ani9 derivative)	0.02
10bm[321]	0.03
Monna[322]	0.08
Niclosamide[241]	0.7
Ani9[323]	0.1
Tannic Acid[324]	0.323
T16A-AO1[325]	1.1
Dichlorophen[321]	5.49
Idebenone[326]	5.52
Shikonin[327]	6.5
Benzbromarone[269]	9.97
CACC-A01[175, 328]	10
9-Phenantrol[329]	12
Nifumic Acid[299]	12
Flufenamic Acid[330]	28
Talniflumate[300]	-
Dehydroandrographolide[331]	20-30
DIDS[332]	10-100
NPPB[333]	15-150
ACTIVATORS	**IC50 (μM)**
Brevenal	-
Eact[334]	3
INO-4995[335]	5
Denufosol[265]	10
Cinnamaldehyde[336]	10
Ginsenoside Rb1[337]	38.4

Table 1 Appendix 2: *Effects of TMEM16A inhibitors and activators.*

Inhibitors: Antioxidative[322], anti-inflammatory, anti-hypertensive, bronchorelaxant, reduce cancer cell proliferation, reduce rotavirus-induced diarrhea[338], reduce capsaicin-induced nocifensive behaviors[116], reduced contractile tone in vascular and airway smooth muscle[249, 325, 339], reduced intestinal motility [327].

Activators: Stimulate epithelial chloride secretion and intestinal contraction[156], elicit pain and hitchy behaviour[334], pro-proliferatory activity, induction of nociceptive responses[70].

ACKNOWLEDGEMENTS

One thing I learned during this path is to believe in myself.
I was a different person when I started my PhD, and I could not become who I am now without all the people surrounding me.

First and foremost my gratitude goes to my advisor Prof. Kunzelmann for his firm and invaluable guidance, for pushing me to do better and overcome my limits and for transmitting me the passion for research.
I am particularly grateful to Prof. Rainer Schreiber, for all his support during these four years. For his significant advices, insightful suggestions, and most of all for his patience and friendship.
This work would have not been possible without the support of the Cystic Fibrosis Trust SRC 003, INOVCF. My deep gratitude goes to Dr. Mike Gray, Prof. Amaral, Dr. Terran, Dr. Vinciane Saint-Criq, Sara and Saira for the intense collaboration and precious discussions.
A special thanks to Dr. Luka Clarke, for helping me in revising the English fluency of my work.

To Ji, for contributing to my growth as a scientist and as a person. Sometimes yelling, sometimes not, but all of it was necessary.
To all the people in the lab that belonged to this huge crazy family in the past four years, especially to Kip, Gam, Raquel and Filipe for being good labmates and great friends. For all the evenings spent together, trips, games, and experiences. To Tini, Patricia, Silvia and Brigitte for all the help and for making our life in the lab so much fun.
A special thank you to Madalena, for all the scientific (and not) discussions, for sharing her experience with me, for the scientific (and not) advices, for all the laughs and the good times together.

To all the people that are my family here in Germany and elsewhere in the world: Valeria, Giuliana, Anna, Nuno, Mario, Paolo and Caterina. You have always been there and you always will be.

To Inês, for staying when I was at my best and at my worst. For not giving up on me and for taking out the best version of me. I could not imagine a better companion for this and for the future journeys.
To Peter, for his support throughout this time, for what we have built (literally), and for what we will. For caring for my success and for making me believe in better things.

Alla mia famiglia. A mia sorella per essere la mia piu grande fonte di orgoglio e ispirazione. Ai miei genitori e ai miei nonni per essere sempre presenti in ogni aspetto della mia vita anche se siamo distanti. Non sarei potuta essere dove sono senza i vostri sacrifici per me, grazie non sarà mai abbastanza.

ERKLÄRUNGEN

Erklärung:

Hiermit erkläre ich, gem. § 6 Abs. 2, Nr. 6 der Promotionsordnung der Math.-Nat.-Fachbereiche zur Erlangung des Dr. rer. nat., dass ich die vorliegende Dissertation selbständig verfasst und mich keiner anderen als der angegebenen Hilfsmittel bedient habe.

Regensburg, den

CURRICULUM VITAE

PERSONAL INFORMATION

Name:	Roberta Benedetto
Date of birth:	June 14th, 1989
Nationality:	Italian
Current address:	Maria Fels Straße 5, 93309 Kelhleim
E-mails:	Roberta.benedetto@ur.de, rb.benedetto1@gmail.com

ACADEMIC BACKGROUND

2014 - Present Ph.D., Faculty of Natural Sciences III: Biology and Preclinical Medicine, University of Regensburg, DE

2012 - 2014 M.Sc. Molecular Biology and Genetics, Faculty of Biology, University of Pavia, IT

2007 – 2012 B.Sc. (Biology), Faculty of Biology, University of Catania, IT

RESEARCH EXPERIENCE AND TRAINING

2014 Erasmus Placement at the ITQB (Institute of chemical and biological technology) Oeiras, district of Lisbon, PT

2012 – 2014 Master thesis (Molecular Microbiology), Department of Biology and Biotechnology, University of Pavia, IT

Thesis title: Transcriptional regulation of genes involved in heme biosynthesis and protection against nitrosative stress in *Staphylococcus aureus* mutant strains.

2013 Tutor for Bachelor students of the course of Biology at the University of Pavia, IT in “Laboratory of Biomolecular methodologies”.

2009 – 2012 Bachelor Thesis (Molecular Microbiology), Departments of Biological, Geological and Environmental Sciences. University of Catania, IT
Thesis title**:** Molecular and phenotypic characterization of isolates of β–

lactamase producing *Enterococcus faecium*

2012 CCO Humanitas (Oncology Center of Catania), Catania, IT
Clinical – Biochemical Analysis of blood and urine of patients. Investigation of genetic marker.

HONOURS AND AWARDS

2018 Best poster presentation winner, Early Career Researcher competition. Europhysiology 2018 London, GB

2017 Travel grant from the Mukoviszidose Institut for the participation to the 14th ECFS basic science conference

2016 Travel grant from the Mukoviszidose Institut for the participation to the 13th ECFS basic science conference

2014 European funding “Erasmus Placement” Fellowship (5 months)

INTERNATIONAL CONFERENCES AND MEETINGS

2018 Europhysiology, London, GB (Poster)

2018 15th ECFS basic science conference, Athens, GR

2017 14th ECFS basic science conference, Albufeira, PT (Poster)

2017 Cystic Fibrosis Trust - Satellite Event - "CF's Got Talent!", UKCF Conference, Nottingham, UK

2016 13th ECFS basic science conference, Pisa, IT (Poster)

2016 Cystic Fibrosis Trust - Satellite Event - "CF's Got Talent !", UKCF Conference Nottingham, UK

2015 12th ECFS basic science conference, Albufeira, PT (Poster)

LIST OF PUBLICATIONS

1. Kunzelmann K., Schreiber R., Ousingsawat J.,Cabrita I., Doušová T., Bähr A., Janda M., **Benedetto, R.** TMEM16A in Cystic Fibrosis: Activating or inhibiting?
Frontiers in Pharmacology, section Pharmacology of Ion Channels and Channelopathies. Review, 2019. In press.

2. **Benedetto R**., Cabrita I., Schreiber R., and Kunzelmann, K. TMEM16A is indispensable for basal ATP-induced mucus secretion in airways and intestine. Faseb J. 2018 Dec:fj201801333RRR.

3. Lérias J, Pinto M, **Benedetto R**, Schreiber R, Amaral M, Aureli M, Kunzelmann K. Compartmentalized crosstalk of CFTR and TMEM16A (ANO1) through EPAC1 and ADCY1. Cell Signal. 2018 Apr; 44:10-19.

4. Simões F, Ousingsawat J, Wanitchakool P, Fonseca A, Cabrita I, **Benedetto R**, Schreiber R, Kunzelmann K. CFTR supports cell death through ROS-dependent activation of TMEM16F (anoctamin 6). Pflügers Arch. 2018 February; 470(2):305-314.

5. Schreiber R, Ousingsawat J, Wanitchakool P, Sirianant L, **Benedetto R**, Reiss K, Kunzelmann K. Regulation of TMEM16A/Ano1 and TMEM16F/Ano6 ion currents and phospholipids scrambling by Ca^{2+} and plasma membrane lipid. J Physiol. 2018 Jan; 596(2):217-229.

6. **Benedetto R**, Ousingsawat J, Wanitchakool P, Zhang Y, Holtzman MJ, Amaral M, Rock JR, Schreiber R, Kunzelmann K. Epithelial Chloride Transport by CFTR requires TMEM16A. Sci Rep. 2017 Sept; 7(1): 12397.

7. Cabrita I, **Benedetto R**, Fonseca A, Wanitchakool P, Sirianant L, Skryabin BV, Schenk LK, Pavenstadt H, Schreiber R, Kunzelmann K. Differential effects of anotamins on intracellular calcium signals. FASEB J. 2017 May; 31(5): 2123-2134.

8. **Benedetto R**, Sirianant L, Pankonien I, Wanitchakool P, Ousingsawat J, Cabrita I, Schreiber R, Amaral M, Kunzelmann K. Relationship between TMEM16A/Anoctamin1 and LRRC8A. Pflügers Arch. 2016 Oct; 468(10): 1751-1763.

9. Sirianant L, Wanitchakool P, Ousingsawat J, **Benedetto R**, Zormpa A, Cabrita I, Schreiber R, Kunzelmann K. Non-essential contribution of LRRC8A to volume regulation. Pflügers Arch. 2016 May; 468(5):805-816.

10. Kunzelmann K, Cabrita I, Wanitchakool P, Ousingsawat J, Sirianant L, **Benedetto R**, Schreiber R. Modulating Ca^{2+} signals: a common theme for TMEM16, Ist2, and TMC. Pflügers Arch. 2016 Mar; 468(3):475-490.

REFERENCE LIST

1. (2004). WHGP. The molecular genetic epidemiology of cystic fibrosis : report of a joint meeting of WHO/IECFTN/ICF(M)A/ECFS, Genoa, Italy, 19 June 2002.
2. Ratjen F, Doring G. Cystic fibrosis. Lancet. 2003;361(9358):681-689.
3. Gibson RL, Burns JL, Ramsey BW. Pathophysiology and management of pulmonary infections in cystic fibrosis. Am J Respir Crit Care Med. 2003;168(8):918-951.
4. Hoppe B, Von Unruh GE, Blank G, Rietschel E, Sidhu H, Laube N, et al. Absorptive hyperoxaluria leads to an increased risk for urolithiasis or nephrocalcinosis in cystic fibrosis. Am J Kidney Dis. 2005;46(3):440-445.
5. Ballard ST, Spadafora D. Fluid secretion by submucosal glands of the tracheobronchial airways. Respir Physiol Neurobiol. 2007;159(3):271-277.
6. Rowe SM, Miller S, Sorscher EJ. Cystic fibrosis. N Engl J Med. 2005;352:1992-2001.
7. Riordan JR. Identification of the cystic fibrosis gene: cloning and characterization of complementary DNA. Science. 1989;245(4922):1066-1073.
8. Riordan JR. CFTR function and prospects for therapy. Annu Rev Biochem. 2008;77:701-726.
9. Liu F, Zhang Z, Csanady L, Gadsby DC, Chen J. Molecular Structure of the Human CFTR Ion Channel. Cell. 2017;169(1):85-95.
10. R K. Conformational States of CFTR Associated with Channel Gating: The Role of ATP Binding and Hydrolysis CELL Press. 1995;82:231-239.
11. Hwang TC, Yeh JT, Zhang J, Yu YC, Yeh HI, Destefano S. Structural mechanisms of CFTR function and dysfunction. J Gen Physiol. 2018;150(4):539-570.
12. Sheppard DN, Welsh MJ. Structure and function of the CFTR chloride channel. Physiol Rev. 1999;79(1 Suppl):S23-S45.
13. Linsdell P, Tabcharani JA, Rommens JM, Hou YX, Chang XB, Tsui LC, et al. Permeability of wild-type and mutant cystic fibrosis transmembrane conductance regulator chloride channels to polyatomic anions. J Gen Physiol. 1997;110(4):355-364.
14. Anderson MP, Berger HA, Rich DP, Gregory RJ, Smith AE, Welsh MJ. Nucleoside triphosphates are required to open the CFTR chloride channel. Cell. 1991;67:775-784.
15. Akabas MH, Kaufmann C, Cook TA, Archdeacon P. Amino acid residues lining the chloride channel of cystic fibrosis transmembrane conductance regulator. J Biol Chem. 1995;269:14865-14868.
16. Linsdell P, Evagelidis A, Hanrahan JW. Molecular determinants of anion selectivity in the cystic fibrosis transmembrane conductance regulator chloride channel pore [In Process Citation]. Biophys J. 2000;78(6):2973-2982.
17. A. MN. Identification of a region of strong discrimination in the pore of CFTR. Am J Physiol Lung Cell Mol Physio. 2001(281):L852–L867.
18. De Boeck K, Amaral MD. Progress in therapies for cystic fibrosis. Lancet Respir Med. 2016;4(8):662-674.
19. P Z. Induction of HSP70 promotes DF508 CFTR trafficking. Am J Physiol Lung Cell Mol Physio. 2001;281:L58–L68.
20. Youker RT, Walsh P, Beilharz T, Lithgow T, Brodsky JL. Distinct roles for the Hsp40

and Hsp90 molecular chaperones during cystic fibrosis transmembrane conductance regulator degradation in yeast. Mol Biol Cell. 2004;15(11):4787-4797.
21. Alberti S, Bohse K, Arndt V, Schmitz A, Hohfeld J. The cochaperone HspBP1 inhibits the CHIP ubiquitin ligase and stimulates the maturation of the cystic fibrosis transmembrane conductance regulator. Mol Biol Cell. 2004;15(9):4003-4010.
22. Cai ZW, Liu J, Li HY, Sheppard DN. Targeting F508del-CFTR to develop rational new therapies for cystic fibrosis. Acta Pharmacol Sin. 2011;32(6):693-701.
23. Vergani P, Lockless SW, Nairn AC, Gadsby DC. CFTR channel opening by ATP-driven tight dimerization of its nucleotide-binding domains. Nature. 2005;433(7028):876-880.
24. Ma T, Vetrivel L, Yang H, Pedemonte N, Zegarra-Moran O, Galietta LJ, et al. High-affinity activators of cystic fibrosis transmembrane conductance regulator (CFTR) chloride conductance identified by high-throughput screening. J Biol Chem. 2002;277(40):37235-37241.
25. Verkman AS, Galietta Luis J.V. Nanomolar affinity small-molecule potentiators of defective F508CFTR chloride channel gating. The Journal of Biological Chemistry. 2003;278(37):35079-35085.
26. Van Goor F, Straley KS, Cao D, Gonzalez J, Hadida S, Hazlewood A, et al. Rescue of DeltaF508-CFTR trafficking and gating in human cystic fibrosis airway primary cultures by small molecules. Am J Physiol Lung Cell Mol Physiol. 2006;290(6):L1117-L11130.
27. Van Goor F, Hadida S, Grootenhuis PD, Burton B, Cao D, Neuberger T, et al. Rescue of CF airway epithelial cell function in vitro by a CFTR potentiator, VX-770. Proc Natl Acad Sci U S A. 2009;106(44):18825-18830.
28. Mospan C, Mospan G, Byland E, Whitaker WB, Xiong L, Dunlap J, Canupp K. Drugs updates and approvals: 20178 in review. Nurse Pract. 2018;43(12):23-32.
29. Wainwright CE, Elborn JS, Ramsey BW, Marigowda G, Huang X, Cipolli M, et al. Lumacaftor-Ivacaftor in Patients with Cystic Fibrosis Homozygous for Phe508del CFTR. N Engl J Med. 2015;373(3):220-231.
30. Deeks ED. Lumacaftor/Ivacaftor: A Review in Cystic Fibrosis. Drugs. 2016;76(12):1191-1201.
31. Cholon DM, Quinney NL, Fulcher ML, Esther CR, Jr., Das J, Dokholyan NV, et al. Potentiator ivacaftor abrogates pharmacological correction of DeltaF508 CFTR in cystic fibrosis. Sci Transl Med. 2014;6(246):246ra96.
32. Health CAfDaTi. Ivacaftor (Kalydeco) 150 mg Tablet: For Treatment of Cystic Fibrosis with G551D, G1244E, G1349D, G178R, G551S, S1251N, S1255P, S549N, S549R, or G970R Mutation. 2015.
33. Sala MA, Jain M. Tezacaftor for the treatment of cystic fibrosis. Expert Rev Respir Med. 2018;12(9):725-732.
34. Veit G, Xu H, Dreano E, Avramescu RG, Bagdany M, Beitel LK, et al. Structure-guided combination therapy to potently improve the function of mutant CFTRs. Nature medicine. 2018;24(11):1732-1742.
35. Han TW, Ye W, Bethel NP, Zubia M, Grabe M, Nung Jan Y, et al. TMEM16F is a Calcium-Activated Phospholipid Scramblase Required for Chemically-Induced Giant Plasma Membrane Vesicles. Biophysical Journal. 2018;114(3):610a.
36. Dorfman R, Taylor C, Lin F, Sun L, Sandford A, Pare P, et al. Modulatory effect of the

SLC9A3 gene on susceptibility to infections and pulmonary function in children with cystic fibrosis. Pediatr Pulmonol. 2011;46(4):385-392.
37. Favia M, Fanelli T, Bagorda A, Di Sole F, Reshkin SJ, Suh PG, et al. NHE3 inhibits PKA-dependent functional expression of CFTR by NHERF2 PDZ interactions. Biochem Biophys Res Commun. 2006;347(2):452-459.
38. Bradford EM, Sartor MA, Gawenis LR, Clarke LL, Shull GE. Reduced NHE3-mediated Na+ absorption increases survival and decreases the incidence of intestinal obstructions in cystic fibrosis mice. Am J Physiol Gastrointest Liver Physiol. 2009;296(4):G886-G898.
39. Scott M, Blackman CWC, Watson C,Kristin M, Arcara L, Strug JRS, Wright Fred A, Rommens JM, Sun L, Pace San RG, Durie PR, Drumm ML, Knowles MR, Cutting GR. Genetic Modifiers of Cystic Fibrosis–Related Diabetes. Diabetes Journal. 2013;62(10):3627-3635.
40. Sun L, Rommens JM, Corvol H, Li W, Li X, Chiang TA, et al. Multiple apical plasma membrane constituents are associated with susceptibility to meconium ileus in individuals with cystic fibrosis. Nat Genet. 2012;44(5):562-569.
41. Xu J, Song P, Miller ML, Borgese F, Barone S, Riederer B, et al. Deletion of the chloride transporter Slc26a9 causes loss of tubulovesicles in parietal cells and impairs acid secretion in the stomach. Proc Natl Acad Sci U S A. 2008;105(46):17955-17960.
42. Chabot H, Vives MF, Dagenais A, Grygorczyk C, Berthiaume Y, Grygorczyk R. Downregulation of epithelial sodium channel (ENaC) by CFTR co-expressed in *Xenopus* oocytes is independent of Cl^- conductance. J Membr Biol. 1999;169(3):175-188.
43. König J, Schreiber R, Voelcker T, Mall M, Kunzelmann K. CFTR inhibits ENaC through an increase in the intracellular Cl^- concentration. EMBO Reports. 2001;2:1-5.
44. Mall M, Bleich M, Greger R, Schreiber R, Kunzelmann K. The amiloride inhibitable Na^+ conductance is reduced by CFTR in normal but not in CF airways. J Clin Invest. 1998;102:15-21.
45. Boucher RC, Stutts MJ, Knowles MR, Cantley L, Gatzy JT. Na+ transport in cystic fibrosis respiratory epithelia: Abnormal basal rate and response to adenylate cyclase. J Clin Invest. 1986;78:1245-1252.
46. Grubb BR, Vick RN, Boucher RC. Hyperabsorption of Na^+ and raised Ca^{2+} mediated Cl^- secretion in nasal epithelia of CF mice. Am J Physiol. 1994;266:C1478-C1483.
47. Zabner J, Smith JJ, Karp PH, Widdicombe JH, Welsh MJ. Loss of CFTR chloride channels alters salt absorption by cystic fibrosis airway epithelia in vitro. Mol Cell. 1998;2(3):397-403.
48. Chen JH, Stoltz DA, Karp PH, Ernst SE, Pezzulo AA, Moninger TO, et al. Loss of anion transport without increased sodium absorption characterizes newborn porcine cystic fibrosis airway epithelia. Cell. 2010;143:911-923.
49. Preston P, Wartosch L, Gunzel D, Fromm M, Kongsuphol P, Ousingsawat J, et al. Disruption of the K^+ channel beta-subunit KCNE3 reveals an important role in intestinal and tracheal Cl^- transport. J Biol Chem. 2010;285(10):7165-7175.
50. Shah VS, Meyerholz DK, Tang XX, Reznikov L, Abou AM, Ernst SE, et al. Airway acidification initiates host defense abnormalities in cystic fibrosis mice. Science. 2016;351:503-507.
51. Scudieri P, Musante I, Caci E, Venturini A, Morelli P, Walter C, et al. Increased

expression of ATP12A proton pump in cystic fibrosis airways. JCI Insight. 2018;3(20).
52. Moss RB. Pitfalls of drug development: lessons learned from trials of denufosol in cystic fibrosis. J Pediatr. 2013;162(4):676-680.
53. Sondo E, Caci E, Galietta LJ. The TMEM16A chloride channel as an alternative therapeutic target in cystic fibrosis. Int J Biochem Cell Biol. 2014;52:73-76.
54. Schreiber R, Uliyakina I, Kongsuphol P, Warth R, Mirza M, Martins JR, et al. Expression and function of epithelial anoctamins. J Biol Chem. 2010;285(10):7838-7845.
55. Yang YD, Cho H, Koo JY, Tak MH, Cho Y, Shim WS, et al. TMEM16A confers receptor-activated calcium-dependent chloride conductance. Nature. 2008;455(7217):1210-1215.
56. Caputo A, Caci E, Ferrera L, Pedemonte N, Barsanti C, Sondo E, et al. TMEM16A, A Membrane Protein Associated With Calcium-Dependent Chloride Channel Activity. Science. 2008;322:590-594.
57. Schroeder BC, Cheng T, Jan YN, Jan LY. Expression cloning of TMEM16A as a calcium-activated chloride channel subunit. Cell. 2008;134:1019-1029.
58. Hartzell C, Putzier I, Arreola J. Calcium-activated chloride channels. Annu Rev Physiol. 2005;67:719-758.
59. Ni YL, Kuan AS, Chen TY. Activation and Inhibition of TMEM16A Calcium-Activated Chloride Channels. PLoS ONE. 2014;9:e86734.
60. Brunner JD, Lim NK, Schenck S, Duerst A, Dutzler R. X-ray structure of a calcium-activated TMEM16 lipid scramblase. Nature. 2014;516:207-212.
61. Paulino C, Kalienkova V, Lam AKM, Neldner Y, Dutzler R. Activation mechanism of the calcium-activated chloride channel TMEM16A revealed by cryo-EM. Nature. 2017;552(7685):421-425.
62. Suzuki J, Umeda M, Sims PJ, Nagata S. Calcium-dependent phospholipid scrambling by TMEM16F. Nature. 2010;468:834-838.
63. Martins JR, Faria D, Kongsuphol P, Reisch B, Schreiber R, Kunzelmann K. Anoctamin 6 is an essential component of the outwardly rectifying chloride channel. Proc Natl Acad Sci U S A. 2011;108:18168-18172.
64. Yang H, Kim A, David T, Palmer D, Jin T, Tien J, et al. TMEM16F Forms a Ca(2+)-Activated Cation Channel Required for Lipid Scrambling in Platelets during Blood Coagulation. Cell. 2012;151:111-122.
65. Juul CA, Grubb S, Poulsen KA, Kyed T, Hashem N, Lambert IH, et al. Anoctamin 6 differs from VRAC and VSOAC but is involved in apoptosis and supports volume regulation in the presence of Ca^{2+}. Pflugers Arch. 2014;466(10):1899-1910.
66. Simoes F, Ousingsawat J, Wanitchakool P, Fonseca A, Cabrita I, Benedetto R, et al. CFTR supports cell death through ROS-dependent activation of TMEM16F (anoctamin 6). Pflugers Arch. 2018;470:305-314.
67. Fujii T, Sakata A, Nishimura S, Eto K, Nagata S. TMEM16F is required for phosphatidylserine exposure and microparticle release in activated mouse platelets. Proc Natl Acad Sci U S A. 2015;112(41):12800-12805.
68. Stohr H, Heisig JB, Benz PM, Schoberl S, Milenkovic VM, Strauss O, et al. TMEM16B, A Novel Protein with Calcium-Dependent Chloride Channel Activity, Associates with a Presynaptic Protein Complex in Photoreceptor Terminals. J Neurosci. 2009;29:6809-6818.

69. Zhang CH, Li Y, Zhao W, Lifshitz LM, Li H, Harfe BD, et al. The transmembrane protein 16A Ca^{2-}-activated Cl^{-} channel in airway smooth muscle contributes to airway hyperresponsiveness. Am J Respir Crit Care Med. 2013;187:374-381.
70. Paulino C, Neldner Y, Lam AK, Kalienkova V, Brunner JD, Schenck S, et al. Structural basis for anion conduction in the calcium-activated chloride channel TMEM16A. Elife. 2017;6.
71. Nicolson SJSaGL. The Fluid Mosaic Model of the Structure of Cell Membranes Science (New Series). 1972;1975(4023):720-731.
72. Simons K. VMG. Lipid sorting in epithelial cells. Biochemistry. 1988;27(17):6197-6202.
73. Korade Z, Kenworthy AK. Lipid rafts, cholesterol, and the brain. Neuropharmacology. 2008;55(8):1265-1273.
74. Pike LJ. The challenge of lipid rafts. J Lipid Res. 2009;50 Suppl:S323-328.
75. Allen JA, Halverson-Tamboli RA, Rasenick MM. Lipid raft microdomains and neurotransmitter signalling. Nature Reviews Neuroscience. 2006;8(2):128-140.
76. Eric J. Smart GAG, Mark A. McNiven, William C. Sessa, Jeffrey A. Engelman, Philipp E. Scherer, Takashi Okamoto, Michael P. Lisanti. Caveolins, Liquid-Ordered Domains, and Signal Transduction. Mol Biol Cell. 1999;19(11):7289-7304.
77. Patel H. IPA. Lipid Rafts and Caveolae and Their Role in Compartmentation of Redox Signaling. Antioxid Redox Signal. 2009;11(6):1357-1372.
78. Murata T, Lin MI, Stan RV, Bauer PM, Yu J, Sessa WC. Genetic evidence supporting caveolae microdomain regulation of calcium entry in endothelial cells. J Biol Chem. 2007;282(22):16631-16643.
79. Jin X, Shah S, Du X, Zhang H, Gamper N. Activation of Ca^{2+}-activated Cl^{-} channel ANO1 by localized Ca^{2+} signals. J Physiol. 2016;594:19-30.
80. Cabrita I, Benedetto R, Fonseca A, Wanitchakool P, Sirianant L, Skryabin BV, et al. Differential effects of anoctamins on intracellular calcium signals. Faseb j. 2017;31:2123-34.
81. Mall MA. Unplugging Mucus in Cystic Fibrosis and Chronic Obstructive Pulmonary Disease. Ann Am Thorac Soc. 2016;13 Suppl 2:S177-S185.
82. Hollingsworth MA, Swanson BJ. Mucins in cancer: protection and control of the cell surface. Nat Rev Cancer. 2004;4(1):45-60.
83. Hattrup CL, Gendler SJ. Structure and function of the cell surface (tethered) mucins. Annu Rev Physiol. 2008;70:431-457.
84. Govindarajan B, Gipson IK. Membrane-tethered mucins have multiple functions on the ocular surface. Exp Eye Res. 2010;90(6):655-63.
85. Sellers L.A., Allen A, Morris ER, Ross-Murphy SB. Mucus glycoprotein gels. Role of glycoprotein polymeric structure and carbohydrate side-chains in gel-formation. Carbohydrate Research. 198; 178:93-110.
86. Johansson ME, Larsson JM, Hansson GC. The two mucus layers of colon are organized by the MUC2 mucin, whereas the outer layer is a legislator of host-microbial interactions. Proc Natl Acad Sci U S A. 2011;108 Suppl 1:4659-4665.
87. Rose MC, Voynow JA. Respiratory tract mucin genes and mucin glycoproteins in health and disease. Physiol Rev. 2006;86(1):245-278.
88. Kreda SM, Davis CW, Rose MC. CFTR, mucins, and mucus obstruction in cystic fibrosis. Cold Spring Harb Perspect Med. 2012;1(2):9.
89. Quinton PM. Role of epithelial HCO_3^- transport in mucin secretion: lessons from cystic

fibrosis. Am J Physiol Cell Physiol. 2010;299(6):C1222-C1233.
90. Gustafsson JK, Ermund A, Ambort D, Johansson ME, Nilsson HE, Thorell K, et al. Bicarbonate and functional CFTR channel are required for proper mucin secretion and link cystic fibrosis with its mucus phenotype. J Exp Med. 2012;209(7):1263-1272.
91. Quinton PM. Role of epithelial HCO3(-) transport in mucin secretion: lessons from cystic fibrosis. Am J Physiol Cell Physiol. 2010;299:C1222-C1233.
92. Okada SF, Zhang L, Kreda SM, Abdullah LH, Davis CW, Pickles RJ, et al. Coupled nucleotide and mucin hypersecretion from goblet-cell metaplastic human airway epithelium. Am J Respir Cell Mol Biol. 2011;45(2):253-260.
93. Garcia MA, Yang N, Quinton PM. Normal mouse intestinal mucus release requires cystic fibrosis transmembrane regulator-dependent bicarbonate secretion. J Clin Invest. 2009;119:2613-2622.
94. Davis CW, Dickey BF. Regulated airway goblet cell mucin secretion. Annu Rev Physiol. 2008;70:487-512.
95. Demetrios Papahadjopoulos SND. Molecular mechanisms of calcium-induced membrane fusion. Journal of Bioenergetics and Biomembranes. 1990;22(2):157-179.
96. Voets T, Moser T, Lund PE, Chow RH, Geppert M, Sudhof TC, et al. Intracellular calcium dependence of large dense-core vesicle exocytosis in the absence of synaptotagmin I. Proc Natl Acad Sci U S A. 2001;98(20):11680-11685.
97. Li Y, Martin LD, Spizz G, Adler KB. MARCKS protein is a key molecule regulating mucin secretion by human airway epithelial cells in vitro. J Biol Chem 2001 Nov;276 (44):40982-90.
98. Li Y, Martin LD, Spizz G, Adler KB. MARCKS protein is a key molecule regulating mucin secretion by human airway epithelial cells in vitro. J Biol Chem. 2001;276(44):40982-90.
99. Sudhof TC. The synaptic vesicle cycle. Annu Rev Neurosci. 2004;27:509-47.
100. Oliver MG, Specian RD. Cytoskeleton of intestinal goblet cells: role of actin filaments in baseline secretion. Am J Physiol. 1990;259(6 Pt 1):991-997.
101. Ehre C, Rossi AH, Abdullah LH, De Pestel K, Hill S, Olsen JC, et al. Barrier role of actin filaments in regulated mucin secretion from airway goblet cells. Am J Physiol Cell Physiol. 2005;288(1):C46-56.
102. Houy S, Groffen AJ, Ziomkiewicz I, Verhage M, Pinheiro PS, Sorensen JB. Doc2B acts as a calcium sensor for vesicle priming requiring synaptotagmin-1, Munc13-2 and SNAREs. Elife. 2017;6.
103. Schroeder TH, Lee MM, Yacono PW, Cannon CL, Gerceker AA, Golan DE, et al. CFTR is a pattern recognition molecule that extracts Pseudomonas aeruginosa LPS from the outer membrane into epithelial cells and activates NF-kappa B translocation. Proc Natl Acad Sci U S A. 2002;99(10):6907-6912.
104. Zar LS, Quittell L, Prince A. Binding of *Pseudomonas aeruginosa* to respiratory epithelial cells from patients with various mutations in the cystic fibrosis transmembrane regulator. Pediatric Infectious Diseases. 1995;126(2):230-233.
105. Pandey KC, De S, Mishra PK. Role of Proteases in Chronic Obstructive Pulmonary Disease. Front Pharmacol. 2017;8:512.
106. Weber A J S, Ryan R., Saba S, Prince A. . Activation of NF-kB in airway epithelial

cells is dependent on CFTR trafficking and Cl^- channel function. Am J Physiol Lung Cell Mol Physio.281(1):71-78.
107. Hartl D, Gaggar A, Bruscia E, Hector A, Marcos V, Jung A, et al. Innate immunity in cystic fibrosis lung disease. J Cyst Fibros. 2012;11(5):363-382.
108. Kieninger SY, Proietti E, Casaulta C, Regamey N, Frey U, Latzin P. Normal lung function in infants with cystic fibrosis shortly after birth. European Respiratory Journal. 2013;42(57).
109. Stoltz DA, Meyerholz DK, Pezzulo AA, Ramachandran S, Rogan MP, Davis GJ, et al. Cystic Fibrosis Pigs Develop Lung Disease and Exhibit Defective Bacterial Eradication at Birth. Science Translational Medicine. 2010;2(29):29ra31
110. Noah TL, Black HR, Cheng PW, Wood RE, Leigh MW. Nasal and Bronchoalveolar Lavage Fluid Cytokines in Early Cystic Fibrosis. Journal of Infectious Diseases. 1997;175(3):638-647.
111. Suzuki J, Fujii T, Imao T, Ishihara K, Kuba H, Nagata S. Calcium-dependent Phospholipid Scramblase Activity of TMEM16 Family Members. J Biol Chem. 2013;288:13305-13316.
112. Pedemonte N, Galietta LJ. Structure and Function of TMEM16 Proteins (Anoctamins). Physiol Rev. 2014;94:419-459.
113. Yang YD, Cho H, Koo JY, Tak MH, Cho Y, Shim WS, et al. TMEM16A confers receptor-activated calcium-dependent chloride conductance. Nature. 2008;455:1210-5.
114. Tian Y, Schreiber R, Kunzelmann K. Anoctamins are a family of Ca^{2+} activated Cl^- channels. J Cell Sci. 2012;125:4991-4998.
115. Heinze C, Seniuk A, Sokolov MV, Huebner AK, Klementowicz AE, Szijarto IA, et al. Disruption of vascular Ca^{2+}-activated chloride currents lowers blood pressure. J Clin Invest. 2014;124:675-686.
116. Takayama Y, Uta D, Furue H, Tominaga M. Pain-enhancing mechanism through interaction between TRPV1 and anoctamin 1 in sensory neurons. Proc Natl Acad Sci U S A. 2015;112:5213-5218.
117. Huang WC, Xiao S, Huang F, Harfe BD, Jan YN, Jan LY. Calcium-Activated Chloride Channels (CaCCs) Regulate Action Potential and Synaptic Response in Hippocampal Neurons. Neuron. 2012;74:179-192.
118. Huang F, Wang X, Ostertag EM, Nuwal T, Huang B, Jan YN, et al. TMEM16C facilitates Na^+-activated K^+ currents in rat sensory neurons and regulates pain processing. Nat Neurosci. 2013;16:1284-1290.
119. Ruppersburg CC, Hartzell HC. The Ca^{2+}-activated Cl^- channel ANO1/TMEM16A regulates primary ciliogenesis. Mol Biol Cell. 2014;25:1793-1807.
120. Duvvuri U, Shiwarski DJ, Xiao D, Bertrand C, Huang X, Edinger RS, et al. TMEM16A, induces MAPK and contributes directly to tumorigenesis and cancer progression. Cancer Res. 2012;72:3270-3281.
121. Ehlen HW, Chinenkova M, Moser M, Munter HM, Krause Y, Gross S, et al. Inactivation of Anoctamin6/Tmem16F, a regulator of phosphatidylserine scrambling in osteoblasts, leads to decreased mineral deposition in skeletal tissues. J Bone Miner Res. 2012;28:246-259.
122. Hammer C, Wanitchakool P, Sirianant L, Papiol S, Monnheimer M, Faria D, et al. A coding variant of ANO10, affecting volume regulation of macrophages, is associated with

Borrelia seropositivity. Mol Med. 2015;21:26-37.
123. Balreira A, Boczonadi V, Barca E, Pyle A, Bansagi B, Appleton M, et al. ANO10 mutations cause ataxia and coenzyme Q deficiency. J Neurol. 2014;261:2192-2198.
124. Griffin DA, Johnson RW, Whitlock JM, Pozsgai ER, Heller KN, Grose WE, et al. Defective membrane fusion and repair in Anoctamin5 -deficient muscular dystrophy. Hum Mol Genet. 2016:ddw063.
125. Fischer MA, Temmerman K, Ercan E, Nickel W, Seedorf M. Binding of plasma membrane lipids recruits the yeast integral membrane protein Ist2 to the cortical ER. Traffic. 2009;10:1084-1097.
126. Jin X, Shah S, Liu Y, Zhang H, Lees M, Fu Z, et al. Activation of the Cl^- Channel ANO1 by Localized Calcium Signals in Nociceptive Sensory Neurons Requires Coupling with the IP3 Receptor. Sci Signal. 2013;6:ra73.
127. Courjaret R, Machaca K. Mid-range Ca^{2+} signalling mediated by functional coupling between store-operated Ca^{2+} entry and IP3-dependent Ca^{2+} release. Nat Commun. 2014;5:3916.
128. Schreiber R, Faria D, Skryabin BV, Rock JR, Kunzelmann K. Anoctamins support calcium-dependent chloride secretion by facilitating calcium signaling in adult mouse intestine. Pflügers Arch. 2014;467:1203-1213.
129. Sirianant L, Ousingsawat J, Tian Y, Schreiber R, Kunzelmann K. TMC8 (EVER2) attenuates intracellular signaling by Zn^{2+} and Ca^{2+} and suppresses activation of Cl^- currents. Cellular signalling. 2014;26:2826-2833.
130. Schreiber R, Uliyakina I, Kongsuphol P, Warth R, Mirza M, Martins JR, et al. Expression and Function of Epithelial Anoctamins. J Biol Chem. 2010;285:7838-7845.
131. Almaca J, Tian Y, AlDehni F, Ousingsawat J, Kongsuphol P, Rock JR, et al. TMEM16 proteins produce volume regulated chloride currents that are reduced in mice lacking TMEM16A. J Biol Chem. 2009;284:28571-2878.
132. Watts SD, Suchland KL, Amara SG, Ingram SL. A sensitive membrane-targeted biosensor for monitoring changes in intracellular chloride in neuronal processes. PLoS ONE. 2012;7:e35373.
133. Lee MY, Song H, Nakai J, Ohkura M, Kotlikoff MI, Kinsey SP, et al. Local subplasma membrane Ca^{2+} signals detected by a tethered Ca^{2+} sensor. Proc Natl Acad Sci U S A. 2006;103:13232-13237.
134. Ousingsawat J, Wanitchakool P, Kmit A, Romao AM, Jantarajit W, Schreiber S, et al. Anoctamin 6 mediates effects essential for innate immunity downstream of P2X7-receptors in macrophages. Nat Commun. 2015;6:6245-6249.
135. Sones WR, Davis AJ, Leblanc N, Greenwood IA. Cholesterol depletion alters amplitude and pharmacology of vascular calcium-activated chloride channels. Cardiovasc Res. 2010;87:476-484.
136. Fischer KG, Leipziger J, Rubini-Illes P, Nitschke R, Greger R. Attenuation of stimulated Ca^{2+} influx in colonic epithelial (HT_{29}) cells by cAMP. Pflugers Arch. 1996;432:735-740.
137. Szentpetery Z, Balla A, Kim YJ, Lemmon MA, Balla T. Live cell imaging with protein domains capable of recognizing phosphatidylinositol 4,5-bisphosphate; a comparative study. BMC Cell Biol. 2009;10(67).
138. Kabouridis PS, Janzen J, Magee AL, Ley SC. Cholesterol depletion disrupts lipid rafts

and modulates the activity of multiple signaling pathways in T lymphocytes. Eur J Immunol. 2000;30(3):954-963.
139. Diaz O, Mebarek-Azzam S, Benzaria A, Dubois M, Lagarde M, Nemoz G, et al. Disruption of lipid rafts stimulates phospholipase d activity in human lymphocytes: implication in the regulation of immune function. J Immunol. 2005;175(12):8077-8086.
140. Sirianant L, Ousingsawat J, Wanitchakool P, Schreiber R, Kunzelmann K. Cellular Volume regulation by Anoctamin 6:Ca^{2+}, phospholipase A2,osmosensing. Pflügers Arch. 2015;468:335-349.
141. Grubb S, Poulsen KA, Juul CA, Kyed T, Klausen TK, Larsen EH, et al. TMEM16F (Anoctamin 6), an anion channel of delayed Ca^{2+} activation. J Gen Physiol. 2013;141:585-600.
142. Zhang WM, Yip KP, Lin MJ, Shimoda LA, Li WH, Sham JS. ET-1 activates Ca^{2+} sparks in PASMC: local Ca^{2+} signaling between inositol trisphosphate and ryanodine receptors. Am J Physiol Lung Cell Mol Physiol. 2003;285(3):680-690.
143. Tones MA, Bootman MD, Higgins BF, Lane DA, Pay GF, Lindahl U. The effect of heparin on the inositol 1,4,5-trisphosphate receptor in rat liver microsomes. Dependence on sulphate content and chain length. FEBS Lett. 1989;252(1-2):105-108.
144. Ohga K, Takezawa R, Arakida Y, Shimizu Y, Ishikawa J. Characterization of YM-58483/BTP2, a novel store-operated Ca^{2+} entry blocker, on T cell-mediated immune responses in vivo. Int Immunopharmacol. 2008;8(13-14):1787-1792.
145. Derler I, Schindl R, Fritsch R, Heftberger P, Riedl MC, Begg M, et al. The action of selective CRAC channel blockers is affected by the Orai pore geometry. Cell Calcium. 2013;53(2):139-151.
146. Maniero C, Zhou J, Shaikh LH, Azizan EA, McFarlane I, Neogi S, et al. Role of ANO4 in regulation of aldosterone secretion in the zona glomerulosa of the human adrenal gland. Lancet. 2015;385 Suppl 1:4.
147. Pritchard HA, Leblanc N, Albert AP, Greenwood IA. Inhibitory role of phosphatidylinositol 4,5 bisphosphate on TMEM16A encoded calcium-activated chloride channels in rat pulmonary artery. Br J Pharmacol. 2014;171(18):4311-4321.
148. Barro Soria R, AlDehni F, Almaca J, Witzgall R, Schreiber R, Kunzelmann K. ER localized bestrophin1 acts as a counter-ion channel to activate Ca^{2+} dependent ion channels TMEM16A and SK4. Pflügers Arch. 2009;459:485-497.
149. Kunzelmann K, Schreiber R, Kmit A, Jantarajit W, Martins JR, Faria D, et al. Expression and function of epithelial anoctamins. Exp Physiol. 2012;97:184-192.
150. Maass K, Fischer MA, Seiler M, Temmerman K, Nickel W, Seedorf M. A signal comprising a basic cluster and an amphipathic alpha-helix interacts with lipids and is required for the transport of Ist2 to the yeast cortical ER. J Cell Sci. 2009;122:625-635.
151. Liu B, Linley JE, Du X, Zhang X, Ooi L, Zhang H, et al. The acute nociceptive signals induced by bradykinin in rat sensory neurons are mediated by inhibition of M-type K^+ channels and activation of Ca^{2+}-activated Cl^- channels. J Clin Invest. 2010;120:1240-1252.
152. Huang F, Zhang H, Wu M, Yang H, Kudo M, Peters CJ, et al. Calcium-activated chloride channel TMEM16A modulates mucin secretion and airway smooth muscle contraction. Proc Natl Acad Sci U S A. 2012;109:16354-16359.
153. Vocke K, Dauner K, Hahn A, Ulbrich A, Broecker J, Keller S, et al. Calmodulin-

dependent activation and inactivation of anoctamin calcium-gated chloride channels. J Gen Physiol. 2013;142:381-404.
154. Zhu MH, Sung TS, O'Driscoll K, Koh SD, Sanders KM. Intracellular Ca^{2+} release from endoplasmic reticulum regulates slow wave currents and pacemaker activity of interstitial cells of Cajal. Am J Physiol Cell Physiol. 2015;308:C608-C620.
155. Singh RD, Gibbons SJ, Saravanaperumal SA, Du P, Hennig GW, Eisenman ST, et al. Ano1, a Ca^{2+}-activated Cl^- channel coordinates contractility in mouse intestine by Ca^{2+} transient coordination between interstitial cells of cajal. J Physiol. 2014;592:4051-4068.
156. Namkung W, Yao Z, Finkbeiner WE, Verkman AS. Small-molecule activators of TMEM16A, a calcium-activated chloride channel, stimulate epithelial chloride secretion and intestinal contraction. FASEB J. 2011;25:4048-4062.
157. Takayama Y, Shibasaki K, Suzuki Y, Yamanaka A, Tominaga M. Modulation of water efflux through functional interaction between TRPV4 and TMEM16A/anoctamin 1. FASEB J. 2014;28:2238-2248.
158. Concepcion AR, Vaeth M, Wagner LE, 2nd, Eckstein M, Hecht L, Yang J, et al. Store-operated Ca^{2+} entry regulates Ca^{2+}-activated chloride channels and eccrine sweat gland function. J Clin Invest. 2016;126(11):4303-4318.
159. Wanitchakool P, Ousingsawat J, Sirianant L, Cabrita I, Faria D, Schreiber R, et al. Cellular defects by deletion of ANO10 are due to deregulated local calcium signaling. Cellular signalling. 2016;30:41-49.
160. Kunzelmann K, Cabrita I, Wanitchakool P, Ousingsawat J, Sirianant L, Benedetto R, et al. Modulating Ca^{2+}signals: a common theme for TMEM16, Ist2, and TMC. Pflügers Arch. 2016;468:475-490.
161. Billet A, Hanrahan JW. The secret life of CFTR as a calcium-activated chloride channel. J Physiol. 2013;591:5273-5278.
162. Namkung W, Finkbeiner WE, Verkman AS. CFTR-Adenylyl Cyclase I Association Is Responsible for UTP Activation of CFTR in Well-Differentiated Primary Human Bronchial Cell Cultures. Mol Biol Cell. 2010;21:2639-2648.
163. Kunzelmann K, Mall M. Electrolyte transport in the colon: Mechanisms and implications for disease. Physiological Reviews. 2002;82:245-289.
164. Ousingsawat J, Martins JR, Schreiber R, Rock JR, Harfe BD, Kunzelmann K. Loss of TMEM16A causes a defect in epithelial Ca^{2+} dependent chloride transport. J Biol Chem. 2009;284:28698-28703.
165. Anagnostopoulou P, Riederer B, Duerr J, Michel S, Binia A, Agrawal R, et al. SLC26A9-mediated chloride secretion prevents mucus obstruction in airway inflammation. J Clin Invest. 2012;122:3629-3634.
166. Veit G, Bossard F, Goepp J, Verkman AS, Galietta LJ, Hanrahan JW, et al. Proinflammatory Cytokine Secretion is Suppressed by TMEM16A or CFTR Channel Activity in Human Cystic Fibrosis Bronchial Epithelia. Mol Biol Cell. 2012;23(21):4188-4202.
167. Liu X, Li T, Riederer B, Lenzen H, Ludolph L, Yeruva S, et al. Loss of Slc26a9 anion transporter alters intestinal electrolyte and HCO_3^- transport and reduces survival in CFTR-deficient mice. Pflugers Arch. 2015;467(6):1261-1275.
168. Yurtsever Z, Sala-Rabanal M, Randolph DT, Scheaffer SM, Roswit WT, Alevy YG, et al. Self-cleavage of human CLCA1 protein by a novel internal metalloprotease domain

controls calcium-activated chloride channel activation. J Biol Chem. 2012;287:42138-42149.
169. Mall MA, Galietta LJ. Targeting ion channels in cystic fibrosis. J Cyst Fibros. 2015;14(5):561-570.
170. Kunzelmann K, Mall M, Briel M, Hipper A, Nitschke R, Ricken S, et al. The cystic fibrosis transmembrane conductance regulator attenuates the endogenous Ca^{2+} activated Cl^- conductance in *Xenopus* ooyctes. Pflügers Arch. 1997;434:178-181.
171. Wei L, Vankeerberghen A, Cuppens H, Eggermont J, Cassiman JJ, Droogmans G, et al. Interaction between calcium-activated chloride channels and the cystic fibrosis transmembrane conductance regulator. Pflugers Arch. 1999;438(5):635-641.
172. Ousingsawat J, Kongsuphol P, Schreiber R, Kunzelmann K. CFTR and TMEM16A are Separate but Functionally Related Cl Channels. Cell Physiol Biochem. 2011;28:715-724.
173. Kunzelmann K, Allert N, Kubitz R, Breuer WV, Cabantchik ZI, Normann C, et al. Forskolin- and PMA-pretreatment alter the acute electrical response of HT_{29} cells to cAMP, ATP, neurotensin, ionomycin and hypotonic cell swelling. Pflügers Arch. 1994;428:76-83.
174. Kubitz R, Warth R, Kunzelmann K, Grolik M, Greger R. Small conductance Cl^- channels induced by cAMP, Ca^{2+}, and hypotonicity in HT_{29} cells: ion selectivity, additivity and stilbene sensitivity. Pflügers Arch. 1992;421:447-454.
175. Gianotti A, Ferrera L, Philp AR, Caci E, Zegarra-Moran O, Galietta LJ, et al. Pharmacological analysis of epithelial chloride secretion mechanisms in adult murine airways. Eur J Pharmacol. 2016:10.
176. Billet A, Luo Y, Balghi H, Hanrahan JW. Role of tyrosine phosphorylation in the muscarinic activation of the cystic fibrosis transmembrane conductance regulator (CFTR). J Biol Chem. 2013;288:21815-21823.
177. Rock JR, O'Neal WK, Gabriel SE, Randell SH, Harfe BD, Boucher RC, et al. Transmembrane protein 16A (TMEM16A) is a Ca^{2+} regulated Cl^--secretory channel in mouse airways. J Biol Chem. 2009;284:14875-14880.
178. Zhang Y, Huang G, Shornick LP, Roswit WT, Shipley JM, Brody SL, et al. A transgenic FOXJ1-Cre system for gene inactivation in ciliated epithelial cells. Am J Respir Cell Mol Biol. 2007;36:515-519.
179. Bebok Z, Collawn JF, Wakefield J, Parker W, Li Y, Varga K, et al. Failure of cAMP agonists to activate rescued deltaF508 CFTR in CFBE41o- airway epithelial monolayers. J Physiol. 2005;569:601-615.
180. Botelho HM, Uliyakina I, Awatade NT, Proenca MC, Tischer C, Sirianant L, et al. Protein traffic disorders: an effective high-throughput fluorescence microscopy pipeline for drug discovery. Sci Rep. 2015;5:9038.
181. Barro Soria R, Schreiber R, Kunzelmann K. Bestrophin 1 and 2 are components of the Ca^{2+} activated Cl^- conductance in mouse airways. BBA. 2008;1783:1993-2000.
182. Mahe MM, Aihara E, Schumacher MA, Zavros Y, Montrose MH, Helmrath MA, et al. Establishment of Gastrointestinal Epithelial Organoids. Curr Protoc Mouse Biol. 2013;3(4):217-240.
183. Ma T, Thiagarajah JR, Yang H, Sonawane ND, Folli C, Galietta LJ, et al. Thiazolidinone CFTR inhibitor identified by high-throughput screening blocks cholera toxin-induced intestinal fluid secretion. J Clin Invest. 2002 ;110 (11):1651-1658.
184. Lefkimmiatis K, Srikanthan M, Maiellaro I, Moyer MP, Curci S, Hofer AM. Store-

operated cyclic AMP signalling mediated by STIM1. Nat Cell Biol. 2009;11:433-442.
185. Nichols JM, Maiellaro I, Abi-Jaoude J, Curci S, Hofer AM. "Store-operated" cAMP signaling contributes to Ca^{2+}-activated Cl^- secretion in T84 colonic cells. Am J Physiol Gastrointest Liver Physiol. 2015;309(8):G670-G679.
186. Kunzelmann K. CFTR: Interacting with everything? News Physiol Sciences. 2001;17:167-170.
187. Sheridan JT, Worthington EN, Yu K, Gabriel SE, Hartzell HC, Tarran R. Characterization of the oligomeric structure of the Ca^{2+}-activated Cl^- channel Ano1/TMEM16A. J Biol Chem. 2011;286:1381-1388.
188. Grubb BR, Boucher RC. Pathophysiology of gene-targeted mouse models for cystic fibrosis. Physiol Rev. 1999;79(1 Suppl):S193-S214.
189. Scudieri P, Caci E, Bruno S, Ferrera L, Schiavon M, Sondo E, et al. Association Of Tmem16a Chloride Channel Overexpression With Airway Goblet Cell Metaplasia. J Physiol. 2012;590:6141-6155.
190. Ruffin M, Voland M, Marie S, Bonora M, Blanchard E, Blouquit-Laye S, et al. Anoctamin 1 Dysregulation Alters Bronchial Epithelial Repair in Cystic Fibrosis. Biochim Biophys Acta. 2013;1832:2340-2351.
191. Faria D, Schreiber R, Kunzelmann K. CFTR is activated through stimulation of purinergic $P2Y_2$ receptors. Pflügers Arch. 2009;457:1373-1380.
192. Lee RJ, Foskett JK. cAMP-activated Ca^{2+} signaling is required for CFTR-mediated serous cell fluid secretion in porcine and human airways. J Clin Invest. 2010;120:3137-3148.
193. Wanitchakool P, Ousingsawat J, Sirianant L, Cabrita I, Faria D, Schreiber R, et al. Cellular defects by deletion of ANO10 are due to deregulated local calcium signaling. Cellular signalling. 2017;30:41-49.
194. Seidler U, Blumenstein I, Kretz A, Viellard-Baron D, Rossmann H, Colledge WH, et al. A functional CFTR protein is required for mouse intestinal cAMP-, cGMP- and Ca^{2+}-dependent HCO_3^- secretion. J Physiol. 1997;505:411-423.
195. Hogan DL, Crombie DL, Isenberg JI, Svendsen P, Schaffalitzky de Muckadell OB, Ainsworth MA. CFTR mediates cAMP- and Ca^{2+}-activated duodenal epithelial HCO_3^- secretion. Am J Physiol. 1997;272(4):872-878.
196. Namkung W, Lee JA, Ahn W, Han W, Kwon SW, Ahn DS, et al. Ca^{2+} activates cystic fibrosis transmembrane conductance regulator- and Cl^--dependent HCO_3^- transport in pancreatic duct cells. J Biol Chem. 2003;278(1):200-207.
197. Moon S, Singh M, Krouse ME, Wine JJ. Calcium-stimulated Cl^- secretion in Calu-3 human airway cells requires CFTR. Am J Physiol. 1997;273:L1208-L1219.
198. Seidler U, Singh AK, Cinar A, Chen M, Hillesheim J, Hogema B, et al. The role of the NHERF family of PDZ scaffolding proteins in the regulation of salt and water transport. Ann N Y Acad Sci. 2009;1165:249-260.
199. Lobo MJ, Amaral MD, Zaccolo M, Farinha CM. EPAC1 activation by cAMP stabilizes CFTR at the membrane by promoting its interaction with NHERF1. J Cell Sci. 2016 ;129(13):2599-2612.
200. Benedetto R, Ousingsawat J, Wanitchakool P, Zhang Y, Holtzman MJ, Amaral M, et al. Epithelial Chloride Transport by CFTR Requires TMEM16A. Scientific Reports. 2017;7:12397.
201. Broadbent D, Ahmadzai MM, Kammala AK, Yang C, Occhiuto C, Das R, et al. Roles of

NHERF Family of PDZ-Binding Proteins in Regulating GPCR Functions. Adv Immunol. 2017;136:353-385.
202. Tian Y, Kongsuphol P, Hug MJ, Ousingsawat J, Witzgall R, Schreiber R, et al. Calmodulin-dependent activation of the epithelial calcium-dependent chloride channel TMEM16A. FASEB J. 2011;25:1058-1068.
203. Ostrom RS, Insel PA. The evolving role of lipid rafts and caveolae in G protein-coupled receptor signaling: implications for molecular pharmacology. Br J Pharmacol. 2004;143:235-245.
204. Kowalski MP, Pier GB. Localization of cystic fibrosis transmembrane conductance regulator to lipid rafts of epithelial cells is required for Pseudomonas aeruginosa-induced cellular activation. J Immunol. 2004;172(1):418-425.
205. Hoque KM, Woodward OM, van Rossum DB, Zachos NC, Chen L, Leung GP, et al. Epac1 mediates protein kinase A-independent mechanism of Forskolin-activated intestinal chloride secretion. J Gen Physiol. 2010;135:43-58.
206. Domingue JC, Ao M, Sarathy J, Rao MC. Chenodeoxycholic acid requires activation of EGFR, EPAC, and Ca^{2+} to stimulate CFTR-dependent Cl^- secretion in human colonic T84 cells. Am J Physiol Cell Physiol. 2016;311(5):C777-C792.
207. Nascimbeni AC, Giordano F, Dupont N, Grasso D, Vaccaro MI, Codogno P, et al. ER-plasma membrane contact sites contribute to autophagosome biogenesis by regulation of local PI3P synthesis. Embo j. 2017;36(14):2018-2033.
208. Maleth J, Choi S, Muallem S, Ahuja M. Translocation between PI(4,5)P2-poor and PI(4,5)P2-rich microdomains during store depletion determines STIM1 conformation and Orai1 gating. Nat Commun. 2014;5:5843.
209. Farinha CM, Matos P, Amaral MD. Control of cystic fibrosis transmembrane conductance regulator membrane trafficking: not just from the endoplasmic reticulum to the Golgi. FEBS J. 2013;280:4396-4406.
210. Fallah G, Roemer T, Detro-Dassen S, Braam U, Markwardt F, Schmalzing G. TMEM16A(a)/anoctamin-1 Shares a Homodimeric Architecture with CLC Chloride Channels. Mol Cell Proteomics. 2010;79:649-661.
211. Knowles MR, Boucher RC. Mucus clearance as a primary innate defense mechanism for mammalian airways. J Clin Invest. 2002;109(5):571-577.
212. Johansson ME, Sjovall H, Hansson GC. The gastrointestinal mucus system in health and disease. Nat Rev Gastroenterol Hepatol. 2013;10(6):352-361.
213. Fahy JV, Dickey BF. Airway mucus function and dysfunction. N Engl J Med. 2010;363(23):2233-2247.
214. Birchenough GM, Johansson ME, Gustafsson JK, Bergstrom JH, Hansson GC. New developments in goblet cell mucus secretion and function. Mucosal Immunol. 2015;8(4):712-719.
215. Dunican EM, Elicker BM, Gierada DS, Nagle SK, Schiebler ML, Newell JD, et al. Mucus plugs in patients with asthma linked to eosinophilia and airflow obstruction. J Clin Invest. 2018;128(3):997-1009.
216. Stoltz DA, Meyerholz DK, Welsh MJ. Origins of cystic fibrosis lung disease. N Engl J Med. 2015;372:351-362.
217. Kunzelmann K, Schreiber R, Hadorn HB. Bicarbonate in cystic fibrosis. Journal of

Cystic Fibrosis. 2017;16:653-662.
218. Kondo M, Tsuji M, Hara K, Arimura K, Yagi O, Tagaya E, et al. Chloride ion transport and overexpression of TMEM16A in a guinea pig asthma model. Clin Exp Allergy. 2017;47(6):795-804.
219. Caci E, Scudieri P, Di Carlo E, Morelli P, Bruno S, De F, I, et al. Upregulation of TMEM16A Protein in Bronchial Epithelial Cells by Bacterial Pyocyanin. PLoS ONE. 2015;10:e0131775.
220. Kondo M, Nakata J, Arai N, Izumo T, Tagaya E, Takeyama K, et al. Niflumic acid inhibits goblet cell degranulation in a guinea pig asthma model. Allergol Int. 2012;61:133-142.
221. Lin J, Jiang Y, Li L, Liu Y, Tang H, Jiang D. TMEM16A mediates the hypersecretion of mucus induced by Interleukin-13. Exp Cell Res. 2015;334:260-269.
222. He M, Ye W, Wang WJ, Sison ES, Jan YN, Jan LY. Cytoplasmic Cl^- couples membrane remodeling to epithelial morphogenesis. Proc Natl Acad Sci U S A. 2017;114(52):E11161-e9.
223. Sirianant L, Wanitchakool P, Ousingsawat J, Benedetto R, Zormpa A, Cabrita I, et al. Non-essential contribution of LRRC8A to volume regulation. Pflügers Arch. 2016;468:1789-1796.
224. Schreiber R, Castrop H, Kunzelmann K. Allergen induced airway hyperresponsiveness is absent in ecto-5´-nucleotidase (CD73) deficient mice. Pflugers Arch. 2008;457:431-440.
225. Zhu Y, Abdullah LH, Doyle SP, Nguyen K, Ribeiro CM, Vasquez PA, et al. Baseline Goblet Cell Mucin Secretion in the Airways Exceeds Stimulated Secretion over Extended Time Periods, and Is Sensitive to Shear Stress and Intracellular Mucin Stores. PLoS One. 2015;10(5):e0127267.
226. Zhu Y, Ehre C, Abdullah LH, Sheehan JK, Roy M, Evans CM, et al. Munc13-2-/- baseline secretion defect reveals source of oligomeric mucins in mouse airways. J Physiol. 2008;586(7):1977-1992.
227. Park KS, Korfhagen TR, Bruno MD, Kitzmiller JA, Wan H, Wert SE, et al. SPDEF regulates goblet cell hyperplasia in the airway epithelium. J Clin Invest. 2007;117(4):978-988.
228. Sala-Rabanal M, Yurtsever Z, Nichols CG, Brett TJ. Secreted CLCA1 modulates TMEM16A to activate Ca^{2+}-dependent chloride currents in human cells. Elife. 2015;4. doi:10.
229. Huang F, Rock JR, Harfe BD, Cheng T, Huang X, Jan YN, et al. Studies on expression and function of the TMEM16A calcium-activated chloride channel. Proc Natl Acad Sci U S A. 2009;106:21413-21418.
230. Morrison KJ, Gao Y, Vanhoutte PM. Epithelial modulation of airway smooth muscle. Am J Physiol. 1990;258(6 Pt 1):254-262.
231. Bates J, Irvin C, Brusasco V, Drazen J, Fredberg J, Loring S, et al. The use and misuse of Penh in animal models of lung disease. Am J Respir Cell Mol Biol. 2004;31(3):373-374.
232. Matos JE, Robaye B, Boeynaems JM, Beauwens R, Leipziger J. K^+ secretion activated by luminal $P2Y_2$ and $P2Y_4$ receptors in mouse colon. J Physiol. 2005;564(Pt 1):269-279.
233. Pei S, Minhajuddin M, Callahan KP, Balys M, Ashton JM, Neering SJ, et al. Targeting aberrant glutathione metabolism to eradicate human acute myelogenous leukemia cells. J Biol Chem. 2013;288(47):33542-33558.
234. Jeon JH, Paik SS, Chun MH, Oh U, Kim IB. Presynaptic Localization and Possible

Function of Calcium-Activated Chloride Channel Anoctamin 1 in the Mammalian Retina. PLoS ONE. 2013;8:e67989.
235. Neureither F, Ziegler K, Pitzer C, Frings S, Mohrlen F. Impaired Motor Coordination and Learning in Mice Lacking Anoctamin 2 Calcium-Gated Chloride Channels. Cerebellum. 2017;16(5-6):929-937.
236. Rossetto O, Seveso M, Caccin P, Schiavo G, Montecucco C. Tetanus and botulinum neurotoxins: turning bad guys into good by research. Toxicon. 2001;39(1):27-41.
237. Rogers DF, Barnes PJ. Treatment of airway mucus hypersecretion. Ann Med. 2006;38(2):116-125.
238. Gorrieri G, Scudieri P, Caci E, Schiavon M, Tomati V, Sirci F, et al. Goblet Cell Hyperplasia Requires High Bicarbonate Transport To Support Mucin Release. Sci Rep. 2016;6:36016.
239. Jung J, Nam JH, Park HW, Oh U, Yoon JH, Lee MG. Dynamic modulation of ANO1/TMEM16A HCO3- permeability by Ca^{2+}/calmodulin. Proc Natl Acad Sci U S A. 2013;110(1):360-365.
240. Wang P, Zhao W, Sun J, Tao T, Chen X, Zheng YY, et al. Inflammatory Mediators Mediate Airway Smooth Muscle Contraction through a GPCR-TMEM16A-VDCC Axis and Contribute to Bronchial Hyperresponsiveness in Asthma. J Allergy Clin Immunol. 2018;141(4):1259-1268.
241. Miner K, Mohn D, Elliot R, Powers D, Chen J, Liu B, et al. The Anthelminthic Niclosamide And Related Compounds Represent Potent Tmem16a Antagonists That Fully Relax Mouse And Human Airway Rings. Journal of paediatrics and child health. 2017;57(2):996-1005.
242. Specian RD, Neutra MR. Mechanism of rapid mucus secretion in goblet cells stimulated by acetylcholine. J Cell Biol. 1980;85(3):626-640.
243. Kurosumi K, Shibuichi I, Tosaka H. Ultrastructural studies on the secretory mechanism of goblet cells in the rat jejunal epithelium. Arch Histol Jpn. 1981;44(3):263-284.
244. Thorn P, Gaisano H. Molecular control of compound Exocytosis: A key role for VAMP8. Commun Integr Biol. 2012;5(1):61-63.
245. Chambers LA, Rollins BM, Tarran R. Liquid movement across the surface epithelium of large airways. Respir Physiol Neurobiol. 2007;159(3):256-270.
246. Boucher RC. Regulation of airway surface liquid volume by human airway epithelia. Pflugers Arch. 2003;445:495-498.
247. Kunzelmann K. The Cystic Fibrosis Transmembrane Conductance Regulator and its function in epithelial transport. Rev Physiol Biochem Pharmacol. 1999;137:1-70.
248. Mall M, Gonska T, Thomas J, Schreiber R, Seydewitz HH, Kuehr J, et al. Modulation of Ca^{2+} activated Cl^- secretion by basolateral K^+ channels in human normal and cystic fibrosis airway epithelia. Pediatric Research. 2003;53:608-618.
249. Gallos G, Remy KE, Danielsson J, Funayama H, Fu XW, Chang HY, et al. Functional Expression of the TMEM16 Family of Calcium Activated Chloride Channels in Airway Smooth Muscle. Am J Physiol Lung Cell Mol Physiol. 2013;305:L625-L634.
250. Danielsson J, Perez-Zoghbi J, Bernstein K, Barajas MB, Zhang Y, Kumar S, et al. Antagonists of the TMEM16A Calcium-activated Chloride Channel Modulate Airway Smooth Muscle Tone and Intracellular Calcium. Anesthesiology (in press). 2015;123(3):569-581.

251. Boucher RC. Airway surface dehydration in cystic fibrosis: pathogenesis and therapy. Annu Rev Med. 2007;58:157-170.
252. Pezzulo AA, Tang XX, Hoegger MJ, Alaiwa MH, Ramachandran S, Moninger TO, et al. Reduced airway surface pH impairs bacterial killing in the porcine cystic fibrosis lung. Nature. 2012;487:109-113.
253. Schultz A, Puvvadi R, Borisov SM, Shaw NC, Klimant I, Berry LJ, et al. Airway surface liquid pH is not acidic in children with cystic fibrosis. Nat Commun. 2017;8(1):1409.
254. Li H, Salomon JJ, Sheppard DN, Mall MA, Galietta LJ. Bypassing CFTR dysfunction in cystic fibrosis with alternative pathways for anion transport. Curr Opin Pharmacol. 2017;34:91-97.
255. Benedetto R, Cabrita I, Schreiber R, Kunzelmann K. TMEM16A is indispensable for basal ATP-induced mucus secretion in airways and intestine. FASEB J. 2019. *In press*
256. Schenk LK, Ousingsawat J, Skryabin BV, Schreiber R, Pavenstadt H, Kunzelmann K. Regulation and Function of TMEM16F in Renal Podocytes. Int J Mol Sci. 2018;19(6).
257. Kunzelmann K, Tian Y, Martins JR, Faria D, Kongsuphol P, Ousingsawat J, et al. Cells in focus: Airway epithelial cells-Functional links between CFTR and anoctamin dependent Cl^- secretion. Int J Biochem Cell Biol. 2012;44:1897-1900.
258. Kunzelmann K, Tian Y, Martins JR, Faria D, Kongsuphol P, Ousingsawat J, et al. Anoctamins. Pflugers Arch. 2011;462:195-208.
259. Danielsson J, Mikami M, Emala CW. Antagonism of the Tmem16A Calcium-Activated Chloride Channel Attenuates Allergic Lung inflammation. Am J Respir Crit Care Med. 2017;195:A5290.
260. Liang L, Huang M, Xiao Y, Zen S, Lao M, Zou Y, et al. Inhibitory effects of Niclosamide on inflammation and migration of fibroblast-like synoviocytes from patients with rheumatoid arthritis. Inflamm Res. 2015;64(3-4):225-233.
261. Solari FA, Mattheij NJ, Burkhart JM, Swieringa F, Collins PW, Cosemans JM, et al. Combined quantification of the global proteome, phosphoproteome and proteolytic cleavage to characterize altered platelet functions in the human Scott syndrome. Mol Cell Proteomics. 2016;15(10):3154-3169.
262. Mazzone A, Gibbons SJ, Bernard CE, Nowsheen S, Middha S, Almada LL, et al. Identification and characterization of a novel promoter for the human ANO1 gene regulated by the transcription factor signal transducer and activator of transcription 6 (STAT6). FASEB J. 2015 Jan;29(1):152-163.
263. Qin Y, Jiang Y, Sheikh AS, Shen S, Liu J, Jiang D. Interleukin-13 stimulates MUC5AC expression via a STAT6-TMEM16A-ERK1/2 pathway in human airway epithelial cells. Int Immunopharmacol. 2016;40:106-114.
264. Kunzelmann K. TMEM16, LRRC8A, bestrophin: chloride channels controlled by Ca and cell volume. Trends Biochem Sci. 2015;40:535-543.
265. Ratjen F, Durham T, Navratil T, Schaberg A, Accurso FJ, Wainwright C, et al. Long term effects of denufosol tetrasodium in patients with cystic fibrosis. J Cyst Fibros. 2012;11(6):539-549.
266. Chen W, Mook RA, Jr., Premont RT, Wang J. Niclosamide: Beyond an antihelminthic drug. Cellular signalling. 2018;41:89-96.
267. Imperi F, Massai F, Ramachandran Pillai C, Longo F, Zennaro E, Rampioni G, et al.

New life for an old drug: the anthelmintic drug Niclosamide inhibits Pseudomonas aeruginosa quorum sensing. Antimicrob Agents Chemother. 2013;57(2):996-1005.
268. Costabile G, d'Angelo I, Rampioni G, Bondi R, Pompili B, Ascenzioni F, et al. Toward Repositioning Niclosamide for Antivirulence Therapy of Pseudomonas aeruginosa Lung Infections: Development of Inhalable Formulations through Nanosuspension Technology. Mol Pharm. 2015;12(8):2604-2617.
269. Gwisai T, Hollingsworth NR, Cowles S, Tharmalingam N, Mylonakis E, Fuchs BB, et al. Repurposing Niclosamide as a versatile antimicrobial surface coating against device-associated, hospital-acquired bacterial infections. Biomed Mater. 2017;12(4):045010.
270. Morin F, Kavian N, Nicco C, Cerles O, Chereau C, Batteux F. Improvement of Sclerodermatous Graft-Versus-Host Disease in Mice by Niclosamide. J Invest Dermatol. 2016;136(11):2158-2167.
271. Li Y, Li PK, Roberts MJ, Arend RC, Samant RS, Buchsbaum DJ. Multi-targeted therapy of cancer by Niclosamide: A new application for an old drug. Cancer Lett. 2014;349(1):8-14.
272. Hwang SJ, Blair PJ, Britton FC, O'Driscoll KE, Hennig G, Bayguinov YR, et al. Expression of anoctamin 1/TMEM16A by interstitial cells of Cajal is fundamental for slow wave activity in gastrointestinal muscles. J Physiol. 2009;587:4887-4904.
273. Zhang RX, Wang XY, Chen D, Huizinga JD. Role of interstitial cells of Cajal in the generation and modulation of motor activity induced by cholinergic neurotransmission in the stomach. Neurogastroenterol Motil. 2011;23(9):e356-371.
274. Huang WC, Xiao S, Huang F, Harfe BD, Jan YN, Jan LY. Calcium-activated chloride channels (CaCCs) regulate action potential and synaptic response in hippocampal neurons. Neuron. 2012;74(1):179-192.
275. R. Marthan CM, T. Amedee, J. Mironneau. Calcium channel currents in isolated smooth muscle cells from human bronchus. J Appl Physiol 1989;66(4):1706-1714.
276. Mounkaila B, Marthan R, Roux E. Biphasic effect of extracellular ATP on human and rat airways is due to multiple P2 purinoceptor activation. Respir Res. 2005;6:143.
277. Flores-Soto E, Carbajal V, Reyes-Garcia J, Garcia-Hernandez LM, Figueroa A, Checa M, et al. In airways ATP refills sarcoplasmic reticulum via P2X smooth muscle receptors and induces contraction through P2Y epithelial receptors. Pflugers Arch. 2011;461(2):261-275.
278. Somlyo AP, Wu, X., Walker, L. A., & Somlyo, A. V. . Pharmacomechanical coupling: the role of calcium, G-proteins, kinases and phosphatases. Reviews of Physiology Biochemistry and Pharmacology. 1999;134(201-234).
279. Chapman DG, Irvin CG. Mechanisms of airway hyper-responsiveness in asthma: the past, present and yet to come. Clin Exp Allergy. 2015;45(4):706-719.
280. Ribeiro CM, Paradiso AM, Carew MA, Shears SB, Boucher RC. Cystic fibrosis airway epithelial Ca^{2+}i signaling. The mechanism for the larger agonist-mediated Ca^{2+} signals in human cystic fibrosis airway epithelia. J Biol Chem. 2005;280(11):10202-10209.
281. Martins JR, Kongsuphol P, Sammels E, Daimène S, AlDehni F, Clarke L, et al. F508del-CFTR increases intracellular Ca^{2+} signaling that causes enhanced calcium-dependent Cl^- conductance in cystic fibrosis. Biochim Biophys Acta. 2011;1812:1385-1392.
282. Shenyuan L. Zhang YY, Jack Roos, J. Ashot Kozak,Thomas J. Deerinck, Mark H. Ellisman, Kenneth A. Stauderman, and Michael D. Cahalan. STIM1 is a Ca^{2+} sensor that

activates CRAC channels and migrates from the Ca^{2+} store to the plasma membrane. Nature. 2006;437(7060):902-905.
283. Maiellaro I, Lefkimmiatis K, Moyer MP, Curci S, Hofer AM. Termination and activation of store-operated cyclic AMP production. J Cell Mol Med. 2012;16(11):2715-2725.
284. Romanenko VG, Catalan MA, Brown DA, Putzier I, Hartzell HC, Marmorstein AD, et al. Tmem16A encodes the Ca^{2+}-activated Cl^- channel in mouse submandibular salivary gland acinar cells. J Biol Chem. 2010;285:12990-3001.
285. Hanzu FA, Gasa R, Bulur N, Lybaert P, Gomis R, Malaisse WJ, et al. Expression of TMEM16A and SLC4A4 in Human Pancreatic Islets. Cell Physiol Biochem. 2012;29:61-64.
286. Hahn A, Salomon JJ, Leitz D, Feigenbutz D, Korsch L, Lisewski I, et al. Expression and function of Anoctamin 1/TMEM16A calcium-activated chloride channels in airways of in vivo mouse models for cystic fibrosis research. Pflugers Arch. 2018;470(9):1335-1348.
287. Raiford KL, Park J, Lin K-W, Fang S, Crews AL, Adler KB. Mucin granule-associated proteins in human bronchial epithelial cells: the airway goblet cell "granulome". Respiratory Research. 2011;12(1).
288. Montoro DT, Haber AL, Biton M, Vinarsky V, Lin B, Birket SE, et al. A revised airway epithelial hierarchy includes CFTR-expressing ionocytes. Nature. 2018;560(7718):319-324.
289. Crystal RG, Randell SH, Engelhardt JF, Voynow J, Sunday ME. Airway epithelial cells: current concepts and challenges. Proc Am Thorac Soc. 2008;5(7):772-777.
290. Laoukili J, Perret E, Willems T, Minty A, Parthoens E, Houcine O, et al. IL-13 alters mucociliary differentiation and ciliary beating of human respiratory epithelial cells. Journal of Clinical Investigation. 2001;108(12):1817-1824.
291. Gomperts BN, Kim LJ, Flaherty SA, Hackett BP. IL-13 regulates cilia loss and foxj1 expression in human airway epithelium. Am J Respir Cell Mol Biol. 2007;37(3):339-346.
292. Turner J, Roger J, Fitau J, Combe D, Giddings J, Heeke GV, et al. Goblet cells are derived from a FOXJ1-expressing progenitor in a human airway epithelium. Am J Respir Cell Mol Biol. 2011;44(3):276-284.
293. Patel AC, Brett TJ, Holtzman MJ. The role of CLCA proteins in inflammatory airway disease. Annu Rev Physiol. 2009;71:425-449.
294. Zu D, Pauli BU. Correlation between the lung distribution patterns of Lu-ECAM-1 and melanoma experimental metastases. Int J Cancer. 1993, 53(4):628-633.
295. Patel AC, Brett TJ, Holtzman MJ. The role of CLCA proteins in inflammatory airway disease. Annu Rev Physiol. 2009;71:425-449.
296. Yuhong Zhou MS, Qu Dong, Louahed J, Weiss C, Shan Hong Wan QC, Dragwa C, Savio D, Huang M, Fuller YT, Nicolaides NC, McLane M and, Levitt RC. A calcium-activated chloride channel blocker inhibits goblet cell metaplasia and mucus overproduction. Mucus Hypersecretion in Respiratory Disease: Novartis Foundation Symposium. 2002.
297. C. A. Bertrand HD, C. T. Poll, C. Laboisse, U. Hopfer,and R. J. Bridges. Niflumic acid inhibits ATP-stimulated exocytosis in a mucin-secreting epithelial cell line. Am J Physiol Cell Physiol. 2004;286:C247-C255.
298. Hauber HP, Daigneault P, Frenkiel S, Lavigne F, Hung HL, Levitt RC, et al. Niflumic acid and MSI-2216 reduce TNF-alpha-induced mucin expression in human airway mucosa. J Allergy Clin Immunol. 2005;115(2):266-271.
299. Walker NM, Simpson JE, Levitt RC, Boyle KT, Clarke LL. Talniflumate increases

survival in a cystic fibrosis mouse model of distal intestinal obstructive syndrome. J Pharmacol Exp Ther. 2006;317(1):275-283.
300. Louise E. Donnelly DFR. Therapy for Chronic Obstructive Pulmonary Disease in the 21st Century. Drugs. 2003;63(19):1973-1998.
301. Lee B, Cho H, Jung J, Yang YD, Yang DJ, Oh U. Anoctamin 1 contributes to inflammatory and nerve-injury induced hypersensitivity. Mol Pain. 2014;10:15 .
302. Sonneville F, Ruffin M, Coraux C, Rousselet N, Le Rouzic P, Blouquit-Laye S, et al. MicroRNA-9 downregulates the ANO1 chloride channel and contributes to cystic fibrosis lung pathology. Nat Commun. 2017;8(1):710.
303. Dai WJ, Qiu J, Sun J, Ma CL, Huang N, Jiang Y, et al. Downregulation of microRNA-9 reduces inflammatory response and fibroblast proliferation in mice with idiopathic pulmonary fibrosis through the ANO1-mediated TGF-beta-Smad3 pathway. J Cell Physiol. 2018. doi: 10.1002/jcp.26961.
304. Cohn L. Mucus in chronic airway diseases: sorting out the sticky details. J Clin Invest. 2006;116(2):306-308.
305. Hansson GC. Role of mucus layers in gut infection and inflammation. Curr Opin Microbiol. 2012;15(1):57-62.
306. Imperi F. MF, Pillai C.R., Longo F., Zennaro E, Rampioni G, Visca P., Leoni L. New Life for an Old Drug: the Anthelmintic Drug Niclosamide Inhibits Pseudomonas aeruginosa Quorum Sensing. Antimicrob Agents Chemother. 2013;57(2):996-1005.
307. Henrik Sengelv LK, Niels Borregaard. Control of Exocytosis in Early Neutrophil Activation. The Journal of Immunology. 1993;150(4):1535-1543.
308. Yong-Dae Kim E-JK, Dae-Won Park, Si-Youn Song, Seok-Keun Yoon and Suk-Hwan Baek. Interleukin-1β Induces MUC2 and MUC5AC Synthesis through Cyclooxygenase-2 in NCI-H292 Cells. Molecular Pharmacology. 2002;62(5):1112-1118.
309. Duvvuri U, Shiwarski DJ, Xiao D, Bertrand C, Huang X, Edinger RS, et al. TMEM16A induces MAPK and contributes directly to tumorigenesis and cancer progression. Cancer Res. 2012;72(13):3270-3281.
310. Baker LY, Hobby CR, Siv AW, Bible WC, Glennon MS, Anderson DM, et al. Pseudomonas aeruginosa responds to exogenous polyunsaturated fatty acids (PUFAs) by modifying phospholipid composition, membrane permeability, and phenotypes associated with virulence. BMC Microbiol. 2018;18(1):117.
311. Charlesworth G, Plagnol V, Holmstrom KM, Bras J, Sheerin UM, Preza E, et al. Mutations in ANO3 cause dominant craniocervical dystonia: ion channel implicated in pathogenesis. Am J Hum Genet. 2012;91(6):1041-1050.
312. Tran TT, Tobiume K, Hirono C, Fujimoto S, Mizuta K, Kubozono K, et al. TMEM16E (GDD1) exhibits protein instability and distinct characteristics in chloride channel/pore forming ability. J Cell Physiol. 2014;229(2):181-190.
313. Whitlock JM, Yu K, Cui YY, Hartzell HC. Anoctamin 5/TMEM16E facilitates muscle precursor cell fusion. J Gen Physiol. 2018;150(11):1498-1509.
314. Jun I, Park HS, Piao H, Han JW, An MJ, Yun BG, et al. ANO9/TMEM16J promotes tumourigenesis via EGFR and is a novel therapeutic target for pancreatic cancer. Br J Cancer. 2017;117(12):1798-809.
315. Li C, Cai S, Wang X, Jiang Z. Identification and characterization of ANO9 in stage II

and III colorectal carcinoma. Oncotarget. 2015;6(30):29324-29324.
316. Oh SJ, Hwang SJ, Jung J, Yu K, Kim J, Choi JY, et al. MONNA, a Potent and Selective Blocker for TMEM16A/Anoctamin-1. Mol Pharmacol. 2013;84(5):726-735.
317. Ko EA, Jin BJ, Namkung W, Ma T, Thiagarajah JR, Verkman AS. Chloride channel inhibition by a red wine extract and a synthetic small molecule prevents rotaviral secretory diarrhoea in neonatal mice. Gut. 2014;63(7):1120-1129.
318. Boedtkjer DM, Kim S, Jensen AB, Matchkov VM, Andersson KE. New selective inhibitors of calcium-activated chloride channels-T16A -A01, CaCC -A01, and MONNA-what do they inhibit? Br J Pharmacol. 2015;172(16):4158-4172.
319. Davis AJ, Shi J, Pritchard HA, Chadha PS, Leblanc N, Vasilikostas G, et al. Potent vasorelaxant activity of the TMEM16A inhibitor T16A(inh)-A01. Br J Pharmacol. 2013;168(3):773-784.
320. Jiang Y, Yu B, Yang H, Ma T. Shikonin Inhibits Intestinal Calcium-Activated Chloride Channels and Prevents Rotaviral Diarrhea. Front Pharmacol. 2016;7:270.
321. Liu S, Feng J, Luo J, Yang P, Brett TJ, Hu H. Eact, a small molecule activator of TMEM16A, activates TRPV1 and elicits pain- and itch-related behaviors. Br J Pharmacol. 2016;173(7):1208-1218.
322. Deba F, Bessac BF. Anoctamin-1 Cl^- channels in nociception: activation by an N-aroylaminothiazole and capsaicin and inhibition by T16A[inh]-A01. Mol Pain. 2015;11:55.
323. Keating D. et al. VX-445–Tezacaftor–Ivacaftor in Patients with Cystic Fibrosis and One or Two Phe508del Alleles. N Engl J Med. 2018; 379(17):1612-1620.
324. Davies J.C. et al. VX-659-Tezacaftor-Ivacaftor in Patients with Cystic Fibrosis and One or Two Phe508del Alleles. N Engl J Med. 2018;379(17):1599-1611.